Synthesis and physico-chemical studies on dithiolene complexes of the closed-shell (d^{10}) metals and trivalent lanthanide ions

Dissertation

Zur Erlangung des Grades
des Doktors der Naturwissenschaften
der Naturwissenschaftlich-Technischen Fakultät III
Chemie, Pharmazie, Bio- und Werkstoffwissenschaften
der Universität des Saarlandes

von

Amadou Latyr NDIAYE

Saarbrücken
2009

Tag des Kolloquiums:	02.04.2009
Dekan:	Prof. Dr. -Ing. Stefan Diebels
Vorsitzender:	Prof. Ulli Kazmaier
Berichterstatter:	Prof. Dr. Dr. h.c. Michael Veith
	Prof. Dr. Michael Knorr
Akad. Mitarbeiter:	Dr. Fabrice Guyon
	Dr. Stefan Stucky

Die vorliegende Arbeit entstand in der Zeit vom Oktober 2004 bis Dezember 2008 in der Anorganischen Chemie der Universität des Saarlandes in Saarbrücken unter Anleitung von Herrn Prof. Dr. Dr. h. c. Michael Veith, und ist eine Zusammenarbeit mit der Institute UTINAM der „Université de Franche Comté“ unter Anleitung von Herrn Prof. Dr. Michael Knorr.

Meinem verehrten Lehrer Herrn Prof. Dr. Dr. h.c. Michael Veith danke ich sehr herzlich für die interessante Themenstellung, die wertvollen Ratschläge und vielen hilfreichen Diskussion sowie für die großzügige Unterstützung während der Durchführung dieser Arbeit.

Meinem zweiten Doktorvater Herrn Prof. Dr. Michael Knorr danke ich recht herzlich für die interessante Themenstellung sowie für die stete Diskussionsbereitschaft und hilfreichen Ratschläge.

Den Mitarbeitern und Angestellten AK Veith, die auf verschiedenste Weise zum Gelingen dieser Arbeit beigetragen haben, bin ich zu großem Dank verpflichtet.

Allen Mitgliedern AK Knorr (UTINAM: „Equipe Matériaux Structurés“), die auf verschiedenste Weise zum Gelingen dieser Arbeit beigetragen haben, sei an dieser Stelle herzlich gedankt.

Herrn Dr. Volker Huch danke ich im Besonderen für die Durchführung der Röntgens-Strukturanalysen.

Herrn Dr. Fabrice Guyon danke ich persönlich für die Zusammenarbeit in diesem Thema, für die guten Ratschläge während dieser Arbeit sowie für die gewissenhafte Durchsicht des vorliegenden Manuskripts.

Weiterhin danke ich Herrn Dr. Markus Ehses für die Diskussionsbereitschaft sowie für die gewissenhafte Durchsicht des vorliegenden Manuskripts.

Frau Helga Feuerhake und Frau Susanne Harling gilt mein Dank für die Durchführung der Elementaranalysen.

Für die gute Arbeitsatmosphäre bedanke ich mich herzlich bei meinen jetzigen und ehemaligen Kollegen vom Labor 290, hier besonders bei Herrn Dr. Markus Ehses, Herrn Dr. Antoine Laurent und Frau Dipl. Chem. Anusch Arezki für ihre Freundschaft und ihre Unterstützung in jeglicher Hinsicht.

Frau Prof. Dr. Claudia Wickleder danke ich ganz herzlich für die Zusammenarbeit sowie für die Diskussionsbereitschaft und die lumineszenz -untersuchungen.

Aber auch meine Familie und meinen Freunden, auch wenn sie wenig mit der eigentlichen chemischen Arbeit zu tun haben, möchte ich mich bedanken, da sie mir immer den nötigen Rückhalt gegeben haben.

Table of Contents

List of abbreviations

BEDT-TTF	Bis-ethylenedithia-tetrathiafulvalene
CF	Crystal field
DFT	Density functional theory
DMIT	Dimercaptoisotrithione (1,3-dithiole-2-thione-4,5-dithiolate)
DMSO	Dimethylsulfoxide
EHMO	Extended Hückel Molecular Orbital
ET	Energy Transfer
EXAFS	Extended X-ray Absorption Fine Structures
HSAB	Hard and Soft Acid and Base
IL	Intraligand
ISC	Intersystem crossing
LC	Ligand centered
LMCT	Ligand-to-metal charge transfer
Ln/Ln^{3+}	lanthanide/ trivalent lanthanides
MLCT	Metal-to-ligand charge transfer
MOF	Metal-organic framework
Nd:YAG	Neodymium doped in Yttrium Aluminium Garnet ($Y_3Al_5O_{12}$)
NIR	Near Infrared
NLO	Nonlinear Optics
OLED	Organic Light emitting Diode
Pm	Probability of formation
ppm	parts per millions
qsal	N-(8-quinolyl)salicylaldimine,
SalEen	N-(2-ethylamino)-ethyl)-salicylaldimine
SOC	Spin–orbit coupling
TCNQ	Tetracyano-p-quinodimethane
THET-TTF	Tetrahydroxyethylthia-tetrathiafulvalene
THF	Tetrahydrofuran
THT	Tetrahydrothiophene
TMTSF	Tetramethyltetraselenafulvalene
TPA	1,3,5-triaza-7-phosphaadamantanetriylphosphine
TTF	Tetrathiafulvalene
UV-Vis	Ultraviolet visible
VDW	Van der Waals
vs.	versus
XLCT	Halide-to-ligand charge transfer
X/MLCT	Halide/metal-to-ligand charge transfer

Zusammenfassung

Heutzutage, ist der Chemie als allgemeines Werkzeug für den Zugang (Synthese), die Beherrschung (Studie von Eigenschaften) und das Verständnis (Parametereinfluss) des Materials. Diese ist auf zwei Ansätze begründet für welche die Anglizismen „Top-down“ und „Bottom-up“ geläufig sind. Das erste Verfahren ist ein Schlüssel zur Nanotechnologie. Der zweite Ansatz besteht darin, dass Mikrosysteme mit spezifischen Eigenschaften zu einem Makrosystem zusammengesetzt werden, welches die gewünschten Eigenschaften in sich vereint. Der Ausdruck „vom Molekül zum Material“ beschreibt die Vorgehensweise dieses Konzeptes wobei die supramolekulare Chemie spielt eine bedeutende Rolle.

Die vorliegende Arbeit überprüft die Synthese und die Eigenschaften von Dithiolen-Systemen, die d^{10} Metallionen oder Lanthanidionen beinhalten. Das erste Kapitel ist eine allgemeine Einleitung über Dithiolene und über Lanthaniden. Das zweite Kapitel beschäftigt sich mit der Synthese und Charakterisierung von supramolekularen Systemen, die auf neutralen Dithiolen-Liganden basiert sind. In diesem Kapitel, die Bedeutung von Funktionsgruppen, die die Fähigkeit besitzen, nichtkovalente Bindungen einzugehen, wird diskutiert. Das dritte Kapitel wird der Reaktivität der neutralen Dithiolen-Liganden gegenüber den d^{10} Übergangsmetallen Cu^{I}, Au^{I} und Hg^{II} gewidmet. Beschrieben werden Synthesemethoden für supramolekulare Komplexe sowie die spektroskopische Eigenschaften. Im letzten Kapitel werden Reaktivität dieser Liganden gegenüber den Lanthaniden Nd, Eu, Gd, Tb und Er und die spektroskopischen Eigenschaften vorgestellt. Der Schwerpunkt liegt auf dem Energieübergangsprozess („Antenna Effekt“), welcher stattfindet, sobald diese Liganden an ein Lanthanoid-Zentrum koordiniert sind.

Abstract

Nowadays, chemistry represents a general tool for accessing (synthesis), controlling (parameters influence) and understanding (study of properties) the material. This is allowed by two possible approaches: the “Top-down” and “Bottom-up”. The first approach is a key to nanotechnology. The second approach consists in assembling small systems, with intrinsic properties, to build up macro system with interesting properties. This concept is generally termed as: “*from molecules to material*” and in this context, supramolecular chemistry plays a crucial role.

The present work examines the synthesis and properties of dithiolene systems bearing metal ions and lanthanides. The first chapter is a general introduction on dithiolene chemistry and lanthanides. The second chapter deals with the synthesis and characterisation of supramolecular systems based on neutral dithiolene-like ligands. In this chapter, importance of non-covalent interactions is discussed. The third chapter concerns the reactivity of these neutral dithiolene-like ligands towards d^{10} transition metals (Cu^{I}, Hg^{II}, Au^{I}). This chapter will describe the synthesis of supramolecular complexes and their spectroscopic properties. The fourth chapter deals with the reactivity of the ligands with lanthanides (Nd, Eu, Gd, Tb, Er) and the characterisation of Ln^{3+}-dithiolene complexes. The discussion will be oriented on the energy transfer process taking place in these coordination compounds (“Antenna Effect”).

Résumé

De nos jours, la chimie est utilisée comme outil général pour accéder (synthèse), contrôler (influence des paramètres) et comprendre (étude des propriétés) le matériau. Ceci est rendu possible grâce à deux approches: l´approche «Top-down» et l´approche « Bottom-up ». La première approche est une des bases de la nanotechnologie. La deuxième approche consiste en l´assemblage de systèmes moléculaires possédant des propriétés intrinsèques pour accéder à des matériaux avec de nouvelles propriétés. Ce concept est généralement appelé: «de la molécule au matériau »; et dans ce contexte, la chimie supramoléculaire occupe une position centrale.

Le présent travail porte sur la synthèse et l´étude de propriétés des systèmes de métal-dithiolene comportant des ions métalliques et des lanthanides. Le premier chapitre est une introduction générale sur la chimie du dithiolene et des lanthanides. Le deuxième chapitre décrit la synthèse et la caractérisation de systèmes supramoléculaires basées sur des ligands dithiolene neutres. Dans ce chapitre, l'importance des groupes fonctionnels capables de former des interactions non covalentes sera discutée. Le troisième chapitre est consacré à la réactivité de ces ligands dithiolene neutres avec les métaux de transition (d^{10}) tels que Cu^{I}, Hg^{II}, et Au^{I}. Ce chapitre décrira la synthèse de complexes supramoléculaires ainsi que leurs propriétés spectroscopiques. Le quatrième chapitre, s´intéresse à la réactivité de ces ligands vis-à-vis des lanthanides trivalents (Nd, Eu, Gd, Tb, Er), la caractérisation des complexes formés ainsi que les propriétés de luminescence en résultant. Notre discussion sera orientée sur le processus de transfert d'énergie («Effet Antenne»), une fois ces ligands coordonnés à un ion lanthanide.

CHAPTER A. INTRODUCTION TO DITHIOLENE AND LANTHANIDE CHEMISTRY

A Introduction

A.1 Dithiolene and neutral derivatives

A.1.1 General features and properties

Synthesis and characterization of heterocyclic compounds containing chalcogen atoms is not a new field in chemistry. Nevertheless, this area of chemistry has increasingly received much attention during the past decades and is still attractive for a lot of researchers. Dithiolene compounds represent a special family in heterocyclic compounds in which the heteroatoms are sulfur atoms. They can be recognised by depicting the terminology dithiolene (dithiole-ene) and represent structural motifs in which two sulfur atoms (di-thio-) are linked through an ethylene bond (-ene-) as displayed below.

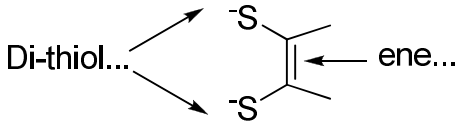

They possess chelating properties and tend to be coordinated to a metal center via ionic or coordinating bonding. In this case, they can be classified as a Hückel-type 6 π-electrons system and possess interesting electrochemical properties resulting from highly electronic delocalization once coordinated to a metal center such as nickel (Ni). Around 1960, three research groups (Holm[1], Gray[2] and Schrauzer[3]) independently discovered the unusual electronic properties of dithiolene complexes. They established the two reversible one-electron electrochemical relationship between a dithiolene complex in its anionic form $[Ni(S_2C_2R_2)_2]^{2-}$ and its neutral form $[Ni(S_2C_2R_2)_2]$ (see Eq. 1).[4]

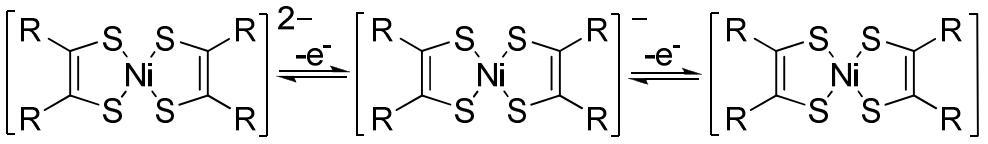

(Eq.1)

Scheme A-1 : Reversible one electron oxidation of the anionic $[Ni(S_2C_2R_2)_2]^{2-}$ leading to the neutral form.

A qualitative description of the bonding in the neutral dithiolene complex involves resonance structures in which the metal possesses a formal oxidation state of 0, II, or

IV[4] while the ligands can be viewed either in its dithiolate form or neutral form.[5] Therefore, these dithiolene complexes should be better described as resonance hybrid of the limiting structure shown in Scheme A-2.

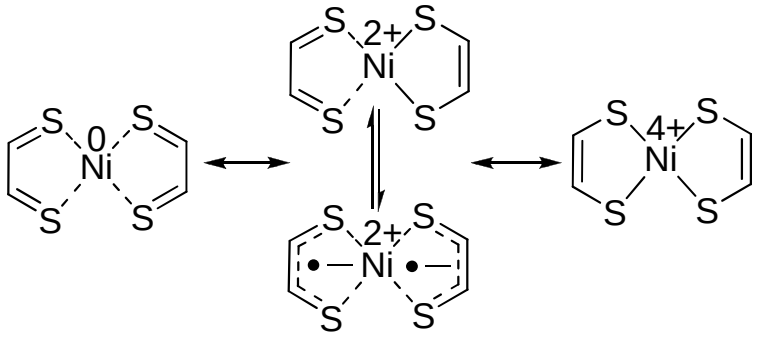

Scheme A-2 : Resonance structures of a neutral [Ni($S_2C_2R_2$)].[4]

In such complexes, the ligand π orbitals interact with the metal dπ orbitals to give frontier orbitals of mixed–ligand and metal character. The electrons are, therefore, not localized at the ligands, but seem to be delocalized within the five-membered ring which exhibits a certain degree of aromaticity.[5]

This aromaticity is demonstrated in the case of the cobaltadithiolene compound (CpCo($S_2C_2R_2$))[6]. In fact, this metalladithiolene which consists of one metal atom, two coordinated sulfur atoms, and two unsaturated carbon atoms; can experience an electrophilic substitution catalyzed by aluminium trichloride (Friedels-Crafts acylation) (see Scheme A-3).

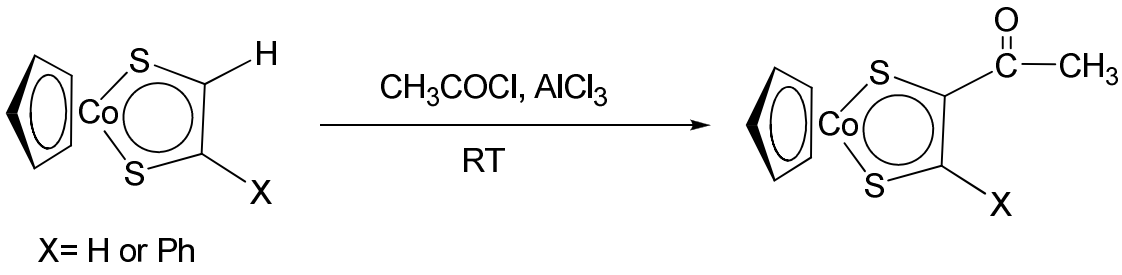

X= H or Ph

Scheme A-3 : Electrophilic substitution on the cobaltadithiolene complex (CpCo($S_2C_2R_2$)), illustrating the aromaticity of the five-membered ring.[6]

Another example illustrating the delocalization in this kind of five-membered ring (metallodithiolene) has been given by Rauchfuss *et al.*[7] He showed that the MS_2C_2-metallacycle can be coordinated to another metal center in a η^5 manner.

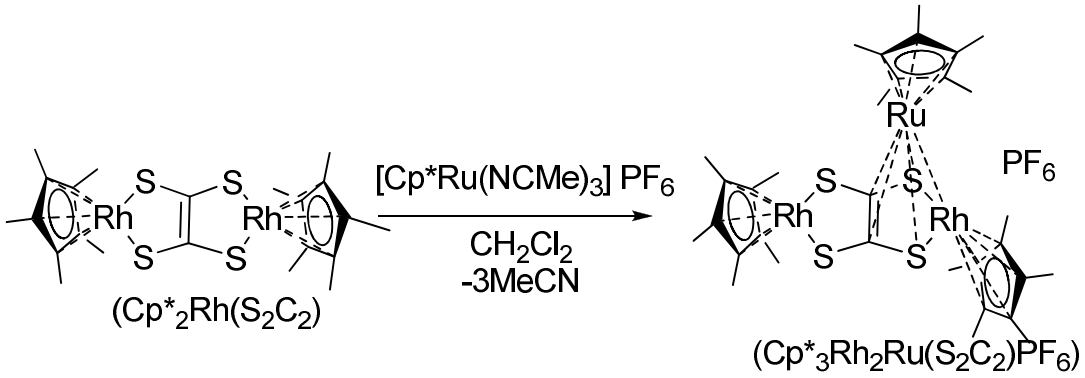

Scheme A-4 : Coordination of a MS_2C_2 moiety to a M´Cp* fragment illustrating the η^5 coordination mode, and evidence for the electrons delocalisation into the MS_2C_2 ring.[7]

The MS_2C_2 moiety acts as a π-ligand, and coordinates to a MCp* moiety to build up a heterotrinuclear complex of general formula ($Cp^*_3M_2M´(S_2C_2)X$) (M=Rh, M´=Ru, X=PF_6) in which the M´Cp* moiety is bonded to the $M(S_2C_2)$ moiety in a η^5 coordination.mode.[7] The crystal structure is shown in Figure A-1.

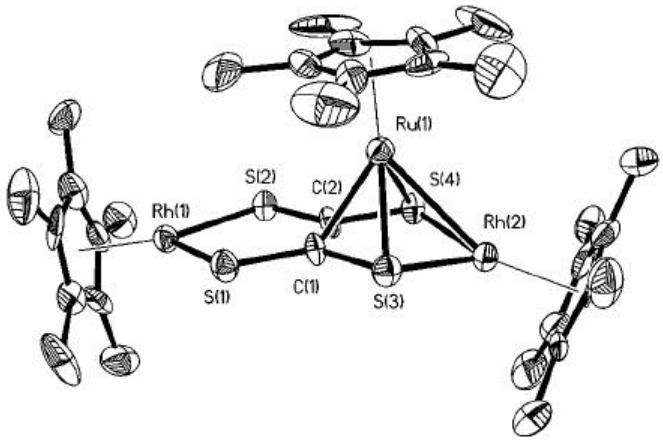

Figure A-1 : Structure of $Cp^*_3Rh_2Ru(S_2C_2)$ showing the coordination of the metallacycle (RhS_2C_2) to a RuCp* in a η^5 way. The PF_6^- counter ion is omitted for clarity. (50 % probability ellipsoids).[7]

As a result of this extensive delocalization in the MS_2C_2 moiety, the oxidation state assignment of the metal and ligands are ambiguous.

These electron-rich sulfur-based heterocyclic compounds are therefore good candidates for investigating and studying phenomena in which electron exchange and/or transfer play an important role, *i.e.* for application in electrochemical, optical and magnetic domains.[5] The presence of sulfur in many biological systems also allows their implication in biochemistry and bioinorganic chemistry.[8-11]

A.1.2 Historical evolution in dithiolene chemistry

Historically, we can divide Dithiolene Chemistry in 2 periods, depending on research orientation, the starting point being the first synthesis of tetrathiafulvalene (TTF) by Wudl *et al.* in 1970.[12]

A.1.3 Early stage of the research on dithiolene complexes

Metal-dithiolene complexes were investigated in the sixties for their electrochemical properties and the unique electronic structure of this class of compounds.[13, 14] They were the object of a renewed interest at the end of the 70's due to their potential applications as building blocks in conducting materials.

This discovery phase was driven by the distinctive redox and structural characteristics of these coordination compounds. In this period, research was emphasized on the metal-dithiolene complexes bearing the MS_2C_2 five-membered ring and much theoretical and experimental effort was made to understand their unique electronic structures relative to their conducting properties.[5]

A.1.3.1 Sulphur rich dithiolene as parent compounds of TTF derivatives.

TTF chemistry has played a major role in the development of synthetic metals, a domain which has emerged in the early 70's after the discovery of the conducting properties of TTF salts. These electronic properties result mainly from the combination of two features of the TTF core.

- The presence of sulfur in these molecules endows them considerable electron-donating properties. TTF, which is a nonaromatic 14 π-electron system, can be reversibly converted to an aromatic 12 π-electron system through two successive-oxidation steps (Scheme A-5).[15, 16]

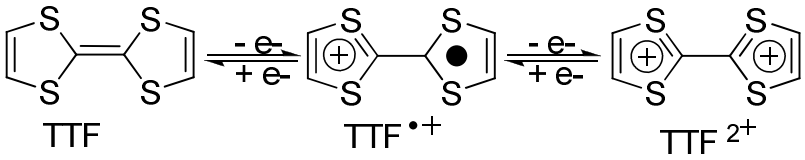

Scheme A-5. Reversible oxidations of TTF showing the formation of a radical cation ($TTF^{\bullet+}$) and the dication (TTF^{2+}) ($E^1_{1/2}$ and $E^2_{1/2}$ are first and second oxidation potential, respectively).

The relatively low oxidation potentials ($E^1_{1/2}$= +0.34 V and $E^2_{1/2}$= +0.73 V *vs.* Ag/AgCl in MeCN[16]) are tuneable by attachment of appropriate substituents (electron-withdrawing group or electron-donating group).

- The planarity and the presence of sulfur atoms on the periphery give rise to a solid state organization where both π•••π and S•••S intermolecular interactions are significantly predominant.

It should be outlined that the following criteria are at least required for the formation of conducting, molecular one-dimensional systems:[17, 18]

- (i) the stacking of planar molecules along one direction.
- (ii) an electronic content, orbital symmetry, and close packing allowing good overlap between stacked molecules.
- (iii) and the partial filling of the conduction band through either partial oxidation or partial electron transfer.

Square planar metal-dithiolene satisfy all the above mentioned conditions and were consequently implicated in materials science, especially after the synthesis of the DMIT ligand in a multigram scale reported by Hoyer *et al.* in 1975. Because of the presence of the C_2S_4 moiety, this ligand possesses a structural motif which approaches nearly that of TTF. The discovery in 1986 by Cassoux *et al.* of a superconducting molecular material, namely the $[TTF][Ni(DMIT)_2]$[19], combining TTF and dithiolene complex, marked a new event in this period. From that time, the number of publications dedicated to $[M(dithiolene)_2]^{2-}$ (where M is a d^8 transition metal and dithiolene ligand is dmit, dmid, mnt or dddt as represented in Scheme A-6), has considerably increased.[20, 21] The plethora of research in this field is well illustrated by two reviews from Olk *et al.* entirely devoted to DMIT systems.[18, 22]

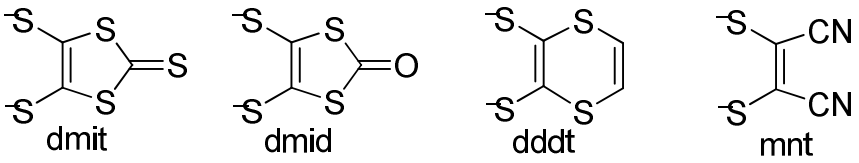

Scheme A-6: Some dithiolene ligands used in the preparation of $[M(dithiolene)_2]^{2-}$ complexes.

A.1.3.2 Recent development: state of the art

A.1.3.2.1 Multifunctional molecular materials

From this point of view, design and preparation of novel materials based on $Ni(dmit)_2$ complexes possessing conducting properties and Fe(III) compounds $(Fe(L)_2^+$ derivatives, where L= saElen[23] or qsal[24]) presenting spin crossover properties have been recently investigated. Faulmann *et al.*, reporting on $Ni(dmit)_2$ derivatives, investigated the possibility to synthesise a molecular system ($[Ni(dmit)_2]_5[Fe(salEen)_2]_2$, 6 CH_3CN), combining semiconducting behaviour from the $Ni(dmit)_2$ unit (in a partial oxidation state) and spin crossover properties from the $Fe(salEen)_2$ moiety.[23]

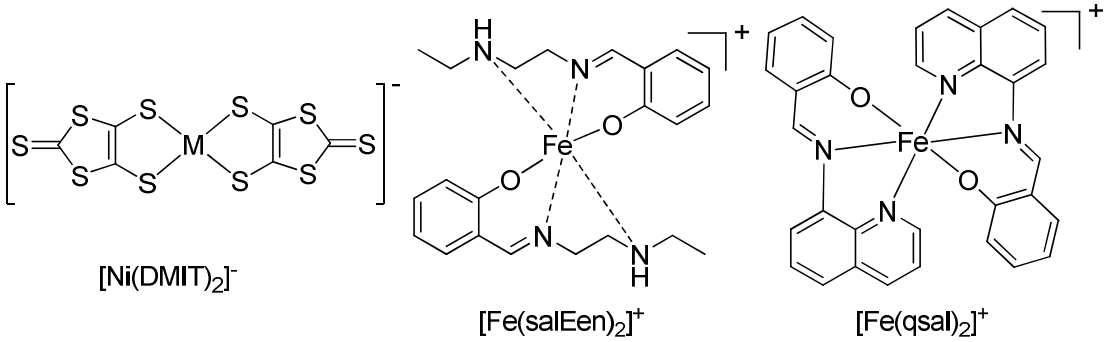

Figure A-2. $Ni(dmit)_2$ derivatives with different counter ions (based on Fe^{III} compounds) used by Faulmann *et al.* [23, 24]

Unfortunately, the electrical conductivity neighbouring the value of 0.12 $S.cm^{-1}$ at 295K is somewhat deceiving with regard to the crystal structure and the fractional oxidation sate of this compound.[23]

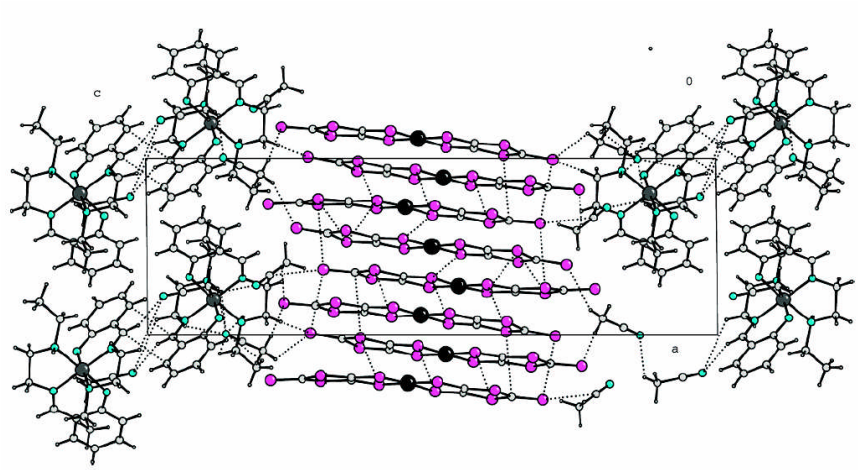

Figure A-3. Projection of ($[Ni(dmit)_2]_5[Fe(salEen)_2]_2$), $6CH_3CN$) along a axis (dotted lines represent short intermolecular contacts).[23]

T. Nakamura and T Akutagawa *et al.* have reported on the synthesis of (anilinium)([18-]crown-6)[$Ni(dmit)_2$] salt, in which a 180° flip-flop motion of the phenyl ring (from the anilinium group) and the rotation of the crown ether group were simultaneously observed in the solid state.[25, 26]

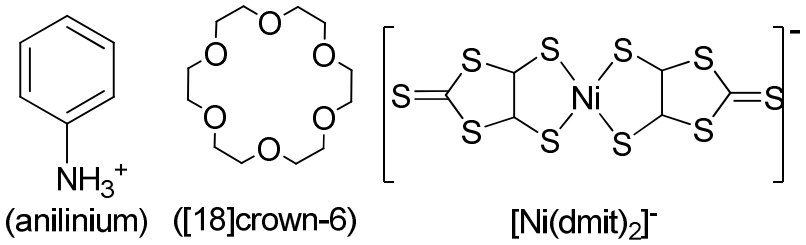

Scheme A-7 : The (anilinium)([18]crown-6)[$Ni(dmit)_2$] salt (of course the supramolecular cation is formed via hydrogen bonding between the ammonium protons and the oxygen of the crown ether)[25].

Development of such supramolecular systems of multimode molecular motions could be useful for dielectric applications, since these motions affect the dielectric response of the crystal.[25] A similar example is the supramolecular rotor based on the same (A^+)([18-]crown-6)[$Ni(dmit)_2$]$^-$ system, but with adamantylammonium as counter ion.[26] The last example on this $Ni(dmit)_2$ series, reported by J. P. Savy *et al.* shows superconductivity of TTF[$Ni(dmit)_2]_2$ films after deposition on silicon wafer substrates.[27]

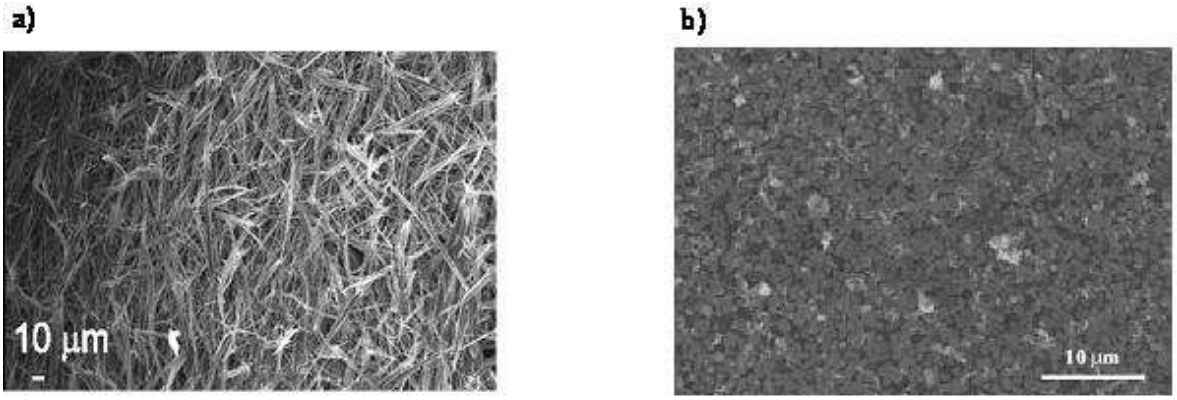

Figure A-4: SEM image of electrodeposited $TTF[Ni(dmit)_2]_2$ thin films deposited from a 3:1 TTF: $NBu4[Ni(dmit)_2]$ ratio in CH_3CN : -a) current density of 6.25 µA. cm^{-2} [27] , -b) current density of 1.5 µA. cm^{-2}. [28]

These fiber-like films (Figure A-4 a) obtained by improving the deposition conditions (current density of 6.25 µA. cm^{-2}) [27], during the electrochemical growth were found to be more resistive than the grain-like films (obtained with a current density of 1.5 µA. cm^{-2}).[28] The latter grain-like film develops cracks due to mechanical stresses at cryogenic temperature, and this has limited its utility for further studies.[27]

Recently, Fourmigué *et al.* reports on a heterobimetallic dithiolene complex composed of copper-dithiolene unit $[Cu(tfadt)_2]^{2-}$ and a nickel-cyclam unit $[Ni(cyclam)_2]^{2+}$ (Scheme A-8).[29]

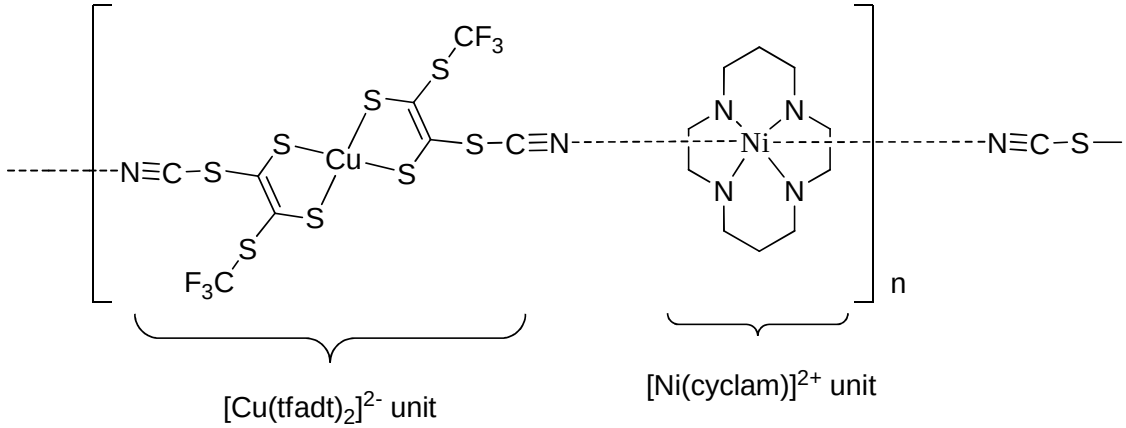

Scheme A-8 : A heterobimetallic complex in which the coordination of the $[Ni(cyclam)_2]^{2+}$ moieties through the nitrile substituents of the dithiolene complexes ($[Cu(tfadt)_2]^{2-}$) ensure the formation of chains.

In the chain-like structure obtained in this heterobimetallic system, the contacts are ensured through secondary coordination of the dithiolene ligand to the nickel metal center through C≡N•••Ni interactions. This material displays ferromagnetic interactions, resulting from the combination of the two units of different spin (S = 1/2 for $[Cu(tfadt)_2]^{2-}$ unit and S = 1 for the $[Ni(cyclam)_2]^{2+}$ unit) (see Scheme A-8).[29]

A.1.3.2.2 The case of metal-cyclopentadienyl dithiolene complexes

Mixed cyclopentadienyl/dithiolene complexes of general formula $[Cp_2M^{IV}(dithiolene)]$ (where M= Mo and W) have been introduced by Fourmigué *et al.* [30] A similar system, bearing *ansa*-metallocenes $Me_2C(\eta^5\text{-}C_5H_4)_2M(dmit)$, has been studied by Guyon *et al.* (Scheme A-9).[31]

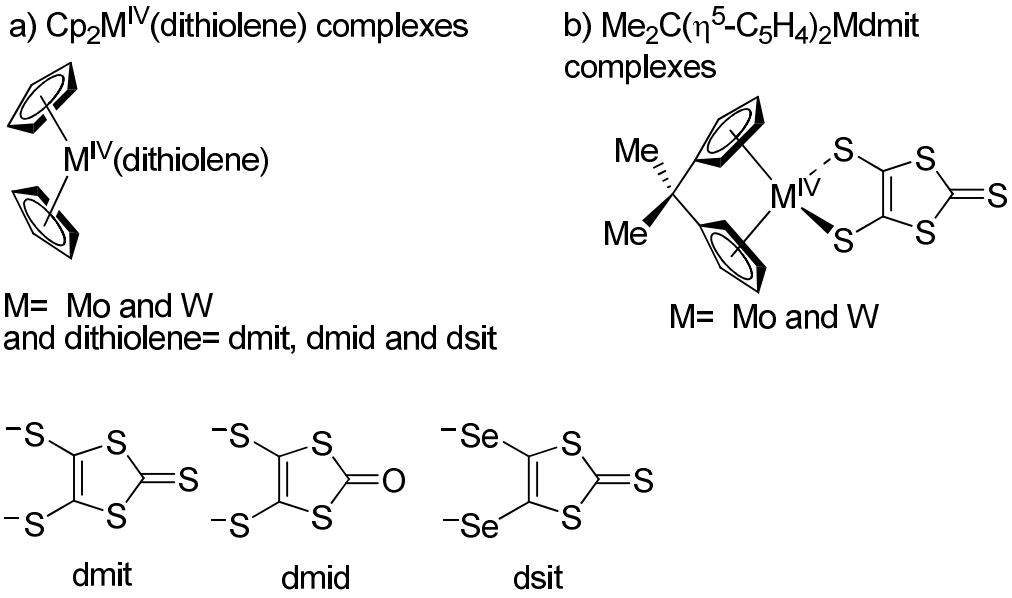

Scheme A-9: Cp_2(dithiolene) complexes reported by Fourmigué[30] and Guyon[31] *et al.*

These complexes were not only interesting for a structural point of view but were also studied for intermolecular interaction. Introducing a non planar, flexible ligand (Cp) avoids π-stacking but, on the other hand, has generated compounds with unique magnetic properties.[30, 31]

Note that heteroleptic cyclopentadienyl/dithiolene complexes of metal such as cobalt[32,33] or titanium[34] were also studied for their redox properties and, more

recently, metallocenes of the f elements have expanded this series by the synthesis of (COT)M(dithiolene) (M = U and COT=η- C_8H_8[35, 36]) and CpM(dithiolene) complexes (M= Ce and Nd).[37]

A.1.3.2.3 Sulfur rich neutral ligand and supramolecular chemistry

Dithiolene-like neutral ligands can be obtained via functionalisation of the dithiolene unit (DMIT in our case) by attaching suitable functional groups. Such a functionalisation is of great importance with regard to supramolecular chemistry. In fact the dithiolene-like neutral ligands combine, on the one hand, the coordination abilities of the DMIT unit and on the other hand, the chemistry of the attached functional group. For example, attaching an OH functional group will probably increase the dimensionality of the system via hydrogen bonding.

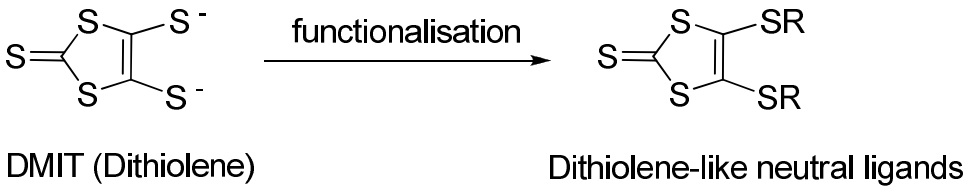

Scheme A-10 : Dithiolene-like neutral ligands obtained by functionalisation of the DMIT unit.

Dithiolene-like neutral ligands form dative coordination bonds rather than covalent bonds. Contrary to the ionic dithiolene ligand, dithiolene-like neutral ligands are quite recent in dithiolene chemistry. They have been introduced because of their various coordination sites and their delocalised π system. An example of such dithiolene-like neutral ligands containing a pyridyl moiety is reported by Noh *et al.* [38] His group investigated the possibility for such ligands to coordinate to a metal center either through coordination via the DMIT skeleton, the nitrogen atom of the pyridyl group or a combination of both.[38]

These systems are also able to generate π–π interactions and Van der Waals S•••S interactions. In addition to π–π and Van der Waals S•••S interactions, supramolecular assemblies can be generated by attaching a functional group at the sulfur atoms. In fact, depending on the functional group, the dimensionality of the system can be increased. They can be coordinated to a metal in a chelating way, a monodentate way or a combination of both.[38] Their electrochemistry is however not well

investigated. Referring to the HSAB principle, such ligands (anionic and neutral) are classified as soft ligands. But their coordination chemistry is not only limited to complexes containing soft metals.

A.1.4 General pathways for the synthesis of sulfur rich ligands

A.1.4.1 Synthesis of the DMIT skeleton

Numerous pathways to synthesise sulfur-based ligands are known.[39] For example, Scheme A-11 resumes various pathways allowing the synthesis of DMIT.

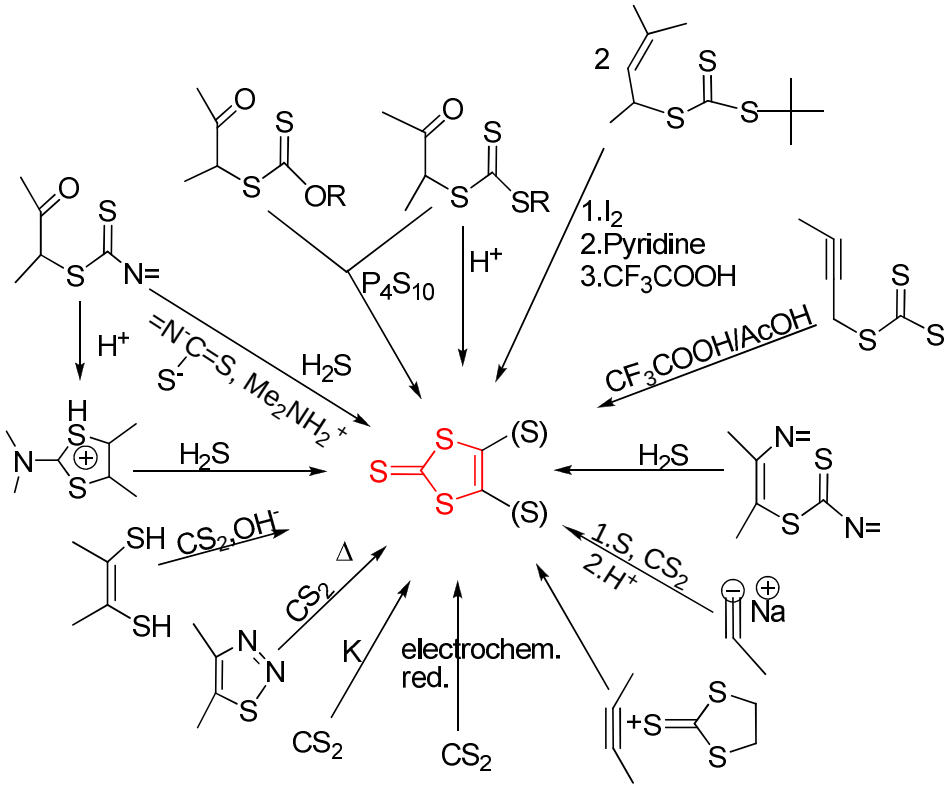

Scheme A-11: Synthetic pathways for dimercaptoisotrithione (DMIT).[39]

All these various synthetical pathways are well established and require one or more steps to isolate the desired product. One of the most efficient method originates from Hoyer's group, which found that DMIT can be conveniently isolated in a multigrame scale as quaternary ammonium salts of $[Zn(DMIT)]^{2-}$.[40] Bryce *et al.* have further improved this method allowing the isolation of $[Zn(DMIT)_2(Et_4N)_2]$ in a 90 g scale.[41] The route developed by Bryce *et al.* used the same reagents but with less sodium

than in the conventional method of Hoyer *et al.* Note that a 70 g scale was also obtained by Becher *et al.* using the same reagents.[42]

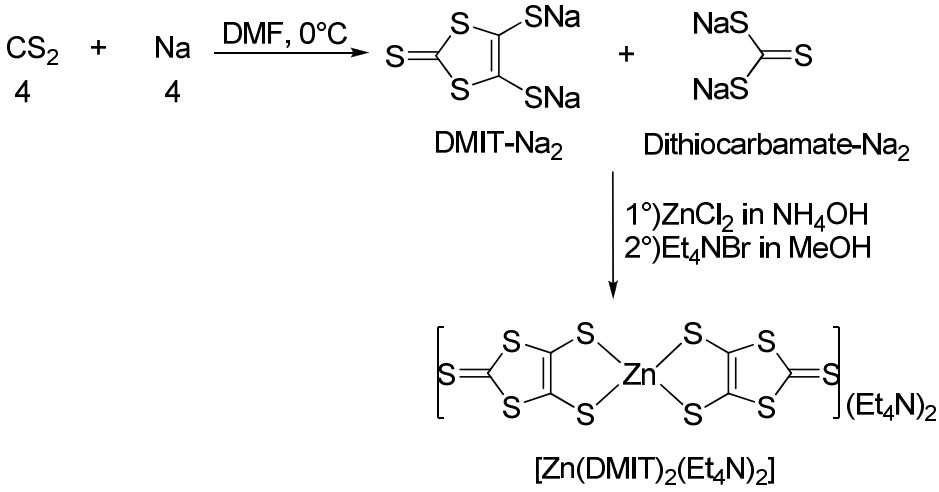

Scheme A-12: Pathway for the synthesis of DMIT isolated as a zinc complex.

DMIT itself as alkali metal salt is not very stable, but in its zinc complex form, it can be isolated and stored under air for several months.[42, 43] This represents the main advantage of this method. Reduction of CS_2 by sodium produces DMIT ($C_3S_5^{2-}$) and dithiocarbamate (CS_3^{2-}) in equimolar proportions.[40] This reduction can be also achieved electrochemically leading to the same products ($C_3S_5^{2-}$ and CS_3^{2-}).[39]
The separation of DMIT ($C_3S_5^{2-}$) from the dithiocarbamate (CS_3^{2-}) is not easy but direct alkylation after reduction allows this separation.[39] In practice, separation of the two anions is readily achieved by treating the mixture with an aqueous solution of $ZnCl_2$, which selectively complexes the DMIT anion, leading to the formation of a zinc chelate which can precipitate as **$[Zn(DMIT)_2](Et_4N)_2$** by addition of NEt_4Br (see Scheme A-12).

A.1.4.2 Functionalisation of the DMIT moiety: the key to supramolecular chemistry.

Of course, research on DMIT-containing compounds has not only been revisited in order to improve their electronic (conducting) properties. The functionalisation of these sulfur electron-rich compounds has also played a central role in their novel application as building block in supramolecular chemistry.[44] This includes the

synthesis and characterisation of DMIT derivatives bearing acid [45, 46], alcohol [47-49], amide[50-52] and pyridine[38] functional groups etc. (Scheme A-13)

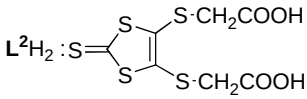

[4,5-bis(carboxymethylthio)-1,3-dithiole-2-thione]

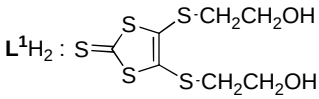

[4,5-bis(2-hydroxyethylthio)-1,3-dithiole-2-thione]

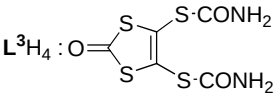

[4,5-diamido-1,3-dithiole-2-one]

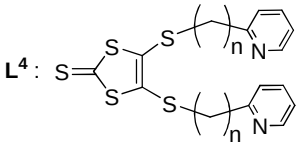

[4,5-bis(pyridil-n-alkylthio)-1,3-dithiole-2-thione]

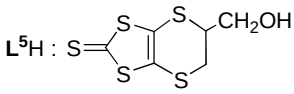

[4,5-(1-Hydroxypropane-2,3-diyldithio)-1,3-dithiole-2-thione]

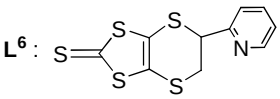

[4,5-(2-pyridyl-ethylendithio)-1,3-dithiole-2-thione]

Scheme A-13: Different types of DMIT-based ligands bearing functional groups.

Such functional groups are of crucial importance since they could introduce additional non-covalent interactions (H-bonding interactions for example) and allowing therefore the assembly of supramolecular systems via increase of dimensionality. This kind of interaction is a basic key in the field of crystal engineering.[53, 54] Hydrogen bonding for example is known to participate in the supramolecular organization via increase of dimensionality. When such ligands bearing functional groups react with metal ions, a self-assembling process often takes place and supramolecular structures are generated. It should be pointed out that the reactivity of such ligands towards metal ions should not involve the cleavage (presence of strong base) of such functional groups since they are a driving force in the supramolecular assembly.

Most of the dithiolene-like neutral ligands can be obtained starting from the DMIT ligand by nucleophilic substitution. In some case, the reaction is effective from the zinc complex **[Zn(DMIT)$_2$(Et$_4$N)$_2$]** as starting material (Route A), while in others cases regeneration of DMIT ligand from the neutral benzoyl-ligand (**DMITCOPh**) (Route B) is a suitable way to access to dithiolene-like neutral ligands (see Scheme A-14).

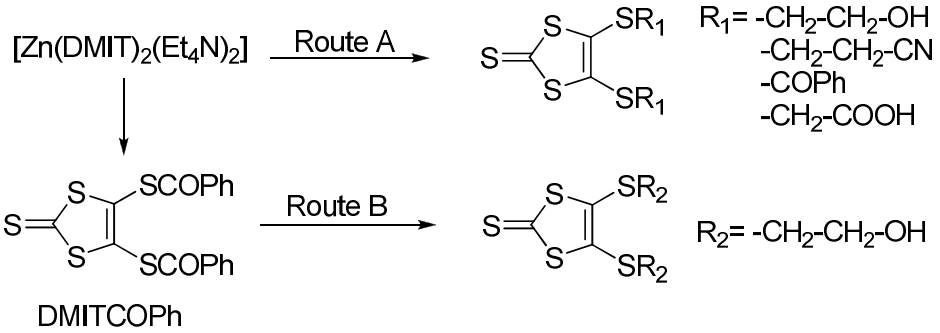

Scheme A-14: Example of functionalisation pathway starting from DMIT unit.

Other derivatives can be obtained by means of classical organic chemistry, mainly a Diels-Alder reaction, starting from the **trithione** (C_3S_5) which is a reduced form of **DMIT** ($C_3S_5^{2-}$) and a suitable functional olefin (see Scheme A-15).

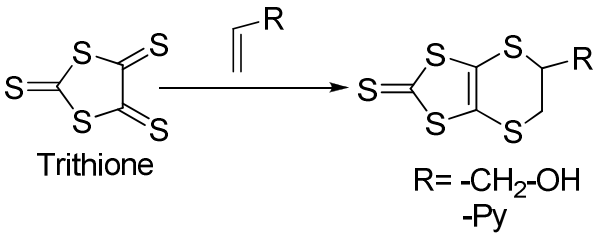

Scheme A-15: Example of ligand´s functionalisation starting from the trithione (a reductive form of DMIT).

Some reports deal with attaching electron-withdrawing groups (CN and CF_3) to the dithiolene unit. This investigation has been motivated by studying the influence of such groups on the stabilization of the radical anion $[Ni(S_2C_2RR´)_2]^{\bullet-}$ (where R=CN and R´=CF_3), since the parent radical anion $[Ni(S_2C_2R_2)_2]^{\bullet-}$ shows tendency to reduce to the diamagnetic dianion $[Ni(S_2C_2R_2)_2]^{2-}$ (where R=CN).[55]

A.1.5 Aim of this work

Since the pioneering research in dithiolene chemistry was essentially orientated in the use of DMIT-derivatives as potential building blocks for TTF derivatives or for the elaboration of conducting molecular materials, the DMIT-compounds have been investigated to a lesser extend for supramolecular purposes.

For this reason, we will report in chapter B on the supramolecular chemistry of dithiolene-like neutral ligands such as **L_0**, **L^1H_2** and **L^2H_2** (bearing potential hydrogen bonding donors or acceptors) while, chapter C will be entirely devoted to the use of such functionalized ligands to elaborate metallo-supramolecular coordination systems. Their photophysical properties will be discussed as well.
Since most of this coordination chemistry is dominated by transition metal dithiolene complexes of the d elements, chapter D will focus on an almost unexplored field combining lanthanide and dithiolene-like neutral ligands. Therefore, the second part of this introduction presents an overview on lanthanide chemistry.

A.2 Lanthanides

A.2.1 Generalities

Lanthanides are localised at the 6th period of the periodical table of the elements.

Table A-1. Electronic configuration of the lanthanides and their common ions [56].

	Atomic	Ln^{3+}	Ln^{2+}	Ln^{4+}
La	[Xe] $5d^1$ $6s^2$	[Xe]		
Ce	[Xe] $5d^1$ $6s^2$ $4f^1$	[Xe] $4f^1$		[Xe]
Pr	[Xe] $6s^2$ $4f^3$	[Xe] $4f^2$		[Xe] $4f^1$
Nd	[Xe] $6s^2$ $4f^4$	[Xe] $4f^3$	[Xe] $4f^4$	[Xe] $4f^2$
Pm	[Xe] $6s^2$ $4f^5$	[Xe] $4f^4$		
Sm	[Xe] $6s^2$ $4f^6$	[Xe] $4f^5$	[Xe] $4f^6$	
Eu	[Xe] $6s^2$ $4f^7$	[Xe] $4f^6$	[Xe] $4f^7$	
Gd	[Xe] $6s^2$ $4f^7$ $5d^1$	[Xe] $4f^7$		
Tb	[Xe] $6s^2$ $4f^9$	[Xe] $4f^8$		[Xe] $4f^7$
Dy	[Xe] $6s^2$ $4f^{10}$	[Xe] $4f^9$	[Xe] $4f^{10}$	[Xe] $4f^8$
Ho	[Xe] $6s^2$ $4f^{11}$	[Xe] $4f^{10}$		
Er	[Xe] $6s^2$ $4f^{12}$	[Xe] $4f^{11}$		
Tm	[Xe] $6s^2$ $4f^{13}$	[Xe] $4f^{12}$	[Xe] $4f^{13}$	
Yb	[Xe] $6s^2$ $4f^{14}$	[Xe] $4f^{13}$	[Xe] $4f^{14}$	
Lu	[Xe] $6s^2$ $4f^{14}$ $5d^1$	[Xe] $4f^{14}$		
Y	[Xe] $5s^2$ $4d^1$	[Kr]		

In this period of the periodical table, the 4f orbitals are gradually filled corresponding to the electronic configuration [Xe] $6s^2 5d^1 4f^n$ (n= 1, 2, 3…..14) (Table A-1).

Their most common oxidation state is +3, giving an electronic configuration where only the f orbitals are filled, the 6s and 5d orbital being empty. However, other oxidation states like +4 and +2 are observed for some of them (see Table A-1).

A.2.2 Comparison of f block with d and s block

Table A-2 presents a comparison of characteristic features between f, d, and s-block metals.

Table A-2. Comparison of 4f, 3d and Group I metals.[56]

	4f	3d	Group I
Electron configurations of ions	Variable	Variable	Noble gas
Stable oxidation states	Usually +3	Variable	1
Coordination numbers in complexes	Commonly 8–10	Usually 6	Often 4–6
Coordination polyhedra in complexes	Minimise repulsion	Directional	Minimise repulsion
Trends in coordination numbers	Often constant in block	Often constant in block	Increase down group
Donor atoms in complexes	'Hard' preferred	'Hard' and 'soft'	'Hard' preferred
Hydration energy	High	Usually moderate	Low
Ligand exchange reactions	Usually fast	Fast and slow	Fast
Magnetic properties of ions	Independent of environment	Depends on environment and ligand field	None
Electronic spectra of ions	Sharp lines	Broad lines	None
Crystal field effects in complexes	Weak	Strong	None
Organometallic compounds	Usually ionic, some with covalent character	Covalently bonded	Ionically bonded
Organometallics in low oxidation states	Few	Common	None
Multiply bonded atoms in complexes	None	Common	None

Reactivity and properties of lanthanides are different from those of the d-block metals.[56] Lanthanides present in coordination chemistry general features which are outlined in the following paragraph:

- A very wide range of coordination numbers (generally 6-12, but also low numbers of 2,3 or 4 are known).
- Coordination geometries are determined by steric factors of the ligand rather than crystal field effects.

- They often form labile 'ionic' complexes that undergo facile exchange of ligands.
- The 4f orbitals in the Ln^{3+} ion do not participate directly in bonding, being well shielded by $5s^2$ and $5p^6$ orbitals. Their spectroscopic and magnetic properties are thus largely uninfluenced by the ligand.
- Small crystal-field splitting and very sharp electronic spectra (in comparison with the d-block metals) are observed.
- They prefer anionic ligands with donor atoms of rather high electronegativity (O, F). Lanthanides are classified as hard according to the HSAB principle.
- They readily form hydrated complexes (on account to the high hydration energy of the small Ln^{3+} ion) and this can cause uncertainty in assigning coordination numbers.
- Their insoluble hydroxide precipitates at neutral pH unless presence of complexing agents.
- The chemistry is largely that of one (3+) oxidation state (certainly in aqueous solution).
- They do not form Ln=O or Ln≡N multiple bonds of the type known for many transition metals and certain actinides.
- Unlike transitions metals, they do not form stable carbonyls and have (virtually) no chemistry in the 0 oxidation state.

Figure A-5 is a schematic representation of the f orbitals.

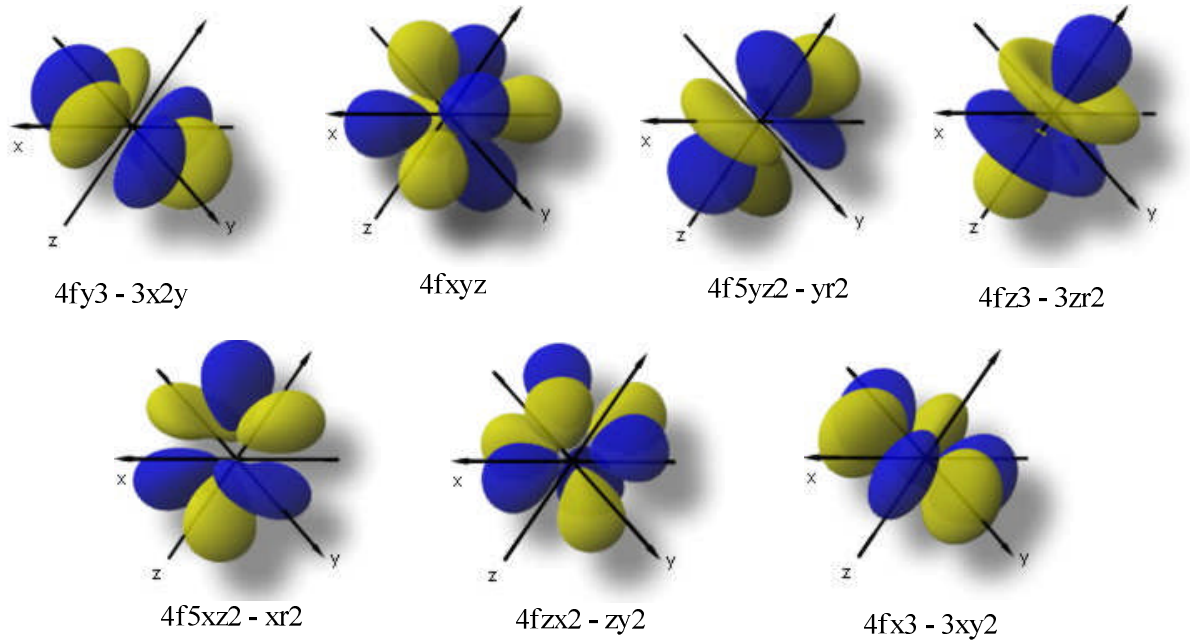

Figure A-5: Schematic representation of the f orbitals[57].

Another effect observed in lanthanides is the contraction of their radius, because 4f electrons are inside the 5s and 5p sub-shell and possess a core-like character (see Figure A-6).[58] The decrease in both atomic and ionic radii is more marked at the beginning of the serie. As the result of this contraction, f electrons are shielded from the ligand, thus taking no part in the bonding, and having spectroscopic and magnetic properties almost independent from the environment.

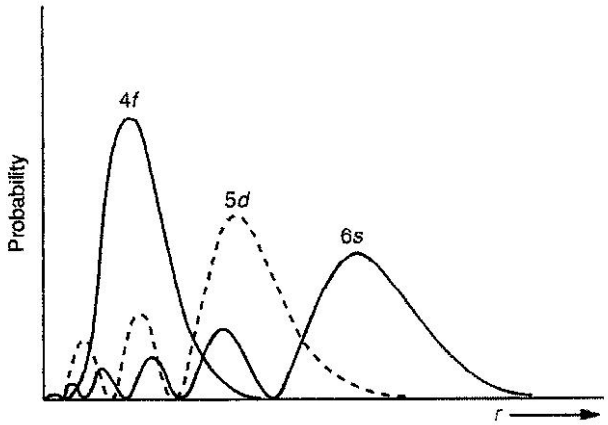

Figure A-6: The radial part of the hydrogenic wave function for 4f, 5d and 6s orbitals of cerium[56, 59].

A.2.3 Coordination chemistry of lanthanides

Lanthanide's coordination chemistry has only been developed in the 60´s. This is a result of their later discovery, but also by the fact that their chemistry is not comparable to that of the d-block metals.

A.2.3.1 Coordination number in lanthanides complexes

For lanthanide ions, it was often assumed that six-coordinated complexes are generally obtained, but various other coordination numbers (CN: 3, 4, …, 12) have been encountered.[60] The coordination number is generally determined by how many ligands can be packed around the metal center. For example, the aqua ions in $[Ln(H_2O)_n]^{3+}$ are stabilised by coordination numbers ranging between 8 and 9.[61]

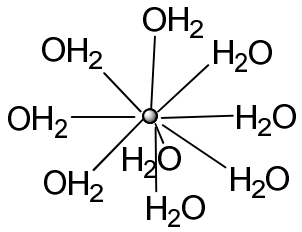

Figure A-7: The structure of the nonaaqualanthanide ion ($[Ln(H_2O)_9]^+$)[56].

The 8-coordinate species adopt a square antiprismatic coordination while the 9-coordinate species are tricapped trigonal prismatic.[56]

A.2.3.2 First and second order effect

Other features, related to this coordination numbers, are the first- and second-order effects. When small ligands (H_2O) are bound to the metal, the coordination number is controlled by the repulsion between the donor atoms directly bound to the metal (first order effect). Whereas, for bulky ligands such as [-$N(SiMe_3)_2$], steric effects generating crowding around the metal shields this later from other ligands (second order effect).[56, 60] Examples of $Ln[N(SiMe_3)_2]_3$ seems to be surprising, since these three-coordinated environment should be unstable. However, if we have a look on the solid-state structure, we can notice that a trigonal pyramidal geometry is obtained instead of the expected trigonal planar one. This low CN can be rationalized by formation of agostic interactions.

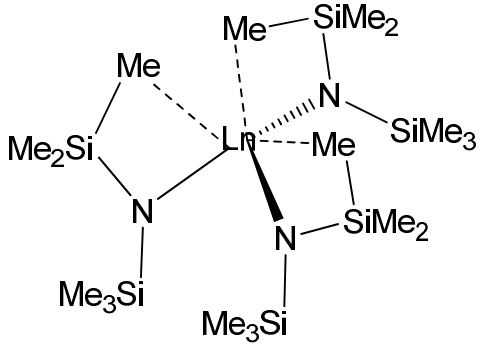

Figure A-8: Solid state structure of $Ln[N(SiMe_3)_2]_3$ (agostic interactions are shown in dotted lines).[56]

The Ln-N angles are 114° rather than 120° expected for a planar structure[56] . This is due to "agostic interactions"[56, 60] between the methyl groups and the lanthanide center (see Figure A-8), participating on the stabilisation of the lanthanide center by

contributing on the high coordination number requirements. $Ln[N(SiMe_3)_2]_3$ compounds are obviously planar in solution.[61]

A.2.4 Properties of the Ln^{3+} Ions

Because of their core-like character, the 4f orbitals cannot overlap with ligands orbitals and therefore do not participate in bonding. As a consequence, lanthanides possess magnetic and spectroscopic properties independent from the environment (surrounding ligands). Among the general properties of Lanthanides, we will only focus on the luminescence as being our field of interest.

A.2.4.1 Spectroscopic properties of the Ln^{3+} Ions

The spectroscopic properties of the lanthanides can be explained using the Russell-Saunders coupling scheme. According to this model, the electron spins are coupled together separately from the coupling of the orbital angular momenta of the electrons, and the orbital moment is unquenched.[56]

-The spins of individual electrons labelled as (s) are coupled together to give the total spin quantum for the ion labelled as (S).

-The orbital angular momenta labelled (l) is similarly coupled to give the total orbital angular momentum quantum number (L).

-Spin-orbit coupling, between L and S, gives rise to the quantum number (J), which can have values of (L+S), (L+S)-1, …., IL-SI.

Therefore a full level symbol of an ion can be written as $^{2S+1}L_J$. The ground term and levels for free ions can be obtained using Hund`s rules:

- Term with highest S lies lowest.
- If there are several terms with the same S, the one with the highest L lies lowest.

-For a shell less than half-filled, J takes the lowest value for the ground state.

-For a shell more than half-filled, J takes the highest value for the ground state.

Table A-3 shows the historical key used for labelling L.

Table A-3 : State symbols for different values of L.

L=	0	1	2	3	4	5	6	...
State symbol	S	P	D	F	G	H	I	...

An example of determination of spectroscopic terms using this model is illustrated in the case of Nd^{3+} ion, which is represented as (Nd^{3+}: [Xe] $4f^3$).
For f-electrons, l = 3 so m_l can take the following values m_l = 3, 2, 1, 0,-1,-2,-3. Electrons have s = 1/2 so m_s presents values of +1/2 (up spin) or -1/2 (down spin).
According to Hund´s rules the arrangement displayed in Table A-4 will be obtained for an f^3 configuration system:

Table A-4 : Spin orientation in an f^3 configuration.

			m_l			
3	2	1	0	-1	-2	-3
↑	↑	↑				

This arrangement allows the determination of S, L, and J values as well as the term symbol ($^{2S+1}L_J$) describing the ground and excited states.

- For **S**: s =1/2 S = 1/2+1/2+1/2= 3/2.
- For **L**: m_l take the value 3,2 and 1, so L = 3+2+1= 6; L= 6 correspond to the label I.
- For **J**: L = 6 and S = 3/2; J = (L+S), (L+S)-1, …., J= 15/2, 13/2, 11/2, 9/2.

The ground state will be defined by the lowest J value as the shell is less than half filled, *i.e.* J= 9/2 for Nd^{3+}.

In summary for Nd^{3+}:
S=3/2, L=6 (label= I), J=9/2; then the ground state level corresponds to $^4\mathbf{I_{9/2}}$.

An energy level diagram (Figure A-9) for all the trivalent lanthanide ions (based on lanthanide halides) has been established, following the above theoretical predictions, coupled with experimental results.[56, 62] Such an energy diagram is a result of tabulated data from Carnall, Fields and Rajnak.[63-66] This energy diagram, usually called “Dieke diagram” by researchers in this field of spectroscopy, is an important tool for understanding and interpreting the luminescence spectra of lanthanides. The

first diagram showing energy levels from 0 to 42000 cm^{-1} reported by Dieke and Crosswhite[67], became a reference for spectroscopists. This was recently extended to 70000 cm^{-1} by Wegh *et al.* using a $LiYF_4$ matrix.[68]

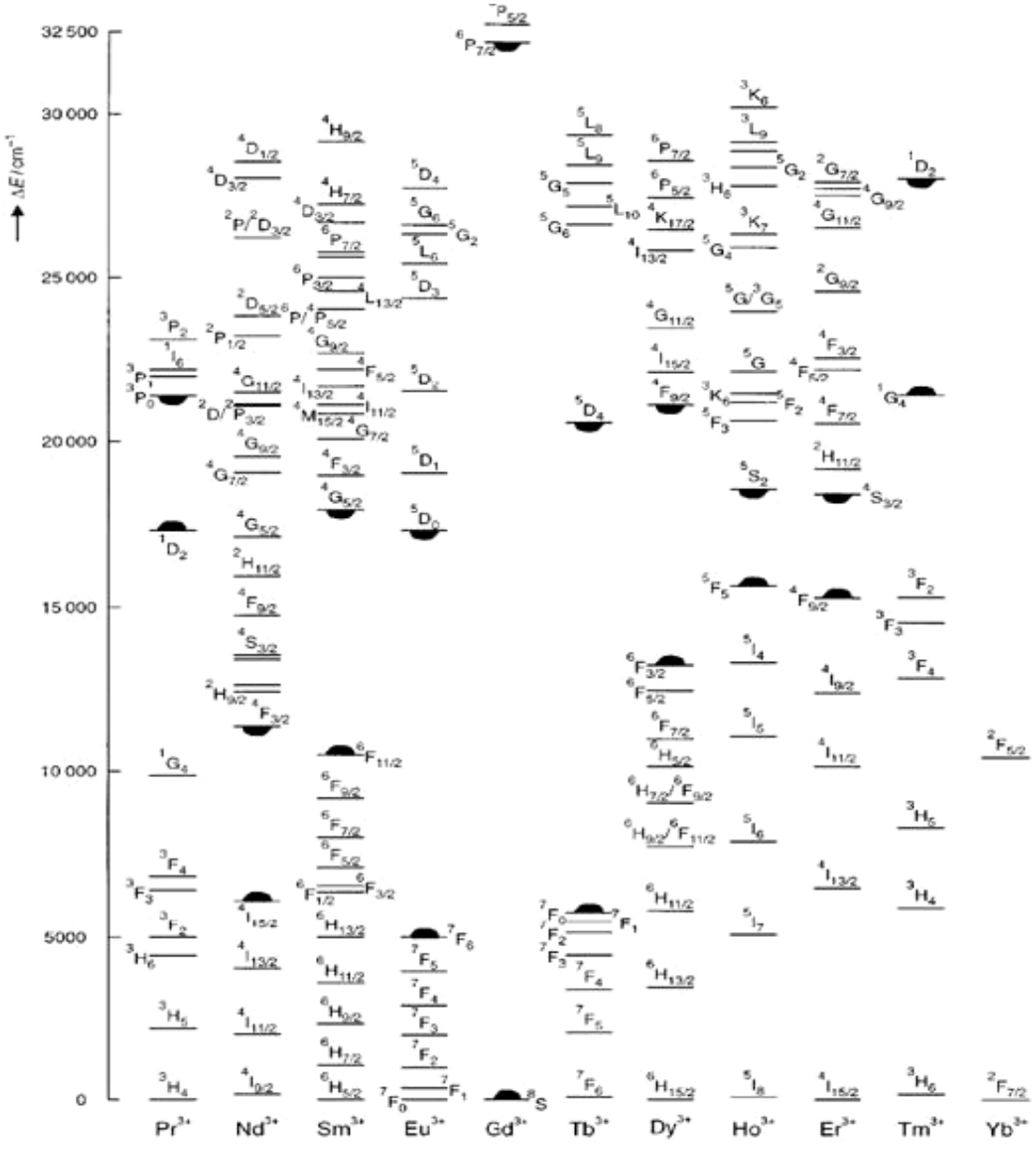

Figure A-9: Energy diagram of the 4f energy levels responsible for the lanthanide's luminescence.[61]

(◓ represent the highest non-luminescent level; ◒ represent the lowest luminescent level).

This diagram is the equivalent of the "Tanabe-Sugabo" diagram for helping the prediction of transitions in d-block transition metals. The d-d transitions as well as f-f transitions are "Laporte forbidden". However, an important difference must be taken into consideration: for the lanthanides, the contribution of the spin-orbit coupling (L-S) is more important than the crystal field contribution, and inversely the contribution of

the crystal filed effect is more important than that of spin orbit coupling in d-block metals. This observation reflects the inner nature of the f orbitals which are sufficiently shielded from the surrounding ligands, and “feel” therefore, no significant effect from these ligands.

A.2.4.2 Luminescence properties of the Ln^{3+} Ions

Luminescence is the response (in form of a radiation or light) of a system which has primarily absorbed energy from a suitable source. The excitation energy may be electromagnetic (X-ray, ultraviolet, Vis- or IR photons), a beam of electrons, heat, electricity, mechanical energy, or energy released by a chemical or biochemical reaction.[69]

Some definitions (underlined below) need to be considered before speaking about luminescence:

-***fluorescence***: is the emission of light from a singlet excited state to the ground state; and a fluorescence lifetime is in the range of nanoseconds (around 10 ns: $10*10^{-9}$ s).

-***phosphorescence***: is the emission of light from a triplet excited state to the ground state; and a fluorescence lifetime range between milliseconds (ms) to seconds (s).

-***lifetime (τ):*** is the reciprocal of radiative rate constants of the transition generating fluorescence or phosphorescence; and represents the average time between excitation and return to the ground state.

-***energy transfer*** (ET): is a process by which an excited sample transfers its excitation energy to an acceptor molecule (lanthanide for example) during the lifetime of the excited state.

-***quenching***: is the partial or total inhibition of luminescence due to the interaction between the luminescent sample and other molecules or ions; it can be static or dynamic.

-***quantum yield*** (Φ): is the ratio of the number of emitted luminescence photons to the number of absorbed photons.

In the case of lanthanide-containing molecular system it is noteworthy to distinguish between overall quantum yield and intrinsic quantum yield. Both are actually related through an equation which will be given in chapter D (Equation D.1).

Regarding IUPAC rules, emission process without spin change will be described as "fluorescence" while that involving a spin change will be described as "phosphorescence".[70] Therefore, we will have fluorescence for Pr^{3+}, Nd^{3+}, Ho^{3+}, Er^{3+} and Yb^{3+} ions, and phosphorescence for Sm^{3+}, Eu^{3+}, Gd^{3+}, Tb^{3+}, and Dy^{3+} ions. Pr^{3+} presents also phosphorescence ($^3P_0 \rightarrow {}^3H_J$).

Prior to emission, the emitting system should absorb energy to populate its excited states. Many lanthanides ions exhibit luminescence characterised by sharp lines due to the f-f transitions within the Ln^{3+} ion. However, they possess low absorption coefficient and consequently a direct excitation is unfavourable. This can be overcome by three possible ways showed in the following scheme (see Scheme A-16).[71]

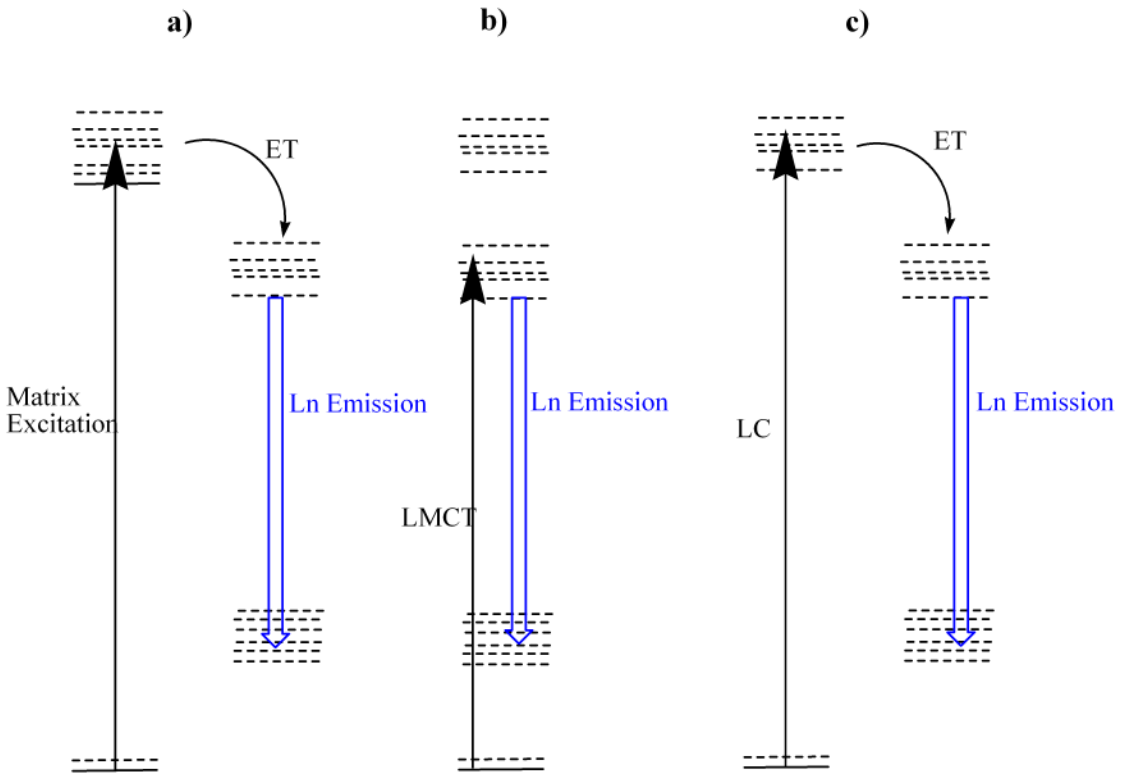

Scheme A-16: Three Pathways to efficient lanthanide luminescence (ET: energy transfer; Ln Emission: lanthanide emission; LMCT: ligand-to-metal charge transfer absorption; LC: ligand centered absorption.[71]

Pathway **a**) is a matrix excitation followed by energy transfer to the lanthanide ion. It proceeds by an excitation above the band gap of a metal oxide matrix (TiO_2, ZrO_2, Al_2O_3 etc…) or zeolithe containing lanthanide ion then through energy transfer to the lanthanide ion leading to emission of this latter.[71] The Eu^{3+} -TiO_2 system shows an intense emission when excited above the band gap while excitation below this band-gap shows weak luminescence.[72]

*Pathway **b**)* is a ligand-to-metal charge transfer which can lead to population of the lanthanide excited states followed by luminescence of this lanthanide center.

*Pathway **c**)* is a ligand-centered absorption followed by an energy transfer to the lanthanide ion which finally luminesces. In this process, the luminescence is enhanced considerably by attaching a suitable organic ligand to the lanthanide.

Scheme A-17 shows the luminescence's process in lanthanide complexes containing a suitable organic ligand able to luminesce. This process corresponds to the pathway **c**) in the Scheme A-16. Here, it describes the real phenomenon taking place as well as the possible deactivation process which have not been shown in Scheme A-16 (pathway **c**)).

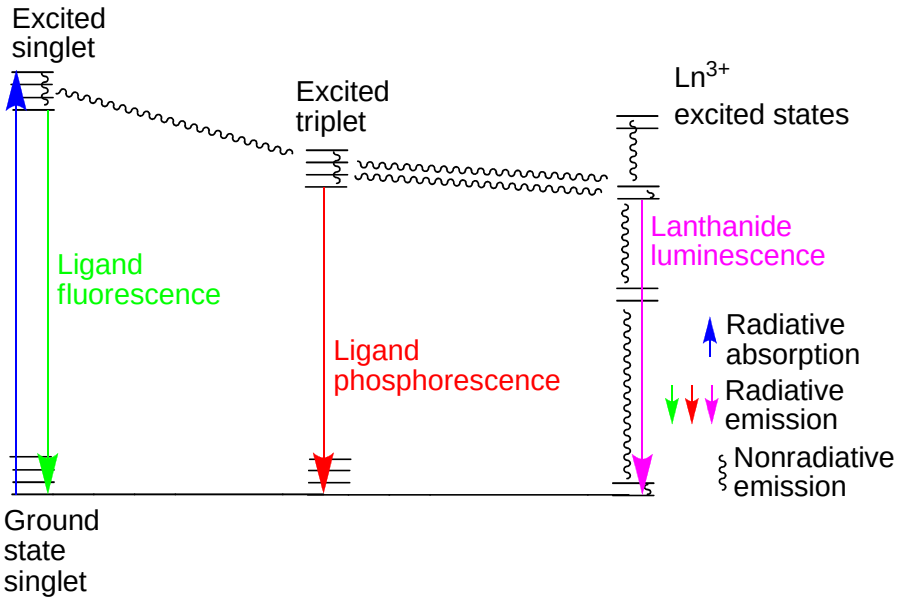

Scheme A-17. Luminescence in lanthanide complexes.[56]

A.2.5 Application of lanthanide's chemistry

Compared to usual luminescent organic dyes, rare earth ions exhibit very sharp emission bands giving rise to a precise color. Lanthanide-containing materials offer emission colors over the whole spectral range from visible (red for Eu^{3+}, Pr^{3+}, Sm^{3+}; green for Er^{3+}, Tb^{3+}; and blue for Tm^{3+}, Ce^{3+}) to NIR (Nd^{3+}, Er^{3+}). For example, Figure A-11, shows an emission spectrum of a fluorescent lamp using $BaMgAl_{10}O_{17}$:Eu, (Ce, Gd, Tb)MgB_5O_{10} and Y_2O_3:Eu.[73, 74] In most of the novel optical materials, like full color glass, the three primary light colors (red, green and blue) are produced only by f–f lanthanide emissions.

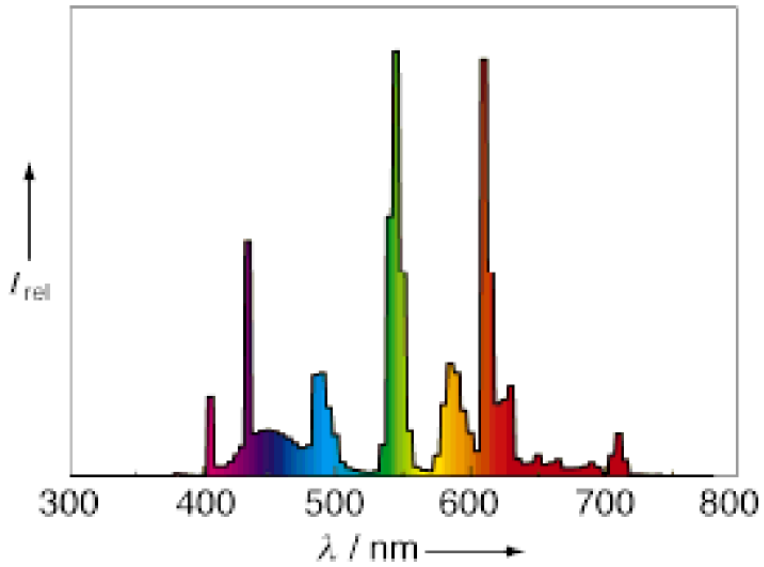

Figure A-10: Emission spectrum of a tricolour fluorescent lamp[73].

Applications of lanthanides cover both the domains of material science and life science.[73] They are used in: (i) lighting industry (lamp phosphors), (ii) the conception of organic light emitting diodes (OLED), (iii) optical amplification (telecommunication), (iv) laser technology, (v) biology, (vi) medicine (medical imaging).

Research in lanthanides has gained in interest because of their unique optical properties which were found as a challenging approach for new optoelectronic devices. Er^{3+} and Pr^{3+} with their emission at ca.1550 nm and 1330 nm respectively, are suitable for telecommunication. In fact, they match well the ´window of transparency, in which, silica used in optical-fiber for data transmission, is transparent. Their emission lines are also called "telecom line"; other lines from Nd^{3+} (1330 nm) and Sm^{3+} (1280-1340 nm) are also within this group.[75]

Another important application concerns lasers. The most common laser is the Nd: YAG laser which can be used as light source for spectroscopy purposes. It is based on the 1064 nm transition of the Nd^{3+}, and is described as a four-level Nd^{3+} laser.[61]
A lamp is used to pump the system to ensure that an excess of Nd^{3+} ions is in an excited state ($^4F_{5/2}$ or $^4F_{7/2}$) so that more ions can emit electrons than can absorb; these excited ions decay rapidly (or cascade), to the long-lifetime $^4F_{3/2}$ state non radiatively, so that a high proportion of Nd^{3+} ions are in this state rather than the ground state, it result in a population inversion (more details can be found in the ref 61).

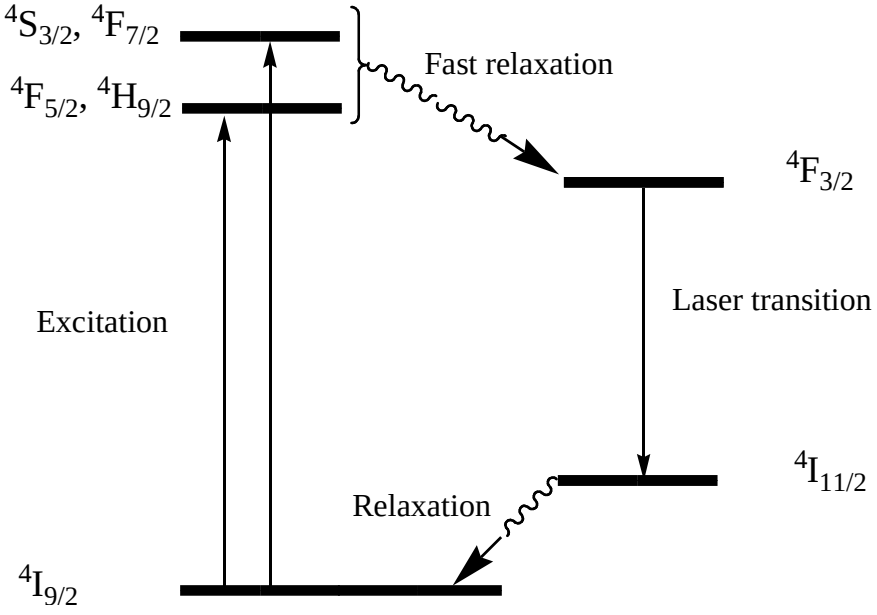

Scheme A-18: Scheme of a four-level Nd^{3+} laser.[61]

Others lines from Er^{3+} (1700 and 2700 nm) are also used as laser line.[75]
For application in life sciences, most of the NIR emitting lanthanides have been investigated because of the transparency of biological tissues above the 1000 nm. Another example used for medical applications is the $^5I_7 \rightarrow {}^5I_8$ transition (2100 nm) of the Holmium ion which has been used in laser surgery.[75]

CHAPTER B. FUNCTIONALISATION OF DITHIOLENE LIGANDS: ROUTE TO SUPRAMOLECULAR CHEMISTRY.

B Synthesis of Dithiolene Ligands

To evaluate and to understand the supramolecular chemistry of dithiolene ligands, we have first to design the ligands. Amongst the large group of dithiolene compounds, those containing the 1,3-dithiole-2-thione unit are of great efficiency since they are known for generating stacking via π–π interactions. They can also introduce S•••S intra- or inter-molecular interactions since the large sulfur atomic orbitals are able to promote effective intermolecular overlap. And finally, they are functionalisable and are potentially good precursors for TTF-derivatives.[76]

B.1 Choice of the ligands

Dithiolene ligands, that we have synthesised here, are typically neutral DMIT derivatives, which are functionalised without modifying the DMIT core (five-ring arrangement). Depending on the attached functional group, additional non-covalent interactions can be generated. Furthermore, by use of hydrogen bonding donor or acceptor groups such as alcohols, carboxylic acids, amines etc. non-covalent interactions may be generated. Hydrogen bonding is one of the famous key interactions for the process of molecular aggregation and recognition in nature.[77]

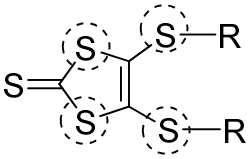

a) S atoms that may be engaged in S...S interactions

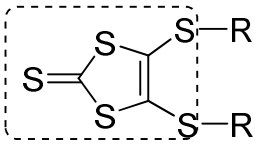

b) Planar DMIT moiety can generate π–π interactions

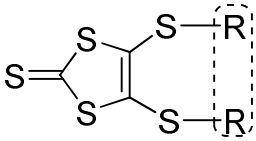

c) If R contain a OH functional headgroup, hydrogen bonding is possible (intra- and inter-molecular interactions).

Scheme B-1: Different interactions sites (- - -) in dithiolene-like neutral ligands.

The synthesised ligands will be described as neutral dithiolene-like derivatives (**L_0**, **L^1H_2** and **L^2H_2**) displaying a DMIT skeleton, which provides π–π interactions and S•••S interactions, while the side chains provide hydrogen bonding interactions (Scheme B-1).

The other idea behind this functionalisation is the fact that introducing hard donor atoms to the soft sulfur moiety (DMIT) will probably be helpful in the synthesis of lanthanide complexes, since lanthanides (hard) will probably better react with hard donor than soft sulfur donors.

B.2 The role of non-covalent interactions in supramolecular chemistry

Supramolecular chemistry represents that part of chemistry that focuses on weak bonding interactions between molecules. In this chapter, those weak and mostly assigned as "non-covalent interactions" are restricted to π–π, S•••S Van der Waals and hydrogen bonding. These features are of potential interest in several fields of modern material science.[77-80] The strength of the hydrogen bond as well as its selectivity, compared to other non-covalent interactions, placed it at the forefront for supramolecular studies.

B.2.1 Some definitions and examples illustrating different types of "non-covalent" interactions.

Non-covalent interactions are classified as weak interactions compared to covalent interactions.

π-π interactions are generally caused by intermolecular overlapping of p-orbital in π-conjugated systems.

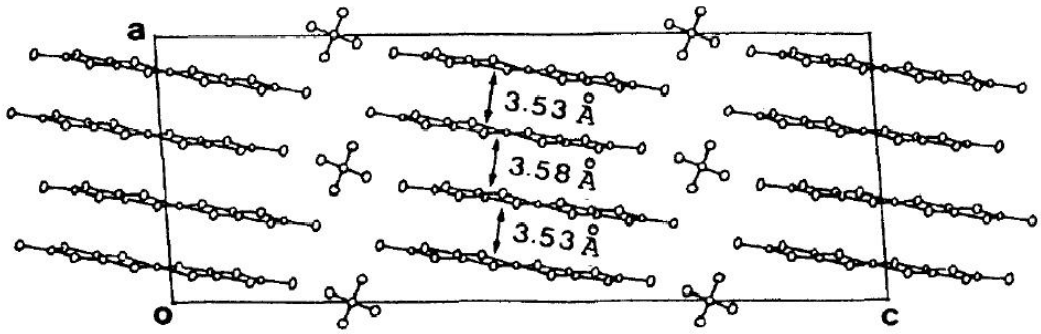

Figure B-1: : π-π interactions in $[(Me_4N)[Ni(dmit)_2]$, the $[Ni(dmit)_2]$ anions, which are almost planar, are stacked along the a axis.[81]

This kind of interactions are involved in the elaboration of conducting or superconducting molecular material.[17, 20] They also help in the generation of supramolecular systems by their non-negligible bonding contribution in keeping the molecule entities close to each other.

The plane to plane separation of ca. 3.5 Å in $[(Me_4N)[Ni(dmit)_2]$[81], is an evidence of strong $\pi-\pi$ interactions. For comparison, the plane-to-plane separation between carbon layers in graphite is about 3.35 Å.[82]

S•••S van der Waals interactions are referred to the S•••S contact distances falling below the sum of Van der Walls (VDW) radii. They can result in intramolecular overlapping; from sulfur atoms situated on the same molecule or intermolecular overlapping, in which case sulfur atoms are situated in adjacent molecules.

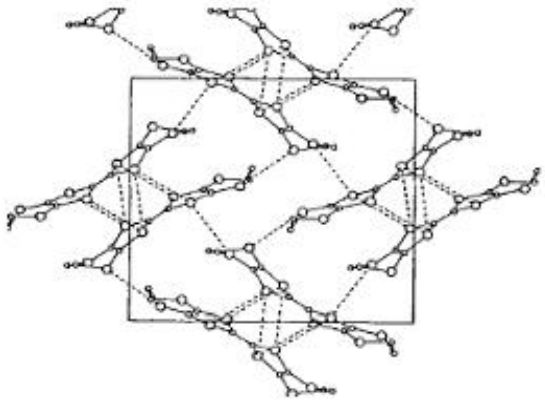

Figure B-2: Shortest S•••S contacts in the BEDT-TTF crystal viewed along the a axis. The square box marks the unit cell in the bc plane.[83]

The strength of S•••S interactions has been evaluated to be about - 0.35 kcal mol^{-1} on the basis of *ab initio* calculations,[83] describing therefore an attractive force. Figure B-2 shows the packing motif in the molecular structure of BEDT-TTF, which displays S•••S interactions.

The ***hydrogen bond*** can be described as a border-line case, and occurs between an electronegative (O, N, F) atom and a hydrogen atom bound to another electronegative atom. Generally, hydrogen bonds occur if a small, highly electronegative atom with a lone pair of electrons shares its nonbonding electrons with a positively polarised hydrogen atom.[84] They can be *intra*molecular and/or *inter*molecular.

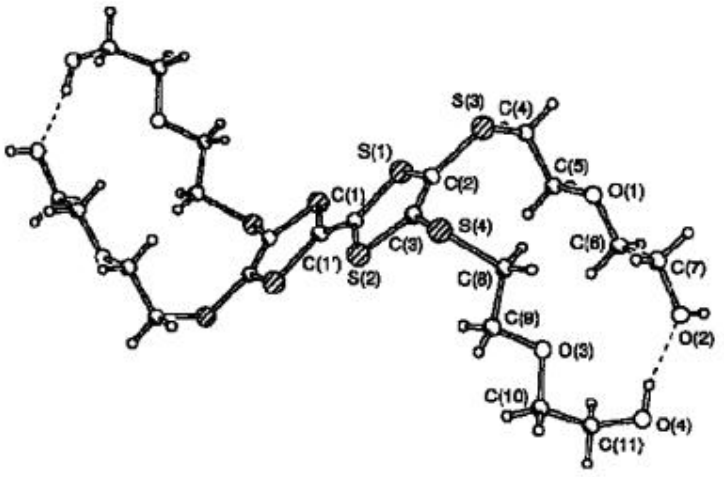

Figure B-3: Intermolecular hydrogen bonding in a TTF-ethyleneglycol derivative.[85]

Depending on the electronegative atom, their energies cover a wide range from over 30 kcal mol^{-1} for the strongest to less than 0.5 kcal mol^{-1} for the weakest one. The bond energies in HO-H•••OH_2 is around 13.5 kcal mol^{-1}.[86] This kind of bonding is, for example, responsible for the high boiling point of water.

B.2.2 Non-covalent interactions in supramolecular chemistry

Pre-organised supramolecular systems could be predicted by the strategic placement of appropriate elements in a ligand and the coordination possibilities of a ligand towards a metal ion.[80] The three types of interactions mentioned above are long-

range interactions, playing therefore an important role in supramolecular organisation. Such interactions can take place simultaneously within the same structure motif, in which case they are in competition with the other “non-covalent” interactions.

This field of chemistry has become an important tool for understanding interaction and/or processes occurring in biological systems, since protein structures are held together by hydrogen bonding interactions, electrostatic interactions, Van der Waal’s packing and hydrophobic interactions.[86, 87] Another importance of these non-covalent interactions in biological molecules is directly related to the phenomenon of molecular recognition in biological systems, which requires rapid formation and breaking of bonds at ambient temperatures.

B.3 Synthesis of dithiolene ligands with OH functional groups (alcohol and acid)

Functionalising the DMIT unit with alcohol or an acidic group should help to organise supramolecular systems through non-covalent interactions by means of crystal engineering. The objective of crystal engineering is the non-casual synthesis of crystal materials having deliberate organisation of molecules in the crystals. For this purpose hydrogen bonding is a fundamental tool which can be used to generate supramolecular architectures,[79, 80, 88] such as rows, layers, sheets, helix strands and networks.

Such substituents (alcohol and acidic functional group) can contribute to the arrangement by helping in the direction of approach of suitable hydrogen bonding agents to the oxygen, thus adding a potential degree of controlling the way two or more molecules are associated.[80, 88]

B.3.1 Synthesis, characterisation and supramolecular description of L^1H_2.

B.3.1.1 Synthesis of ligand L^1H_2

The synthesis of $\mathbf{L^1H_2}$, by Bryce[48] and Hansen[47] , was designed for accessing to alkylthio-TTF and crown ether-annelated-TTF derivatives, respectively. Hansen *et al*. use a one pot reaction using the zinc complex $\mathbf{[Zn(DMIT)_2](Et_4N)_2}$ which is refluxed in the presence of 2-bromoethanol, while Bryce *et al.* use a two step reaction. This two-step reaction starts with a cleavage of the 4,5-bis(benzoylthio)-1,3-dithiole-2-thione ($\mathbf{L_0}$) using 2 equivalents of sodium ethanolate to generate the Na_2DMIT, characterised by the red colour of the solution. The second step is a nucleophilic reaction between Na_2DMIT and the added 2-chloroethanol. This reaction is generally followed by a colour change from red to orange and later to yellow after one day under stirring.

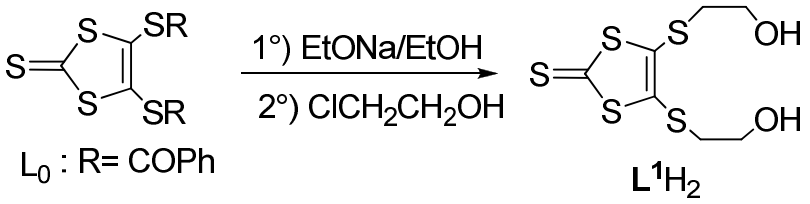

Scheme B-2: Reaction pathway for the synthesis of L^1H_2 according to Bryce *et al.* [48]

$\mathbf{L^1H_2}$ was characterised by elemental analysis, IR, NMR and X-ray diffraction analysis.

NB: There are various techniques for the detection of hydrogen bonds. The most important methods are IR spectroscopy, X-ray and neutron diffraction, and ^{1}H NMR spectroscopy, in this order.[89] It is commonly accepted that neutron diffraction finds hydrogen atoms better than X-ray diffraction. The neutron diffraction experiment, with an accuracy of ca. ± 0.001 Å, locates the hydrogen atom's nucleus, while with the X-ray diffraction the hydrogen atom's electron cloud is detected with an accuracy of ca. ± 0.02 Å.[88] However, the difference between these two diffraction methods exceeds rarely 0.15 %.[78]

B.3.1.2 Crystal structure determination of L^1H_2.

Yellow crystals of $\mathbf{L^1H_2}$ are obtained from a concentrated THF solution cooled at a temperature between -5 and -10°C. A single crystal was isolated for X-Ray diffraction

analysis. As depicted in Table B-1, ligand $\mathbf{L^1}H_2$ (*4*,5-bis[(2´-hydroxyethyl)thio]1,3-dithiole-2-thione) crystallises in the monoclinic system [$P2_1/n$]. The molecular structure with the atom numbering for $\mathbf{L^1}H_2$ is shown in Figure B-4.

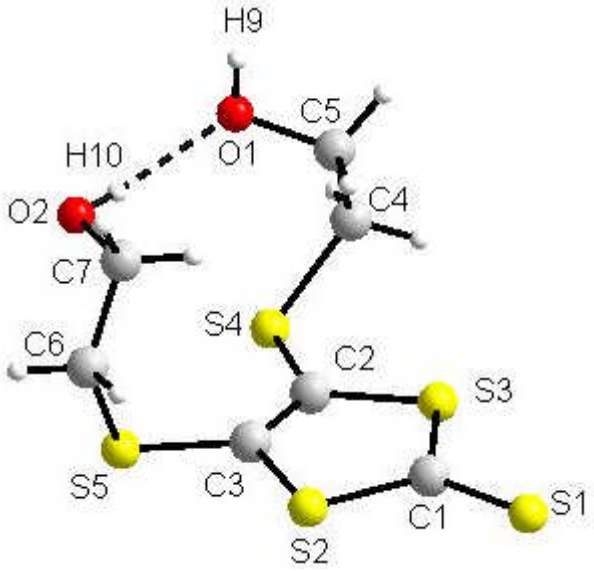

Figure B-4: Molecular structure of L^1H_2. Dotted lines represent hydrogen bonding interactions.

The crystal structure was solved by direct methods and refined by full-matrix least squares on F^2 using the SHELX software package for crystal structure solution and refinement.[90] All non-hydrogen atoms were refined with anisotropic thermal parameters in the later cycles of refinement. Selected bond lengths and angles are reported on Table B-2.

Table B-1: Crystal data and structure refinements for L^1H_2.

Compound	$\mathbf{L^1}H_2$
Empirical formula	$C_7 H_{10} O_2 S_5$
Formula weight	286.45
Temperature	103(2) K
Wavelength	0.71073 Å
Crystal system	Monoclinic
Space group	$P2_1/n$
Unit cell dimensions	a = 5.2765(5) Å α= 90°
	b = 25.853(3) Å β= 105.124(6)°
	c = 8.6152(10) Å γ = 90°

Volume	1134.5(2) $Å^3$
Z	4
Density (calculated)	1.677 Mg/m^3
Absorption coefficient	0.991 mm^{-1}
F(000)	652
Crystal size	0.5 x 0.4 x 0.2 mm^3
Theta range for data collection	1.58 to 29.46°
Index ranges	-7<=h<=7, -34<=k<=35, -11<=l<=10
Reflections collected	13208
Independent reflections	3138 [R(int) = 0.0406]
Completeness to theta = 24.00°	99.7 %
Absorption correction	None
Refinement method	Full-matrix least-squares on F^2
Data / restraints / parameters	3138 / 0 / 167
Goodness-of-fit on F^2	1.008
Final R indices [I>2sigma(I)]	R1 = 0.0296, wR2 = 0.0568
R indices (all data)	R1 = 0.0475, wR2 = 0.0633
Largest diff. peak and hole	0.445 and -0.312 $e.Å^{-3}$

Table B-2: Selected bond lengths (Å) and angles (°) for L^1H_2.

S(1)-C(1)	1.644(2)	C(2)-S(4)-C(4)	102.28(9)
S(2)-C(1)	1.734(2)	C(3)-S(5)-C(6)	99.41(9)
S(2)-C(3)	1.751(2)	S(1)-C(1)-S(3)	122.02(1)
S(3)-C(1)	1.733(2)	S(1)-C(1)-S(2)	125.65(1)
S(3)-C(2)	1.753(2)	S(3)-C(1)-S(2)	112.29(1)
S(4)-C(2)	1.756(2)	C(3)-C(2)-S(3)	115.53(1)
S(4)-C(4)	1.824(2)	C(3)-C(2)-S(4)	124.16(1)
S(5)-C(3)	1.757(2)	S(3)-C(2)-S(4)	120.19(1)
S(5)-C(6)	1.829(2)	C(2)-C(3)-S(2)	116.36(1)
C(2)-C(3)	1.347(3)	C(2)-C(3)-S(5)	126.18(1)
C(4)-C(5)	1.512(3)	S(2)-C(3)-S(5)	117.43(1)
C(5)-O(1)	1.431(2)	C(5)-C(4)-S(4)	114.02(1)
C(6)-C(7)	1.508(3)	O(1)-C(5)-C(4)	109.60(2)

C(7)-O(2)	1.433(2)	C(7)-C(6)-S(5)	114.39(1)
C(1)-S(2)-C(3)	97.72(9)	O(2)-C(7)-C(6)	111.45(2)
C(1)-S(3)-C(2)	98.08(9)		

B.3.1.3 Supramolecular description of L^1H_2.

Figure B-5 shows a block structure where molecules of $\mathbf{L^1H_2}$ are held together via hydrogen bonding interactions. The side chains bound to C2 and C3 are approximately stretched perpendicular to the DMIT plan (Figure B-4). Oxygen atoms are both donor and acceptor of hydrogen bonds giving rise to a polymer-like structure. We could identify two types of hydrogen bonding: *intra*-molecular ($O_2H_{10}\bullet\bullet\bullet O_1$) and *inter*-molecular ($O_1H_9\bullet\bullet\bullet O_2$) (Figure B-5).

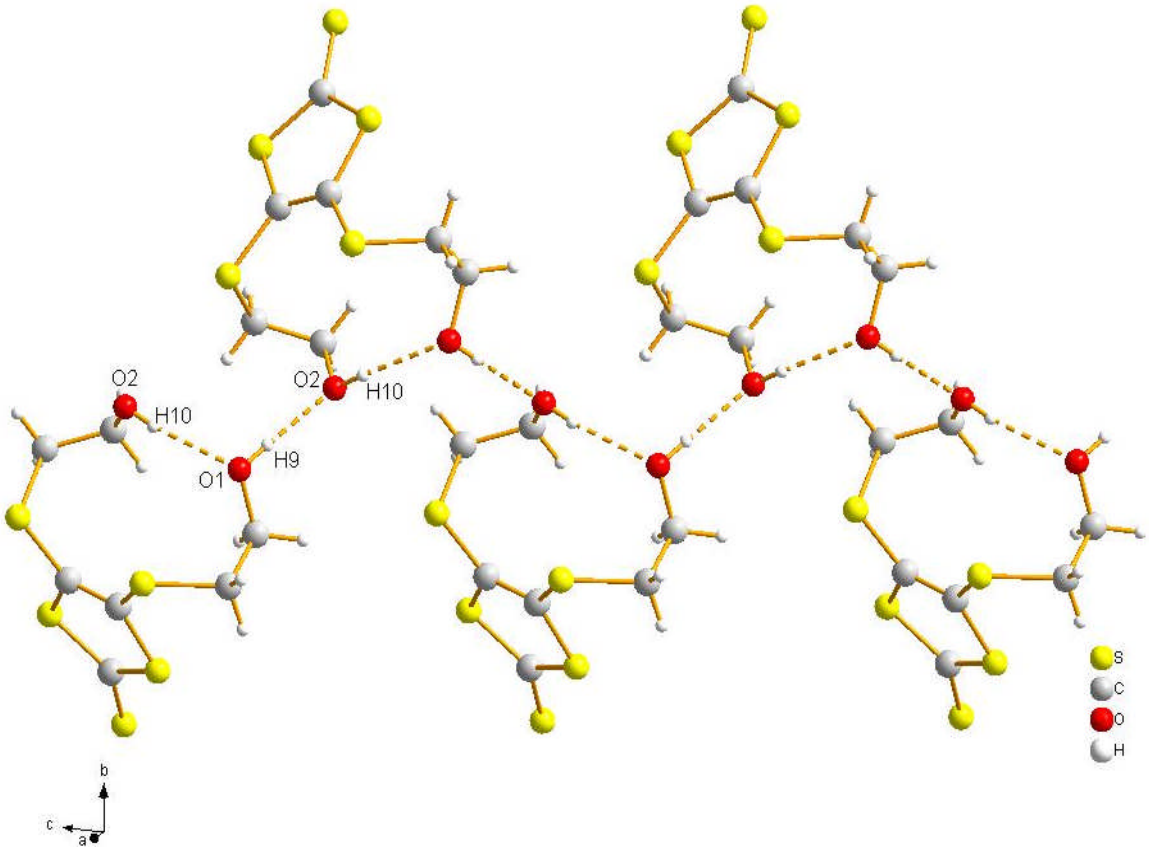

Figure B-5: Crystal structure of L^1H_2: projection on the *bc* plane showing the intra- and inter-molecular hydrogen bonding (hydrogen bridges are shown as dashed lines).

Such interactions have not been observed in the TTF analogue (THET-TTF) reported by *Becher et al.* [85] where only intermolecular hydrogen bonding between the

molecules and the solvent (methanol in that case) were observed. It should be noted that *inter*-molecular O_1H_9•••O_2 (2.72 Å) distances are slightly shorter than *intra*-molecular O_2H_{10}•••O_1 (2.78 Å) distances (see Table B-3).

Table B-3: Distances and angles data for the hydrogen bonding network in L^1H_2.

Distances in Å	**O_1…O_2intra**	2.79(3)
	O_1…O_2inter	2.72(2)
	O_1-H_9	0.81(1)
	O_2-H_{10}	0.76(1)
Angles in °	**O_1-H_9…O_2**	165.25(8)
	O_2-H_{10}…O_1	178.88(6)

Not only, the OH•••O distances are of crucial importance but the OH•••O angle is also a helpful parameter. It has been demonstrated that longer and weaker hydrogen bonds are more likely to deviate from a linear arrangement.[88] Furthermore, it is more common for N-H•••O bonds to deviate from linear arrangements than it is for O-H•••O bonds, even when their bond distances are similar.[88]

Discussing hydrogen bonding in terms of weakness or strength is not evident. The distance range ($r_{A\text{-}H\cdots B}$) is an important factor but not the only limiting factor. But we can assume that a combination of the distance ($r_{A\text{-}H\cdots B}$) and the deviation of the corresponding angle from linearity (180 °) are good factors which need to be taken into account when considering the strength of hydrogen bonds in crystal engineering.

Table B-4 summarised some hydrogen bonding parameters found in TTF functionalised by hydroxyl groups.

Table B-4: Selected distances (Á) and angles (°) of the hydrogen bonds found in TTF-hydroxylated derivatives. (For better comparison, only derivatives in which hydrogen bond linked oxygen atoms are represented. The structures of the compounds are represented in the annexe; see Scheme H-2, in the Appendix, for more details).

Compounds	Nature of the O-H---O# bond	d(O-H) Á	d(H---O#) Á	d(O----O#) Á	(O-H---O#) Angle °	Ref
L^1H_2	**O-H---O# inter**	**0.807(1)**	**1.916(1)**	**2.723(2)**	**178.88(6)**	**this work**
L^1H_2	**O-H---O# intra**	**0.764(1)**	**2.039(2)**	**2.785(3)**	**165.25(8)**	**this work**
$(Me_3TTF)_{2d}(OH)Me$	O-H---O# inter[a]		2.44	3.47(2)	174.7(5)	[91]
HETMT-EDTTTF (A)	O-H---O# inter	0.82	2.16	2.943	161	[92]
HETMT-EDTTTF (B)	O-H---O# inter	0.82	2.27	3.015	151	
HETMT-EDTTTF (C)	O-H---O# inter	0.82	2.51	2.907	111	
$(SC_8H_8O_4S)$-TTF$(CH_2OH)_2$	O-H---O# inter		2	2.82	172	[49, 78]
			2.29	3.04	153	
			2.02	2.8	156	
DHMT-DHTTTF	O-H---O# inter		1.85	2.705	165	[78, 93]
	O-H---O# inter		1.99	2.707	133	
THET-TTF	O-H---O# inter[b]		1.70(1)	2.703(1)	161.2(1)	[85, 78]
	O-H---O# inter[b]		2.05(2)	2.75(1)	165.3(2)	
	O-H---O# intra		1.92(1)	2.65(1)	152.4(4)	
THEGT-TTF	O-H---O# inter		1.95(2)	2.673(3)	174.5(1)	[85, 78]
	O-H---O# intra		1.88(1)	2.652(3)	165.4(2)	

NB: the missing standard deviations for bond length and angles have not been found in the original publication.

[a] intermolecular interaction between molecules and ethanol (solvent)

[b] intermolecular interaction between molecules and methanol (solvent)

(A) and (B) are referred to two different phases found in the electrocrystalisation of HETMT-EDTTTF with ClO_4^-

(C) is referred to charge transfer complex of HETMT-EDTTTF with TCNQ

Taylor *et al.* plotting the mean N-H•••O angle as function of the H•••O distance range (based on 1357 examples), have found an almost linear decay when the distance increased.[94] However, the donor-acceptor distance ($r_{A\text{-}H\bullet\bullet\bullet B}$) do not always fit with the linearity of the A-H•••O angle as seen in the examples in Table B-4.

Table B-5 gives an overview of some helpful parameters in relationship with the strength or weakness of hydrogen bonds (the classification follows that of Jeffrey[86]).

Table B-5: Strong, moderate, and weak hydrogen bonding (X-H•••A) parameters.(X= O, N, halogen and A= O, N, S, halide, etc.) [95]

	Strong	Moderate	Weak
Interaction type	strongly covalent	mostly electrostatic	electrostat./dispers.
bond lengths [Å] H•••A	1.2-1.5	1.5-2.2	>2.2
X-H versus H•••A	X-H ~ H•••A	X-H < H•••A	X-H << H•••A
X-H•••A [Å]	2.2-2.5	2.5-3.2	>3.2
bond angles [°]	170-180	>130	>90
bond energy [kcal.mol^{-1}]	15-40	4-15	<4
^{1}H downfield shift	14-22	<14	

In the case of **L**^{1}H$_2$, the OH•••O distances average the 2.70 Å which would suggest that we are in the case of moderate interaction, but having a look on the O-H•••O angle which average the 170° would suggest strong interaction.

At this stage we could not conclude in the strength of the hydrogen bonding interaction. Furthermore, the presence of π–π interactions can also have an influence on the hydrogen bonding interaction.

Apart from the hydrogen bonding interaction, π–π interactions have been also observed. These π–π interactions help molecules to stack in the way showed in Figure B-6.

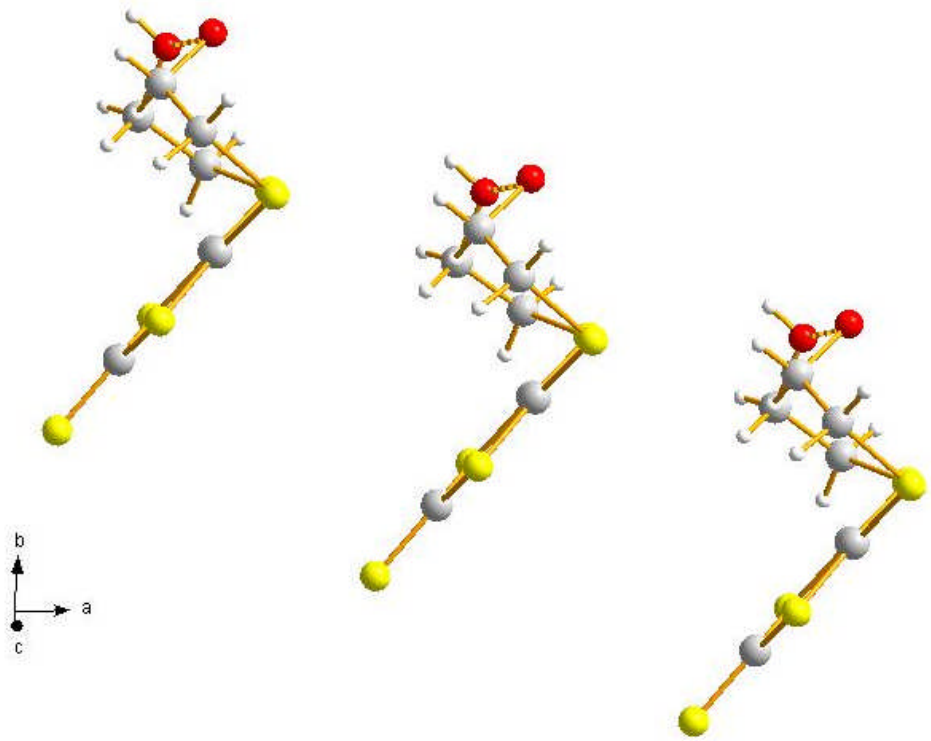

Figure B-6: Packing diagram viewed along the *a* axis showing the stacking of "dmit" units in L^1H_2[96]. (The hydrogen bonds and other molecules omitted for clarity)

The plane to plane separation amounts to 3.66(1) Å (π-stacking). Furthermore, two S•••S contacts of 3.838(1) Å and 3.762(1) Å, somewhat shorter than the corresponding Van-der-Waals radii of two S atoms, are also observed.

B.3.1.4 NMR studies

Basically, the chemical shift observed in ^{1}H-NMR investigations of OH headgroups (engaged in hydrogen bonding or not) depends on several parameters such as solvent, temperature etc.. The nature of the hydrogen bonding (*intra*- and *inter*-molecular, strength, etc...) can also be deduced from proton-NMR investigations[97]. To get more insight into our system (namely $\mathbf{L^1}H_2$) we have performed the NMR studies at variable temperature. This NMR experiment of $\mathbf{L^1}H_2$ reveals only little change when the temperature is raised up. But addition of a donor solvent (DMSO) leads to significant changes in the NMR shifts, when the concentration of DMSO is increased. Figure B-7 represents the evolution of the proton NMR shift of the alcohol group of $\mathbf{L^1}H_2$ by successive addition of DMSO-$_{D6}$.

For clarity the hydrogen atoms will be indexed with the subscripts a,b,c following the structure of $\mathbf{L^1}H_2$, as displayed in the following scheme.

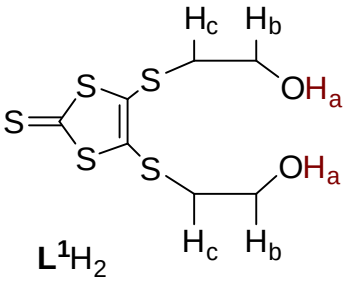

$\mathbf{L^1}H_2$

Increasing the DMSO-d6 concentration has not only an effect in chemical shift but also on the multiplicity (see Figure B-7).

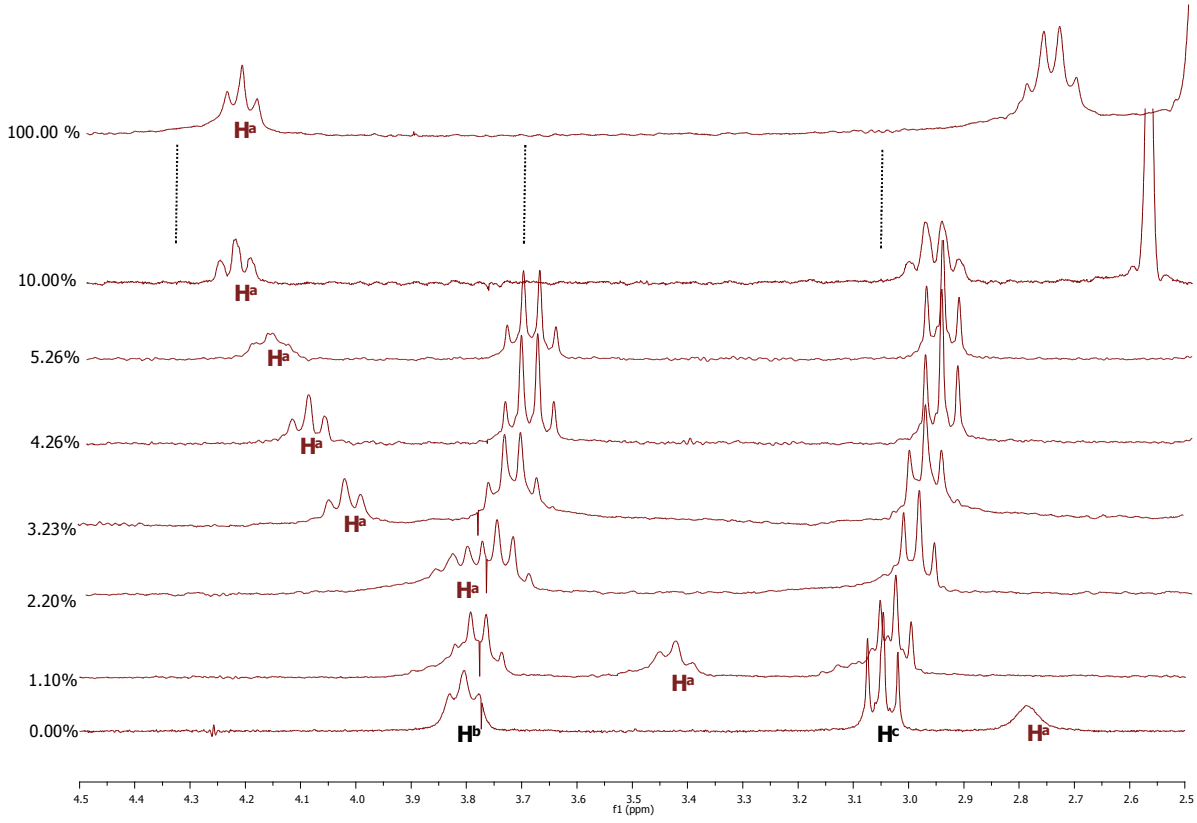

Figure B-7: Variation of the NMR shift of the OH of $\mathbf{L^1}H_2$ as a function of the % DMSO (Volume), (after 10% of DMSO no significant shift was noticed).

Starting from two triplets representing the two -CH_2- groups ($\mathbf{H_b}$ and $\mathbf{H_c}$) and one broad singlet for the –OH ($\mathbf{H_a}$) group in $CDCl_3$ we can identify, after addition of DMSO, appearance of a triplet ($\mathbf{H_c}$) and a pseudo-quadruplet ($\mathbf{H_b}$) representing the two -CH_2- groups and one triplet for the -OH group. By addition of DMSO, the hydrogen atoms ($\mathbf{H_a}$) of the hydroxyl group become fixed (no more free) and participate in the coupling.

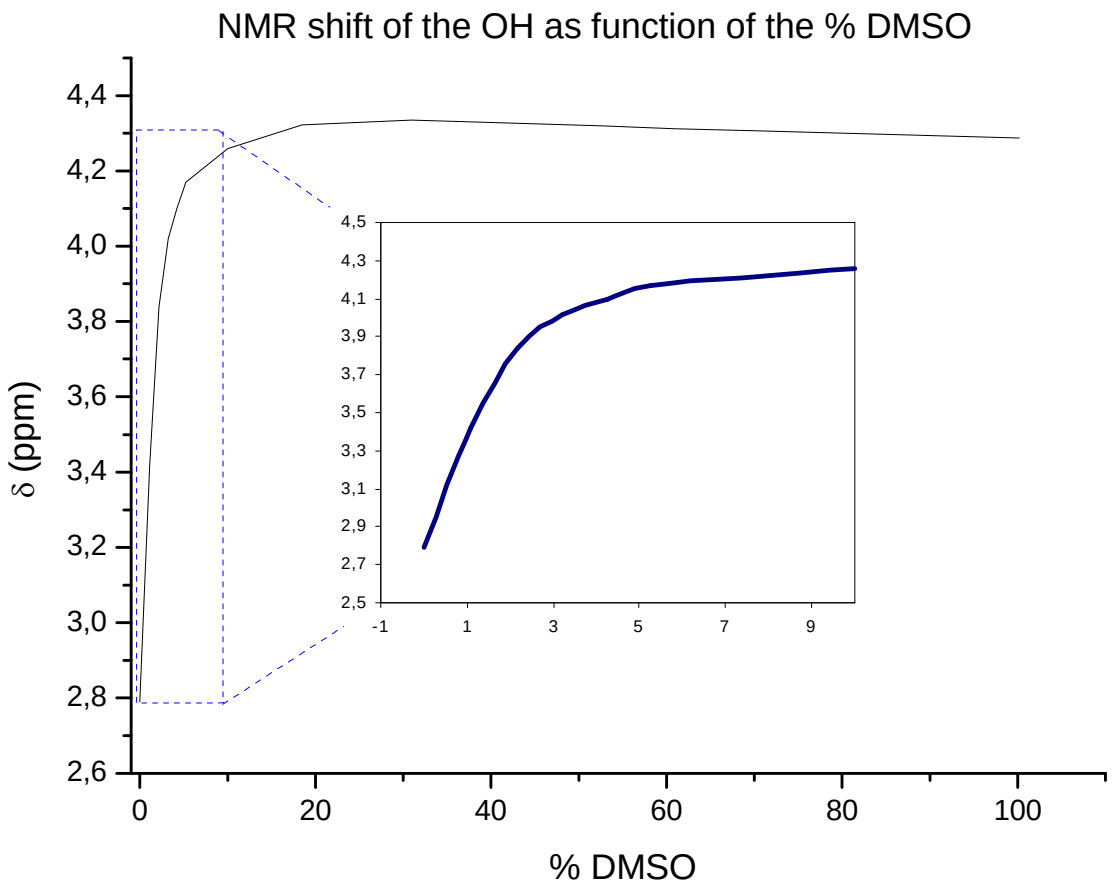

Figure B-8: Plot of the NMR shift of the OH proton as function of the percentage DMSO (d_6).

In Figure B-7, the broad signal at 2.80 ppm (singlet) in pure $CDCl_3$ corresponds to the OH group. The broadness of this peak is tentatively explained by a rapid exchange phenomenon between intermolecular and intramolecular OH bonds, since both OH groups (of the two side chains) can be engaged in *intra*- or *inter*-molecular hydrogen bonding.

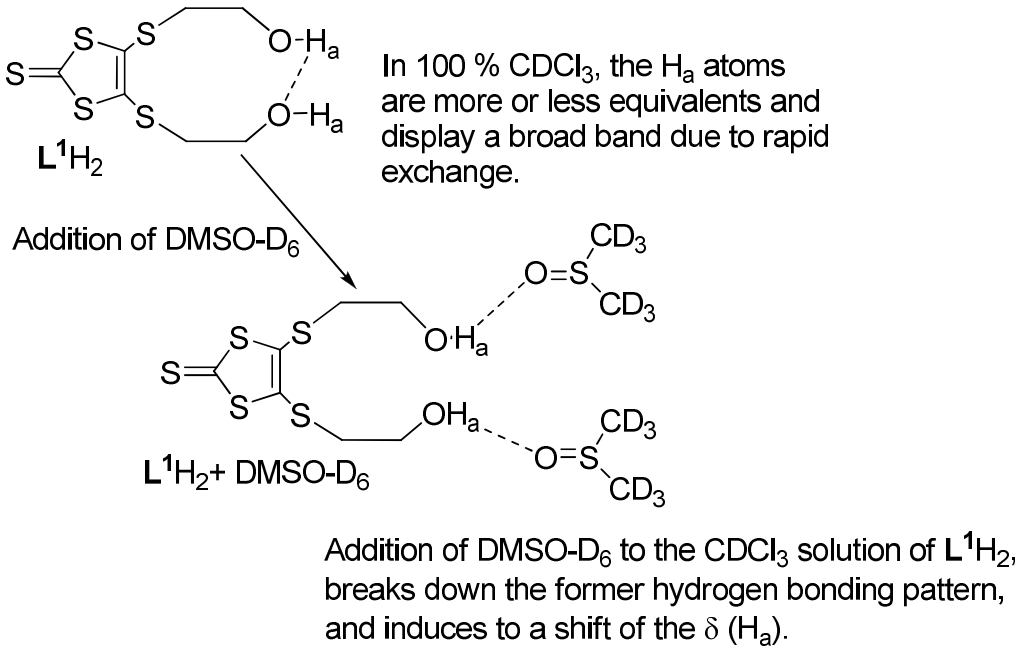

Scheme B-3: Possible schematic representation of the change following the addition of DMSO-D_6 in the $CDCl_3$ solution of L^1H_2.

Increasing the percentage of DMSO-D_6 to 1 % causes a shift of this peak to 3.42 ppm. The multiplicity changes to a triplet. DMSO-D_6, as a proton acceptor may block the propensity for these OH arms to be engaged in both intra- or inter-molecular fashion, by breaking the previous network. Since *intra*- and *inter*-molecular interactions are perturbed by DMSO-D_6 as acceptor of hydrogen bonds, we will probably see only intermolecular interaction between OH groups of the ligand and DMSO-D_6. As a result of this addition, the exchange phenomenon is no more possible. At increased percentage of DMSO-D_6, the OH tends to be shifted downfield and reaches a value of 4.18 ppm at 5.26 % volume of DMSO-D_6, corresponding to saturation.

The sensitivity of the OH headgroup toward DMSO agrees with a classification of the hydrogen bonding in the case of $\mathbf{L^1}H_2$ as weak interactions.

A study on intramolecular O-H•••O in molecules bearing β-diketone enol fragment by Bertolasi *et al.*, has shown a nearly linear relationship between ^{1}H NMR chemical shift and bond distances.[97] The proton chemical shifts, measured in $CDCl_3$, solutions have been found to be in the range 8.6–10.1ppm for O-H•••O distances between 2.59 Å and 2.64 Å and 14.9–19.0 ppm for distances between 2.41 Å and 2.55 Å.[97] Note however that their systems are different to $\mathbf{L^1}H_2$, in this sense that in this later

the π-system is not conjugated to the hydrogen bond of the thio-alkohol rest and plays no significant role in the delocalisation influencing the δ (OH) shift.

B.3.2 Synthesis, characterisation and supramolecular description of L^2H_2 and L^2H_2.THF

B.3.2.1 Hydrogen bonding in carboxylic acids

Hydrogen bonding in carboxylic acids has been widely investigated and the most frequently observed pattern is the closed dimer (Scheme B-4).

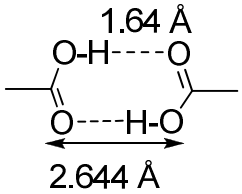

Scheme B-4: Mean geometry of the carboxylic acids dimer in crystals.[95]

In a conventional way, such hydrogen bonds arrangement can be defined using graph sets established by M. C. Etter.[98] To assign a graph set to an arrangement, we have first to identify the different types of hydrogen bonds as well as the nature of the donors and acceptors engaged in a hydrogen bonding. Generally the graph set is specified using the pattern designator (**G**), the degree of this pattern (**n**), and finally the number of donors (**d**) and acceptors (**a**) involved in this pattern:

$$G^a_d\,(n)$$

For intermolecular hydrogen bonds, the following designators are used: **C** (for chain), **R** (for ring), **D** (for dimer or other finite set), while **S** denotes intramolecular hydrogen bonds. The number of donors and acceptors used in each motif are assigned as subscripts and superscripts respectively and finally, the number of atoms in a repeat unit is indicated in parentheses.[98] Some examples are given in the following scheme to illustrate this model.

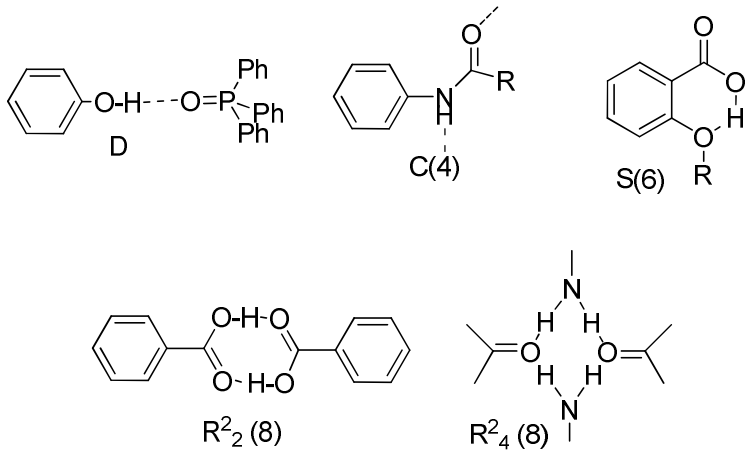

Scheme B-5: Graph-Set assignment for representative Hydrogen-Bond Motifs according to Etter.[98]

Surprisingly, the probability of formation (*Pm*) of a carboxylic acid dimer synthon (example **e** in Scheme B-6) in crystals, calculated by Allen *et. al*.[99] is somewhat lower than in the oxime-heterodimer (example **b** in Scheme B-6) form.[95] This lowered value was explained by a possible competition from other hydrogen bond donors and acceptors (water molecules or carboxylate groups), and could rise to a value of 0.86 to 0.95 in the absence of such competing groups.[54, 99]

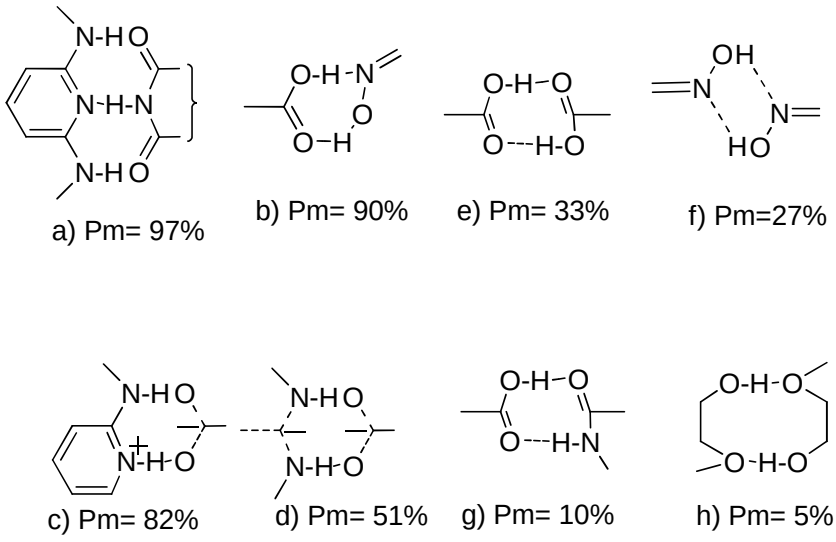

Scheme B-6: Examples of intermolecular hydrogen bond motifs with their probability of formation (Pm) in crystals. Notice that Pm of the carboxy-oxime heterodimer (b) is much higher than that of the carboxylic acid (e) and oxime homodimers (f). [99]

B.3.2.2 Synthesis of ligand L^2H_2

L^2H_2 could be synthesised by refluxing a solution of di(tetraethyl-ammonium) bis(1,3-dithiole-2-thione-4,5-dithiolate)zincate with the suitable α-halogenido-carboxylic acid XCH_2COOH (X = Br, Cl). This synthetic route was first described by Hoyer *et al* [40] using $ClCH_2COOH$. Later, the crystal structure of a $L^2H_2.H_2O$ was resolved by Zhao *et al*[46] using $BrCH_2COOH$. In our group, we have slightly modified the Hoyer's procedure not only for improving the overall yield but also for isolating a water free ligand since this ligand will be engaged in water-sensitive reactions (see chapter D).

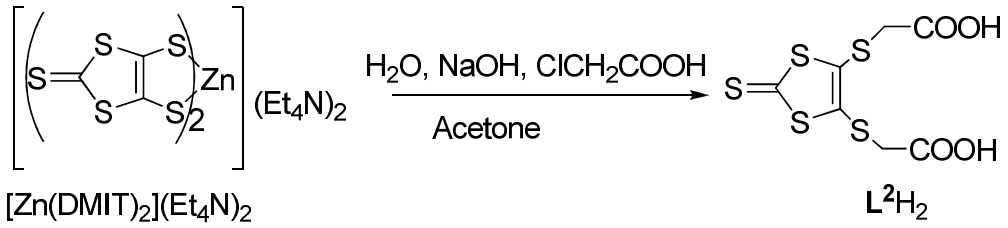

$[Zn(DMIT)_2](Et_4N)_2$ L^2H_2

Scheme B-7: Reaction pathways for the synthesis of L^2H_2.

In that respect the recrystallisation process was conducted in diethyl ether instead of dilute NH_3. Slow evaporation of the diethyl ether solution allowed the isolation of air-stable yellow crystals. No solvated-Et_2O molecules were found in the crystal structure (Figure B-9). In contrast, if THF is used as solvent in the crystallisation process, a solvated-THF was found in the crystal structure. The oxygen of this THF solvate builds hydrogen bonding with hydroxyl group of the carboxylic group of the sulfur-rich ligand giving rise to a structural orientation completely different from that observed in L^2H_2 (see **B.3.2.5** subhead)

The difference in orientation between these two structures of ligand L^2H_2 argues the influence of hydrogen bonding in the arrangement of a system in the solid-state. Characterisation of L^2H_2 was completed by standard methods (elemental analysis, IR, NMR, etc…). In the IR spectra, L^2H_2 presents a broad band situated between 2000 and 3200 cm^{-1}, in the typical region for OH groups. A strong band, characteristic of a C=O function was found at 1692 cm^{-1}, and in the fingerprint region, strong bands representing C=S (1065 cm^{-1}) and C-S (850 cm^{-1}) were identified.

B.3.2.3 Crystal structure determination of L^2H_2.

Yellow crystals of L^2H_2 were obtained from a concentrated diethyl ether solution at room temperature. A single crystal was isolated and the crystal structure determination performed at -170°C. As depicted in Table B-6, ligand L^2H_2 (*4*,5-bis[carboxymethylthio]1,3-dithiole-2-thione) crystallises in the triclinic system in the centrosymmetric space group $P\bar{1}$. The molecular structure with the atom numbering for L^2H_2 is shown in Figure B-9.

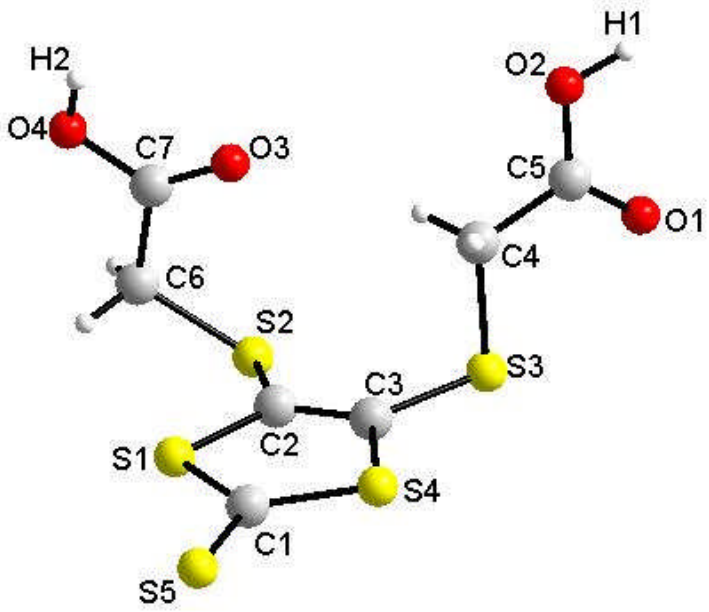

Figure B-9: Molecular structure of L^2H_2.

The crystal structure was solved by direct methods and refined by full-matrix least squares on F^2 using the SHELX software package for crystal structure solution and refinement.[90] Selected bond lengths and angles are listed in Table B-7.

Table B-6: Crystal data and structure refinements for L^2H_2.

Compound:	L^2H_2
Identification code	sh2498
Empirical formula	C7 H6 O4 S5
Formula weight	314.42
Temperature	200(2) K
Wavelength	0.71073 Å
Crystal system	Triclinic
Space group	$P\bar{1}$

Unit cell dimensions	A = 5.1049(10) Å, α= 108.07(3)°.
	B = 10.755(2) Å, β= 101.06(3)°.
	C = 11.638(2) Å, γ = 91.18(3)°.
Volume	594.0(2) $Å^3$
Z	2
Density (calculated)	1.758 Mg/m^3
Absorption coefficient	0.968 mm^{-1}
F(000)	320
Crystal size	0.6 x 0.44 x 0.2 mm^3
Theta range for data collection	3.15 to 27.93°.
Index ranges	6≤h≤6, -13≤k≤13, -15≤l≤15
Reflections collected	5383
Independent reflections	2612 [R(int) = 0.0476]
Completeness to theta = 27.93°	91.6 %
Absorption correction	None
Refinement method	Full-matrix least-squares on F^2
Data / restraints / parameters	2612 / 0 / 169
Goodness-of-fit on F_2	0.784
Final R indices [I>2sigma(I)]	R1 = 0.0334, wR2 = 0.0608
R indices (all data)	R1 = 0.0720, wR2 = 0.0677
Largest diff. peak and hole	0.361 and -0.322 $e.Å^{-3}$

Table B-7: Selected bond lengths (Å) and angles (°) for L^2H_2.

S(1)-C(1)	1.749(3)	C(1)-S(4)-C(3)	97.94(1)
S(1)-C(2)	1.753(3)	S(5)-C(1)-S(4)	123.84(2)
S(2)-C(2)	1.761(3)	S(5)-C(1)-S(1)	123.64(2)
S(2)-C(6)	1.800(3)	S(4)-C(1)-S(1)	112.51(2)
S(3)-C(3)	1.766(3)	C(3)-C(2)-S(1)	115.3(2)
S(3)-C(4)	1.818(3)	C(3)-C(2)-S(2)	123.7(2)
S(4)-C(1)	1.732(3)	S(1)-C(2)-S(2)	120.70(1)
S(4)-C(3)	1.749(3)	C(2)-C(3)-S(4)	116.3(2)
S(5)-C(1)	1.651(3)	C(2)-C(3)-S(3)	125.6(2)
O(1)-C(5)	1.234(3)	S(4)-C(3)-S(3)	118.06(2)

O(2)-C(5)	1.305(3)	O(1)-C(5)-O(2)	125.2(2)
O(3)-C(7)	1.228(3)	O(3)-C(7)-O(4)	124.6(3)
O(4)-C(7)	1.314(3)	O(3)-C(7)-C(6)	124.2(2)
C(2)-C(3)	1.371(4)	O(4)-C(7)-C(6)	111.3(2)
C(4)-C(5)	1.505(4)	C(1)-S(1)-C(2)	97.94(1)
C(6)-C(7)	1.514(4)		

B.3.2.4 Supramolecular description of L^2H_2.

Figure B-9 shows the molecular structure of $\mathbf{L^2}H_2$ in which the side chains are stretched almost perpendicularly to the dmit plan. Analysis of $\mathbf{L^2}H_2$ (Figure B-10) revealed a one-dimensional chain-like structure which has its origin in intermolecular hydrogen bond interactions (O-H•••O) in the R^2_2 (8) arrangement motif, mostly found in systems possessing a carboxylic acid functional group.[95] The building of this $R^2_2(8)$ arrangement is favoured by the presence of two good proton donors (OH) and acceptors (C=O) following the general rules given by Etter.[98]

The O-H•••O distances of 2.66 (3) Å are in the range of the mean values (2.644 Å) found in crystals of carboxylic acid dimer.[95] Assuming that these O•••O distances are shorter than 3 Å, the supramolecular structure can be described as assembled by columns of alternating parallel molecules linked together by hydrogen bond networks. The carboxylic functional groups out of the DMIT plan are engaged in an intermolecular way following the arrangement found in carboxylic acid dimers.

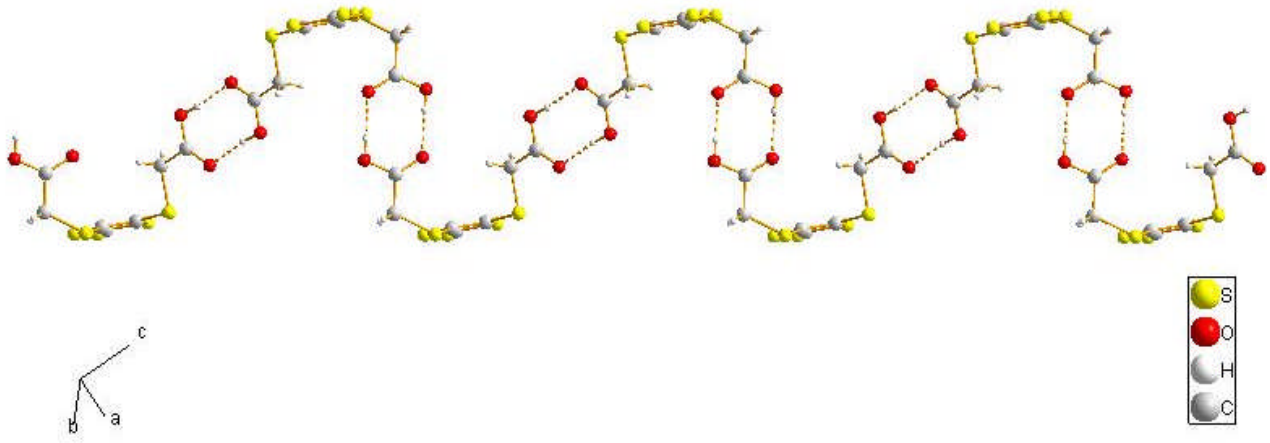

Figure B-10: One dimensional molecular structure arrangement with an emphasis on the formation of ribbons built through $R^2_2(8)$ pattern.

No short intermolecular S•••S contacts have been identified in the solid state. This situation differs from that observed in the case of **L²H₂.H₂O** since in this case the one-dimensional chain-like structure results from S•••S contacts of 3.56 Å (Figure B-11).[46] The common $R^2_2(8)$ arrangement was also observed in the structure of **L²H₂.H₂O**, as well as other intermolecular hydrogen bonding interactions between carboxylic chains and water molecules.[46]

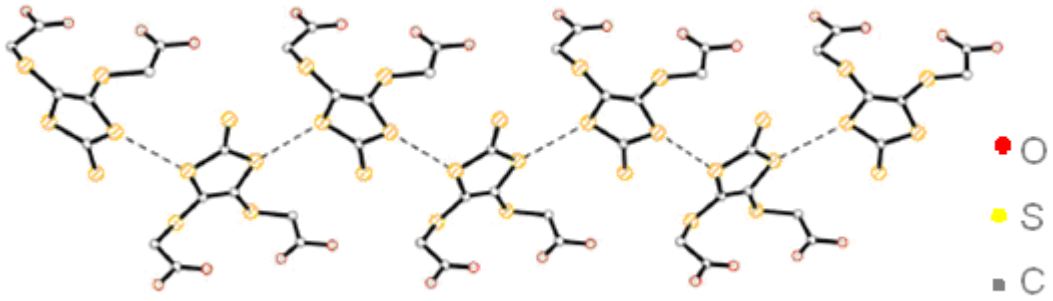

Figure B-11: The one dimensional chain-like structure of $L^2H_2.H_2O$, formed by S•••S interactions (dashed lines) along the b axis.[46]

B.3.2.5 Influence of an acceptor in the hydrogen bonding pattern of L^2H_2.

As stated previously, a good hydrogen donor should be sensitive to the presence of different hydrogen bond acceptors, leading to a possible competition in the hydrogen bonding pattern formed. This idea was investigated by introducing in the crystallisation process of **L²H₂** a solvent able of building hydrogen bonding.

The synthesis followed the method performed in Scheme B-7 with the only difference that re-crystallisation was performed using THF as a solvent.

Since the **L²H₂** alone crystallised without Et_2O molecules, we did not expect to observe big differences. But surprisingly, the X-ray analysis revealed the formation of a **L²H₂.THF** adduct (Figure B-12).

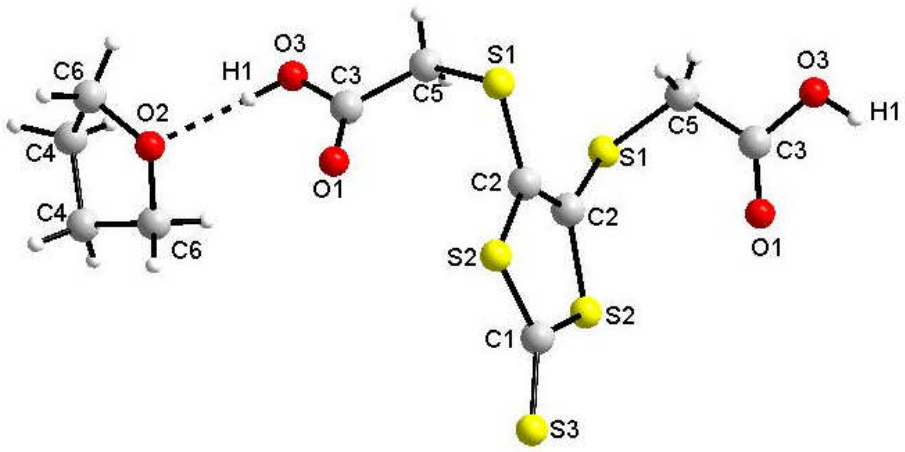

Figure B-12: Molecular structure of L^2H_2.THF

The crystallographic data are shown in Table B-8 and selected bonds and Angles in Table B-9.

Table B-8: Crystal data and structure refinements for L^2H_2.THF

Identification code	sh2594	
Empirical formula	C11 H14 O5 S5	
Formula weight	386.52	
Temperature	180(2) K	
Wavelength	0.71073 Å	
Crystal system	Orthorhombic	
Space group	Pnna	
Unit cell dimensions	a = 7.9656(4) Å	α= 90°.
	b = 21.0885(11) Å	β= 90°.
	c = 9.5192(5) Å	γ = 90°.
Volume	1599.06(14) $Å^3$	
Z	4	
Density (calculated)	1.606 Mg/m^3	
Absorption coefficient	0.740 mm^{-1}	
F(000)	800	
Crystal size	0.66 x 0.40 x 0.30 mm^3	
Theta range for data collection	1.93 to 27.32°.	

Index ranges	-10<=h<=10, -27<=k<=27, -12<=l<=12
Reflections collected	28804
Independent reflections	1800 [R(int) = 0.0520]
Completeness to theta = 27.32°	99.9 %
Absorption correction	Multiscan
Max. and min. transmission	0.8085 and 0.6409
Refinement method	Full-matrix least-squares on F^2
Data / restraints / parameters	1800 / 0 / 125
Goodness-of-fit on F^2	1.080
Final R indices [I>2sigma(I)]	R1 = 0.0302, wR2 = 0.0585
R indices (all data)	R1 = 0.0420, wR2 = 0.0619
Largest diff. peak and hole	0.257 and -0.258 e.$Å^{-3}$

Table B-9: Selected bond lengths [Å] and angles [°] for L^2H_2.THF

S(1)-C(2)	1.762(2)	C(1)-S(2)-C(2)	97.74(9)
S(1)-C(5)	1.806(2)	C(6)#1-O(2)-C(6)	108.3(2)
S(2)-C(1)	1.730(1)	S(3)-C(1)-S(2)#2	123.73(7)
S(2)-C(2)	1.744(2)	S(3)-C(1)-S(2)	123.73(7)
S(3)-C(1)	1.653(3)	S(2)#2-C(1)-S(2)	112.55(1)
O(1)-C(3)	1.198(2)	C(2)#2-C(2)-S(2)	115.98(6)
O(2)-C(6)#1	1.466(2)	C(2)#2-C(2)-S(1)	126.40(6)
O(2)-C(6)	1.466(2)	S(2)-C(2)-S(1)	117.57(1)
O(3)-C(3)	1.331(2)	O(1)-C(3)-O(3)	124.11(2)
C(1)-S(2)#2	1.730(1)	O(1)-C(3)-C(5)	126.16(2)
C(2)-C(2)#2	1.350(3)	O(3)-C(3)-C(5)	109.70(2)
C(3)-C(5)	1.507(3)	C(6)-C(4)-C(4)#1	102.98(1)
C(4)-C(6)	1.493(3)	C(3)-C(5)-S(1)	115.12(1)
C(4)-C(4)#1	1.507(4)	O(2)-C(6)-C(4)	105.65(2)
C(2)-S(1)-C(5)	101.09(8)		

(Symmetry transformations used to generate equivalent atoms: #1 x,-y+1/2,-z+3/2 #2 -x+1/2,-y+1,z)

The arrangement in the crystal structure is totally different to that detected for $\mathbf{L^2}H_2$ and $\mathbf{L^2}H_2\mathbf{.H_2O}$[46], The first point concerns the $\mathbf{R^2_2(8)}$ arrangement which disappears by the coordination of a THF molecule and is replaced by a **C(5)** motif (following the graph set analogy from Etter[98]). As a consequence, the side chains adopt an *anti*-conformation compared to the DMIT plane (Figure B-12). Tail-to-tail arrangements, bridged through the oxygen atoms of the THF molecules, ensure the one-dimensional polymer-like chain (see Figure B-13).

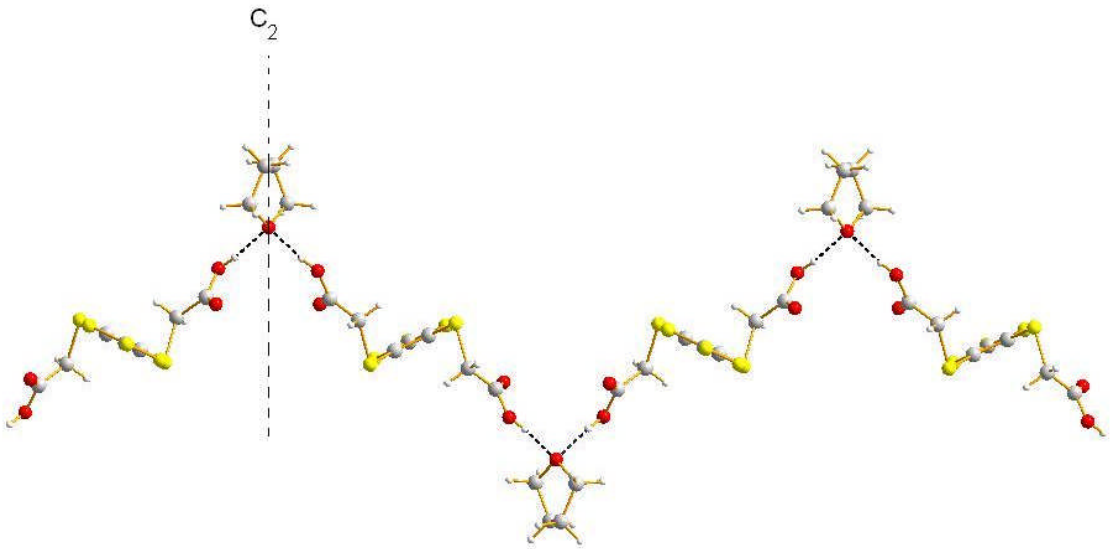

Figure B-13: Molecular structure of the $\mathbf{L^2}H_2$.THF showing a one dimensional polymer-like chain supported by hydrogen bonding. (The vertically dashed line shows the C_2 axis).

The oxygen of the THF molecule hosts two different hydrogen atoms (three-center bonding) from two different donors (-COOH groups localised on two different adjacent ligands). This kind of double acceptor ability could be related to the lone-pair directionality which, according to previous studies, rejects a possible tendency for hydrogen bonds to be formed along the lone-pair directions.[94] The chains are also linked in up and down fashion through OH•••O•••HO bridges. Having a closed look in the structure, we can identify a symmetry element. In fact the oxygen atom of the THF is situated in the C_2 axis as represented in the Figure B-13. In our case we could state without any ambiguity that the hydrogen bonds are formed along the lone pair directionality. This is further confirmed by the quasi-tetrahedral geometry around the oxygen of the THF (angles are between 105 and 109°) in Figure B-14. This observation is in agreement with a sp^3-hybridised oxygen atom. The O-H•••O distances of about 2.665(1) Å are in good agreement with the mean value reported

for similar systems possessing a carboxyl group as a donor and a -C-O-C- fragment (only acceptor ability, THF in our case).[95]

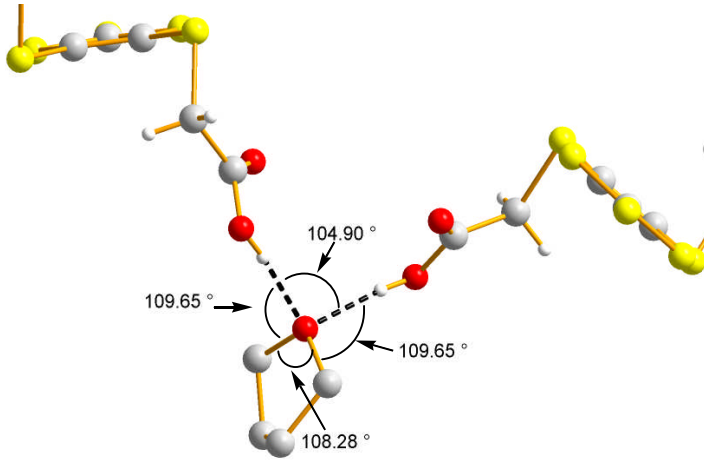

Figure B-14: Zoom on the hydrogen pattern showing the quasi-tetrahedral geometry around the oxygen of the THF.

The DMIT unit, which is the common part of the molecular skeleton in these compounds (**L^2H_2**, **$L^2H_2.H_2O$** and **$L^2H_2.THF$**), remains almost planar. Figure B-15 represents an overview showing the structural changes induced by the presence of an acceptor molecule on the hydrogen bonding networks in the case of ligand **L^2H_2**.

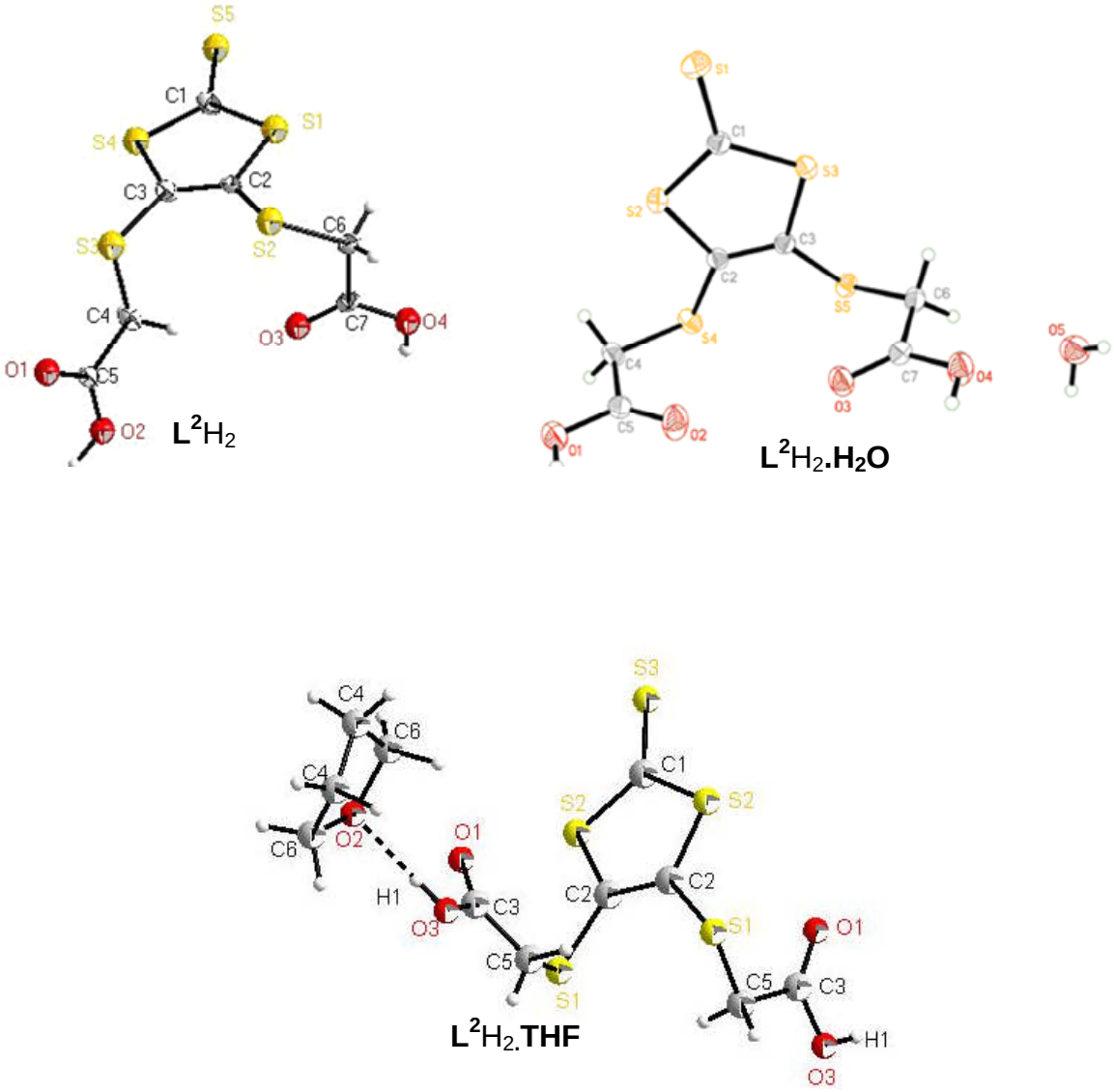

Figure B-15: Structural changes induced by a hydrogen bond acceptor in the L^2H_2 motif.

In **L^2H_2.H_2O**, the difference in orientation is a result of a hydrogen bonding between oxygen of the water molecule and the hydrogen from the C-H (C6-H•••O5 in Figure B-15), this distance O5•••H-C is about 2.44(9) Å.[46]

Between two DMIT moieties, the shortest S•••S intermolecular contacts have been identified at 7.57 Å to each other. This distance is far away from the sum of the Van der Waals radii of sulfur atoms. Therefore, in the structural arrangement, contribution of intermolecular S•••S interactions are negligible. π–π interactions are completely absent in this structural arrangement.

All in all, the driving force leading to the formation of such a structure is unambiguously the hydrogen bonding.

B.4 Synthesis of dithiolene ligands with C=O functional groups

Carbonyl groups (C=O) can be considered, in a certain extent, as acceptor of hydrogen bonding, because of their lone pairs residing on the oxygen atom. Here we will present a ligand bearing carbonyl groups as representative of an exceptional case of ligands bearing only acceptor moiety, but nevertheless able to undergo hydrogen bonding, namely a C-H•••O hydrogen bond.

This ligand (**L_0**) has been already structurally characterised and present a disorder (from the O of the C=O) when measured at 288 K.[100] This disorder disappears when measurement are performed at 120K.[101]

But, when we performed the crystallographic analysis at a still lower temperature, namely at 102 K, we discovered a structural organisation which was not observed in the precedent investigations. The most salient feature of this low-temperature study was the identification of unexpected hydrogen bonding interactions.

B.4.1 Synthesis and characterisation of L_0.

The synthesis of **L_0** is an acylation of the DMIT moiety. **L_0** is prepared by reaction between one equivalent of the zinc complex **$[Zn(DMIT)_2(Et_4N)_2]$** with fifteen equivalents of benzoyl chloride in acetone at room temperature, following literature methods.[42]

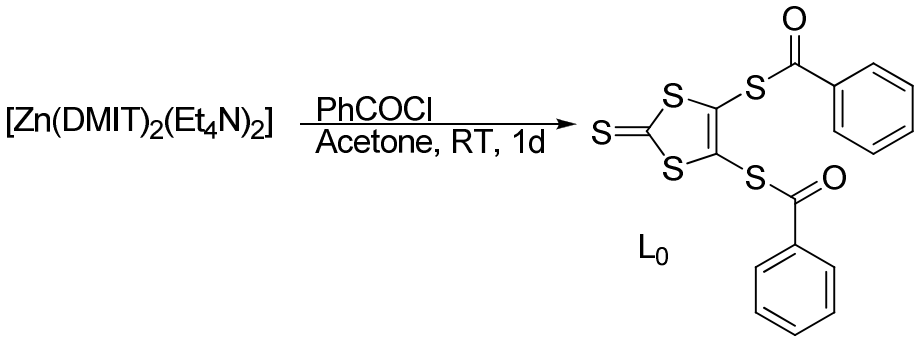

Scheme B-8: Reaction pathway for the synthesis of L_1 according to Becher et.al.[42]

The end of the reaction is indicated by a strong color change from deep red (at the beginning) to yellow–orange. **L_0** can be re-crystallised in pure $CHCl_3$ solution and single crystals could be obtained at room temperature within one day.

B.4.2 Crystal structure determination and description of L_0

A single crystal was isolated for X-Ray diffraction analysis and the crystal structure determination performed at -170°C. As depicted in Table B-10, ligand **L_0** (*4*,5-bis(benzoylthio)-1,3-dithiole-2-thione) crystallises in the monoclinic system [$P2_1/c$].

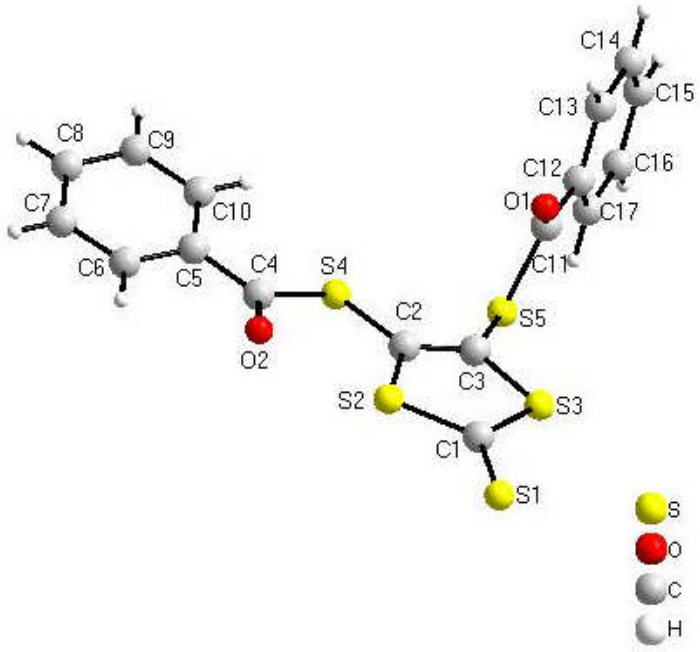

Figure B-16: Molecular structure of L_0 (Hydrogen atoms are not numbered for clarity).

The molecular structure with the atom numbering for **L_0** is shown in Figure B-17 and selected bond lengths and angles are reported on Table B-11.

Table B-10: Crystal data and structure refinements for L_0.

Identification code	sh2281
Empirical formula	C17 H10 O2 S5
Formula weight	406.595
Temperature	103(2) K
Wavelength	0.71073 Å
Crystal system	Monoclinic
Space group	P2(1)/c
Unit cell dimensions	a = 9.6204(3) Å α= 90°.
	b = 10.5705(3) Å β= 92.783(2)°.
	c = 16.9777(5) Å γ = 90°.

Volume	1724.47(9) $Å^3$
Z	3
Density (calculated)	1.566 Mg/m^3
Absorption coefficient	0.679 mm^{-1}
F(000)	832
Crystal size	0.65 x 0.43 x 0.25 mm^3
Theta range for data collection	2.40 to 40.55°.
Index ranges	-16<=h<=17, -19<=k<=18, -29<=l<=30
Reflections collected	39084
Independent reflections	10615 [R(int) = 0.0231]
Completeness to theta = 40.55°	96.1 %
Absorption correction	Multiscan
Max. and min. transmission	0.8486 and 0.6667
Refinement method	Full-matrix least-squares on F^2
Data / restraints / parameters	10615 / 0 / 217
Goodness-of-fit on F^2	1.067
Final R indices [I>2sigma(I)]	R1 = 0.0312, wR2 = 0.0835
R indices (all data)	R1 = 0.0376, wR2 = 0.0893
Largest diff. peak and hole	1.366 and -0.752 $e.Å^{-3}$

Table B-11: Selected bond lengths (Å) and angles (°) for L_0.

S(1)-C(1)	1.647(8)	S(1)-C(1)-S(3)	125.72(5)
S(2)-C(1)	1.737(8)	S(1)-C(1)-S(2)	120.64(4)
S(2)-C(2)	1.750(7)	S(3)-C(1)-S(2)	113.65(4)
S(3)-C(1)	1.729(8)	C(3)-C(2)-S(2)	115.62(6)
S(3)-C(3)	1.745(8)	C(3)-C(2)-S(4)	118.98(6)
S(4)-C(2)	1.756(8)	S(2)-C(2)-S(4)	125.30(4)
S(4)-C(4)	1.785(8)	C(2)-C(3)-S(3)	116.68(6)
S(5)-C(3)	1.749(8)	C(2)-C(3)-S(5)	124.54(6)
S(5)-C(11)	1.814(8)	S(3)-C(3)-S(5)	118.52(4)
O(1)-C(11)	1.207(1)	O(2)-C(4)-C(5)	123.04(8)
O(2)-C(4)	1.211(1)	O(2)-C(4)-S(4)	122.13(7)
C(2)-C(3)	1.360(1)	C(5)-C(4)-S(4)	114.83(6)

C(4)-C(5)	1.479(1)	C(10)-C(5)-C(6)	120.33(7)
C(5)-C(10)	1.400(1)	C(9)-C(8)-C(7)	120.63(8)
C(5)-C(6)	1.401(1)	C(10)-C(9)-C(8)	120.01(8)
C(6)-C(7)	1.390(1)	O(1)-C(11)-C(12)	125.08(7)
C(7)-C(8)	1.393(1)	C(12)-C(11)-S(5)	112.99(6)
C(8)-C(9)	1.392(1)	C(17)-C(12)-C(13)	120.18(7)
C(9)-C(10)	1.392(1)	C(13)-C(14)-C(15)	120.07(8)
C(11)-C(12)	1.487(1)	C(16)-C(15)-C(14)	120.21(8)
C(12)-C(17)	1.397(1)	C(15)-C(16)-C(17)	119.93(8)
C(12)-C(13)	1.400(1)	C(16)-C(17)-C(12)	119.81(7)
C(1)-S(2)-C(2)	97.06(4)		
C(1)-S(3)-C(3)	96.93(4)		

The molecular structure shows the same orientation of the phenyl groups towards the DMIT plane, as previously observed.[100, 101] The phenyl rings (of the benzoyl groups) are inclined at angle of 83.32(4)° with respect to one another. One phenyl ring (C5.-C10) is nearly coplanar with the DMIT ring and the second one (C12-C17) is inclined about 82.7(5)° with respect to the DMIT ring. In the precedent cases, the determined structure consisted of discrete molecules of **L_0** kept together by Van der Waals packing forces.[100-102] The sulfur atom of the thione function (C=S) is situated at 0.217(1) Å from the plane of the five-membered ring, compared to a value of 0.178 (5) Å observed by Solans *et al.,* for the same molecule.[100]

In the present case, hydrogen bonding between the hydrogen in para position of the phenyl group and oxygen from the adjacent carbonyl group supports the polymer-like structure as shown in Figure B-17. Molecules of **L_0** are connected in a tail-to-tail fashion. No $\pi-\pi$ interaction or short S•••S contacts were detected.

Figure B-17: One dimensional molecular structure arrangement of L_0 with an emphasis on the hydrogen bonding.

These C(sp^2)-H•••O distances of 2.330(1) Å evidence the presence of such interaction. This distance is clearly shorter than that observed in the EDT-TTF-COOH and EDO-TTF-COOH with C(sp^3)-H•••O distances of 2.63(3) and 2.54(5) Å, respectively.[78] The angle C(sp^2)-H•••O of 164.51(2)° is slighted deviated from linearity. This kind of interaction contributes to keep the molecules in the way they are arranged. [103]

This unusual hydrogen bonding interaction arranges the molecules in a one-dimensional structure (see Figure B-17) which is different from the 3D structure (due to packing forces[101]). Such a one dimensional structure was not expected since the DMIT ring and the phenyl ring are appropriate candidates for building π–π interaction more than hydrogen bonding interaction.

B.5 Conclusion

We have focussed in this chapter on the ease of chemical modification of the DMIT moiety to access to functionalised dithiolene ligands. By introducing functional groups such as carboxylic acid or alcohol on the DMIT core, we have demonstrated that the solid-state organisation of the structure results from several non-covalent interactions, which in our opinion are important tools for supramolecular assemblies.

In all cases, hydrogen bonding play an dominant role in the stabilisation of the supramolecular structure, which are more important than other interactions such as π–π interactions, and intermolecular S•••S van der Waals interactions, which are also present in some molecular structures.

Functionalisation as tool for the synthesis of Dithiolene-like neutral ligands

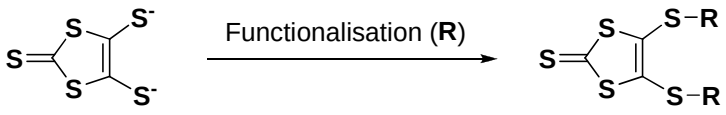

Examples of Dithiolene-like neutral ligands:

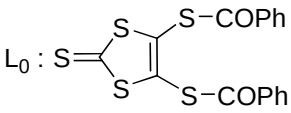

[4,5-bis(benzoylthio)-1,3-dithiole-2-thione]

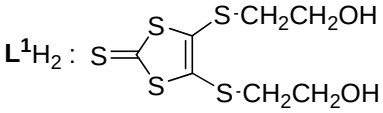

[4,5-bis(2-hydroxyethylthio)-1,3-dithiole-2-thione]

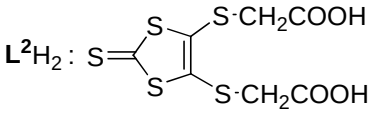

[4,5-bis(carboxymethylthio)-1,3-dithiole-2-thione]

The structural features of **L^2H_2.THF** represent a typical model showing that lone-pair directionality can be, to a certain extent, related to the propensity of an acceptor molecule to form hydrogen bonding in the direction of the lone-pairs. Such ligands could be used to coordinate metal centers by either coordination through sulphur from the DMIT ring (for soft metals) or through oxygen from the functional groups (for hard metals). These possibilities will be studied in chapters C and D, respectively.

CHAPTER C. PREPARATION OF DITHIOLENE COMPLEXES CONTAINING CLOSED-SHELL (d^{10}) TRANSITION METALS: Supramolecular Metallo-Dithiolene Frameworks.

C Supramolecular Metallo-dithiolene Frameworks

C.1 Background

As stated by Pyykkö, between closed–shell species of zero charge or same nominal charge, no strong attractions have to be expected.[104] Contrarily, strong covalent bonds are expected between open-shell species if more bonding molecular orbitals than antibonding MOs are filled. The detection of metal•••metal contacts shorter than the sum of van der Waals radii between linear d^{10} transition metal complexes in numerous crystal structures has stimulated research in the area of coordination complexes containing closed-shell (d^{10}) metals.[104] Recent developments in the coordination chemistry have emphasised on synthesis of supramolecular architectures, as a flourishing domain. These architectures are obtained via self-assembly processes involving metal ions and in-organic ligands. In our team, we have investigated the synthesis of metallo-supramolecular systems by using ligands that present themselves non-covalent bonding.

C.1.1 Generalities

The synthesis and characterization of new metal-organic architectures is a current research interest in coordination and supramolecular chemistry owing to the enormous variety of structures and topologies, as well as their potential applications as functional materials. Remarkable luminescence properties are at the origin of the increasing interest of scientists with the aim of constructing metal-organic frameworks (MOF) that could find potential applications in the area of optoelectronic devices, chemical sensors[105], biological imaging, photochemical catalysis, light-driven fuel production[106], gas storage, molecular recognition, etc. [107]

The coordination complexes of d^{10} metals present in some cases significant advantages over the derivatives made of opened-shell like d^6 coordination compounds complexes. For example, they offer a large variety of coordination geometries, compared to the almost octahedral geometry of d^6 metals, which make them ideal building blocks for the synthesis of sophisticated molecular architectures.[108]

C.1.2 Closed-shell systems (d^{10}-d^{10} interactions)

Among the metals used for the elaboration of MOF containing short M•••M distances, those having a closed-shell (d^{10}) electronic configuration have been successfully used. Such metal•••metal interaction was observed for copper (Cu^{I}) with distances lying between 2.63 to 3.5 Å,[104] gold (Au^{I}) with distances lying between 2.7 to 3.5 Å [109], silver (Ag^{I}) with distances lying between 2.97 [110] to 3.07 Å.[111] In the case of mercury (Hg^{II}), metal•••metal interactions, with distances ranging the 2.84 Å, were also detected.[112] In some mercury (II) acetylides [$Hg(C\Xi CR)_2$; where R= -Ph or -$SiMe_3$], obtained as aggregates, Hg•••Hg distances between 3.5 Å and 4.25 Å were also found.[113, 114] In the case of gold, this metal•••metal interaction was termed as aurophilicity by Schmidbaur.[115] By extension, the term metallophilicity was commonly used to denote the metal•••metal interaction.

It is also important to mentioned that this interaction is not only restricted to homometallic species, di-coordinated complexes or group 11 metals. For instance, heterometallic species (Cu•••Hg[116] and Au•••Hg[117]), tri-coordinated d^{10} compounds, but also group-10-metal complexes have been reported.[118]

Metal-metal interactions are observed in different structural motifs varying from unbridged (A), singly bridges (B), doubly bridges (C), chain-like (D), cluster-like (E) and connected through hydrogen bonding (F) (see Scheme C-1).

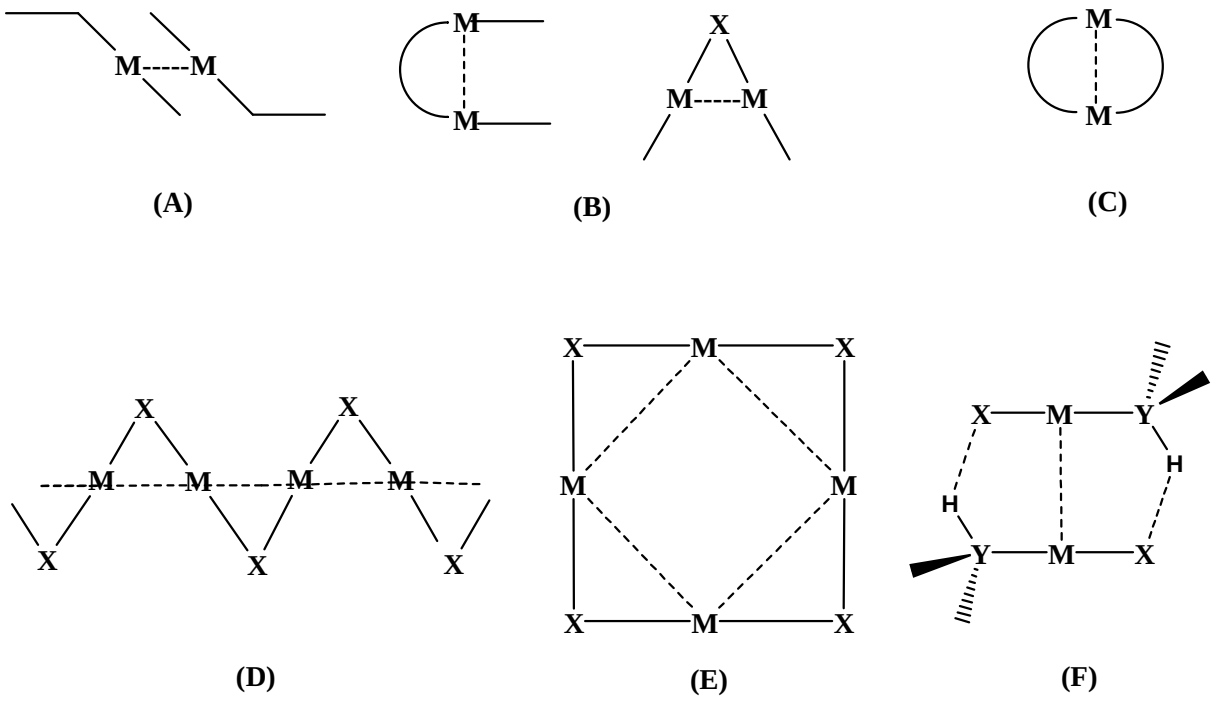

Scheme C-1: Various coordination modes and structural motifs found in di- and polynuclear d^{10}•••d^{10} metal coordination complexes.[119]

According to EHMO (extended Hückel molecular orbital) calculations, the origin of the metal-metal interaction in the case of copper is repulsive if only the filled 3d orbitals are considered. However, the same calculations taking also into account the contribution of the empty 4s and 4p orbitals, have argued on the attractive nature of this kind of interaction.[120, 121]

Such coordination complexes have been targeted because of their potential application in material science, especially in photoluminescence and /or electroluminescence.[122] The first luminescent study of such metallo-complexes build up through self-assembly in the presence of a coinage metal can be traced back to 1970.[123]

C.2 Spectroscopic properties

C.2.1 Spin-orbit coupling (SOC) and crystal field (CF) splitting

Electronic transitions within the same orbital type (d-d, f-f, etc…) are Laporte forbidden[69]. However this rule is relaxed by spin–orbit coupling (SOC) and/or ligand

field (crystal field (CF)) effects. Both (SOC and CF) can split the energy levels, which are degenerated in the free metal ion configuration. The influence of these two factors in the splitting of the energy levels depends on the nature of the orbital and the geometry around the metal center. For instance, SOC has a stronger influence on f metal group elements than on d elements. In contrast, the CF splits the energy level in d metal to levels separated approximately about 10000 cm^{-1} compared to 100 cm^{-1} for f elements.[61]

C.2.2 Electronic transitions in d^{10} transition metal complexes

Because of the completely filled metal d-sub-shell (d^{10}), the electronic ground states of the coordination compounds containing a d^{10} metal center can not be subject to the CF effect, contrarily to other transition metals (d^{1-9}). Furthermore, they do not experience the Jahn-Teller effect, which is encountered in paramagnetic Cu(II) compounds with an electronic d^9 configuration.

These factors (SOC and CF) are not the only ones governing the spectroscopic properties giving rise to electronic transitions. Other types of electronic transitions such as LMCT (Ligand-to-Metal Charge Transfer), MLCT (Metal-to-Ligand Charge Transfer) and IL (Intra-Ligand) transitions may influence the spectroscopic properties of metal complexes. Figure C-1 shows a schematic representation of transitions that can take place in a coordination compound.[124]

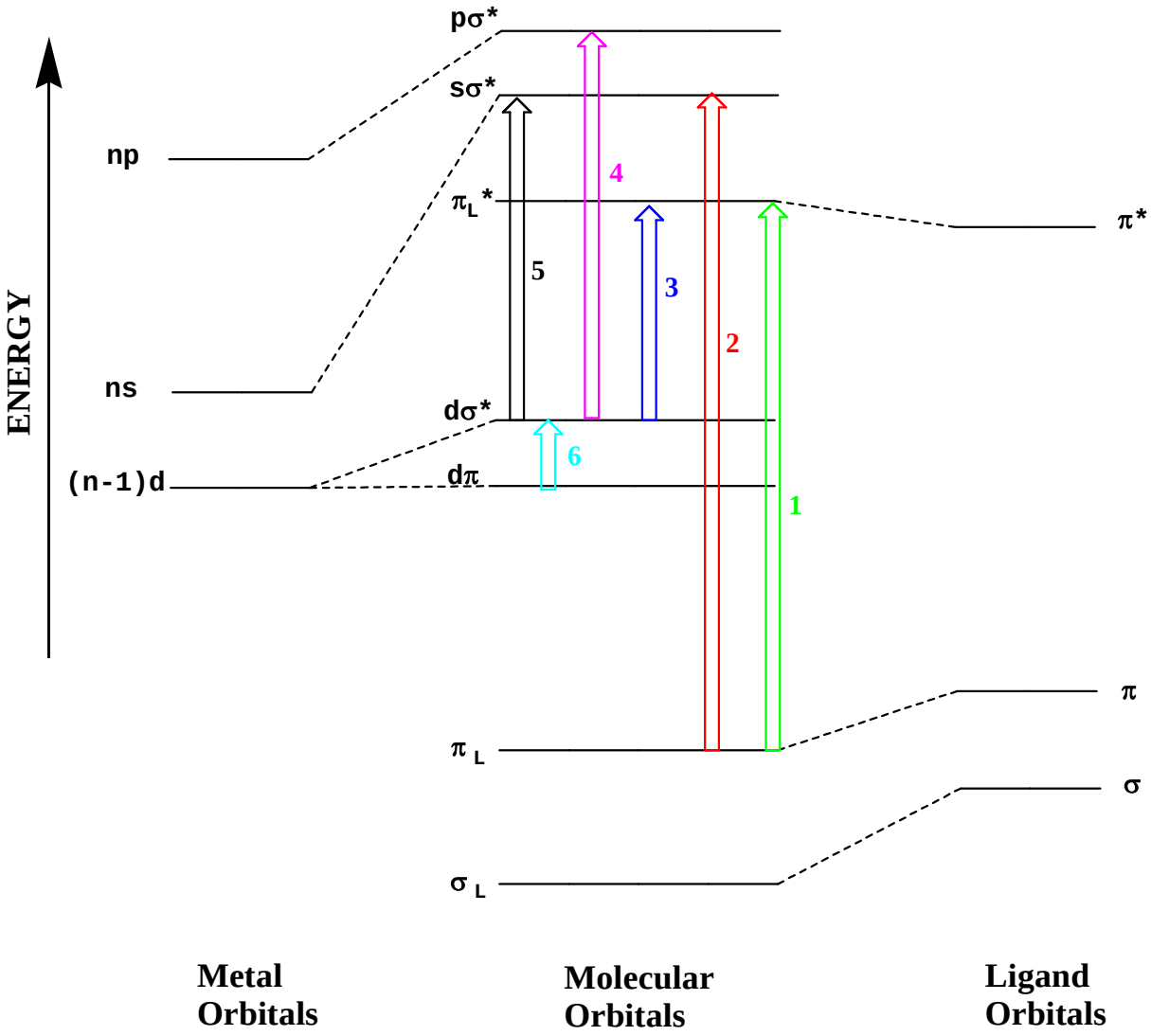

Figure C-1: Schematic energy level diagram of molecular orbitals and electronic transition in an octahedral coordination compound. (NB: for simplicity, all orbitals of a given type are represented by a single energy level. The p orbitals, for example, may be bonding, non-bonding or anti-bonding in character).[124]

Six different transitions may be observed:

- (**1**) is an intraligand (IL) transition:
- (**2**) is a LMCT transition:
- (**3**) is a MLCT transition:
- (**4**) is an intraconfigurational metal-centered, d-p transition:
- (**5**) is an intraconfigurational metal-centered, d-s transition:
- (**6**) is a ligand field transition (absent in d^{10} complexes).

C.2.3 Why are dithiolene-d^{10} transition metal complexes interesting?

Research on metallo-dithiolene based complexes and their photophysical properties is not new (former use in detection[125]). Dithiolene-like neutral ligands with their π-system are potential candidates for spectroscopic studies in which electronic transitions represent the basic key.

On the other hand, closed-shell d^{10} metal complexes are known to exhibit luminescent properties that are sensitive to a subtle change in the environment and/or arrangement around the metal atoms. The modification of the ligand skeleton is a way for finely tuning the luminescence of ligand-metal based complexes.[126, 127]

Dithiolene which is a sulfur-rich system fits well to the database of ligands suitable for building coordination complexes with metals in a d^{10} electronic configuration. In fact, these d^{10} metals in their respective oxidation state Cu^{+}, Ag^{+}, Au^{+}, Hg^{2+} etc., are classified as “soft” according to HSAB (Hard and Soft Acid and Base) principle.

Functional groups like alcohol and carboxyl are potential candidates for building supramolecular structure by increase of the dimensionality through hydrogen bonding. The combination of electron-rich dithiolene ligand with closed-shell d^{10} metal appears tempting for the elaboration of coordination complexes exhibiting both intriguing photoluminescent properties and presenting unique supramolecular arrangements in the solid-state.

C.2.4 The d^{10} “Avenue”

The d^{10} “Avenue” represents the elements of the IB and IIB columns of the periodical table.[108] The term “d^{10} Avenue” is in relation with their electronic configuration in certain oxidation states, namely +1 for IB column and +2 for the IIB column.

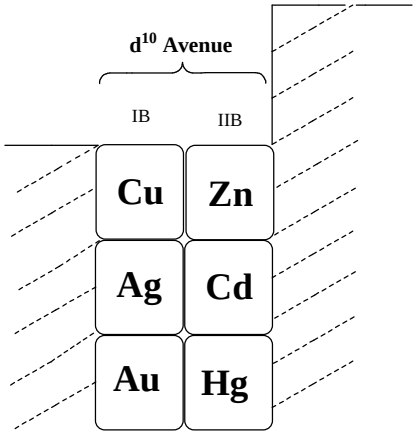

In their coordination complexes, these elements adopt a wide variety of structural arrangements from linear chains to 3D (three-dimensional) networks. Another collective property in these d^{10} metals complexes is that they display M•••M contacts that are shorter than the sum of the van der Walls radii (3.32 Å for Au(I), 3.44 Å for Ag(I) and 2.80 Å for Cu(I)).[128]

Among these elements, copper, silver and gold form also a sub-group known as "coinage metals[129]" because of their former usage and their resistance to corrosion. They are also known for their biochemical activity. Copper and silver have antibacterial activities whereas gold (Au^{I}) thiol has found increasing use in the treatment of rheumatoid arthritis.[58]

C.3 Objectives

In this study, we intend to investigate the possibility of building metallo-supramolecular systems based on the ligands presented in the chapter B (**L_0**, **L^1H_2** and **L^2H_2**) and d^{10} transition metals like Hg^{II}, Cu^{I} and Au^{I}. The combination of non-bonding interactions taking place in these complexes will be discussed in term of supramolecular assemblies. Structural modification in the ligand arrangement, (compared to the free ligands) induced by the closed-shell metal center will be also analysed. And finally, luminescent studies on these complexes will be investigated.

C.4 Synthesis, characterisation and luminescent properties of dithiolene complexes containing closed-shell (d^{10}) transition metals

C.4.1 Synthesis and characterisation of copper (I)-dithiolene complexes

Here we will present complexes of type **L^i-CuI** where **L^i** represents a dithiolene-like neutral ligand ligated on copper Iodide. This work was motivated by previous results, in our group, on copper coordination polymers assembled by using dithioether ligands.[130] Various structural topologies have been found in copper halide coordination polymers and they can vary from square rhomboid to hexagonal grid chains.[131] Apart from their fascinating architectures the interest in assembling copper iodide coordination compounds results in their remarkable photophysical properties.
The synthetic pathway is outlined in Scheme C-2 and the procedure follows that from reference 130.

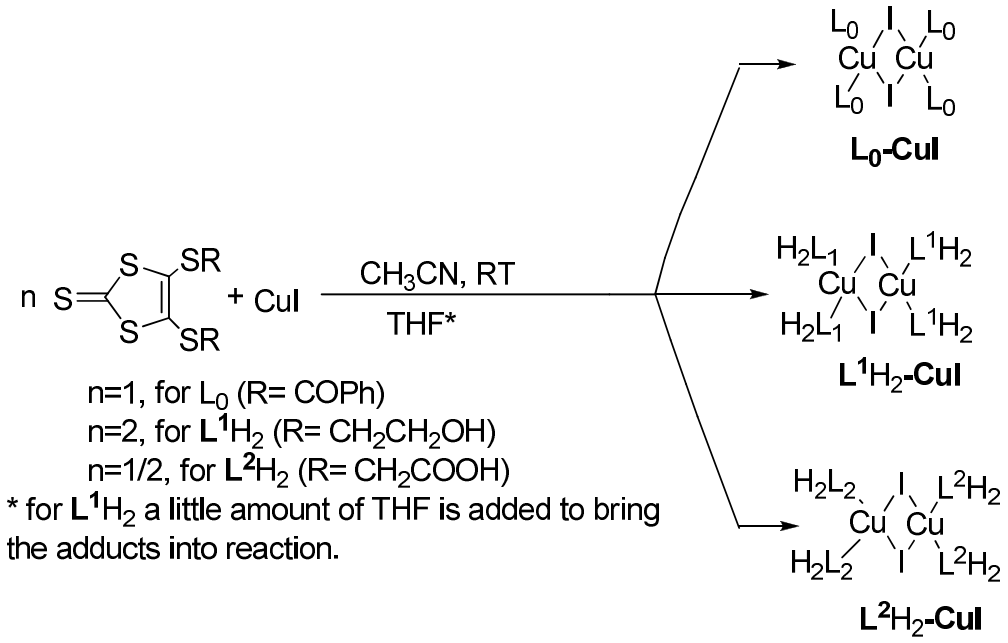

Scheme C-2: Reaction pathways for the synthesis of copper complexes.

The clear solution obtained after stirring a suspension of CuI in acetonitrile at room temperature, turns immediately red when equimolar amounts of the ligands dissolved in acetonitrile (for **L_0** and **L^2H_2**) and THF (for **L^1H_2**) are added. The mixture is stirred for additional 1h during which the intensity of the red color is growing. The mixture is then filtrated and reduction of the volume followed by cooling to a lower temperature

allowed the isolation of red crystals (for **L_0-CuI** and **L^2H_2-CuI**) suitable for X-ray measurements. In the case of **L^1H_2-CuI**, we failed in isolating crystals suitable for X-ray analysis. The characterisation was completed by NMR, infrared spectroscopy, elemental analysis and UV-Vis spectroscopy. For a better comparison, characteristic data in the infrared spectroscopy and UV-Vis of the free ligands are also presented.

C.4.1.1 Synthesis and characterisation of L_0-CuI

C.4.1.1.1 IR and UV-Vis results for L_0-CuI

The different analytical data are presented in Table C-1. For clarity, only the characteristic data (of the ligands) able to present changes (or shift) due to the coordination on the metal are reported.

Table C-1: Analytical data from IR and UV-Vis measurements.

		L_0	L_0-CuI
IR	ν (C=S) in cm-1	1055	1026
	ν (C=O) in cm-1	1670	1668
Uv-Vis (CH_3CN)	λ^{max} in nm (ε)	366.6 (36333)	366 (27599)

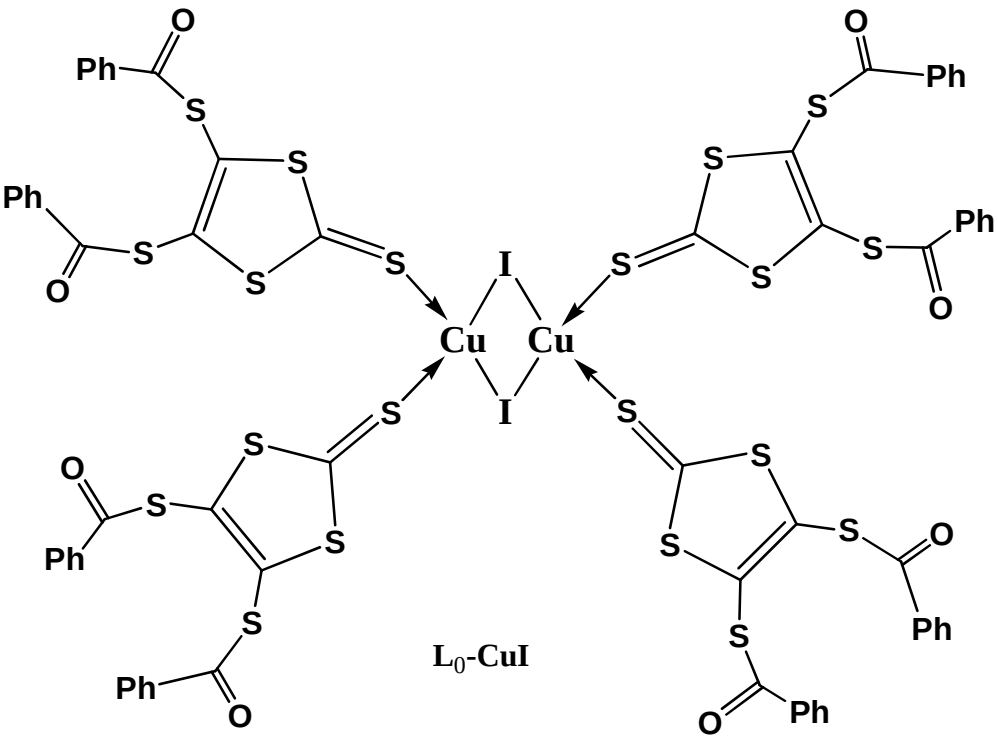

L_0-CuI

The first evidence that coordination occurs via the thiocarbonyl function (C=S) is provided by the shift of the ν C=S band from 1055 to 1026 cm^{-1}. Such a coordination is not new and has been previously observed in the case of 4,5-ethylenedithio-1,3-dithiole-2-thione[132] and 4,5-bis(methylthio)-1,3-dithiole-2-thione[133] with copper iodide. In the later case a shift of 23 cm^{-1} to lower wavenumbers was recorded for the C=S stretching frequency[133] compared to the free ligand. The position of the carbonyl ν(C=O) vibration remains unchanged indicating that no C=O group is involved in a coordination bond. In the UV-Vis part, the absorption band at 366 nm assigned to π–π* transition was not affected by this coordination. However, a slightly decrease of the extinction coefficient was observed.

C.4.1.1.2 Structural description of L_0-CuI

Red crystals of **L_0-CuI** were grown within a period of 1 day from a concentrated acetonitrile solution of the reaction mixture. A crystal was isolated and a single crystal X-ray diffraction analysis was performed at 170 K. **L_0-CuI** crystallises in the triclinic system in the centrosymmetric space group $P\bar{1}$. The molecular structure with the atom numbering for **L_0-CuI** is shown in Figure C-2 and selected bond lengths and angles are reported in Table C-2.

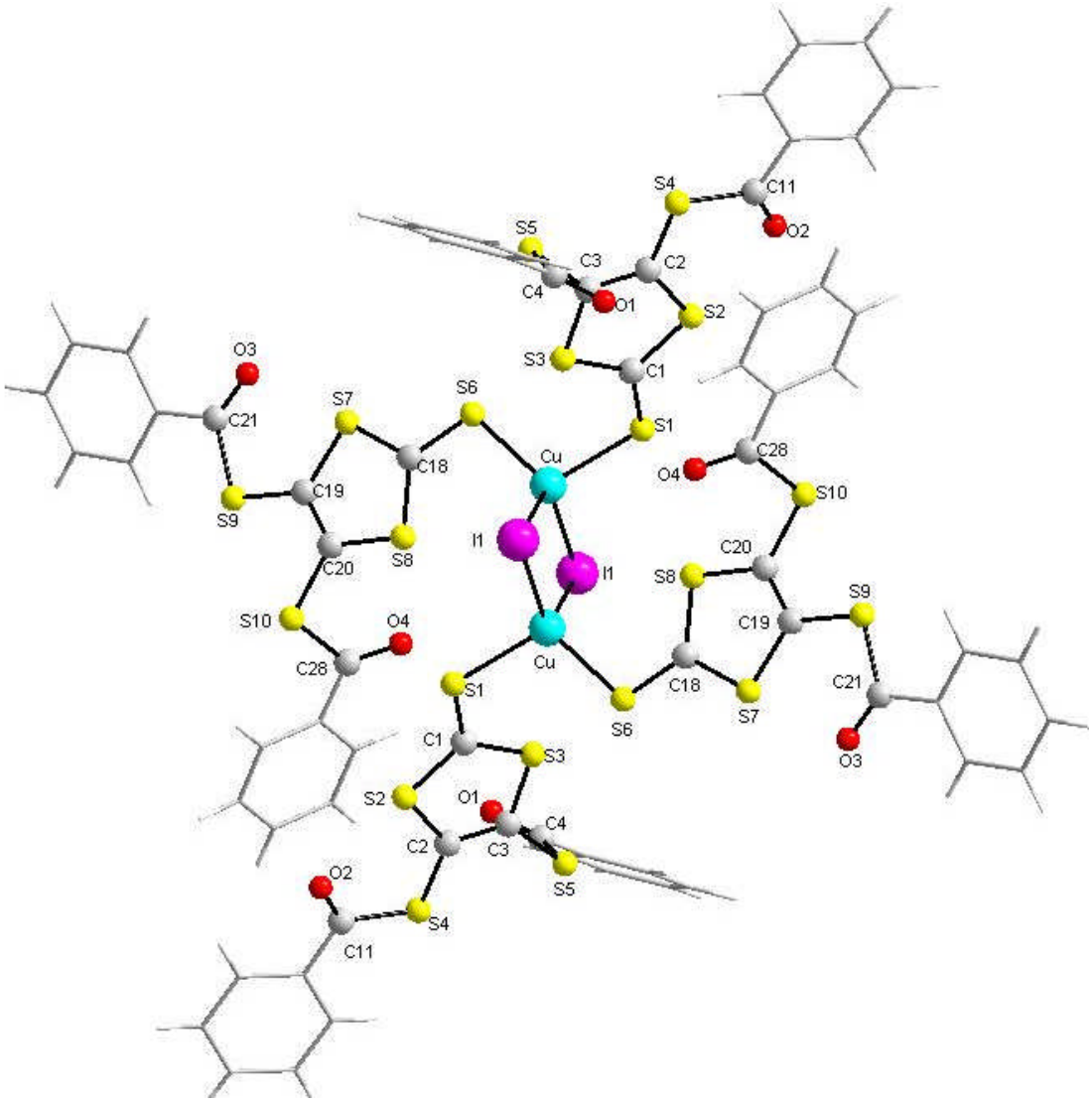

Figure C-2: The molecular structure for L_0-CuI (for clarity the numbering of the phenyl groups is not included, and the phenyl groups are represented as wires).

Table C-2: Crystal data and structure refinement for L_0-CuI.

Identification code	sh2465
Empirical formula	C74H40Cu2I2O8S20
Formula weight	2079.14
Temperature	170(2) K
Wavelength	0.71073 Å
Crystal system	Triclinic
Space group	$P\bar{1}$

Unit cell dimensions	a = 12.1861(6) Å α= 62.198(2)°.
	b = 13.5080(6) Å β= 84.796(2)°.
	c = 13.5835(6) Å γ = 87.493(2)°.
Volume	1969.71(16) $Å^3$
Z	1
Density (calculated)	1.753 Mg/m^3
Absorption coefficient	1.909 mm^{-1}
F(000)	1032
Crystal size	0.6 x 0.3 x 0.15 mm^3
Theta range for data collection	1.68 to 36.34°.
Index ranges	-20<=h<=18, -20<=k<=22, -22<=l<=22
Reflections collected	55470
Independent reflections	18876
Completeness to theta = 36.34°	98.7 %
Absorption correction	None
Refinement method	Full-matrix least-squares on F^2
Data / restraints / parameters	18876 / 0 / 463
Goodness-of-fit on F^2	0.967
Final R indices [I>2sigma(I)]	R1 = 0.0347, wR2 = 0.0844
R indices (all data)	R1 = 0.0618, wR2 = 0.0969
Largest diff. peak and hole	1.438 and -0.681 $e.Å^{-3}$

Figure C-3 represents different structural motifs found in copper complexes. The cubane tetramer (**I**) is the most frequently observed form,[131, 134-138] but in some cases the rhomboid $Cu_2(\mu_2\text{-}I)_2$ dimer form (**III**) has been encountered. [127, 131, 139, 140]

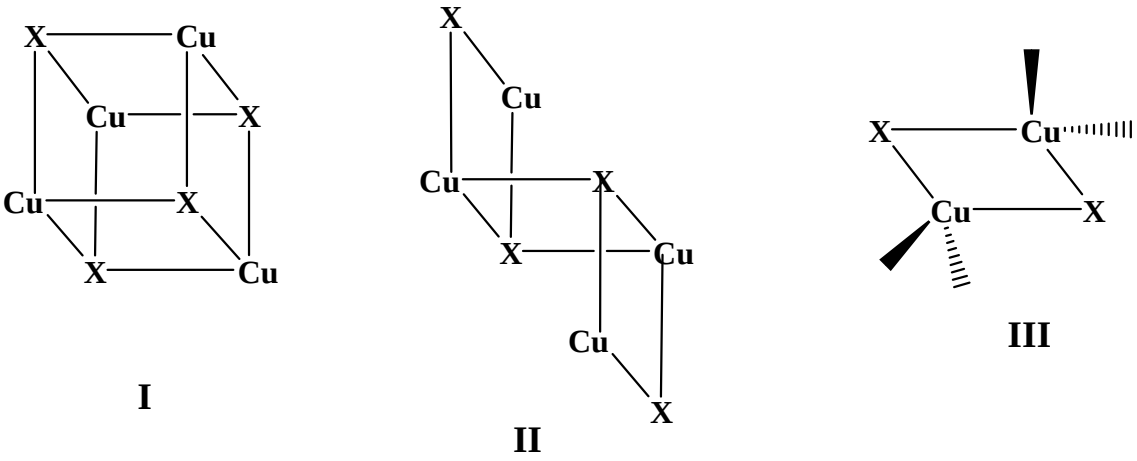

Figure C-3: Different structural motifs found in copper halide coordination compounds: the "cubane-like " form (I) , the "step" form (II) and the "rhombohedral dimer" form (III).

As evidenced by the X-ray analysis (see Figure C-2), the molecule is found in a rhomboid $Cu_2(\mu_2\text{-}I)_2$ dimer form (**III**).

The orientation of the benzoyl groups towards the DMIT plane is similar in **L_0** and **L_0-CuI**. The metal lies in a distorted tetrahedral environment formed by two S atoms of distinct **L_0** ligands and two bridging iodine atoms, with I-Cu-I and S-Cu-S angles of 109.29(1)° and 106.63(2)° respectively (Figure C-4).

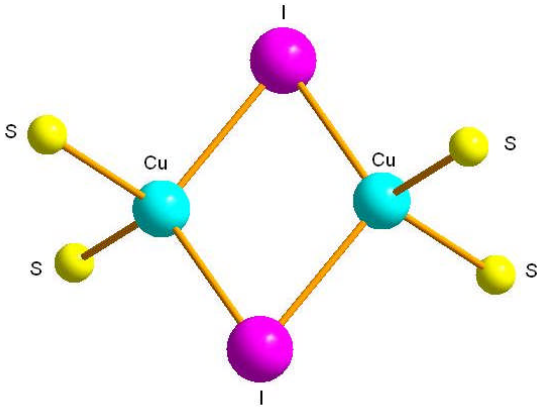

Figure C-4: Zoom in the Cu_2I_2 core in L_0-CuI showing the rhombohedral dimer form and the tetrahedral environment around the copper atoms (the rest of the complex is omitted for clarity).

The average distance of the two Cu-S bonds of 2.314(2) Å is slightly longer than the value of 2.284(1) Å reported for a dithiolene-like neutral –copper complex $[(Cu_2(\mu^2\text{-}I)_2(DMIT\text{-}Me_2)]$, exhibiting the similar rhombohedral Cu_2I_2 core. [133]

The average Cu•••Cu separations length of 3.051(1) Å in **L_0-CuI** is somewhat longer than that of 2.806(1) Å reported for a similar rhomboid dimer form $[(Cu_2(\mu^2\text{-}I)_2(\mu\text{-}PhS(CH_2)_2SPh)_2]$ using a dithioether ligand.[130] The Cu•••Cu separations in **L_0-CuI** is in

the upper limit range representing metallophilic interactions[139] for homopolynuclear copper complexes. As stated by Novoa *et al.*[119] such an weak intermolecular Cu•••Cu contact could not be considered as an attractive interaction since the bridging iodide can geometrically impose the two Cu centers to come closer. According to Novoa *et al*., the best Cu•••Cu interactions are localized in dimer without bridging ligands. A view of the packing mode presented in Figure C-5 showed the existence of a network which is probably supported by packing forces, since no close contacts between adjacent motifs was identified. The C=S bond is 0.013 Å longer than in the uncoordinated ligand (**L_0**). [100]

Table C-3: Bond lengths [Å] and angles [°] for L_0-CuI.

C(1)-S(1)	1.660(2)	S(6)-C(18)-S(8)	124.52(1)
C(1)-S(3)	1.715(2)	S(6)-C(18)-S(7)	120.41(1)
C(1)-S(2)	1.731(2)	S(8)-C(18)-S(7)	115.06(1)
C(2)-C(3)	1.359(2)	C(20)-C(19)-S(7)	115.44(1)
C(2)-S(4)	1.747(2)	C(20)-C(19)-S(9)	118.99(1)
C(2)-S(2)	1.750 (2)	S(7)-C(19)-S(9)	125.56(1)
C(3)-S(3)	1.741(2)	C(19)-C(20)-S(8)	117.08(1)
C(3)-S(5)	1.749(2)	C(19)-C(20)-S(10)	121.98(2)
C(4)-O(1)	1.202(2)	S(8)-C(20)-S(10)	120.87(1)
C(4)-C(5)	1.479(3)	O(3)-C(21)-C(22)	124.41(2)
C(4)-S(5)	1.825(2)	O(3)-C(21)-S(9)	121.88(2)
C(5)-C(10)	1.382(3)	O(4)-C(28)-C(29)	125.03(2)
C(5)-C(6)	1.385(3)	O(4)-C(28)-S(10)	120.94(2)
C(6)-C(7)	1.390(3)	C(33)-C(34)-C(29)	120.0(2)
C(7)-C(8)	1.372(4)	S(1)-Cu(2)-S(6)	106.626(2)
C(8)-C(9)	1.364(4)	S(1)-Cu-I(1)	111.146(2)
C(9)-C(10)	1.392(3)	S(6)-Cu-I(1)	114.295(2)
C(11)-O(2)	1.205(2)	S(1)-Cu-I(1)#1	102.493(1)
C(11)-C(12)	1.490(2)	S(6)-Cu-I(1)#1	112.335(2)
C(11)-S(4)	1.793(2)	I(1)-Cu-I(1)#1	109.292(1)
C(16)-C(17)	1.394(3)	S(1)-Cu-Cu#1	119.882(2)
C(18)-S(6)	1.664(2)	S(6)-Cu-Cu#1	133.143(2)

C(18)-S(8)	1.705(2)	I(1)-Cu-Cu#1	54.922(9)
C(18)-S(7)	1.725(2)	I(1)#1-Cu-Cu#1	54.370(8)
C(19)-C(20)	1.355(2)	Cu-I(1)-Cu#1	70.708(1)
C(19)-S(7)	1.743(2)	C(1)-S(1)-Cu	108.40(6)
C(19)-S(9)	1.753(2)	C(1)-S(2)-C(2)	96.70(8)
C(20)-S(8)	1.734(2)	C(1)-S(3)-C(3)	96.33(8)
C(20)-S(10)	1.750(2)	C(2)-S(4)-C(11)	103.22(8)
C(21)-O(3)	1.209(2)	C(3)-S(5)-C(4)	100.55(9)
C(21)-C(22)	1.474(3)	C(18)-S(6)-Cu(2)	106.60(6)
C(21)-S(9)	1.785(2)	C(18)-S(7)-C(19)	96.18(9)
C(26)-C(27)	1.378(4)	C(18)-S(8)-C(20)	96.15(9)
C(28)-O(4)	1.199(2)	C(19)-S(9)-C(21)	103.84(9)
Cu-S(1)	2.304(5)	C(20)-S(10)-C(28)	99.58(9)
Cu-S(6)	2.325(6)	C(36)-C(35)-C(37)	124.3(8)
Cu-I(1)	2.627(3)	C(35)-C(36)-C(37)#2	131.6(9)
Cu-I(1)#1	2.645(3)	C(36)#2-C(37)-C(35)	98.6(8)
Cu-Cu#1	3.051(5)	C(3)-C(2)-S(4)	119.22(1)
I(1)-Cu#1	2.645(3)	C(3)-C(2)-S(2)	115.09(1)
C(35)-C(36)	1.314(9)	S(4)-C(2)-S(2)	125.68(1)
C(35)-C(37)	1.483(1)	C(2)-C(3)-S(3)	117.23(1)
C(36)-C(37)#2	1.322(1)	C(2)-C(3)-S(5)	126.12(1)
C(37)-C(36)#2	1.322(1)	S(3)-C(3)-S(5)	116.58(1)
		O(1)-C(4)-C(5)	125.73(2)
S(1)-C(1)-S(3)	124.56(1)	S(3)-C(1)-S(2)	114.54(9)
S(1)-C(1)-S(2)	120.90(1)		

(Symmetry transformations used to generate equivalent atoms; #1 -x+1,-y,-z+1 ; #2 -x+1,-y+1,-z+1)

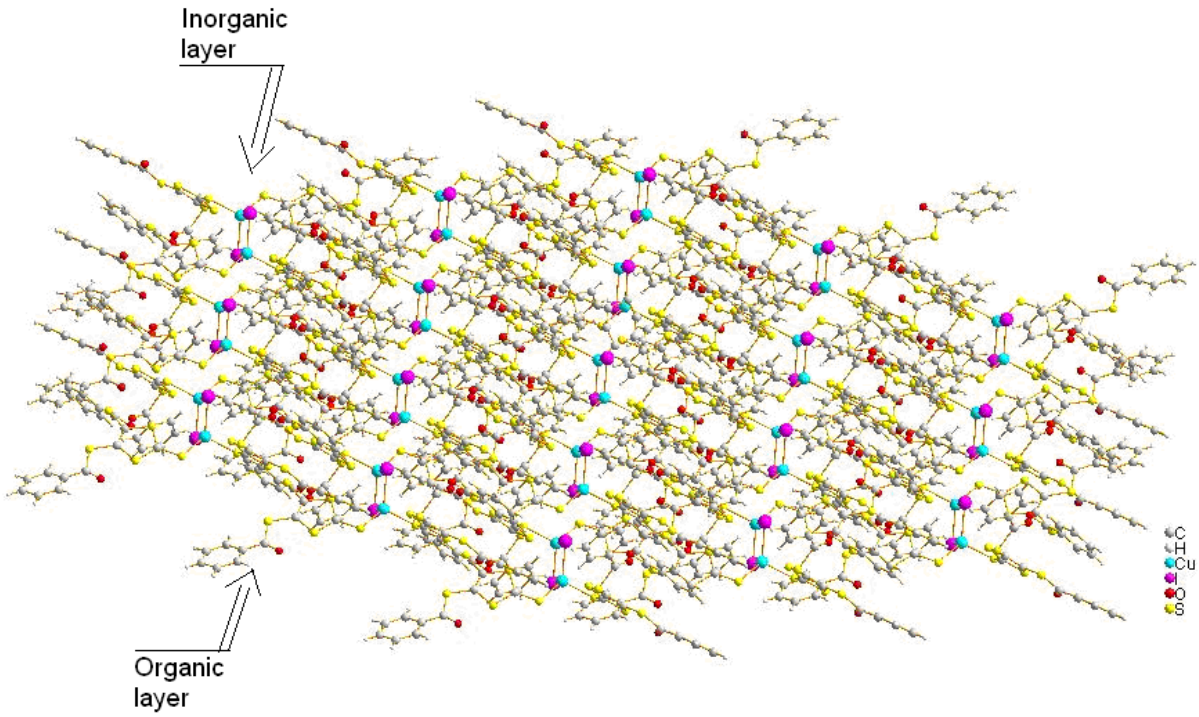

Figure C-5: Block structure showing dimers kept together by packing forces. The network is formed by a succession of inorganic and organic layers.

Another view shows a network formed by a succession of inorganic (Cu_2I_2 layers) and "organic" (organic layers are formed by dithiolene-like neutral ligands) layers.

C.4.1.2 Synthesis and characterisation of L^1H_2-CuI

L^1H_2-CuI was obtained as a yellow-orange powder from the concentrated acetronitrile-THF solution of the reaction mixture. Attempts to grow crystals were unsuccessful and a rapid formation of agglomerates within a period of minutes was always observed. But, elemental analysis and IR permits to conclude in a 2:1 ligand-metal ratio and a coordination mode via the sulfur of the thiocarbonyl bond. Table C-4 shows the analytical data obtained from the IR and UV-Vis analysis.

Table C-4: Analytical data from IR and UV-Vis measurements for L^1H_2-CuI.

		L^1H_2	L^1H_2-CuI
IR	ν (C=S) in cm^{-1}	1074	1033
	ν (O-H) in cm^{-1}	3272	3245
Uv-Vis (CH_2Cl_2)	λ^{max} in nm (ε)	380 (47820)	380 (24840)

The band at 1074 cm^{-1} corresponding to the thiocarbonyl function (C=S) is shifted to lowers values in the complex (1033 cm^{-1}). This means that the complex (**L^1H_2-CuI**) is formed by coordination via the C=S. The O-H vibration bands are situated in the 3200 cm^{-1} region showing a hydrogen bonding network (non-bonded or free O-H are generally localised around 3500 cm^{-1} [141]). The absorption spectrum of the complex shows no significant difference compared to that of the free ligand. Both **L^1H_2-CuI** and the free ligand **L^1H_2** present a maximum at 380 nm. The only difference is the lower extinction coefficient in **L^1H_2-CuI** (24840 $M^{-1}.cm^{-1}$ for **L^1H_2-CuI** against 47820 $M^{-1}.cm^{-1}$ for **L^1H_2**).

C.4.1.3 Synthesis and characterisation of L^2H_2-CuI

C.4.1.3.1 IR and UV-Vis results for L^2H_2-CuI

The Table C-5 gives some analytical data on **L^2H_2-CuI**, and **L^2H_2** for comparison.

Table C-5: Analytical data from IR and UV-Vis measurements.

		L^2H_2	L^2H_2-CuI
IR	ν (C=S) in cm^{-1}	1065	1028
	ν (C=O) in cm^{-1}	1692	1685
	ν (O-H) in cm^{-1}	2800-3273 br	2800-3272 br
Uv-Vis (CH_3CN)	λ^{max} in nm (ε)	378.6 (40560)	376 (9090)

The shift of the C=S at 37 cm^{-1} is representative of a coordination involving the C=S moiety. This shift is intermediate between the value of 29 cm^{-1} and 43 cm^{-1} observed in the cases of **L_0-CuI** and **L^1H_2-CuI**, respectively. The absorption relative to the carboxyl functional group remains unchanged indicating that these groups are not engaged in the coordination around the copper center, although their chelating ability is well established. The broad band observed between 2800 and 3300 cm^{-1} reveals that the carboxyl groups are engaged in hydrogen bonding networks.

C.4.1.3.2 Structural description of $\underline{L^2H_2}$-CuI

The crystal structure of the **L^2H_2-CuI** will not be presented here because of the poor quality of the crystals rendering the structure difficult to be resolved. But the analysis of this latter confirms a similar arrangement than that in **L_0-CuI** fraction.

C.4.2 Synthesis and characterisation of mercury (II)-dithiolene complexes

In this section, we will present the synthesis and characterisation of dithiolene complexes bearing the ligand **L^1H_2** and mercury halide (**HgI_2, $HgCl_2$**). This work was started after we observed that coordination complexes of dithiolene-like neutral ligands based on neutral **DMIT** derivatives and mercury halide are ligated through the thiocarbonyl function when the 4,5-bis(methylthio)-1,3-dithiole-2-thione is reacted with mercury halide.[142] (Scheme C-3)

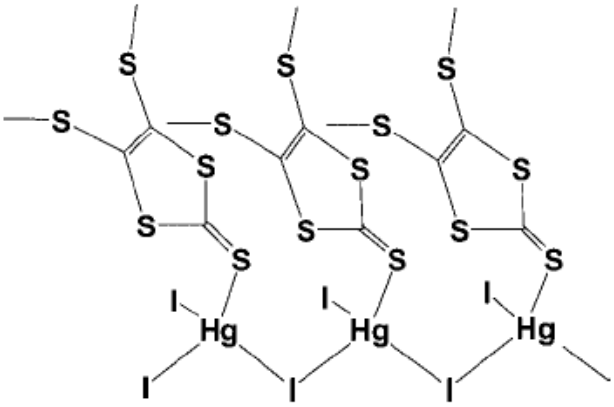

Scheme C-3: 1-D polymeric molecular structure resulting from reaction of 4,5-bis(methylthio)-1,3-dithiole-2-thione with HgI_2.[142]

C.4.2.1 Synthesis and characterisation of $\underline{L^1H_2}$-$\underline{HgX_2}$ (X= I and Cl)

L^1H_2-HgX_2 (X= I, Cl) were obtained by reaction between **L^1H_2** and **HgX_2** in a ratio 1:1. Ligand **L^1H_2** is too sensitive to heat (or high temperature) starting to decompose between 50-60°C (melting point for **L^1H_2** were found at 65-67°C [48] and 58-60°C [96]).

Therefore, after dissolving the **HgX_2** (in toluene at 110°C), the reaction temperature should be lowered down to 50-60 °C before adding the THF solution of **L^1H_2**. No complex was isolated when the reactants are mixed at room temperature. A rapid cooling of the mixture gives rise to the formation of aggregates.

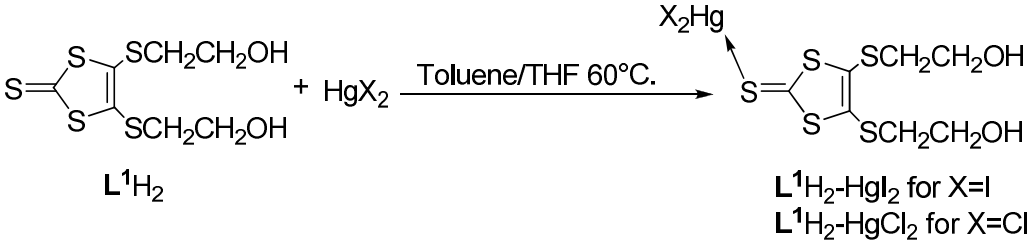

Scheme C-4: Reaction pathways for the synthesis of L^1H_2-HgX_2 complexes.

After stirring at 60° C during 1 h, the reaction mixture was slowly cooled down (**NB**: the flask was maintained under stirring under the oil bath, to avoid rapid cooling) and filtered. The filtrate was then reduced under vacuum until the solution gets turbid, and after cooling, yellow crystals (for **L^1H_2-HgX_2**) were grown within a period of 2-3 days. (**NB**: crystals could be also obtained at room temperature).

In the case of **L^1H_2-$HgCl_2$**, we failed in growing crystals suitable for X-ray measurements. But analysis of the isolated product reveals a similar ratio metal: ligand as in **L^1H_2-HgI_2** but with a THF solvate.

Table C-6: Analytical data from IR and UV-Vis measurements for L^1H_2-HgX_2 (X= Cl and I)[96].

		L^1H_2	L^1H_2-HgI_2	L^1H_2-$HgCl_2$. 0.25 THF
IR	ν (C=S) in cm^{-1} ν (O-H) in cm^{-1}	1074 3272	1031 3240	1015 3229
Uv-Vis (CH_2Cl_2)	λ^{max} in nm	380 (47820)	380 (11820)	380 (7280)

IR analysis of both **L^1H_2-HgI_2** and **L^1H_2-$HgCl_2$** illustrates the coordination of ligand **L^1H_2** via the thiocarbonyl function as observed in the previous copper compounds (see paragraph C.4.1.1.1.). The shift of the C=S bond is more pronounced for **L^1H_2-$HgCl_2$** (59 cm^{-1}) than for **L^1H_2-HgI_2** (43 cm^{-1}) and both are more significant than in the copper derivatives described above (shifted between 29 and 43 cm^{-1}). The OH bands around 3200 cm^{-1} illustrates that the complexes exhibit hydrogen-bonded networks. This is confirmed by the crystal structure analysis (see below).

C.4.2.2 Crystal structure determination of L^1H_2-HgI_2

The single crystal X-ray diffraction analysis was performed on a Stoe imaging plate diffractometer (IPDS) at -70 °C, using graphite monochromated Mo Kα radiation (λ = 0.71073 Å). The crystal structures were solved by direct methods and refined by full-matrix least squares on F^2 using the SHELX software package for crystal structure solution and refinement.[90] All non-hydrogen atoms were refined with anisotropic thermal parameters in the later cycles of refinement. The hydrogen atoms were placed in idealized positions and refined using the riding model with general isotropic temperature factors.[96] Table C-7 shows the crystallographical data and structure refinement for **L^1H_2-HgI_2**.

C.4.2.3 Crystal structure description of L^1H_2-HgI_2

Since we have additional hydroxyl groups in **L^1H_2**, hydrogen bonding networks could be formed once the mercury is coordinated via the thiocarbonyl and giving rise to supramolecular structure with a sustainable di- or tri-dimensional organisation.

Table C-7: Crystal data and structure refinement for L^1H_2-HgI_2.

Compound	**L^1H_2-HgI_2**
Identification code	sh2303
Empirical formula	$C_7 H_{10} Hg I_2 O_2 S_5$
Formula weight	740.84
Temperature	200(2) K
Wavelength	0.71073 Å
Crystal system	Triclinic
Space group	$P\bar{1}$
Unit cell dimensions	a = 4.4760(10) Å α= 116.30(3)°
	b = 13.973(3) Å β= 92.86(3)°
	c = 14.900(3) Å γ = 93.97(3)°
Volume	830.0(3) $Å^3$
Z	2
Density (calculated)	2.964 Mg/m^3

Absorption coefficient	13.607 mm^{-1}
F(000)	668
Crystal size	0.4 x 0.2 x 0.18 mm^3
Theta range for data collection	2.75 to 24.00°
Index ranges	-4<=h<=5, -15<=k<=15, -16<=l<=16
Reflections collected	5130
Independent reflections	2394 [R(int) = 0.0464]
Completeness to theta = 24.00°	92.0 %
Absorption correction	Numerical
Refinement method	Full-matrix least-squares on F^2
Data / restraints / parameters	2394 / 0 / 156
Goodness-of-fit on F^2	1.027
Final R indices [I>2sigma(I)]	R1 = 0.0248, wR2 = 0.0627
R indices (all data)	R1 = 0.0273, wR2 = 0.0637
Largest diff. peak and hole	1.374 and -1.154 e.$Å^{-3}$

The molecular structure with the atom's numbering is shown in Figure C-6.

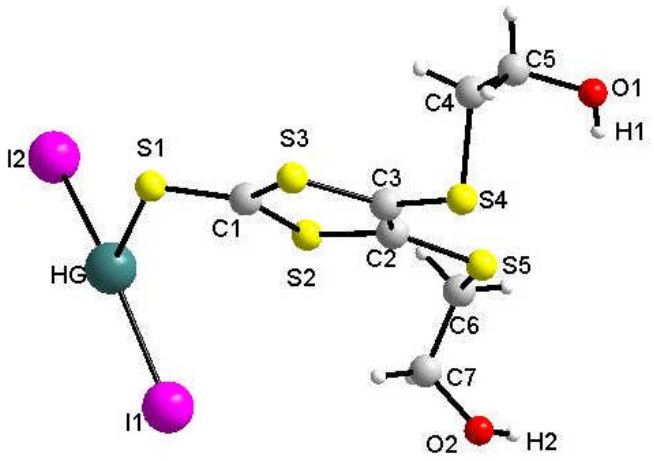

Figure C-6: Molecular structure with the atom's numbering for L^1H_2-HgI_2.

Single crystal X-ray diffraction reveals that **L^1H_2** is complexed on Hg (II) via the sulfur of the thiocarbonyl function (Figure C-6). This coordination mode has already been observed with other dithiolene-like neutral derivatives.[143, 144] Moreover, a recent study based on theoretical and experimental data, has shown that in the case of the related

4,5-bis(methylthio)-1,3-dithiole-2-thione ligand, the formation of the thiocarbonyl adduct is preferred rather than the dithioether adduct resulting from a chelating mode.[142]

Surprisingly, the side chains bounded to C2 and C3 adopt an *anti* position regarding to the DMIT plane (compared to a *syn* position in $\mathbf{L^1}H_2$). Therefore, no intramolecular hydrogen bond is observed. Intermolecular hydrogen bonds with O•••O distance of 2.724(1) Å and O•••H•••O angles of 168.03(4)°, in the same order of magnitude to those observed in the hydrogen bonds network of $\mathbf{L^1}H_2$**,** organize the adduct as a centrosymmetrical dimer in the solid state, thus generating a 22-membered cycle (Figure C-7).

The Hg-S distance (2.812(2) Å) is longer than that reported for HgI_2 ligated with *Me_2DMIT* (2.583(4) Å)[142] or 4,5-ethylenedithio-1,3-dithiole-2-thione (2.567(2) Å).[144] Both Hg-I distances are similar (2.633(9) and 2.655(8) Å) and the I-Hg-I angle of 154.08(1)° reflects a distorted trigonal planar environment around the mercury center.

C.4.2.4 Supramolecular description

Figure C-7 shows the unit cell of $\mathbf{L^1}H_2$**-HgI_2** composed of dimers. Every monomer is connected via hydrogen bonding to its “frontal” neighbour situated more or less in the same plane and simultaneously to the neighbour situated under or over this plan. Figure C-8 gives a view on the structure with the bonding mode through the hydrogen.

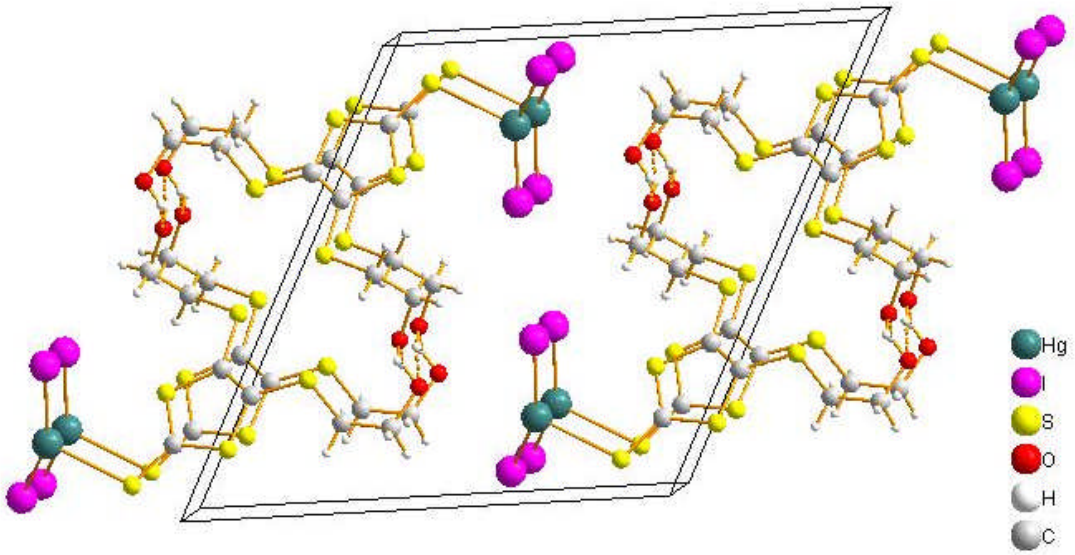

Figure C-7: Unit cell showing the crystal packing in L^1H_2-HgI_2.

An additional weaker intermolecular (Hg•••I) contact of 3.333(1) Å with the iodo ligand of a second motif adds a further lozange like HgI_4 coordination to the trigonal $SHgI_2$ coordination in an almost perpendicular orientation (Figure C-8). Overall, the bonding situation encountered for **L^1H_2-HgI_2** is quite different to that reported for $[HgI_2(Me_2dmit)]_n$. In this later compound, one iodo ligand in a *terminal* mode and one in an almost symmetrically *bridging* mode between two Hg atoms are clearly identified and the coordination around the Hg centre is distorted tetrahedral.[142] Besides the hydrogen bonding network also intermolecular Hg•••I interactions seem to contribute to the stabilisation of the network as may be seen from Figure C-8.

In Figure C-8 we can see several details. First, the DMIT moieties are planar and stacked through π–π interaction. The plane to plane separation amounts to 3.65 Å, the shortest S•••S distance being 3.820(1) Å. The Hg•••Hg separation of *ca.* 4.476(1)

Å is far too long to take into account any “mercurophilic” interaction.

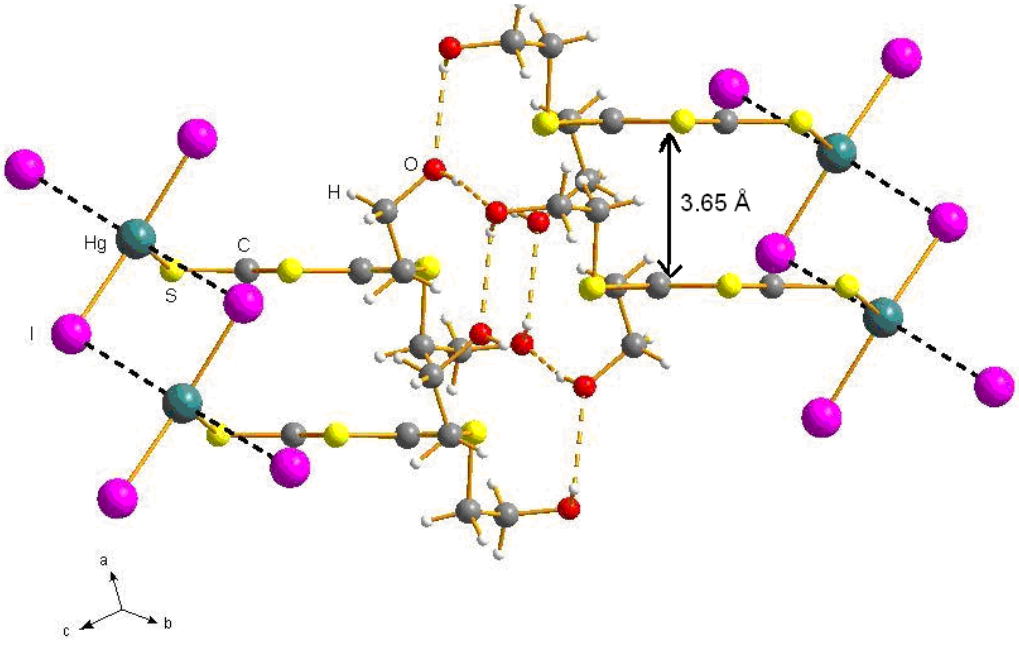

Figure C-8: Packing diagram viewed along the a axis showing the weak intermolecular interaction Hg•••I (dashed lines) (for clarity only neighbouring iodine atoms are represented).

Hydrogen bonding, π-π and S•••S Van-der-Waals interactions are altogether present both in free ligand **L^1**H$_2$ and **L^1**H$_2$**-HgI$_2$** with similar strengths. The major impact of HgI_2 complexation results in the *anti* orientation of hydroxylethyl side chains and consequently in the rupture of the intramolecular hydrogen bonds. The propensity of HgI_2 to build-up chains via μ^2-iodo bridges may be at the origin of the conformational change. Indeed, a weaker bridging contribution of one iodo ligand was identified in **L^1**H$_2$**-HgI$_2$**. The relative orientation of the adjacent *dmit* planes becomes less favourable for a *syn* orientation of the hydroxyethyl substituents. So, they adopt now an *anti* conformation minimizing the steric hindrance. In the free ligand, the oxygen atoms are located at 2.70(2) and 3.02(2) Å from the *dmit* plane, whereas theses distances amount to 2.20(2) and 1.62(1) Å in the adduct (Scheme C-5).

The supramolecular organisation can be imagined as resulting from three different steps as outlined in the following Scheme C-5.

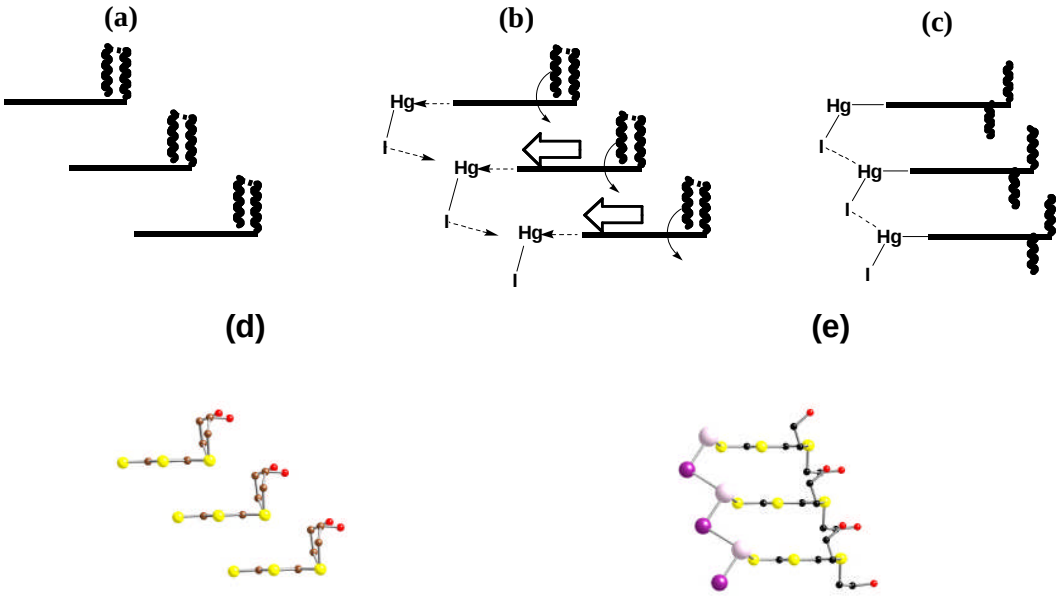

Scheme C-5: (a) Schematic representation and crystal structure showing the stacking of L^1H_2 ((a) and (d)) and L^1H_2-HgI_2 ((c) and (e)); the terminal iodo ligands and hydrogen atoms are omitted for clarity. (b) Stretching of the HgI_2-induced solid state rearrangement of the π-stacking interactions of ligated L^1H_2.

Channel formation (Figure C-9) is also promoted by weak inter-dimer hydrogen bond along the *a* axis with O•••O distances of 2.727(9) Å and O•••H•••O angles of 100.86(3)°.

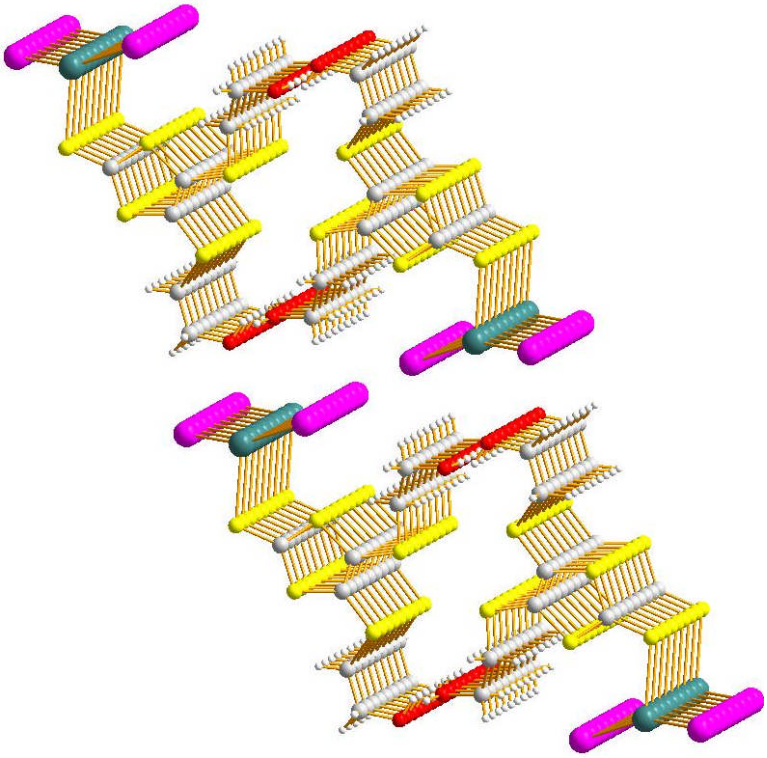

Figure C-9: Channels formation view along the a axis.

C.4.3 Synthesis and characterisation of gold (I)-dithiolene complexes

To follow our idea on the preparation of supramolecular structure incorporating dithiolene-like neutral ligands and metal centers with d^{10} electronic configuration, we have also investigated on gold (I). Apart from its fascinating properties[109, 145] this noble metal has gained an increasing interest illustrated by the "explosive growth" [109] of the literature on gold research. Our study was oriented on ligands $\mathbf{L^1}H_2$ and $\mathbf{L^2}H_2$ which possess, on the one hand, hydroxyl functional group for potential hydrogen bonding interaction, and on the other hand, a DMIT moiety able of coordinating the gold center via the thiocarbonyl function as already observed by other soft metals (copper and mercury , see section C.4.1 and C.4.2, respectively). In the case of gold, we can introduce another type of weak interaction (aurophilic) in addition to the other weak interactions (π–π, S•••S and hydrogen bonding interactions), in which case competition can occur.

C.4.3.1 Background

Gold occupies a central position in the elements of the "d^{10} Avenue". It was classified as a potential "cure-all" for diseases many centuries ago[146], and possess antiarthritic properties. Its central position in chemical science is partly due to the bonding interactions between gold centers in different coordination modes varying from two-coordinated to clustering. The metal•••metal interaction in the case of gold has been attributed to relativistic effects.[147, 148] As we can see in Figure C-10, gold occupies the local minimum in the plot of the ratio $\mathbf{r}_{rel}/\mathbf{r}_{non\text{-}rel}$ versus atomic number (Z) of the element ($\mathbf{r}_{rel}$: relativistic radius, $\mathbf{r}_{non\text{-}rel}$: non-relativistic radius of the valence electrons).

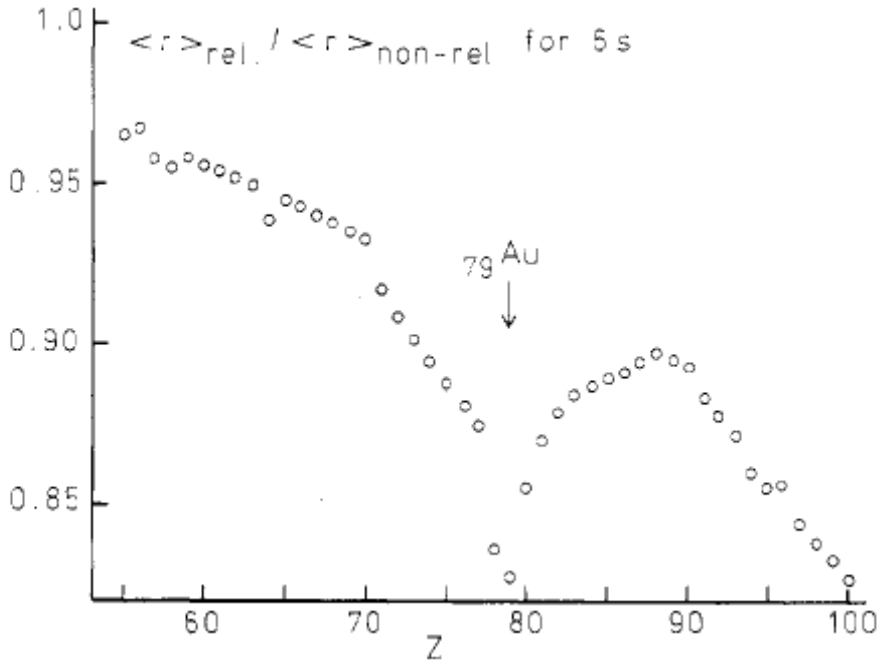

Figure C-10: The relativistic contraction of the 6s shell in the elements Cs (Z=55) to Fm (Z=100)[147].

The relativistic effect in gold can be summarised in 3 points: **i**) s-orbital and (-to a smaller extent-) p-orbital contraction, **ii**) spin –orbit coupling and **iii**) d-orbital expansion.[109]

C.4.3.2 Gold•••Gold interaction energy

This attractive gold•••gold interaction has been termed “Aurophilicity” by Schmidbaur *et al.*[115] This interaction is energetically in the same order than a hydrogen bonding interaction. Theoretical calculations combined with structural investigations have allowed to estimate it at ca. 6-12 kcal/ Au•••Au at gold distances of 3.0±0.2 Å.[149-151]

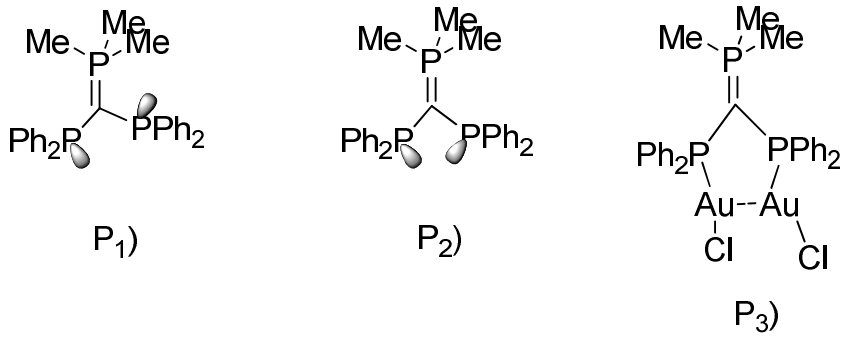

Scheme C-6: Phosphino-substituted ylides in syn/anti (P_1) and syn/syn (P_2) conformation as well as the resulting gold complex (P_3), used for estimation of a gold…gold interaction energy.[150]

Such a determination is based on the fact, that from phosphino-substituted ylide in *syn/anti* conformation (**P_1**) to *syn/syn* conformation (**P_2**), corresponding to a rotation around the P-C axis, an activation energy of 9 kcal.mol^{-1} is needed. Since the gold complex (**P_3**) formed by gold•••gold interaction adopt the same *syn/syn conformation*, the Au•••Au energy is estimated to be more or less the energy needed to bring the ylide from a *syn/anti* to a *syn/syn* conformation (Scheme C-6).[150] This was, of course, not the only model used for estimation of the gold•••gold. Other investigations based on gold-phosphine complexes have determined similar Au^{I}•••Au^{I} interaction strengths between 29 and 46 kJ.mol^{-1} for intermolecular gold-gold distances lying between 3.00 and 3.12 Å. [152-154] Gold centers do attract mutually and this attraction has a strength comparable with hydrogen bonding. It follows that like hydrogen bonding interaction, the mutual attraction between gold centers could be used, in a certain extent, to build-up supramolecular complexes via self-assembly. But more interesting, is the combination of these two weak forces (aurophilicity and hydrogen bonding) within the same complex, since competition or synergy between these two energetically equivalent forces can take place.

C.4.3.3 Synthesis and characterisation of $\underline{L^1H_2\text{-AuCl}}$

Gold complexes containing ligands functionalised by alcohol headgroup are not new,[149, 155] but those combining dithiolene-like neutral ligands functionalised by alcohol headgroup are, to the best of our knowledge, unknown.

L^1H_2-AuCl was obtained by ligand exchange reaction from **L^1H_2** and **AuCl(tht)** as reactants. The commonly used gold precursor [**AuCl(tht)**] (**tht** = tetrahydrothiophene) is known for the lability of the sulphide ligand, facilitating its substitution by other neutral or anionic ligands.[156] The synthetic pathway is outlined in Scheme C-7.

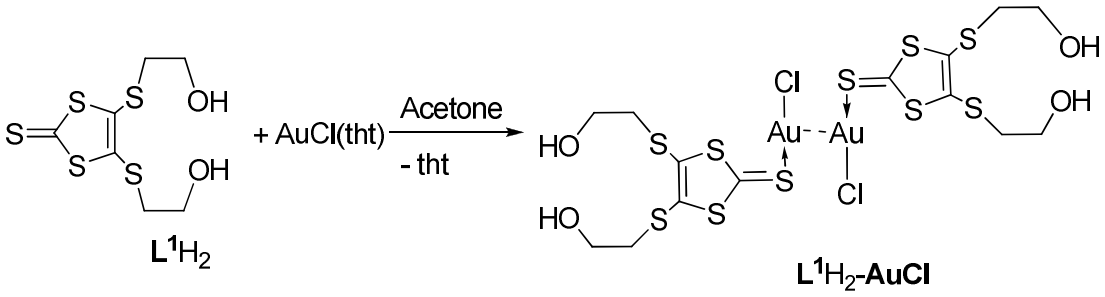

Scheme C-7: Synthetic pathway for ligand displacement reaction between AuCl(tht) and L^1H_2.

Thus, **L^1H_2** reacts with [AuCl(tht)] in a 1:1 metal to ligand ratio at room temperature to afford yellow crystals of **L^1H_2-AuCl**. The nature of the products was established by elemental analysis and single crystal X-ray diffraction study. Once more, the coordination occurred exclusively via the thiocarbonyl (C=S) group of the DMIT .

C.4.3.3.1 IR and UV-Vis results for $\underline{L^1H_2\text{-AuCl}}$

As in precedent cases (complexes with Cu^I and Hg^{II}) we have reported in Table C-8 analytical data useful to approve the coordination mode and the reactivity of **L^1H_2** towards **Au** (I).

Table C-8: Analytical data from IR and UV-Vis measurements.

		$\underline{L^1H_2}$	$\underline{L^1H_2\text{-AuCl}}$
IR	ν (C=S) in cm^{-1}	1074	1008
	ν (O-H) in cm^{-1}	3272	3252
Uv-Vis (Solvent *)	λ^{max} in nm	380 (47820)	424 (11782)

Solvent *: CH_2Cl_2 for L^1H_2 and THF for L^1H_2-AuCl.

The first evidence of the coordination through the thiocarbonyl group (C=S) is given by the considerable shift of this later in the IR spectrum. This shift averages the 66 cm^{-1} compared to the free ligand and illustrates probably a relatively strong interaction between the sulfur atom (of the C=S) and the gold center. The presence of a broad band in the region around 3200 cm^{-1} indicates that the alcohol groups are engaged in a hydrogen bonding arrangement.

The absorption spectrum of **L^1H_2-AuCl** exhibits a maximum at 424 nm, whereas it appears at 380 nm for **L^1H_2**. This difference indicates that the presence of Au(I) has an influence in the absorption transition.

C.4.3.3.2 Crystal structure determination of L^1H_2-AuCl

Yellow crystals of **L^1H_2-AuCl** were grown within a period of several days from a concentrated acetone solution of the reaction mixture. The single crystal X-ray diffraction analysis was performed on a Stoe imaging plate diffractometer (IPDS) at 293 K, using graphite monochromated Mo Kα radiation (λ = 0.71073 Å). All structures were solved applying direct and Fourier methods (SHELXL-97).[90] The non-hydrogen atoms were refined anisotropically. All of the H-atoms were placed in geometrically calculated positions and to each was assigned a fixed isotropic displacement parameter based on a riding-model. Refinement of the structure was carried out by full-matrix least-squares methods based on F_o^2 using SHELXL-97.[90]

C.4.3.3.3 Crystal structure description of L^1H_2-AuCl

Complex **L^1H_2-AuCl** displays a supramolecular architecture, which consists of a dimeric structural motif build through aurophilic interaction. The dimeric configuration results from a surprisingly close aurophilic contact of 3.078(6) Å between the two metal centers as depicted in Figure C-11. This anti-parallel orientation of the ligand towards the Au•••Au axis remembers that found in the n-alkylisonitrile complexes of gold (I) chloride, $C_3H_7NCAuCl$.[157] The Au•••Au contact is about 3.547(1) Å in that case. [157] This kind of short Au•••Au contact in **L^1H_2-AuCl** is rare for non-supported aurophililic interaction.

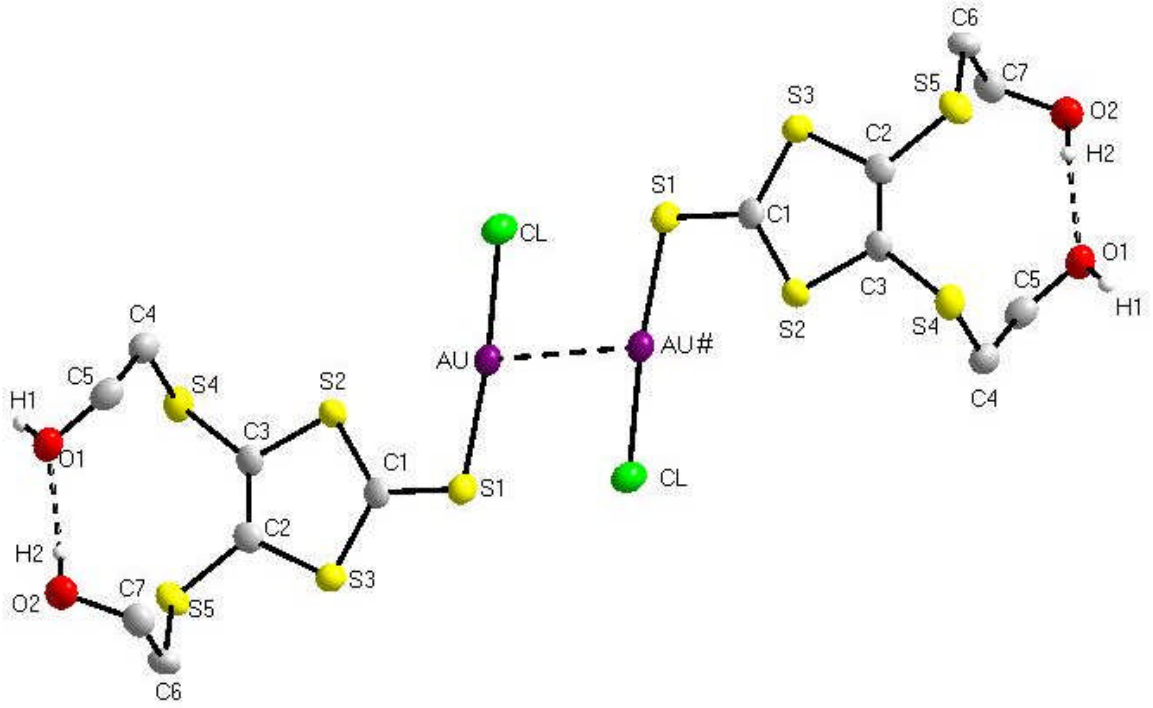

Figure C-11: Molecular structure with atoms numbering for L^1H_2-AuCl (for clarity hydrogen atoms of the ethyl groups are omitted).

A similar arrangement in anti-parallel pairs was reported for the thione complex [AuCl($C_3H_4S_3$)] ($C_3H_4S_3$ = ethylenthiocarbonate) with a Au•••Au separation of 3.366 Å.[158] More recently, an Au•••Au contact of 3.149(7) Å was established in the dimeric association of two gold(I) macrocycles.[159] The S(1)-Au-Cl angle about 174 ° is slightly deviated from linearity and could be accounted for a possible repulsion between S(1) and the chloride (Cl) atom situated in direct neighbourhood. In gold (I) complexes ((TPA)AuX; where TPA=1,3,5-triaza-7- phosphaadamantanetriylphosphine and X= Cl, Br, I) the gold-gold interaction has been found to increase proportionally to the softness of the ligand X.[160]

C.4.3.3.4 Supramolecular description

The presence of hydroxyl groups in **L^1H_2** suggests that we will probably deal with supramolecular structure in **L^1H_2-AuCl**. The combination of the metal•••metal interaction with other secondary non-covalent interactions such as hydrogen bonding, in thiobarbiturate gold(I) complexes[155], and $\pi-\pi$ interaction, in gold(I) thiolate complexes[161], has been proven to be an interesting approach for designing supramolecular networks. It is not always obvious that association of ligands bearing

hydrogen bonding initiator (OH or COOH) and gold(I) fragments lead to supramolecular structures built through hydrogen bonding and gold-gold attraction simultaneously. The thiobarbituric acid is a good example to illustrate this later point (see Scheme C-8). Using PPh_3-Au-(O_2CCF_3) as a gold fragment, Puddephatt *et.al.*[155] have shown that only hydrogen bonding helps the molecules to self-assemble in the solid state. In contrast, the use of (O_2CCF_3)-Au-Ph_2P-$(CH_2)_3$-PPh_2-Au-(O_2CCF_3) as a gold (I) fragment gives rise to an organised structure where both hydrogen bonding and aurophilic interaction are present (Scheme C-8).[155]

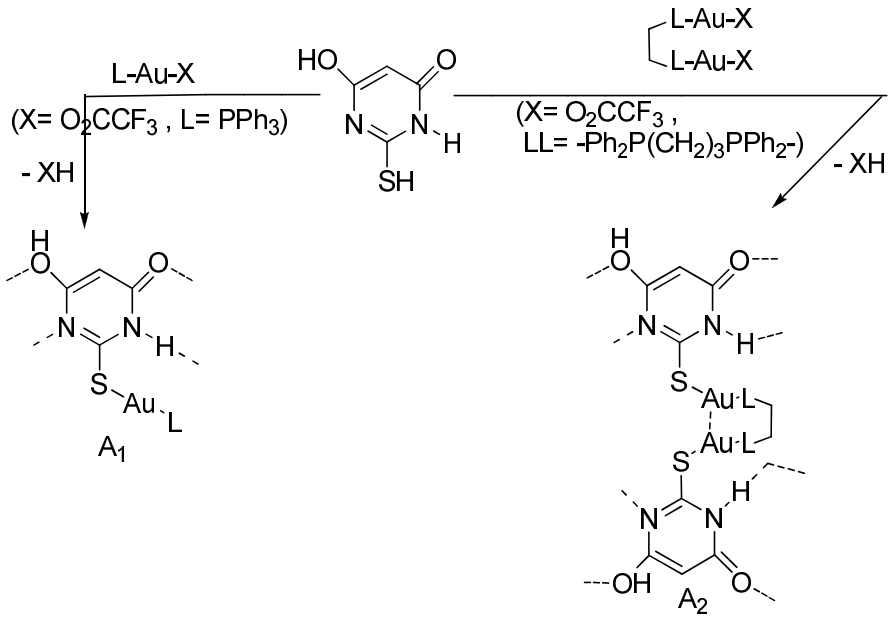

Scheme C-8: Gold(I)-thiobarbituric complexes involving hydrogen bonding interaction and aurophilic interaction. In $\underline{A_1}$, the obtained structure is build through hydrogen bonding, while in $\underline{A_2}$ both the hydrogen bonding and aurophilic interaction are present (dashed lines indicate the presence of hydrogen bonded N-H•••O or O-H•••N).[155]

In our case the hydroxyl group of the thioethanol group readily assists the self-assembly through hydrogen bonding interaction. But, we observe an aurophilic interaction although we have not used a bridging ligand to bring the gold centers in close proximity. This illustrates once more, the fascinating behaviour of gold and its intriguing position in the periodical table of the elements.

In terms of crystal engineering, we could propose the following Scheme C-9, as illustrating the process taking place during the self-assembly and giving rise to the supramolecular network (Figure C-12).

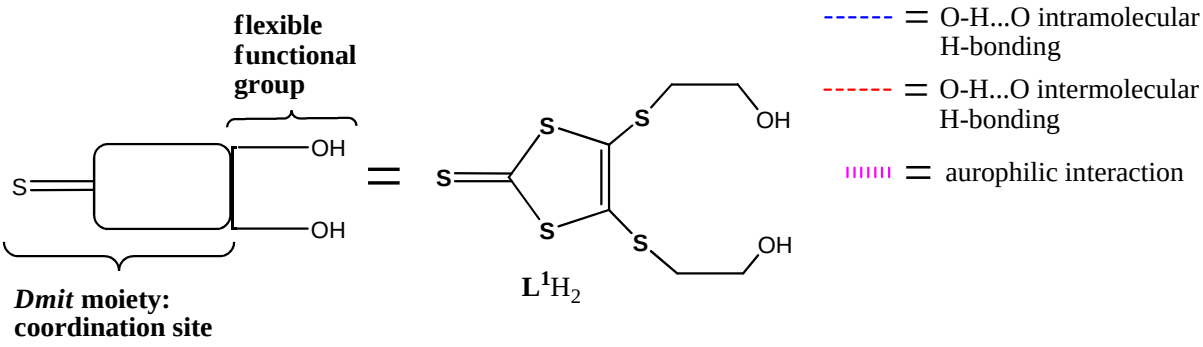

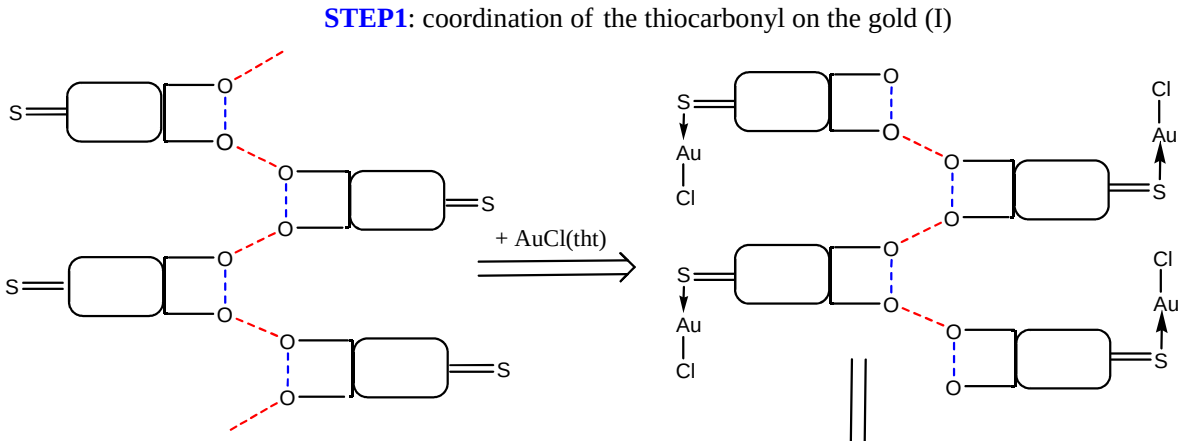

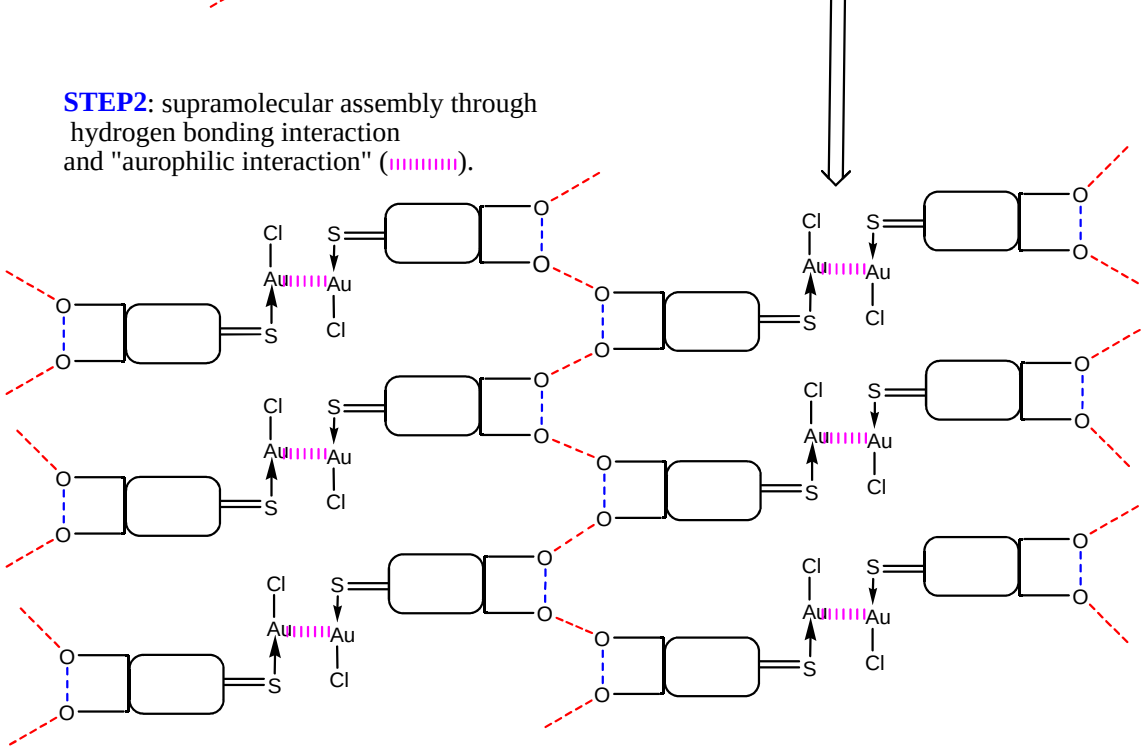

Scheme C-9: Proposed scheme based on three steps for explanation of the supramolecular self-organisation.

Step1*:* the ligand is coordinated to the gold center via the thiocarbonyl group as already observed in other thione function. This coordination is activated via displacement of the labile **tht** from the **AuCl(tht)** fragment. Having a look on the

solid state organisation of ligand **L^1**H$_2$ we can see that the hydrogen bonding interaction (intra and inter-molecular) are also already present. From this observation, we have represented **L^1**H$_2$ as displayed in step1 (Scheme C-9). This statement is also supported by the fact that the hydrogen bonding network is unchanged by the coordination of the thiocarbonyl bond on the metal center. The arrangement resulting from this first step (Step1) is a combination of Au-S interaction and hydrogen bonding (O-H•••O) interaction.

Step2: Gold atoms are known to exercise strong attractions termed as aurophilic interactions. Therefore we can imagine that such an attraction between two gold atoms in different **L^1**H$_2$**-AuCl** fragments will lead to the formation of a network. In this network we can recognize at least three types of non-covalent interactions namely the gold•••gold interaction, the Au-S interaction and the hydrogen bonding interactions. The resulting network is dominated by three kinds of non-bonding interactions: intramolecular one (blue dashed lines), aurophilic interaction (wavy bond) and intermolecular one (red dashed lines), see Scheme C-9.

If we have a look on the structure as presented in Figure C-12, we could also imagine that regular distance between adjacent dimers are resulting from $\pi-\pi$ interaction, but the shortest S-S contact lying between 6.76 Å excludes possible stacking between molecules. Then, we can conclude that the resulting supramolecular structure is predominately formed via aurophilic interaction and hydrogen bonding, a contribution of intramolecular S—S contact in the dmit moiety can be also envisaged.

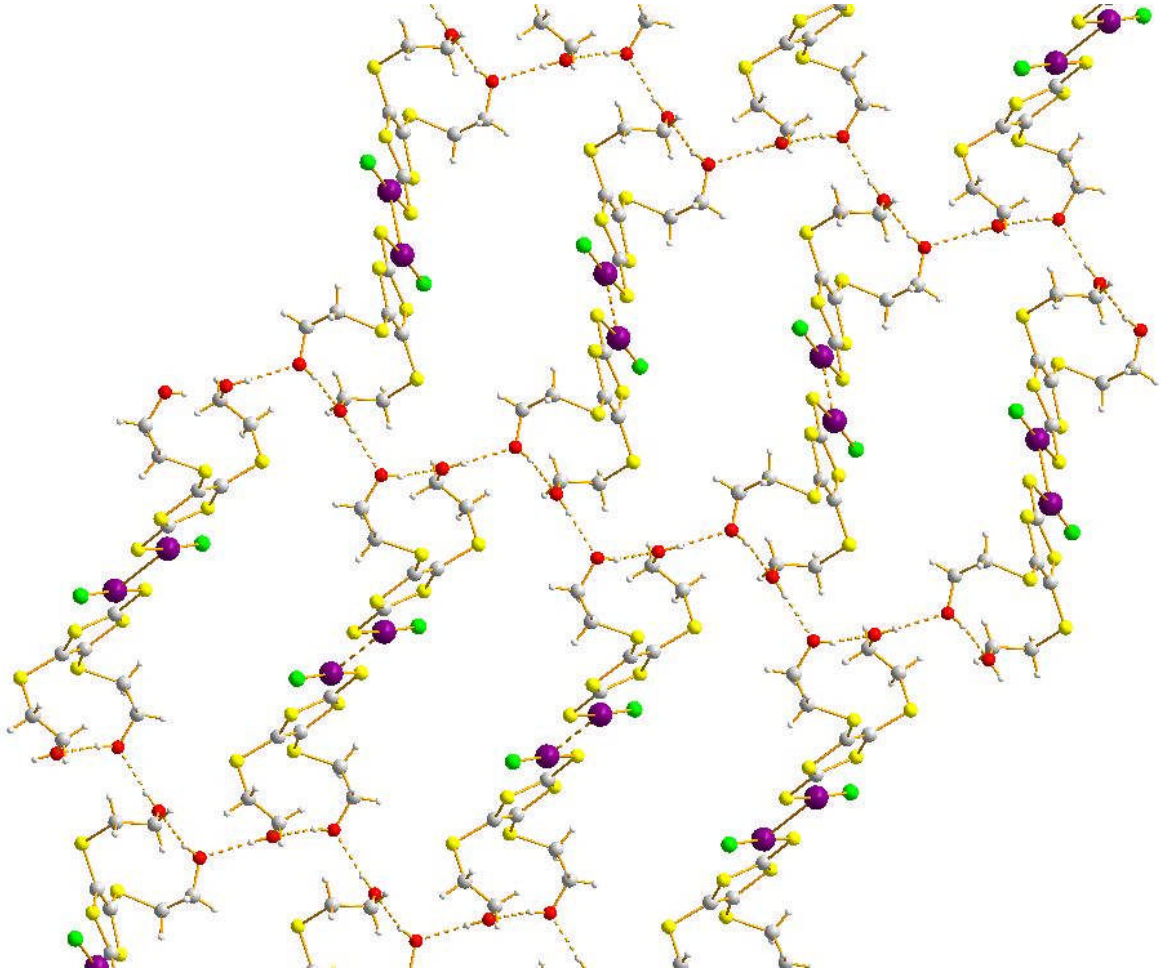

Figure C-12: Structure of L^1H_2-AuCl showing the resulting supramolecular networks built through combination of different non-bonding interactions.

NB: As member of the group of coinage metals, Ag^I presents also similar behaviour compared to Cu^I and Au^I. To complete this group of the coinage metals, we have also desperately attempted to isolate silver complexes of ligands $\mathbf{L^1}H_2$ and $\mathbf{L^2}H_2$ without success. Reaction of silver nitrate ($AgNO_3$) or silver p-toluenesulfonate ($AgO_3S(C_6H_4)CH_3$) with $\mathbf{L^1}H_2$ or $\mathbf{L^2}H_2$ gives rise to unstable oily products which are difficult to crystallise and the elemental analysis results are not convenient enough to propose a structure.

C.4.3.4 Synthesis and characterisation of L^2H_2-AuCl

Like in $\mathbf{L^1}H_2$**-AuCl** complex, the $\mathbf{L^2}H_2$**-AuCl** complex was obtained by ligand exchange reaction between $\mathbf{L^2}H_2$ and **AuCl(tht)**. This reaction is performed in

acetone and the **L²H₂-AuCl** complex is isolated with acetone molecules (**CH_3COCH_3**) as solvates. No crystals could be obtained by performing the reaction into THF. The synthetic pathway is outlined in Scheme C-10.

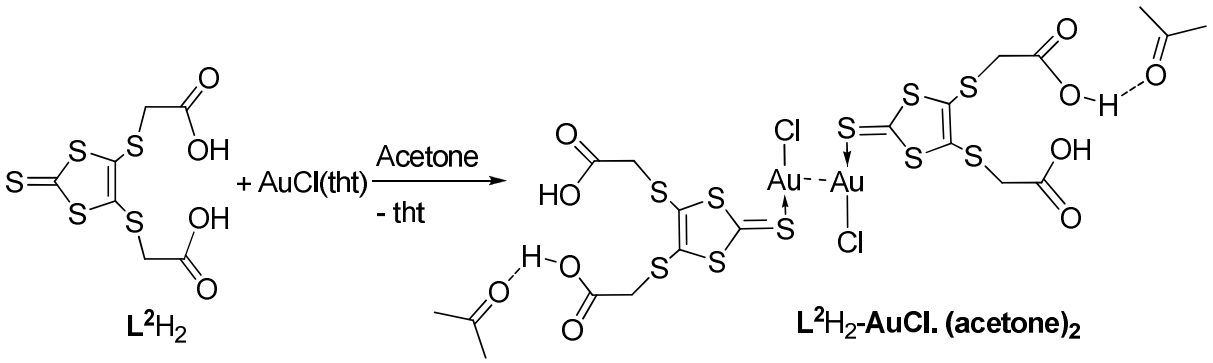

Scheme C-10: Synthetic pathway for ligand displacement reaction between AuCl(tht) and L^2H_2.

L^2H_2 reacts with [AuCl(tht)] in a 1:1 metal to ligand ratio at room temperature to afford yellow crystals of **L^2H_2-AuCl. CH_3COCH_3**. Similarly to **L^1H_2-AuCl**, the coordination occurred exclusively via the thiocarbonyl (C=S) group of the DMIT moiety and one carboxylic group is further linked to an acetone molecule solvate by intermolecular hydrogen bonding interaction.

Table C-9 represents analytical data useful to approve the coordination mode and the reactivity of **L^2H_2** towards **Au (I)**.

Table C-9: Analytical data from IR and UV-Vis measurements.

		L^2H_2	**L^2H_2-AuCl. (CH_3COCH_3)**
IR	ν (C=S) in cm^{-1} ,ν(C=O) in cm^{-1} ν (O-H) in cm^{-1}	1065 1692 2800-3273 br	1013 1694 2800-3377 br
Uv-Vis (THF)	λ^{max} in nm	378.6 (40560).	416 (12820)

As seen in the IR spectrum, the thiocarbonyl group (C=S) is shifted about 52 cm^{-1} compared to the free ligand and illustrates probably a relatively strong interaction between the sulfur atom (of the C=S) and the gold center. The presence of a broad band in the region around 2800-3377cm^{-1} indicates that the acidic group is engaged in a hydrogen bonding arrangement.

As previously observed in the **L^1H_2-AuCl** complex, the absorption peak of the **L^2H_2-AuCl** complex in the UV-Vis spectrum appears at 416 nm, compared to 378 nm for

L^{2}H$_2$ and indicates that the presence of Au(I) has an influence in the absorption transition.

C.4.3.4.1 Crystal structure description of L^{2}H$_2$-AuCl

The molecular structure with the atom numbering for **L**^{2}H$_2$**-AuCl** is shown in Figure C-13 and the crystallographic data are reported in Table C-10.

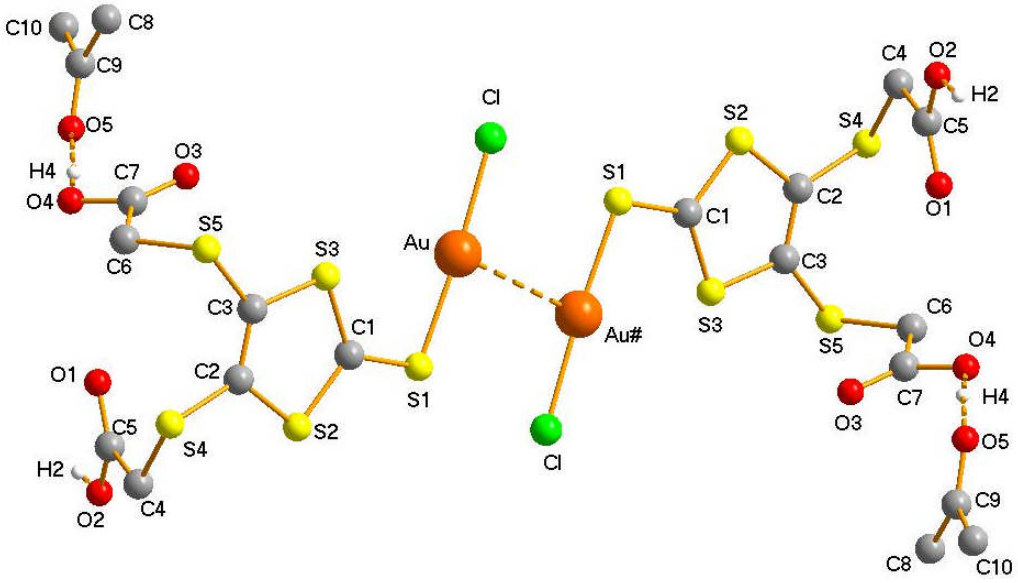

Figure C-13: Molecular structure with atoms numbering for L^{2}H$_2$-AuCl.(CH$_3$COCH$_3$)(for clarity hydrogen atoms of the ethyl groups are omitted).

Table C-10: Crystal data and structure refinement for L^{2}H$_2$-AuCl.

Identification code	sh2793	
Empirical formula	C13 H18 Au Cl O6 S5	
Formula weight	662.99	
Temperature	153(2) K	
Wavelength	0.71073 Å	
Crystal system	Triclinic	
Space group	$P\bar{1}$	
Unit cell dimensions	a = 5.6607(3) Å	α= 71.359(2)°.
	b = 14.1790(6) Å	β= 88.234(3)°.
	c = 14.3137(6) Å	γ = 85.486(3)°.
Volume	1085.20(9) Å^3	
Z	2	
Density (calculated)	2.029 Mg/m^3	

Absorption coefficient	7.408 mm^{-1}
F(000)	640
Crystal size	1.21 x 0.09 x 0.06 mm^3
Theta range for data collection	1.50 to 32.41°.
Index ranges	-8<=h<=8, -17<=k<=21, -19<=l<=21
Reflections collected	25482
Independent reflections	7708 [R(int) = 0.0552]
Completeness to theta = 32.41°	98.8 %
Absorption correction	Multiscan
Max. and min. transmission	0.6818 and 0.0403
Refinement method	Full-matrix least-squares on F^2
Data / restraints / parameters	7708 / 0 / 235
Goodness-of-fit on F^2	1.054
Final R indices [I>2sigma(I)]	R1 = 0.0448, wR2 = 0.0915
R indices (all data)	R1 = 0.0691, wR2 = 0.0995
Largest diff. peak and hole	1.801 and -3.112 e.$Å^{-3}$

The same dimeric structural motif build through aurophilic interaction observed in the complex **L^1H_2-AuCl** is also identified in the case of the complex **L^2H_2-AuCl**. Two remarkable differences are the presence of the acetone solvates and the length of the Au•••Au contact. This later is about 3.270(4) Å, and is slightly longer than the Au•••Au contact of 3.078(6) Å found in **L^1H_2-AuCl**.

The S(1)-Au-Cl angle about 176.37(5)° is slightly deviated from linearity and is probably a result of the a possible repulsion between S(1) and the chloride (Cl) atom situated in direct neighbourhood. Since these two structures are similar (at least in their dimeric motif) the structural description of the **L^2H_2-AuCl** complex will not be completely specified here. Some selected bond lengths and angles are reported in Table C-11.

Table C-11: Bond lengths [Å] and angles [°] for L^2H_2-AuCl.

Au-S(1)	2.264(13)	Cl-Au-Au#1	91.74(4)
Au-Cl(1)	2.274(1)	C(1)-S(1)-Au(1)	103.24(2)
Au-Au#1	3.270(4)	C(1)-S(3)-C(3)	96.7(2)
S(1)-C(1)	1.697(5)	C(1)-S(2)-C(2)	96.3(2)
S(3)-C(1)	1.688(5)	C(2)-S(4)-C(4)	100.7(2)
S(3)-C(3)	1.740(5)	C(3)-S(5)-C(6)	99.4(2)
S(2)-C(1)	1.715(5)	S(3)-C(1)-S(1)	125.4(3)
S(2)-C(2)	1.739(5)	S(3)-C(1)-S(2)	115.0(3)
S(4)-C(2)	1.750(5)	S(1)-C(1)-S(2)	119.6(3)

S(4)-C(4)	1.810(5)	C(5)-C(4)-S(4)	114.5(3)
S(5)-C(3)	1.758(5)	O(1)-C(5)-O(2)	124.7(5)
S(5)-C(6)	1.800(6)	O(1)-C(5)-C(4)	124.7(5)
C(4)-C(5)	1.517(7)	O(2)-C(5)-C(4)	110.5(4)
C(5)-O(1)	1.214(6)	C(3)-C(2)-S(2)	115.7(4)
C(5)-O(2)	1.309(6)	C(3)-C(2)-S(4)	123.9(4)
C(2)-C(3)	1.348(7)	S(2)-C(2)-S(4)	120.3(3)
C(6)-C(7)	1.501(8)	C(2)-C(3)-S(3)	116.2(4)
C(7)-O(3)	1.196(7)	C(2)-C(3)-S(5)	125.9(4)
C(7)-O(4)	1.327(7)	S(3)-C(3)-S(5)	117.8(3)
O(5)-C(9)	1.230(7)	C(7)-C(6)-S(5)	115.1(4)
C(9)-C(8)	1.487(9)	O(3)-C(7)-O(4)	122.6(6)
C(9)-C(10)	1.489(9)	O(3)-C(7)-C(6)	126.6(6)
O(6A)-C(12A)	1.457(2)	O(4)-C(7)-C(6)	110.7(5)
C(11A)-C(12A)	1.492(2)	O(5)-C(9)-C(8)	122.3(6)
C(12A)-C(13A)	1.562(2)	O(5)-C(9)-C(10)	119.4(6)
O(6B)-C(12B)	1.649(2)	C(8)-C(9)-C(10)	118.3(6)
C(12B)-C(13B)#2	1.51(3)	O(6A)-C(12A)-C(11A)	114.8(11)
C(12B)-C(11B)	1.58(2)	O(6A)-C(12A)-C(13A)	128.5(11)
C(13B)-C(12B)#3	1.51(3)	C(11A)-C(12A)-C(13A)	115.0(11)
		C(13B)#2-C(12B)-C(11B)	125.6(16)
S(1)-Au-Cl	176.37(5)	C(13B)#2-C(12B)-O(6B)	134.3(16)
S(1)-Au-Au#1	90.30(3)	C(11B)-C(12B)-O(6B)	100.1(12)

Symmetry transformations used to generate equivalent atoms: #1 -x,-y+1,-z
#2 x+1,y,z #3 x-1,y,z

C.4.3.4.2 Supramolecular description of L^2H_2-AuCl: comparison with L^1H_2-AuCl

We have previously seen that the combination of the metal•••metal interaction with other secondary non-covalent interaction such as hydrogen bonding can be, to a certain extent, an interesting approach for designing supramolecular networks. Similarly to the precedent case, the anti-parallel orientation of the ligand towards the Au•••Au axis is also identified in the crystal structure.

However, the presence of solvent molecules gives rise to an orientation growth completely different to that we observed in the **L^1H_2-AuCl** complex:

a) In the **L^1H_2-AuCl** complex, the gold-gold attraction ensures the dimerisation whereas the two hydroxyl groups (attached to the DMIT) contribute to the direction of growth through intra- and inter-molecular hydrogen bonding interactions leading to the formation of a sheet-like network (Scheme C11).

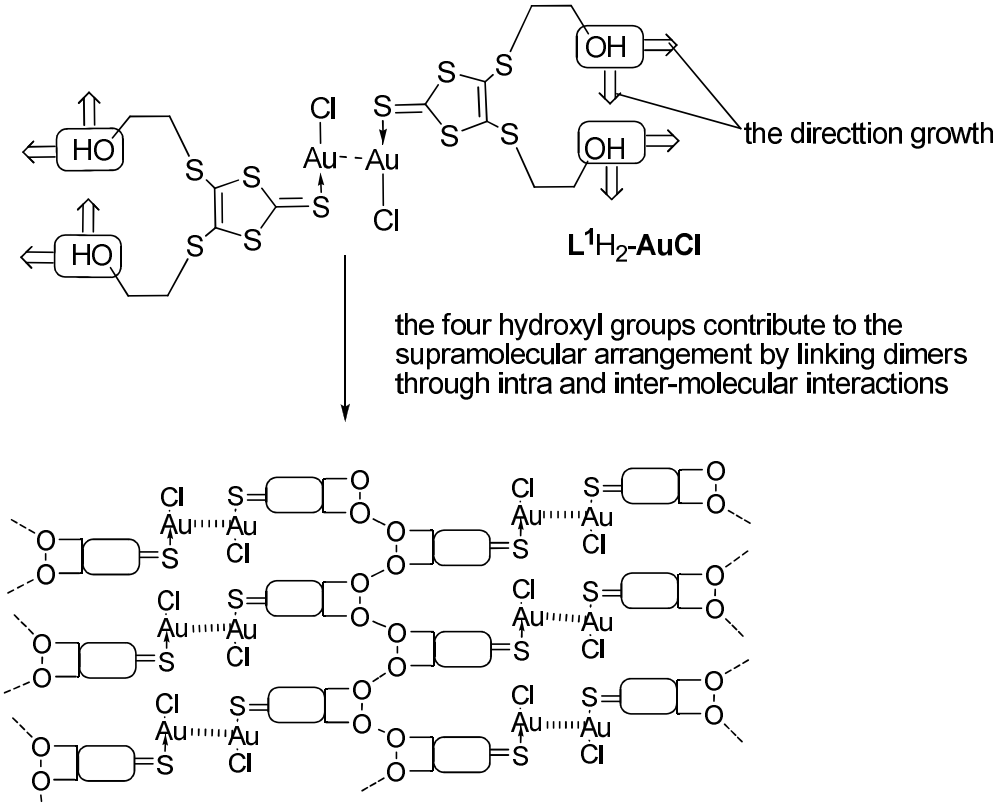

Scheme C-11: Formation of a sheet like structure in the case of L^1H_2-AuCl.

b) In the case of **L^2H_2-AuCl** complex, a similar gold-gold attraction ensures the dimerisation, but only one carboxyl group contributes to the direction growth through intermolecular hydrogen bonding , the second carboxyl group is hampered by the acetone molecule and do not therefore participate in the growing process. As a result of this blockade, a one dimensional polymer-like arrangement is obtained instead of the sheet-like network.

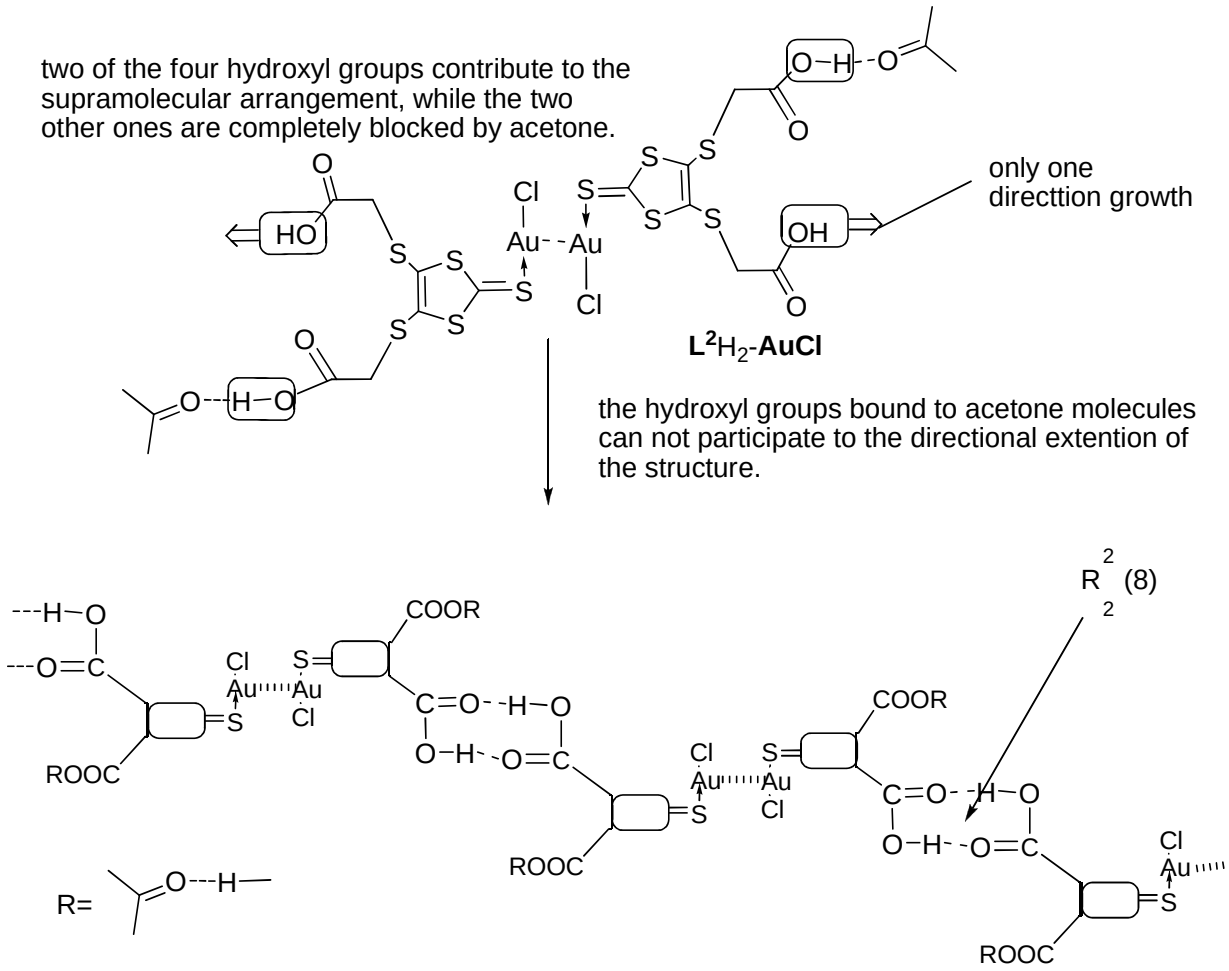

Formation of a one dimensional polymer-like structure resulting from the a combination of aurophilic and hydrogen bonding intermolecular interactions

Scheme C-12: Formation of a one dimensional polymer-like structure in L^2H_2-AuCl complex.

Another projection of this structure allows identifying a stair-like structure arranged through a succession of Au•••Au interactions and hydrogen bonding interactions (with a R^2_2 (8) arrangement) (see Figure C-14).

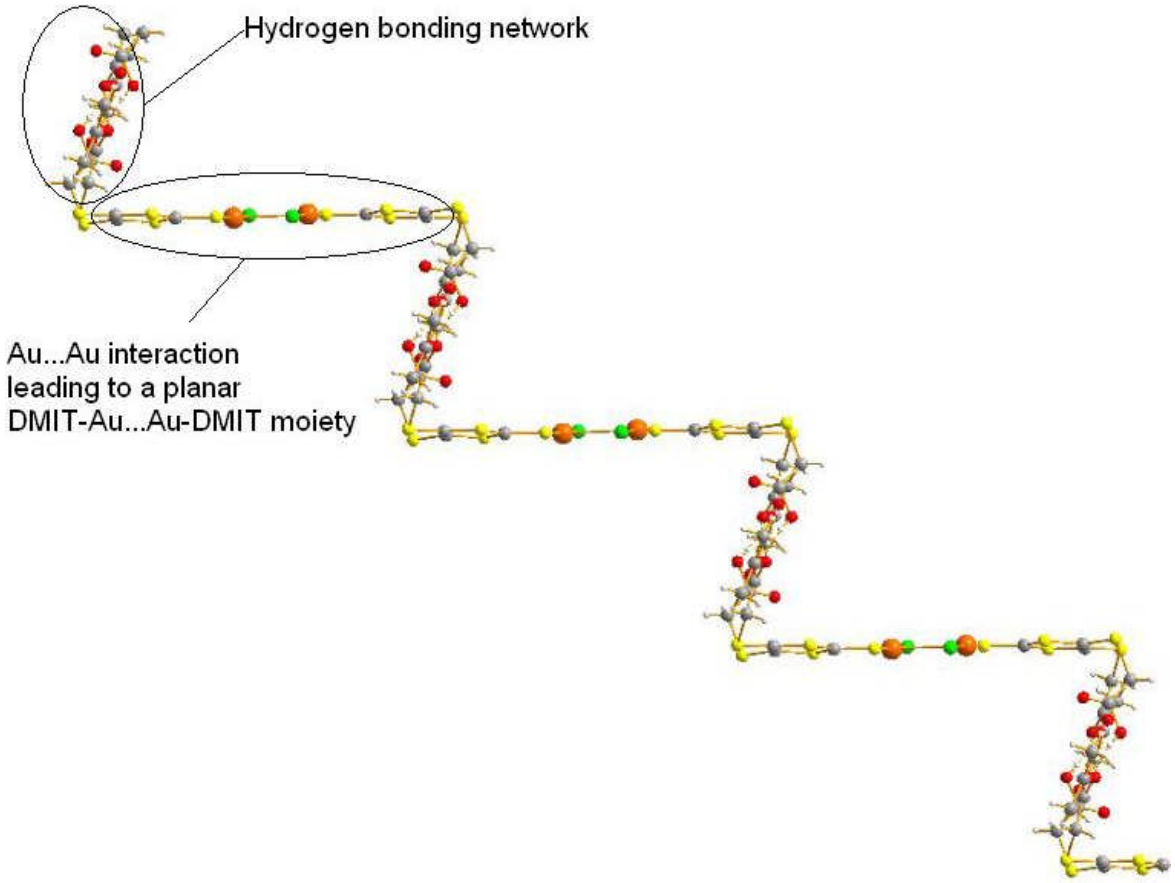

Figure C-14: Projection of the molecular structure of L^2H_2-AuCl complex showing a stair-like structure.

These results show that the combination of ligand bearing functional groups suitable for non-bonding interactions and aurophilic interaction lead to fascinating supramolecular structures. Structural orientations have been also induced, by the presence of a coordinating solvent for example. The aurophilic interaction seems to be a driving force in the formation of these gold complexes, but the hydrogen bonding interactions play also a non-negligible role.

C.5 Photophysical properties of the ligand based metal (d^{10}) complexes: luminescence

Coordination polymers presenting luminescent properties have been widely studied because of their potential application in optoelectronic area.[105, 122, 162-164]

C.5.1 Generalities

Photoluminescent properties are often affected by the metal(d^{10})-metal(d^{10}) interaction (the presence of metal-metal interaction is related to the solid state luminescence in some cases[131, 139]). However in other cases no metal-metal interaction is needed for a complex to luminesce (some mononuclear complexes are luminescent, although no metal-metal interaction has been evidenced[123]). As generally observed, emissions are known to involve ligand-centred (IL), metal-ligand charge transfer (MLCT) or ligand-metal charge transfer (LMCT) and metal-centred transitions. While the metal centred transition is mostly related to the presence of metal-metal interaction, the others transitions are not obviously attributed. A theoretical investigation is generally needed, to get insight into the origin of the luminescence in such complexes.

C.5.1.1 Luminescence in copper (I) complexes

Copper(I) complexes present potential application in the domains of optoelectronic and are interesting because of their low cost compared to others luminescent transition metals based complexes (Pt^{II}, Pd^{II}, Rh^{II} etc…).[108] The first observation of the luminescent in copper (I) complexes dates back to 1981 from Hardt *et.al.*[140], and earlier in 1970 from Ziolo *et al.* [123] who have observed luminescence in the family of CuI • L (L= ligand) adducts. Later on, crystallographic studies combined with DFT calculations have brought more light to assignment of the excited states responsible of the luminescence[106, 119, 138, 139, 165-168].

For example, in the case of tetranuclear copper (I) complexes (Cu_4I_4-py_4) possessing a tetrahedral core with significant metal-metal interactions, the strong lower energy emission was assigned to a triplet cluster-centred excited states, a combination of iodide to copper charge transfer (XMCT) and d-s transitions, and the weaker higher energy to a triplet halide-to-ligand charge transfer (^{3}XLCT).[139]

The case of copper (I) complexes (Cu_2I_2-L_x, x= 2 or 4) possessing a rhombohedral core has been investigated to lesser extends. In the case of luminescence arising from an intraligand transition, a comparison between the ligand emission and the complex emission is sufficient to conclude in the nature of the luminescence.[124]

C.5.1.2 Luminescence in mercury (II) complexes

Compared to copper (I), mercury (II) complexes have been poorly investigated for their photophysical interest.[169] Mercury itself is known to quench luminescence in ligand by heavy atom effect. The number of mercury (II) complexes displaying metal-metal interactions is relatively low compared to other d^{10} elements (Cu^{I}, Au^{I}…).[114] But mercury ions (Hg^{2+}) are known to enhance the inter system crossing (ISC) from a singlet state to a triplet state.[169]

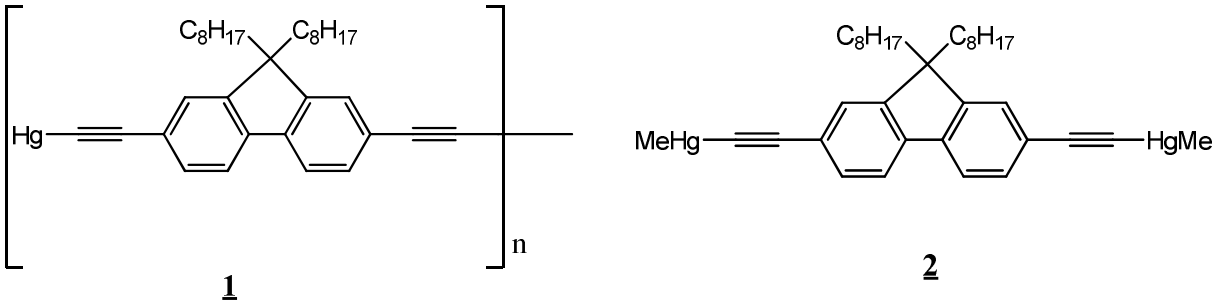

Scheme C-13: Example of mercury (II) polyyne polymers showing intraligand transitions.[169]

Despite the paucity of literature reports on their photophysical properties, intraligand emissions are identified in metallo-dithiolene complexes.[170] Similar results have been observed in the case of mercury (II) polyyne polymers, where the emissions were attributed to intraligand transitions.[169] The metal-metal contacts in the range of 3.738 and 4.183 Å interactions were in the upper limit corresponding to metallophilic interaction.

C.5.1.3 Luminescence in gold (I) complexes

Gold is the most investigated system in the metal (d^{10}) based complexes. Because of its various structural topology in the solid state combined with the highly luminescent properties, there have been increasing interests notified by the number of report on gold chemistry through the years. Contrary to the above mentioned examples, gold (I) complexes have been well investigated theoretically and their photophysics are more and more investigated. EXAFS (Extended X-ray Absorption Fine Structures), which is a sophisticated technique for analysing the environment of an atom, has

been proved to be well suited for investigating gold-gold interaction both in solution[171, 172] and solid state.[171, 173] NMR and X-ray have also allowed to understand the gold systems.

It should be argued that gold-gold interactions do not necessarily lead to luminescence. Some mononuclear species (in which there is no evidence for a gold-gold interaction) are luminescent.[174-176] Luminescence in polynuclear gold complexes has been mostly attributed as arising from the excited states involving gold-gold bonding.[177] Taking the direction of aggregation as the z axis, and having in mind that d orbitals are filled and p orbital are empty, the diagram depicted in Figure C-15 can be used as representing molecular orbitals in such systems.[178]

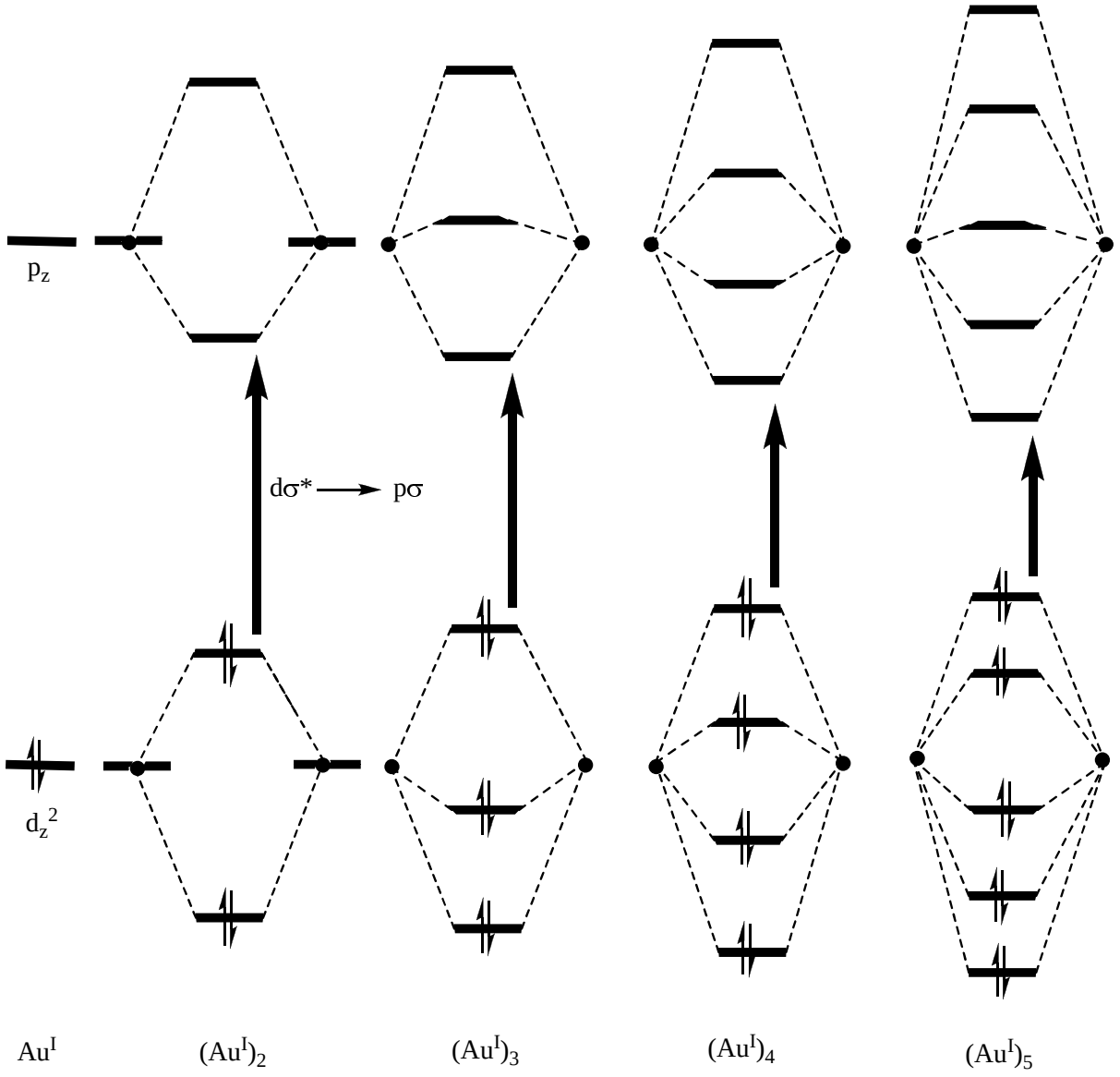

Figure C-15: Molecular orbital diagrams showing the interactions between the filled d_z^2 and the empty p_z orbitals for a chain of 2, 3, 4 and 5 gold(I) ions.[178]

As we can see in this figure, gold-gold association created a filled band of d_z^2 orbital and an empty band of p_z orbitals. These two bands resulting from gold attraction or aggregation tend to be closer to each other as the number of gold centers increases. The absorption process in polynuclear gold complexes results in a promotion of electrons from a filled band of d_z^2 orbital to an empty band of p_z orbitals, corresponding to the $d\sigma^* \rightarrow p\sigma$ transition.[178] This transition is favoured because it implied a promotion of an electron from anti-bonding ($d\sigma^*$) orbital to a bonding one ($p\sigma$).[178] From mononuclear gold (I) to dinuclear gold (I) (*i.e.* from Au^I to $(Au^I)_2$ see Figure C-15), this transition is expected to be shifted to higher wavelength. Generally, the attribution of luminescence in gold complexes can be achieved by coupling information given by structure analysis (X-ray) and theoretical calculations[119, 179-181] (DFT for example).

C.5.2 Luminescence in dithiolene-based metal (d^{10}) complexes

C.5.2.1 Luminescence studies of the L_0-CuI complex

L_0-CuI presents in its absorption spectrum bands situated between 240-390 nm. These peaks are attributed as intraligand transition arising from $n-\pi^*$ and $\pi-\pi^*$ transition.[182] The ligand **L_0** presented similar transitions with a maximum at about 367 nm. No noticeable shift was observed upon coordination of the thione to the metal center, contrary to what was observed in the gold (I) thione complexes showing the same coordination mode (AuCl←S=CR; where R= -S-CH_2-CH_2-S-).[158] In the same context we have not detected a transition which could arise from the metal-centred excited states (as observed in some copper complexes[139]). Luminescence spectra of complex **L_0-CuI** and that of the free ligand **L_0** are shown in Figure C-16.

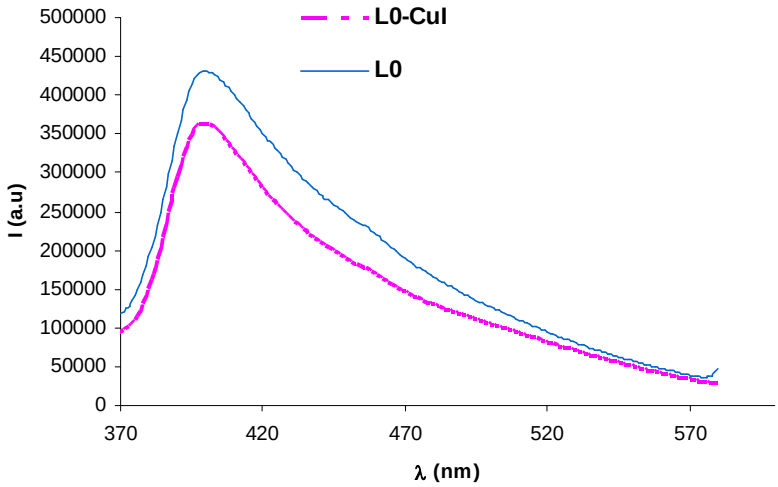

Figure C-16: luminescence spectra recorded at room temperature in CH_3CN for L_0 (solid line) and L_0-CuI (dotted line) (λ^{ex}= 300 nm).

Upon excitation at 300 nm, the neutral ligand **L_0** shows an emission maximum at λ=400 nm in solution. This luminescence could be attributed to the π*-π transition. Such transitions are known as intraligands transitions.[124] The complex **L_0-CuI** shows in its emission spectrum an intense band at λ=400 nm under the same excitation at λ=300 nm (excitation at 350 nm in the same conditions showed an emission at 418 nm but with a weaker intensity). Compared to the free ligand, the emission observed in **L_0-CuI** is not shifted, proof of insignificant influence of the metal on the luminescence properties. Therefore, we conclude that the luminescence observed in the case of complex **L_0-CuI** is an intraligand process. The lack of transitions involving excited states centered on the metal can be explained by the absence or weakness of the metal-metal interactions (Cu•••Cu contacts are about 3.051(1) Å).

C.5.2.2 Luminescence studies of the L^1H_2-HgI_2 complex

Similarly to **L_0-CuI**, the **L^1H_2-HgI_2** presents in its absorption spectrum bands in the region 210- 430 nm. These peaks are attributed as intraligand transitions arising from n–π* and π–π* transition as previously discussed. The ligand **L^1H_2** presents similar transitions with a maximum around 380 nm (Figure C-17).

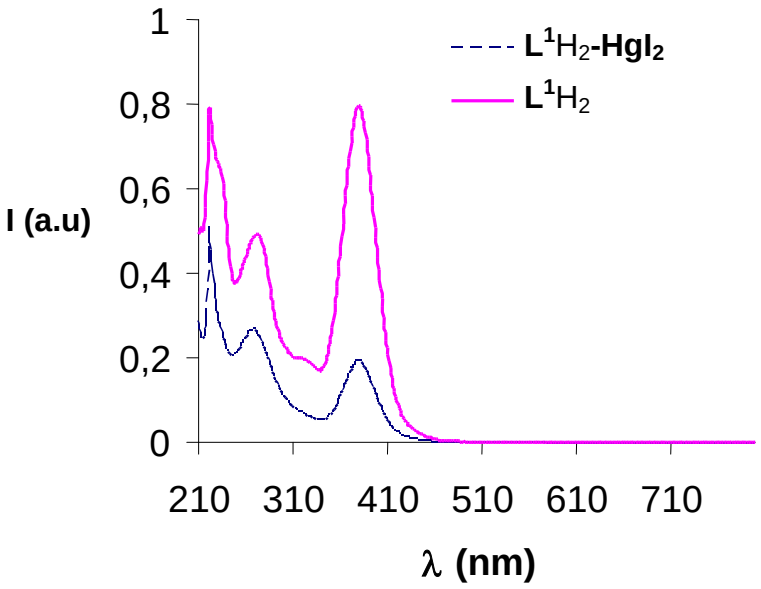

Figure C-17: Absorption spectrum of L^1H_2 and L^1H_2-HgI_2 at room temperature in CH_2Cl_2.

As complex **L^1H_2-HgI_2** exhibits only weak metal-metal interactions, we are not expecting to observe luminescent properties stemming from metal-centered excited states. Figure C-18 displayed emission spectra of **L^1H_2-HgI_2** and the free ligand **L^1H_2**.

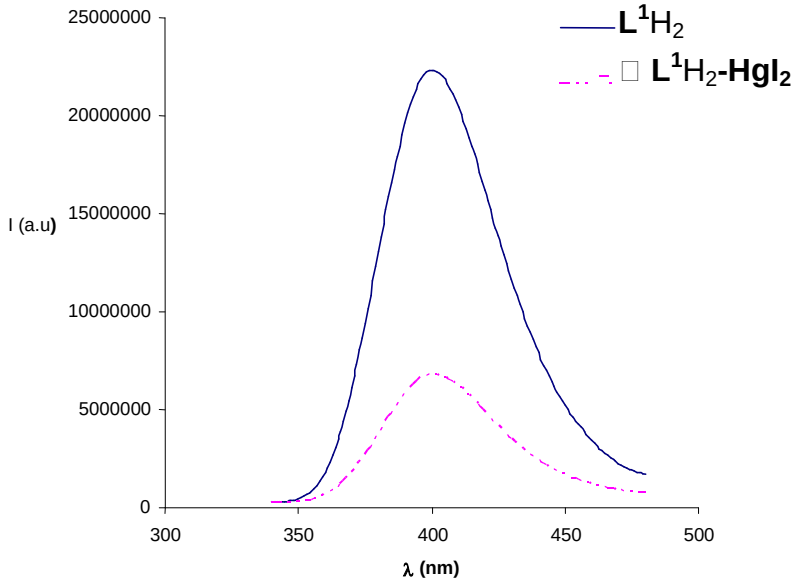

Figure C-18: Solid-state luminescence spectra recorded at room temperature for L^1H_2 (solid line) and L^1H_2-HgI_2 (dotted line) (λ^{ex}= 260 nm).

Upon excitation at 260 nm, the neutral ligand shows an emission with a maximum at λ=400 nm in the solid state, which can be also attributed to intraligands transitions (π^*- π). The emission spectrum of **L^1H_2-HgI_2** displays an emission band centered at λ=404 nm, almost equal to that of the free ligand, but with a drastically decrease in intensity (Figure C-18). No significant red shift traducing a possible metal effect was noted. The observed luminescence can again be attributed as originating from an intraligand process. This result parallels with those observed in the metallo-dithiolene complexes[170] and mercury (II) polyyne polymers[169] reported. In both case the luminescence was dominated by intraligand processes.

C.5.2.3 Luminescence studies of the L^1H_2-AuCl complex

We have discussed above the supramolecular structure of this gold complex as being one of the best model showing, how combination of inter- and intra-molecular hydrogen bonding interactions (weak) and aurophilic interaction could be used to settle supramolecular structure. The resulting luminescent properties are fascinating as well. Figure C-19 shows the luminescence spectra of **L^1H_2-AuCl** both in the solid state and in solution (2MeTHF at 77K).

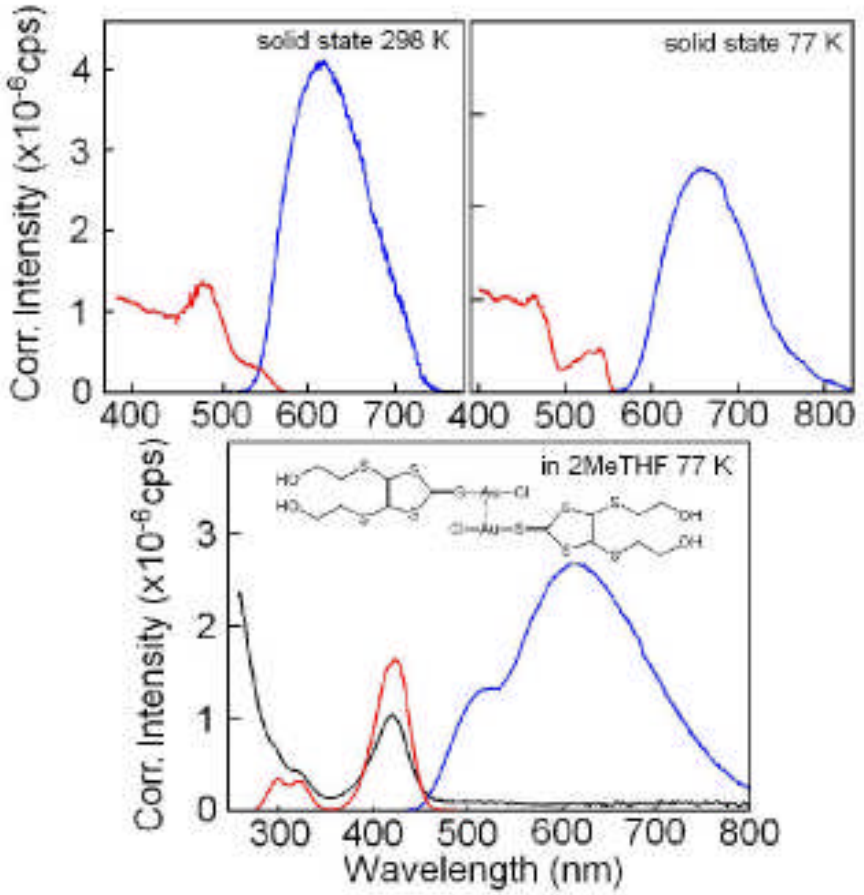

Figure C-19: Emission (blue), excitation (red), and absorption spectra (black) of L^1H_2-AuCl in the solid state and in 2-MeTHF solution at 77 and 298 K. No luminescence was observed in solution at 298 K.

The absorption spectrum of the free ligand $\mathbf{L^1}H_2$ displays an intense peak centered at 380 nm and the corresponding gold complex $\mathbf{L^1}H_2$**-AuCl** present a peak at 412 nm (lowest energy transition). This is the first observation illustrating the originality of this gold system compared to the above studied metal-dithiolene complexes. The assignment of this transition is not easily attributed.

The π–π^* transition of a thione ligand is expected to be shifted by 4200 cm^{-1} when the thione function binds to a gold center[158], if assignment of these transitions are based upon the model of Spanget-Larsen.[182] Compared to the free ligand the shift observed in the complex average the 2500 cm^{-1}. On the other hand, the electronic transitions in absorption spectra of gold complexes are mainly dominated by IL (intraligand) and LMCT (ligand to metal charge transfer)[153, 173] transitions rather than metal centered transitions.

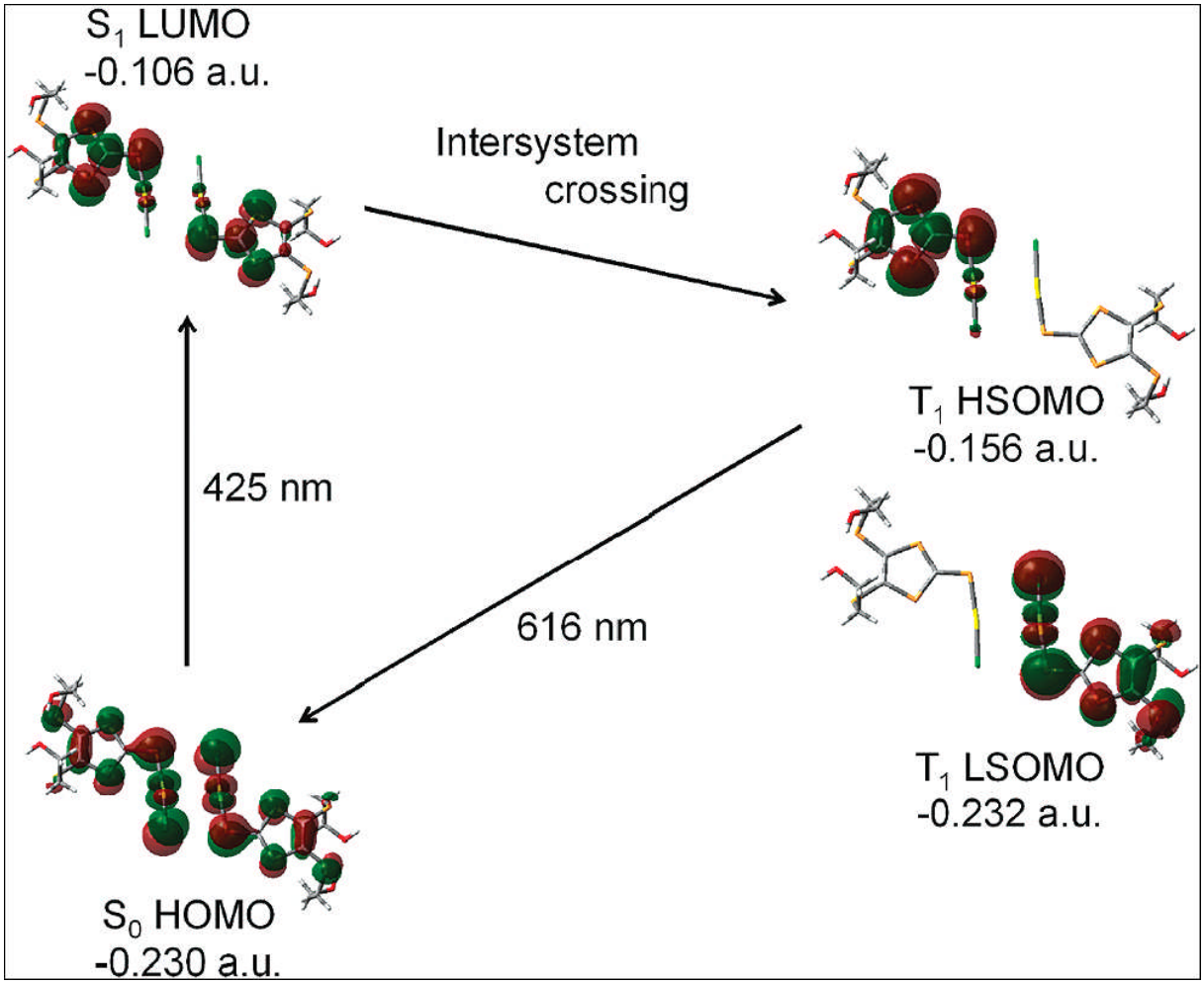

Figure C-20: Calculated MOs involved in the absorption and emission spectra of two interacting complexes L^1H_2-AuCl.

To correctly assign this absorption we have used computing methods based on density functional theory (DFT).[183] Figure C-18 represents the molecular orbitals resulting from these calculations using X-ray data of **L^1H_2-AuCl**.

The HOMO (highest occupied molecular orbital) is composed primarily of the chlorine lone pair, Au d_{xy} and p orbital of the sulfur atom of the C=S bond (Figure C-18). Some minor contributions of the π system of the dithiolene ligand are also noted. The LUMO (lowest unoccupied molecular orbital) is now mainly composed of the π system of the trithiocarbonate part of the dithiolene. Thus, these computations indicate that the lowest energy transition is X/MLCT (i.e., halide/metal-to-ligand charge transfer). The computed transition wavelength is 425 nm, which fits favourably to that observed in the spectra (i.e., about 480 nm in the solid and 420 nm in solution; Figure C-19).

The fact that the emission maximum is red-shifted in the solid state with respect to the solution is due to Au•••Au interactions, generating sets of Au_2-centered bonding and antibonding orbitals mixed with the MLCT manifolds.[176, 178] Indeed, the gold d_{xy} orbital calculated in the HOMO combines in the dimer to form the dδ* contribution to the overall MO. So, we assign the MLCT transition for **L^1H_2-AuCl** in solution to an isolated complex and for **L^1H_2-AuCl** in the solid state to a dimer-like complex.

The emission spectra of **L^1H_2-AuCl** are presented in Figure C-19. The spectra are characterized by an emission band centered at 615 nm at 298 K, which is red-shifted at 77 K to 670 nm.

The diradical nature of the triplet state consists of one electron of the LUMO on one complex **L^1H_2-AuCl** (-0.156 au) of the Au•••Au interacting dimer and one electron located on the HOMO (-0.232 au) of the other complex **L^1H_2-AuCl**.[183] The computed emission wavelength is 616 nm, which fits nicely with that observed at room temperature. Evidence for Au•••Au interactions comes from the red-shift of the emission band which is expected upon contraction of the unit cell (the crystal structure of **L^1H_2-AuCl** exhibits a Au•••Au separation of 3.078(6) Å). **L^1H_2-AuCl** is not luminescent at 298 K. At 77 K, a strong emission band is observed with a maximum at ~ 610 nm, which is blue-shifted with respect to the solid state emission spectrum (680 nm) at this temperature and to the one at 298 K (615 nm). On the basis of this blue shift and the assignment made for the absorption band in solution, a MLCT assignment for an isolated molecule is also suggested.

C.6 Conclusion

From the light of this study it comes out that, supramolecular architectures are generated by using suitable functional ligands which can further coordinate to metal centers. The presence of functional groups such as alcohol or acid group (hydrogen bonding ability) in a DMIT skeleton (π–π stacking ability and coordination of the sulfur) plays an important role in the supramolecular organisation. Using d^{10} metals which allow unusual metal-metal interaction is also an attractive method for building supramolecular coordination complexes.

In all the metallo-dithiolene complexes (**L_0-CuI**, **L^1H_2-HgI_2**, **L^1H_2-AuCl** and **L^2H_2-AuCl**) studied in this chapter, we have identified different non-bonding interactions

(π–π, S•••S, hydrogen bonding, metal•••metal interactions). They can simultaneously coexist in a complex, and they can also act independently. However, according to these studies, we can not order these interactions in terms of strength. We can not summarise this study without pointing out the conformation change of the ligand **L_1** upon coordination on Au (I) and Hg (II).

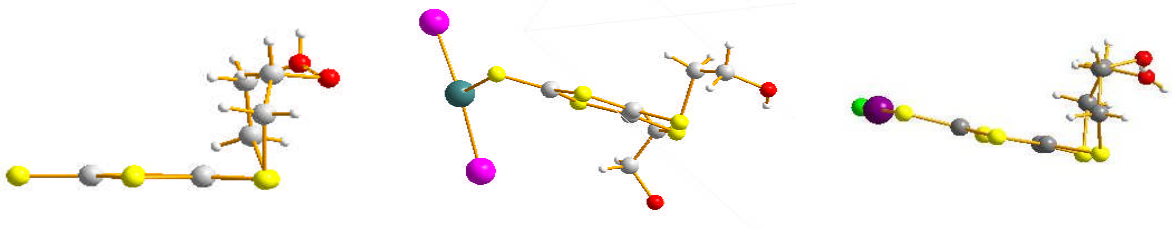

L^1H_2 **L^1H_2-HgI_2** **L^1H_2-AuCl**

From a *syn*-configuration (in the free ligand), **L^1H_2** adopts an *anti*-configuration upon coordination by Hg (II) and a *syn*-configuration upon coordination on gold (I). This is intriguing since the coordination occurred in the same thione (C=S) position. But, this observation support that the metal-metal interaction is the driving force in complex **L^1H_2-AuCl** (the dimer-like nature of the complex). Thus, no change in the ligand conformation was observed. While in the case of **L^1H_2-HgI_2**, the bridging nature of the iodine induces a steric factor which results in conformation change of the ligand (*anti*-configuration). Therefore in the case **L^1H_2-HgI_2**, the bridging nature of the iodine can be accounted for driving forces.

The other point concerns their luminescent properties. Once more the gold (I) complex gives the most fascinating results. It emits an intense red emission as shown in the following picture. In the case of the copper and mercury complex the luminescent is dominated by an intraligand process.

NB: the **L^2H_2-CuI** complex have not been described because of the poor quality of the crystals. But, the emission observed under UV irradiation seems to be promising for investigating photoluminescent properties.

Gold complex evaporated in a round bottom flask and irradiated under UV lamp (366 nm).

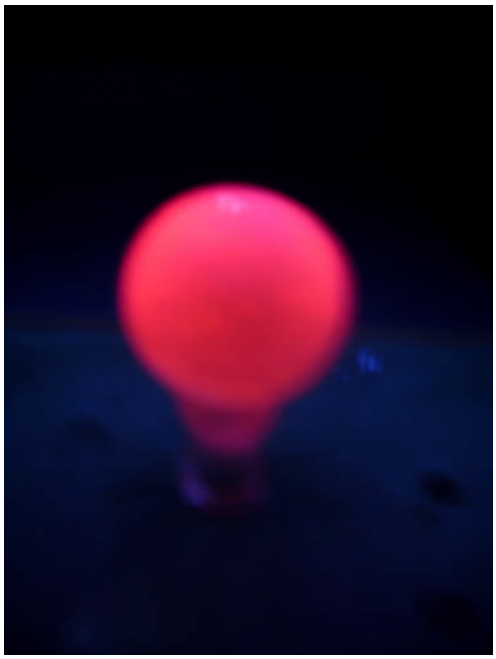

L_2-CuI complex in solution (THF- Acetonitrile) irradiated under UV lamp at low temperature:

366 nm **254 nm**

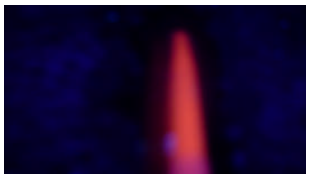

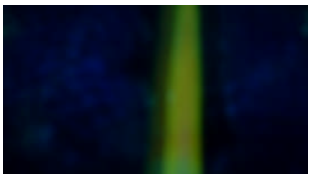

CHAPTER D. NIR- AND VIS-EMITTING LANTHANIDE-DITHIOLENE COMPLEXES (Ln^{3+}-Dithiolene)

D Reactivity of dithiolene-like neutral ligands towards trivalent lanthanide (Ln^{3+}): luminescence studies

The chemistry of lanthanide started in 1794 in Scandinavia when Johan Gadolin succeeded in obtaining an earth oxide (composed of different elements) from a black mineral that he named "Yttria".[61] The pronounced similarity of lanthanide rendered their classification and separation so difficult that more than 100 years were needed to completely isolate them from each other.[61]

The challenge behind this area of chemistry is not only due to their later discovery (compared to others elements of the periodical table) but to the wealth knowledge of their chemistry (f-block chemistry). The first approach consisted in their treatment as d-block metals (transition metals). But some observations in their behaviour and reactivity indicated that their chemistry does not fit well to transition metals chemistry. Their spectroscopic and magnetic properties are largely uninfluenced by the ligand etc.[61]

D.1 Properties of lanthanides

The terminology "rare earths" is referred to the group of lanthanide elements (from lanthanum (La) to lutetium (Lu)) including yttrium (Y) and scandium (Sc) which display similar chemical properties to those of lanthanides.[59] They are all stable as trivalent (Ln^{3+}) cations and research on lanthanides is mainly focussed on spectroscopic and magnetic properties. These properties are dominated by their electrons localised in the f sub-shell. In the following, we will only deal with the trivalent lanthanides (Ln^{3+}), although, some of them are also stable in divalent or tetravalent states.

D.1.1 Magnetic properties

Except for La (f^0) and Lu (f^{14}) the lanthanides are all paramagnetic and possess unpaired electrons. Since their excited states are well separated from the ground state (see Dieke Diagram in chapter A (Figure A-9)), it results that their magnetic

properties are largely dominated by their ground state. The f-electrons do not participate in the formation of the bonding in lanthanide complexes. Thus, the magnetic moment of the Ln^{3+} ions is independent of the surrounding ligand (contrarily to transition metal complexes).[61]

Magnetic moments are given by the following equation:

$$\mu_{eff} = g_J \sqrt{J(J+1)}$$

where g is the Landé factor and is defined by $g_J = 3/2 + [S(S+1)-L(L+1)] / 2J(J+1)$ and S is the spin quantum number; L is the total angular momentum quantum number, and J is defined by values between (L+S), (L+S)-1; (L-S).
Table D-1 gives magnetic moments of Ln^{3+} ions at room temperature[61].

Table D-1: Magnetic Moments of Ln^{3+} ions at room temperature[61].

	f^n	Ground term	Predicted μ_{eff}	Calculated μ_{eff}
La	0	$^1S_0$	0,00	0,00
Ce	1	$^2F_{5/2}$	2,54	2,46
Pr	2	$^3H_4$	3,58	3,48
Nd	3	$^4I_{9/2}$	3,68	3,44
Pm	4	$^5I_4$	2,83	??
Sm	5	$^6H_{5/2}$	0,85	1,64
Eu	6	$^7F_0$	0,00	3,36
Gd	7	$^8S_{7/2}$	7,94	7,97
Tb	8	$^7F_6$	9,72	9,81
Dy	9	$^6H_{15/2}$	10,63	10,60
Ho	10	$^5I_8$	10,60	10,70
Er	11	$^4I_{15/2}$	9,59	9,46
Tm	12	$^3H_6$	7,57	7,51
Yb	13	$^2F_{7/2}$	4,53	4,47
Lu	14	$^1S_0$	0,00	0,00

The magnetic moment in the second half of the lanthanide's serie is stronger than that of the elements in the first half. This is due to the selection rules in the determination of the ground state, since J= L+S for more than half-filled shells and J= L-S for less than half filled shells. Irregularities observed in the case of Eu^{3+} and Sm^{3+} are caused by contributions of others terms in the ground states accessible by thermal population.[61, 184]

D.1.2 Spectroscopic properties: luminescence

Trivalent lanthanides are interesting for spectroscopic purposes, because of their unusual transitions within the f sub-shell normally forbidden by Laporte's selection rules. They display sharp f-f electronic transitions resulting from rearrangement of electrons within the f sub-shell and therefore producing narrow bands with absorption coefficients lower than 10 $M^{-1}.cm^{-1}$ (compared to 100000 $M^{-1}.cm^{-1}$ for transition metals or organic chromophore).[75]

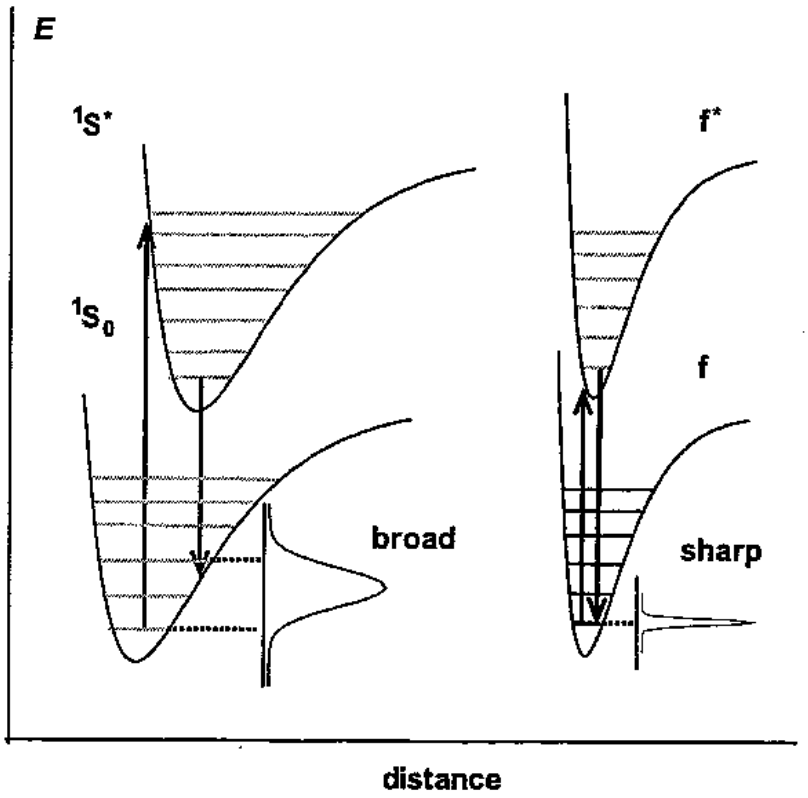

Scheme D-1: Sharp emission from the Ln^{3+} ions due to the small offset of the electronic levels as shown from the configuration coordinate (right); as comparison, the case of an organic molecule is depicted on the left ($^1S_0$ and $^1S^*$ denotes the singlet ground state and singlet excited states respectively) (adapted from reference 75).[75]

They do not experience a ligand field because the f electrons are shielded from the ligand field by the 5s and 5p electrons. Scheme D-1 represents the configurational coordinate diagrams in the case of Ln^{3+} compared with organic molecules.

D.1.2.1 Electronic transitions

The crystal field splitting in lanthanide is about a couple of hundreds cm^{-1}.[184] As a consequence, electronic spectra of lanthanide complexes resemble closely to those of the free ions. A reduced energy diagram of the elements involved in our studies (Nd^{3+}, Eu^{3+}, $Tb^{3+}$and Er^{3+}) is represented in Figure D-1 (the full version can be found in Figure A-9 in chapter A).

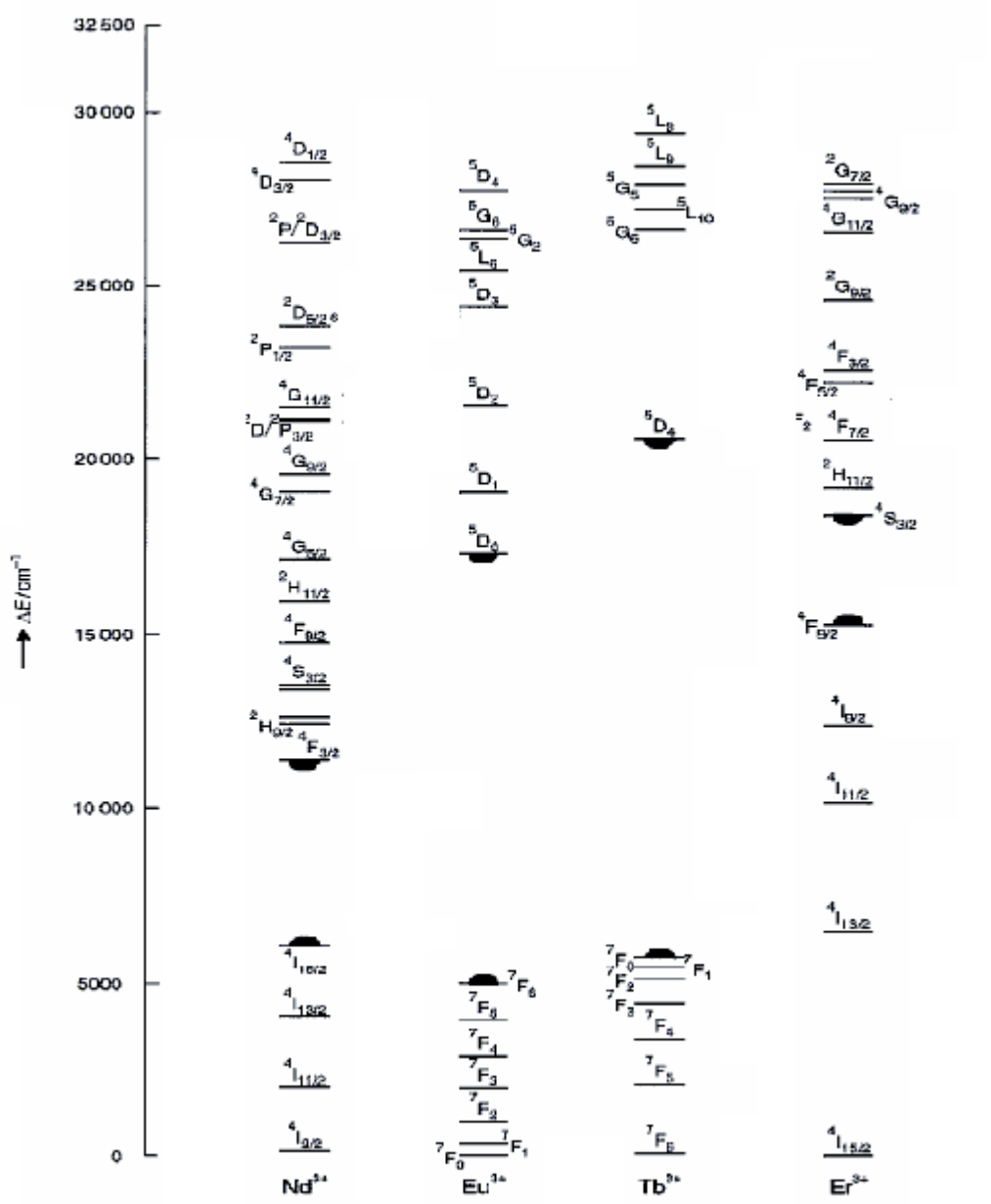

Figure D-1: A reduced energy diagram showing energy level of trivalent lanthanides involved in our studies.(: lowest luminescent level, : highest non-luminescent level).

The different terms in the energy level diagram result from a combination of electronic repulsion, spin-orbit coupling and ligand field as shown in Scheme D-2.

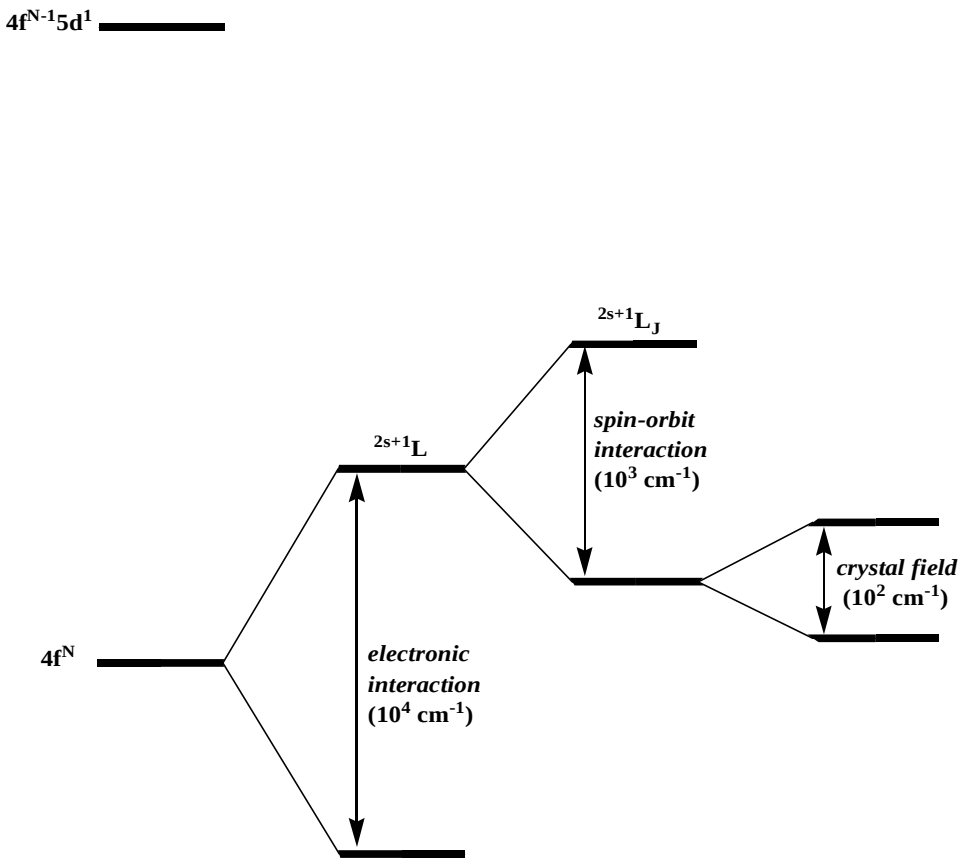

Scheme D-2: diagram illustrating the relative strength of the different parameters involved in the splitting of the $4f^N$ configuration in the Ln^{3+}.

First of all, interelectronic repulsion (ER) gives terms separated energetically by ca. 10^4 cm^{-1}. The spin-orbit (SOC) contribution splits the resulting terms in different levels separated by energy around 10^3 cm^{-1} and finally, these degenerated levels are partially splitted by the crystal field (CF)(in complexes) in such a way that the resulting sub-levels are separated only by 10^2 cm^{-1}.[184] It should be noted that the amplitude of the energy difference resulting from levels splitted by spin-orbit contribution (10^3 cm^{-1}) and crystal field contribution (10^2 cm^{-1}) is inversed in the case of transition metals.

D.1.2.2 Type of electronic transitions in complexes

Generally, transitions in trivalent lanthanides arise within the f-levels. But, here we will mention about three possible electronic transitions that have been identified in lanthanides complexes. Those arising from charge transfer transitions (MLCT and LMCT) which are Laporte's allowed, those corresponding to promotion of a 4f electron into the 5d sub-shell (parity allowed) and finally those from pure f-f transitions which are Laporte's forbidden.[75]

LMCT or MLCT appears normally at higher energy > 40000 cm^{-1} except for ions which are easily reduced to their +2 oxidation states (Sm^{3+}, Eu^{3+}, Tm^{3+}, Yb^{3+}) or oxidised to their +4 states (Ce^{3+}, Pr^{3+}, Tb^{3+}) in which cases they can be observed at energies as low as 30000 cm^{-1}.

Transitions corresponding to a promotion of electrons from the f level to the d level are parity allowed and results in absorption coefficients between 10^{-2} to 10^{3} $M^{-1}.cm^{-1}$. They are largely depending upon the environment because the 5d orbitals are external and feel the crystal field effect. These transitions are quite energetic and are sometimes observed in the region below 50000 cm^{-1} for Ce^{3+}, Pr^{3+} and Tb^{3+}.

Finally, the f-f transitions which represent our matter of interest are Laporte's forbidden and present low absorption coefficients. They gain in intensities through mixing in higher electronic states of opposite parity (d states) or "vibronic coupling" (destroying any center of symmetry) although this effect is relatively weak in lanthanides.[61]

D.1.2.3 Antenna effect

Because of their low absorption coefficient, a direct excitation of lanthanide is unfavourable, leading to weak emission. A possibility to overcome this problem consists of using a chromophore to enhance the luminescence properties. This is known as "antenna effect". It was first observed in 1942 by Weissman[185] and interpreted as an intramolecular energy transfer. Later on, Lehn[87] proposed a conversion of light via a three step "absorption – energy transfer – emission" mode. This feature is nowadays termed as antenna effect and a schematic representation of the process has been proposed by Bunzli *et al.*[186, 187]

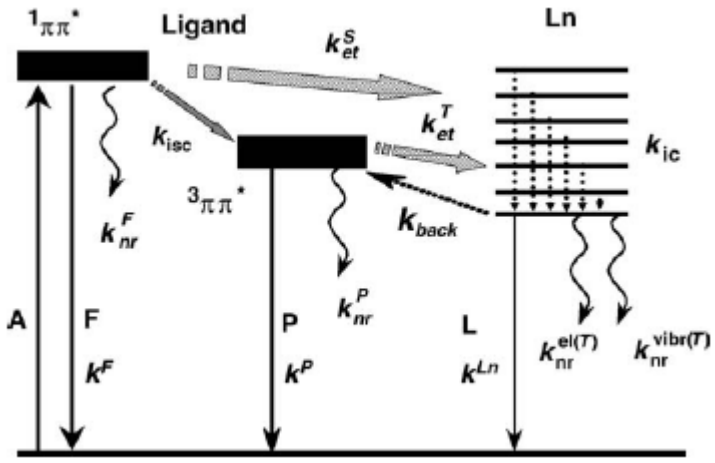

Scheme D-3: Simplified diagram showing the energy migration paths in a trivalent lanthanide complex.(1ππ*, singlet state; 3ππ*, triplet state; A, absorption; F, fluorescence; P, phosphorescence; L, luminescence (either fluorescence or phosphorescence); isc, intersystem crossing; nr, nonradiative; ic, internal conversion; et, energy transfer; back, back transfer; T, temperature-dependent; el, electronic; vibr, vibrational).[186]

Once the ligand is excited to its singlet states, it can release its energy by radiative way (fluorescence) or nonradiative way. It can also populate the triplet states via intersystem crossing (ISC). At this stage, the deactivation by radiative deactivation (phosphorescence) or energy transfer to populate the lanthanide's excited states is possible. The lanthanide can either luminesce or depopulate the excited levels by loosing its energy. The "antenna effect" represents the whole process from absorption of the energy to emission of the lanthanide. It should be argued that all radiative processes (fluorescence, phosphorescence or luminescence) are in strong competition with nonradiative ones (electronic, vibration or thermal). Note that the ISC (intersystem crossing) is facilitated by the heavy atom effect, enhancing therefore the luminescence properties of a lanthanide ion.[70]

D.1.3 Luminescence properties: case of europium (Eu^{3+}) and terbium (Tb^{3+})

Because of the originality of their transitions, lanthanides are easily recognisable (through their narrow and sharp bands) and are ideal candidates for optical probes.[70] Amongst the lanthanides, Eu^{3+} and Tb^{3+} have been well investigated[70, 184, 188-190] and fully characterised, so that they represent nowadays well-known models for

optoelectronic application. This is partly due to their luminescence in the visible region but also to their longer lifetimes[187] and their high quantum yield.[191-193] Another feature is that their configuration $4f^6$ and $4f^8$ are conjugated, which means that their energy matrices are identical.[61]

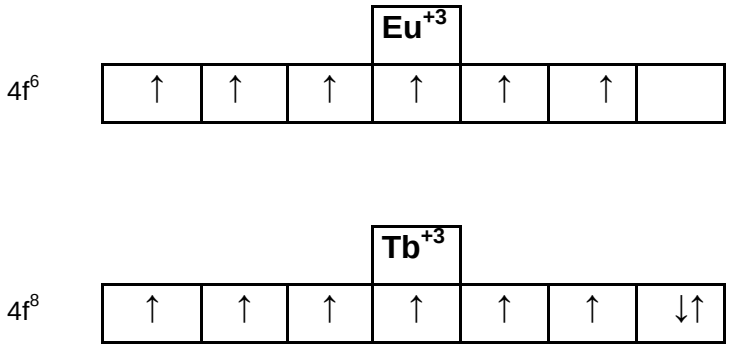

Since we are interested in optical transitions and since light is an electromagnetic wave, two operators can performed the transition: the electric dipole (**ED**) operator and magnetic dipole (**MD**) operator (NB: transitions caused by quadrupolar and octopolar operators could be envisaged but their intensities would be extremely faint).[184]

D.1.3.1 The Eu^{3+} ion

Europium (III) has a $4f^6$ electronic configuration which gives rise to the following terms ^7F_J with the different J values (J= 0, 1, 2 ,3 ,4 ,5 and 6) in the ground states, the term symbol for the ground state corresponds to the $^7F_0$ (determined by Hund´s rule) since the shell is less than half-filled. A partial energy diagram for Eu^{3+} showing the magnitude of the different splitting interaction (**ER** for electronic repulsion, **SOC** for spin-orbit coupling and **CF** for crystal field) is shown in Scheme D-4.

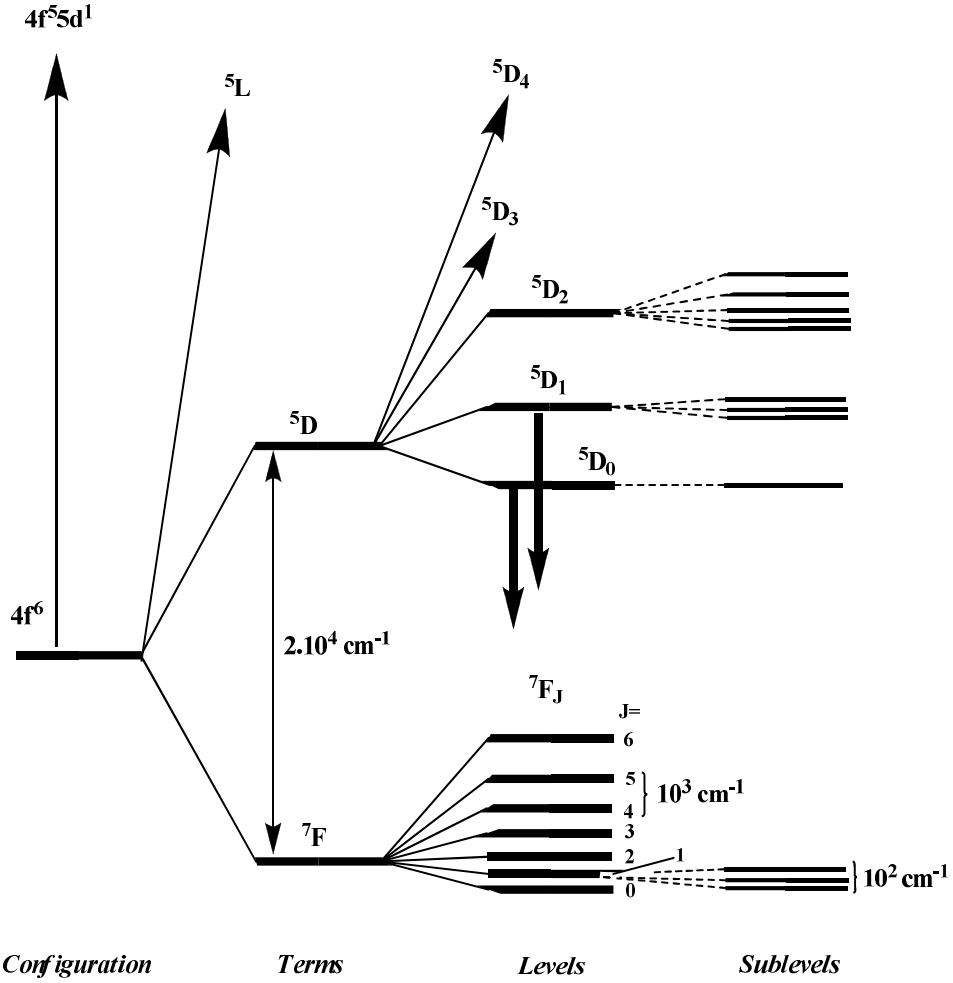

Scheme D-4: Partial energy diagram for Eu^{3+} ion showing the relative strength of the ER, SOC and CF effects; (ER for electronic repulsion, SOC for spin-orbit coupling and CF for crystal field) Downward arrows indicate the most luminescent excited levels.[184]

In solution, the most observed lines for Eu^{3+} complexes are associated to transitions arising from the $^5D_0$ level to the ^7F_J levels, while in the solid state strong lines originating from the $^5D_{1,2,3}$ levels are sometimes observed.[184] Table D-2 gives typical features of the luminescent transitions for Eu^{3+} complexes in solutions (the transitions discussed here are from $^5D_{0,1}$ levels to the ^7F_J levels).

Table D-2: Principal luminescent transitions for Eu^{3+} in solution (the luminescent levels considered are the $^5D_0$ and $^5D_1$)[184].

^7F_J	Principal Dipole Character	Range (nm)	Intensity	Comments
From $^5D_0$				
0	Electric Dipole (ED)	577-581	vw	non degenerate forbidden transition; gains intensity through J-mixing in Cs, Cn and Cnv symmetries
1	Magnetic Dipole (MD)	585-600	s	allowed; intensity almost independent from environment, strong optical activity
2	ED	610-625	s-vs	hypersensitive ($\Delta J=2$); absent if the ion lies on an inversion center
3	ED	640-655	vw	forbidden, always very weak
4	ED	680-710	m-s	sensitive to the Eu-environment
5	ED	740-770	vw	forbidden, seldom observed
6	ED	810-840	vw	seldom measured
From $^5D_1$				
0	MD	524-528	vw	
1	ED	530-540	vw	sensitive to Eu-environment
2	ED	550-565	vw	

As we can see in this table, transitions are magnetic or electric dipole in character and can in a certain extent give information about the environment or symmetry of the ion. For example, the number of component of the $^5D_0 \rightarrow {}^7F_0$ transition can be related to the number of chemically distinct environments occupied by an ion in a complex. In fact, since both the initial and final states are nondegenerate this transition is unique for each Eu^{3+} in a given chemical environment.[184]

The second point concerns the ***hypersensitive*** $^5D_2 \rightarrow {}^7F_0$ transition. This transition is electric dipole in character and is absent if the ion lies in an inversion center. It possesses very strong intensities and is useful to confirm whether a system possesses an inversion center or not.

D.1.3.2 The Tb^{3+} ion

As for Eu^{3+}, the same data are available for Tb^{3+} ions in a complex. The terms in the case of Tb^{3+} are the same that in Eu^{3+} (^7F_J levels with J= 0, 1, 2 ,3 ,4 ,5 and 6). This arises from the fact that their configurations are conjugated. The only difference is in the determination of the ground state since the shell is more than half-filled giving $^7F_6$ as ground state using Hund´s rule.

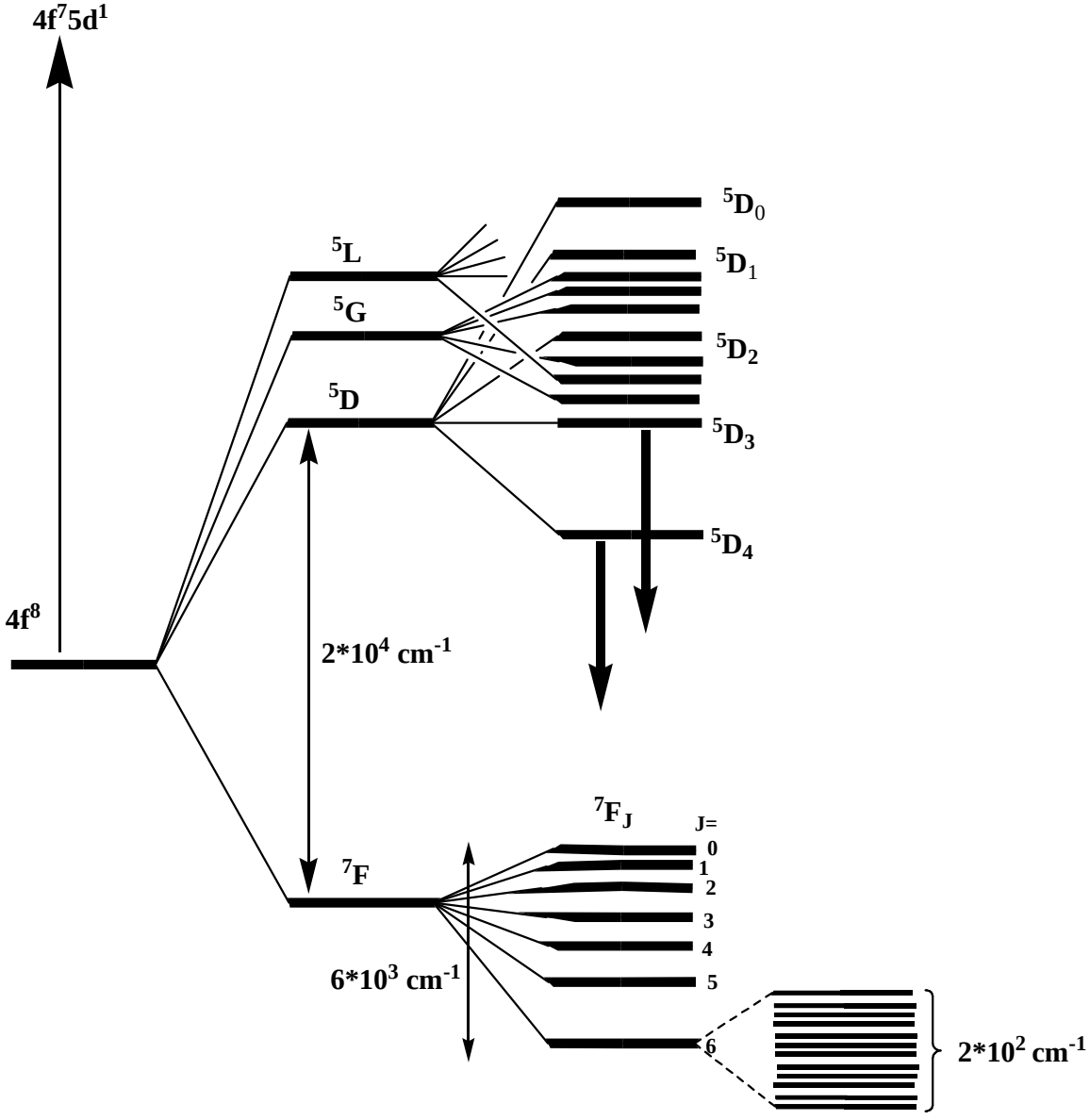

Configuration *Terms* *Levels* *Sublevels*

Scheme D-5: Partial energy diagram for Tb^{3+} ion showing the relative strength of the ER, SOC and CF effects (ER for electronic repulsion, SOC for spin-orbit coupling and CF for crystal field) (Downward arrows indicate the most luminescent excited levels).[184]

Similarly to the case of Eu^{3+}, the partial energy diagram for Tb^{3+} showing the magnitude of the different splitting interaction is displayed in Scheme D-5.
The following Table D-3 presents typical features of the luminescent transitions for Tb^{3+} complexes in solution.

Table D-3: Principal $^5D_4 \rightarrow {}^7F_J$ luminescent transitions for Tb^{3+} in solution[184].

J	Range (nm)	Intensity	Comments
6	480-505	m-s	sensitive to the metal environment
5	535-555	s-vs	best probe transition(e.g. for titration; displays strong optical activity
4	580-600	m-s	sensitive to the metal environment; displays medium optical activity
3	615-625	m	displays strong optical activity
2	640-655	w	sensitive to the metal environment
1	660-670	vw	always weak
0	675-680	vw	always weak

Contrarily to its homolog (Eu^{3+}), the terbium ion (Tb^{3+}) cannot be used to probe the structure of the complexes because of the degeneracy of the $^5D_4$ level. But, the $^5D_4 \rightarrow {}^7F_{3,5}$ transitions possess strong magnetic dipole character.

D.1.4 Photophysical data: lifetime and quantum yield in lanthanide complexes

Lifetime and quantum yield are the most significant parameters to assess the suitability of lanthanides complexes for practical applications.

D.1.4.1 Lifetime

The lifetime determines the average time that a system can spend in the excited states prior to return to the ground states by deactivation pathways. The higher the lifetime the best the system can be used for optical application. This parameter is of course very sensitive. It decreases as function of different process such as presence

of oscillator in the metal surrounding. The energy gap between the lowest emitting level of excited states and highest non luminescent level of the ground states of the lanthanide is a determinant parameter in the quenching by OH oscillators.[70] The smaller this gap, the easier for non-radiative deactivation process to govern the luminescence.[70]

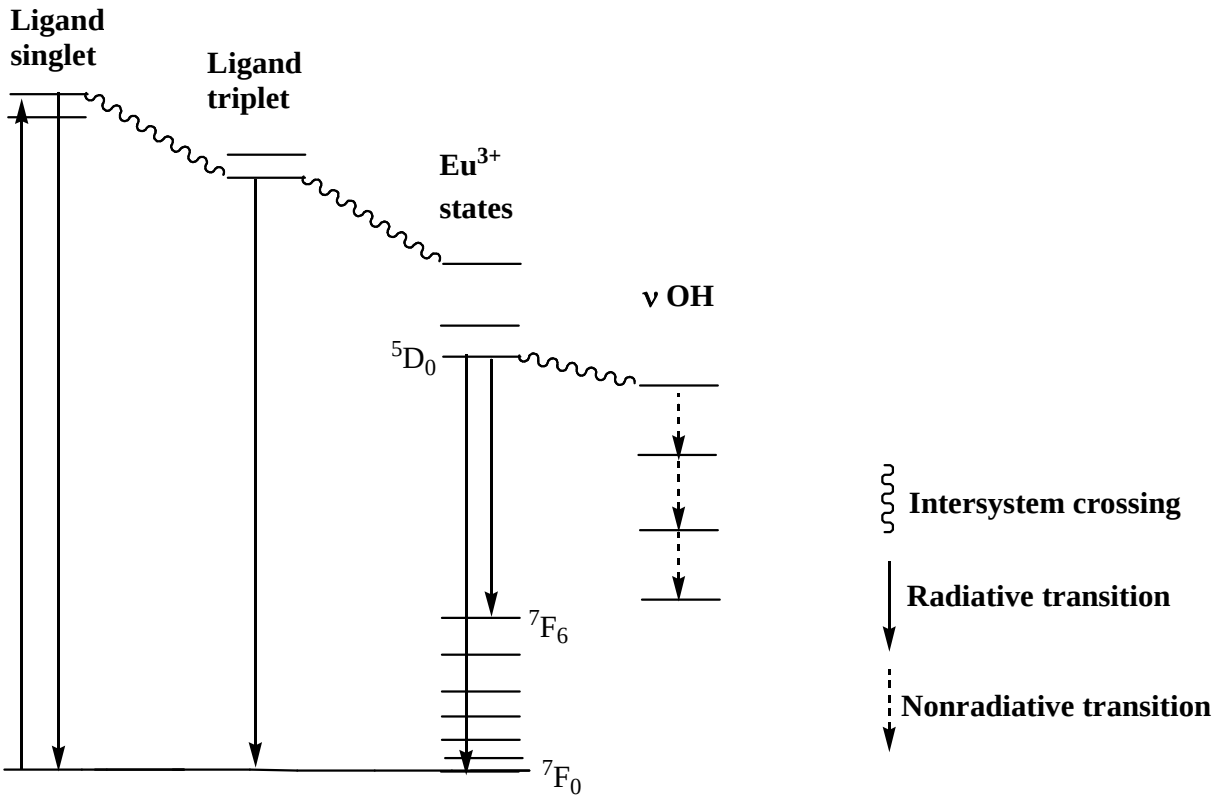

Figure D-2: Example based on Eu^{3+} showing the quenching of luminescence by OH oscillators.[61]

Oscillators such as C-H, N-H and OH are efficient quenchers. They act in the deactivation process taking place in the excited states as represented in Figure D-2. It is noteworthy to precise that these quenchers are only effective when they are localised in the first coordination sphere of the metal ions. In solution, the quenching by OH oscillators can be reduced using deuterated solvents while solid state measurements give the highest values. For example, the luminescence lifetime of the Eu^{3+} $^5D_0$ level which is about 0.1-1 ms in aqueous solution can reach 4-4.5 ms using deuterated solvents and may be as long as 5-6 ms in the solid state.[184] The luminescence lifetimes of the Eu^{3+} $^5D_1$ level are much shorter and are usually < 0.05 ms.

The following table gives lifetimes measured in europium and terbium complexes.

Table D-4: Lifetimes in ms for $^5D_0$ (Eu) and $^5D_4$ (Tb) excited states in diluted solutions of $Ln(NO_3)_3$ (C < 0.1 M).[184]

	H_2O	D_2O	CH_3CN	DMSO
Eu $(NO_3)_3$	**0.114**	**3.71**	**1.35**	**1.4**
Tb $(NO_3)_3$	**0.478**	**3.2**	**1.85**	**2.61**

It should be noted that the luminescence lifetimes of the Tb^{3+} $^5D_4$ level are much longer than those of Eu^{3+} $^5D_0$ level.

D.1.4.2 Quantum yield

The quantum yield is basically defined by the ratio between the number of photons emitted and the number of photons absorbed by a sample.[73, 194] It is often given in %. But its determination is somewhat tricky and the data are scarce and less reliable.[184]
Generally, the quantum yield can be determined by comparison with standard phosphors, whose quantum yields have been measured.[194] While, for determination in solution, some standards are available, those measured in the solid state remains, critical and needs careful consideration.
The best method for the determination of the quantum yield in the solid state has been proposed by Wrighton *et al.* [195] and consists in using an integration sphere. This method was improved by de Mello *et al.* [196]
However, one has to distinguish between overall quantum yield (Q^{L}_{Ln}) and intrinsic quantum yield (Q^{Ln}_{Ln}). In the case of ligand sensitization, they are related by a factor efficiency (η_{sens}) through the following equation: [70, 197, 198]

$$Q^{L}_{Ln} = \eta_{sens} \bullet Q^{Ln}_{Ln} \qquad \text{(Equation D.1)}$$

η_{sens} represents the efficiency of the energy transfer through ligand excitation. This value can not be measured directly, but it can be estimated using the overall and intrinsic quantum yields. The overall quantum yield can be measured by using standard phosphors in solution or the above mentioned integration sphere device for

solid samples.[196] The intrinsic quantum yield can be calculated by using the following equation[190, 198]:

$$Q_{Ln}^{Ln} = \tau / \tau_0 \qquad \text{(Equation D.2)}$$

where τ_0 is the natural luminescence lifetime and τ is the observed luminescence lifetime. Estimated τ_0 values for some lanthanides in the solid state are available,[199] whereas τ can be calculated by direct measurement.

The quantum yield determination in solution suffers from the necessity to perform the measurement in identical conditions (solvent, concentration, and excitation and emission range) than the standard solution (fluorescein for example) and this is not always easy to handle. As an illustration the quantum yield for europium is solvent-dependent (Table D-5).[184]

Table D-5: Quantum yield (in %) of lanthanide perchlorates ($Ln(ClO_4)_3$) in different solvents.

Lanthanides	H_2O	D_2O	CH_3CN	DMSO
Eu	0.5	78	20	27
Tb	8,40	.	.	.

D.2 Motivation for Ln^{3+}-dithiolene systems

To date, most of the reported Ln-S systems are concerning with lanthanide thiolate[200] or chalcogenates[201, 202] but also Ln-S clusters. Lanthanide sulfido clusters are obtained by reacting lanthanide thiolate [$Ln(SPh)_3$) with Pr, Nd, Gd] and elemental sulphur.[203] Lanthanide thiolates can be prepared by metathesis or by oxidative addition of disulfide RSSR (R= Ph) to metallic lanthanide.[202] Most of these lanthanide thiolates are obtained by using aryl-, isopropyl-, butyl- or benzene-thiolate ligands.[204]

Investigation on Ln^{3+}-dithiolene complexes is limited to three literature reports.[37, 205, 206] However, none of these works[205, 206] describes the luminescent properties of such Ln^{3+}-dithiolene complexes. Therefore, we have found necessary to investigate on the luminescence properties of Ln^{3+}-dithiolene complexes. Indeed, the unique electronic structure of dithiolene makes them potential candidate for the enhancement of the lanthanide luminescence by “antenna effect”.

D.3 Synthesis and characterisation of Ln^{3+}-dithiolene complexes

Contrary to the previous chapters where the reactivity of the dithiolene ligand was exclusively dominated by coordination on metals through the DMIT skeleton (the thiocarbonyl group), here, we will deal with the reactivity of the dithiolene ligand involving the use of functional groups (OH and COOH). To achieve the formation of Ln^{3+}-dithiolene complexes we have used a general method starting from lanthanide silyl-amide ($Ln[N(TMS)_2]_3$; TMS= $-SiMe_3$) as outlined in Scheme D-6.

$$Ln[N(TMS)_2]_3 \ + \ 3\ ROH \xrightarrow[-\ HN(SiMe_3)]{} Ln[OR]_3$$

(TMS= $-SiMe_3$)

Scheme D-6: General procedure for the synthesis of lanthanide alkoxide using lanthanide silyl-amide.

This method has been proven to be appropriate for the synthesis of many alkoxydes[207-209] and is well suited because the hexamethyldisilazane [$HN(SiMe_3)_2$] is a volatile non-coordinating liquid and is readily removed in vacuum.

D.3.1 Synthesis and characterisation of $Ln[N(TMS)_2]_3$ (TMS= $-SiMe_3$)

The metalamides $Ln[N(TMS)_2]_3$ (TMS= $-SiMe_3$) are prepared using literature method.[210] They are isolated by salt elimination reactions starting from the lanthanide chloride and lithium hexamethyldisilasane as shown below.

$$LnCl_3 + 3\ LiN(SiMe_3)_2 \xrightarrow[-LiCl]{THF/\ Toluene} Ln[N(TMS)_2]_3$$

Anhydrous lanthanide chlorides ($LnCl_3$) were dried under vacuum at temperatures between 100 and 150°C. They are then dissolved in THF (by -196°C) and three equivalent of $LiN(SiMe_3)_2$ dissolved in toluene are successively added. $Ln[N(TMS)_2]_3$ compounds are obtained after 48h and purified by sublimation. Traces of air or humidity destroy the $Ln[N(TMS)_2]_3$ complexes which rapidly turn from their respective color to colorless, therefore, they should be handled under nitrogen atmosphere using “Stock apparatus”.

The **$La[N(TMS)_2]_3$** is obtained as a colorless powder, the **$Nd[N(TMS)_2]_3$** as a blue-violet powder, the **$Eu[N(TMS)_2]_3$** as red-orange, the **$Tb[N(TMS)_2]_3$** as colorless, **$Er[N(TMS)_2]_3$** as pink and the **$Ce[N(TMS)_2]_3$** as yellow-brown powder.
The **$Ce[N(TMS)_2]_3$** has not be fully investigated because of its sensitivity. It readily oxidizes and shows color changes even when kept under argon atmosphere. This is probably due to its electronic configuration (f^1).
The metalamides ($Ln[N(TMS)_2]_3$) are soluble in organic solvents and are purified by sublimation at temperature ranging from 100 to 150°C.

D.3.2 Reactivity of the $Ln[N(SiMe_3)_2]_3$ towards dithiolene ligands (L^1H_2 and L^2H_2)

$Ln[N(SiMe_3)_2]_3$ is sensitive to the presence of proton sources since the amide $N(SiMe_3)_2^-$ reacts strongly via protonolysis to liberate $HN(SiMe_3)_2$. Ligands **L^1H_2** and **L^2H_2** bearing alcohol and acid functional group respectively, are particularly appropriate for this purpose.

D.3.2.1 Reactivity of the $Ln[N(SiMe_3)_2]_3$ towards ligand L^1H_2

We have seen in chapter B and C that such 4,5-bis(hydroxyethyl)thio-1,3-dithiol-2-thione (**L^1H_2**) is a potential building block for supramolecular systems. In this context, the DMIT skeleton is used as the reactive part while the side chains (alcohols groups) remain unchanged. However, **L^1H_2** is a versatile ligand and shows reactivity via the functional group. Thus, **L^1H_2** was reacted with **$Nd[N(TMS)_2]_3$** and **$Er[N(TMS)_2]_3$** in a ratio 2:1 to allow for the formation of complex **$Nd_2(L^1)_3$** and **$Er_2(L^1)_3$**, respectively, following the Scheme D-7.
This reaction proceeds by protonolysis and occurs instantaneously. The limpid solution of **$Ln[N(TMS)_2]_3$** turns trouble as the ligand solution is added and a rapid precipitation was observed within a period of few seconds. The resulting mixture is stirred during 1 h after complete addition of the ligand. No change was observed even by heating or by stirring more than one hour (one week). A yellow powder was isolated by filtration and dried under vacuum. The NMR of the reaction solution after isolation of **$Ln_2(L^1)_3$** revealed the presence of free $HN(SiMe_3)_2$.

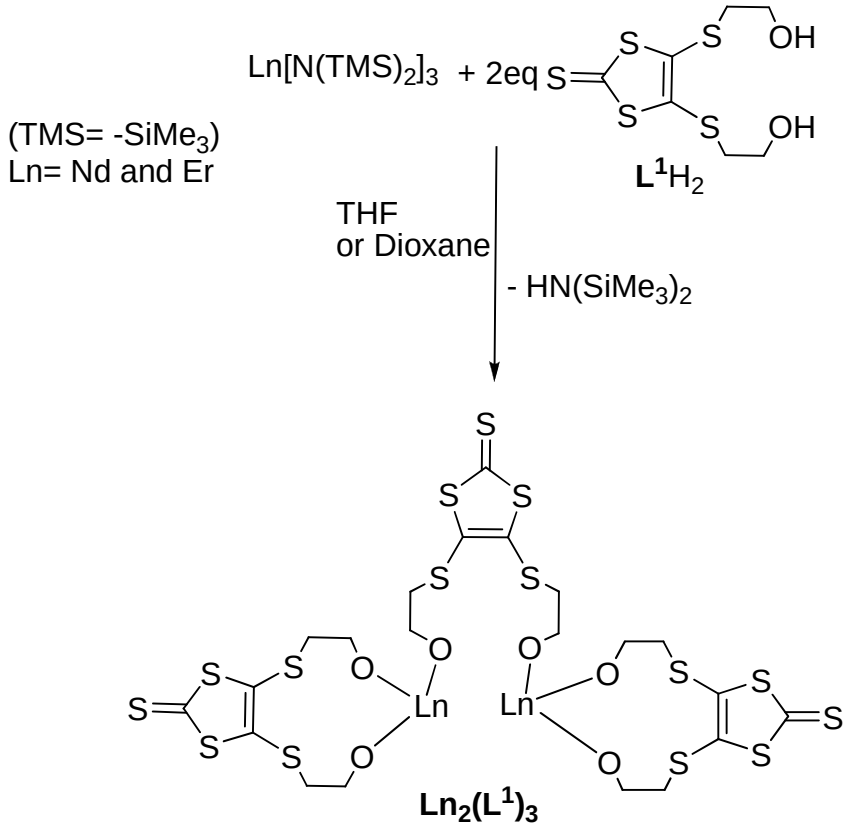

Scheme D-7: Synthetic pathways for the synthesis of $Nd^{3+}$and Er^{3+} dithiolene-alkoxide complexes and proposition of the structure.

These powders show no solubility in common solvents. Therefore we presume that the product may be polymeric in nature as already observed in the case of $[Ln(SBu)_3]$.[204]

Elemental analysis of the powder give a metal-to-ligand ratio of 2:3 as presented in Scheme D-7. The polymeric character of the product limits the characterisation by NMR and UV-vis method. Nevertheless, we have run an IR analysis using an ATR Golden gate device. The IR spectrum of the **$Nd_2(L^1)_3$** together with that of the free ligand **L^1H_2** are presented in Figure D-3. These spectra deliver important information that can help to understand the polymeric nature of the complex.

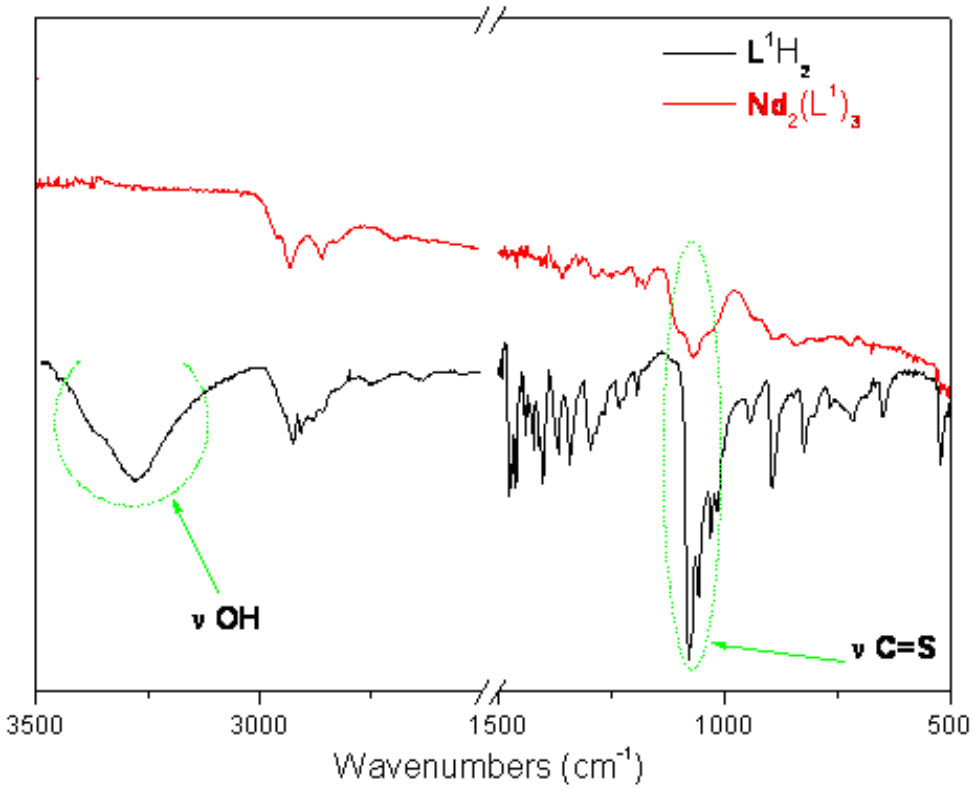

Figure D-3: IR spectra of the $Nd_2(L^1)_3$ complex (red) compared with the free ligand L^1H_2 (black).

The first important information concerns the disappearance of the OH vibration bands around 3200-3400 cm^{-1} illustrating the reactivity through the OH groups. Secondly, the C=S bands which are normally intense, are shifted in both intensity and wavenumbers suggesting the coordination of the thiocarbonyl function as observed in the **L^1H_2-M(d^{10})** (developed in chapter C) and in the thiomaltol-lanthanide complexes.[211] Consequently, we have proposed the following structure where the thiocarbonyl are coordinated on the neodymium center to explain the polymer-like nature of **$Nd_2(L^1)_3$** complex.

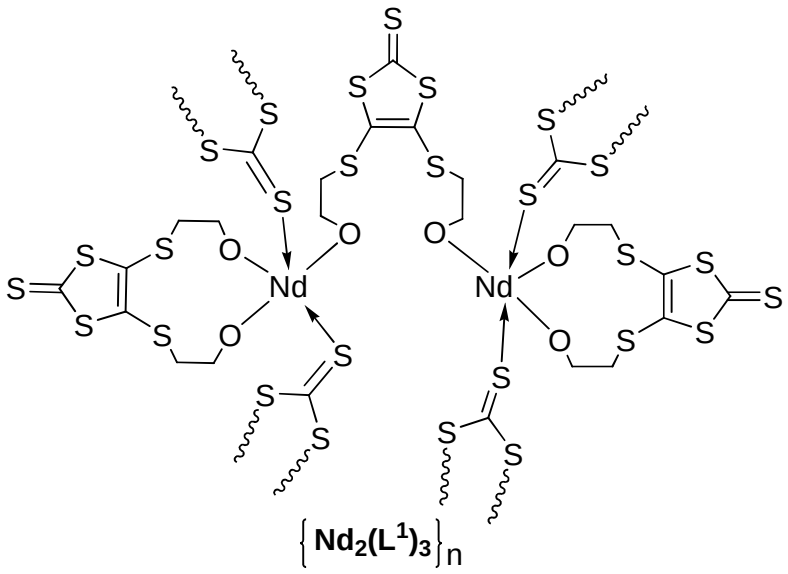

Figure D-4: Proposed polymeric structure for the $Nd_2(L^1)_3$ complex.

This additional coordination of the thiocarbonyl function is an evidence since lanthanides require high coordination number,[60] and explains therefore the polymeric nature of the complexes. The same observations apply also to the erbium complex (**$Er_2(L^1)_3$**). Attempts to synthesise these complexes by salt metathesis failed because of the difficulty to control the formation of the alkolate (from Na and Li) since a ring opening occurs or the reduction of the ligand in elemental sulfur.

D.3.2.2 Reactivity of the $Ln[N(SiMe_3)_2]_3$ towards ligand L^2H_2

Compared to **L^1H_2**, ligand **L^2H_2** is more suitable for coordinating a lanthanide center since the carboxylate group ($-COO^-$) contributes more on stabilising the metal center by chelating effect than an alkohol group. The synthetic pathway is the same that for **L^1H_2** as outlined in Scheme D-8.

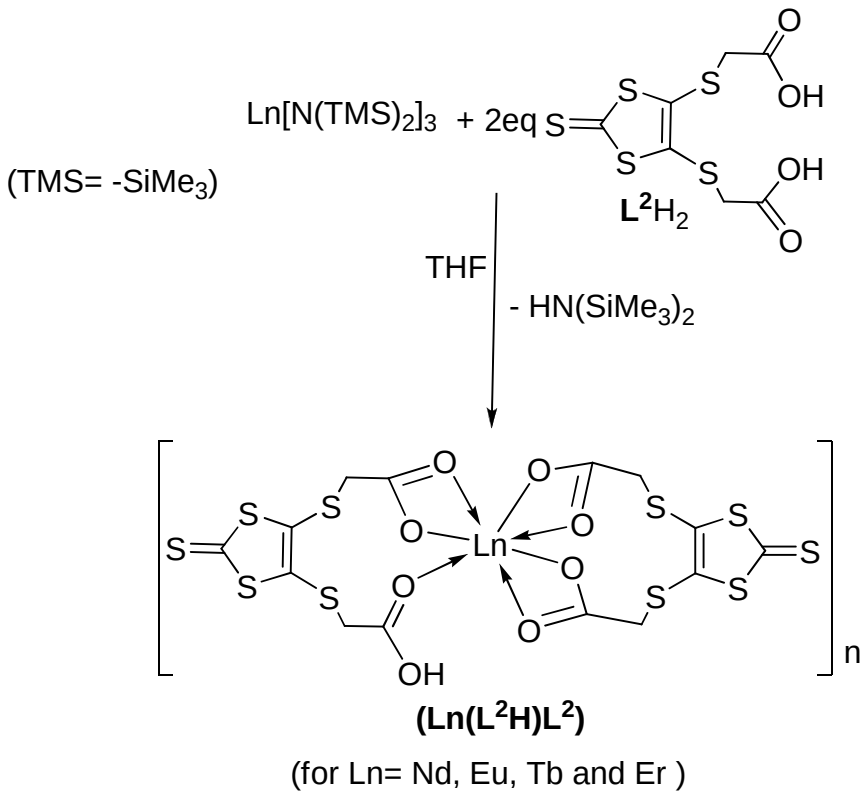

(Ln(L^2H)L^2)

(for Ln= Nd, Eu, Tb and Er)

Scheme D-8: Synthetic pathways for the synthesis of Nd^{3+}, Eu^{3+}, Er^{3+} dithiolene-carboxylate complexes.

$\mathbf{L^2}H_2$ reacts with **Ln[N(TMS)$_2$]$_3$** in a ratio 2:1 to allow the formation of **Ln(L^2H)L^2** complexes (Ln= Nd, Eu, Tb and Er). Similarly to the case of $\mathbf{L^1}H_2$, addition of a solution of $\mathbf{L^2}H_2$ to the lanthanide solution gives rise to the formation of a precipitate. Most probably it possesses a similar polymer-like nature. But in contrast to **$Nd_2(L^1)_3$** a band corresponding to an OH group is detected around 3200 cm^{-1}. Figure D-5 shows the ATR-IR spectrum of the **Eu(L^2H)L^2** complex as well that of the free ligand $\mathbf{L^2}H_2$ for comparison.

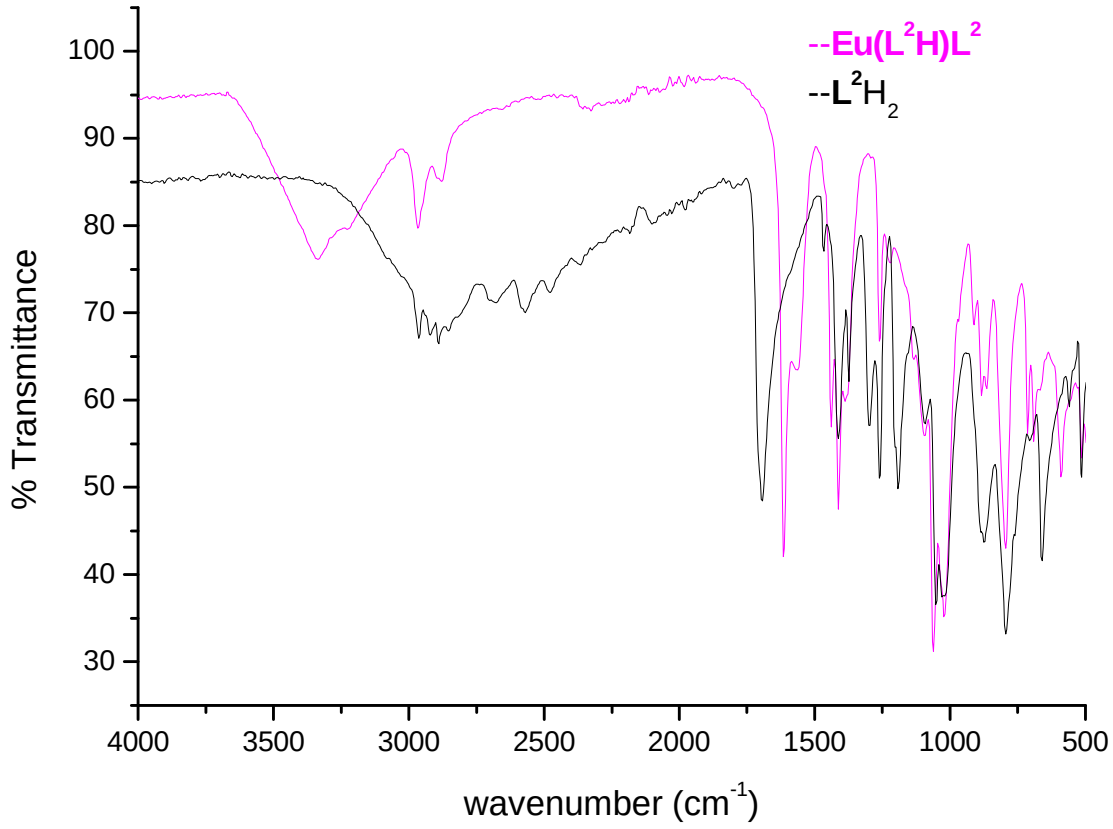

Figure D-5: ATR-IR spectra of $Eu(L^2H)L^2$ (pink) and the free ligand L^2H_2 (black).

The presence of a broad band in the range 3000-3600 cm^{-1} displayed by the europium complex is the evidence that one carboxylate group remains protonated after the reaction. Compared to the free ligand $\mathbf{L^2}H_2$ (νOH= 2800-3200 cm^{-1}), this band is shifted to higher wavenumbers proving that the OH groups are not engaged in hydrogen bonding interaction as observed in $\mathbf{L^2}H_2$.

The second point concerns the carbonyl function (C=O) which is localised at 1647 cm^{-1} compared to 1692 cm^{-1} in the free ligand $\mathbf{L^2}H_2$. This shift argues with the coordination of the carbonyl group on the lanthanide center. This coordination of the C=O groups is expected since it helps to reach a high coordination number at the lanthanide center. The C=S band in $\mathbf{Eu(L^2H)L^2}$, shifted about 14 cm^{-1} compared to the free ligand, could be also considered as a result of the coordination of the C=S to the lanthanide center. Similar statements are reliable for the other lanthanide complexes.

D.3.3 Attempts to prepare mixed d-f elements (heterometallic compounds)

Synthesis of molecular heteronuclear systems combining 5d-4f metals have been documented recently.[212-214] Such a combination give rise to the enhancement of NIR luminescence of lanthanides by attaching a suitable transition metals acting as a chromophore.[212, 215]

Our idea was motivated by the propensity of ligand **L^1H_2-HgI_2** to act as molecular system able of hosting molecules. Since the ligand in **L^1H_2-HgI_2** is coordinated via its thiocarbonyl function, it could be involved in further reaction through the alkohol rest. On the other hand, we have seen that the C=S bond participates to the coordination of the metal center and leads probably to the formation of a polymer-like material. Therefore the immobilisation of the C=S by mercury could help to avoid the polymerisation problem.

Before describing the reaction between **L^1H_2-HgI_2** and $ErCl_3$, we will introduce the existing heterobimetallic Er-Hg systems.

D.3.3.1 Er-Hg systems as rare examples of 4f-5d heterobimetallic systems

Few literature reports on heterobimetallic systems containing Er and Hg ions are known. Goodgame *et al.* reported on a Er-Hg system where the Er^{3+} and Hg^{2+} ions are connected via organic ligands such as propiolactam[216] or fused-ring lactams[217] (see Scheme D-9). These complexes are isolated from the reaction of mercury (Hg^{II}) acetate with the organic ligand (lactam) and lanthanide nitrate.

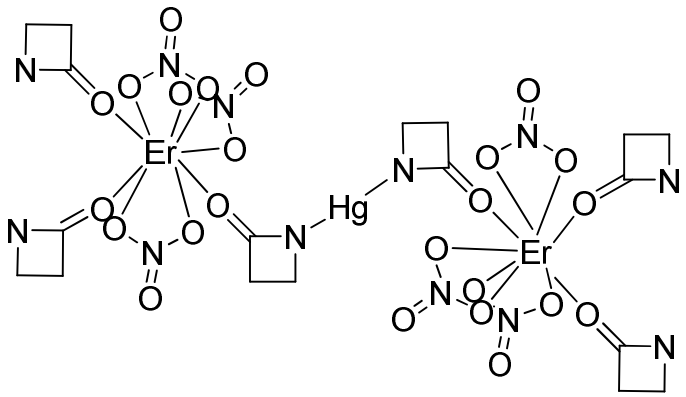

Scheme D-9: Example of Er-Hg complex obtained by Goodgame et al.[216] (NB: the propiolactam ligand (L^p) ensures the connection between the Er and Hg metal centers).

As displayed in Scheme D-9, the propiolactam (**L^p**) acts as a bridging ligand and coordinates the Er metal center via the oxygen atom (of the carbonyl group) and the Hg^{II} ion through the nitrogen atom of the lactam ring. All metal-metal contacts (Er-Er or Er-Hg) are greater than 4 Å.

Chen *et al.* have reported on another Er-Hg system obtained by hydrothermal synthesis .[218] But in this latter, the Er^{III} ion and the Hg^{II} ion are located at 9 Å from each other and there is no connection between these two ions. [218]

D.3.3.2 Ion-pair based Erbium compounds

Erbium compounds have been described as ion-pairs, in which the monocation is composed of $ErCl_2$ fragment and the monoanion part contains the $ErCl_4$ fragment. Willey *et al.* reports on a erbium ion-pair $[ErCl_2(thf)_5][ErCl_4(thf)_2]$ in which the anion is six-coordinated with an octahedral metal geometry comprising four equatorial chlorine atoms and two axial THF molecules.[219]

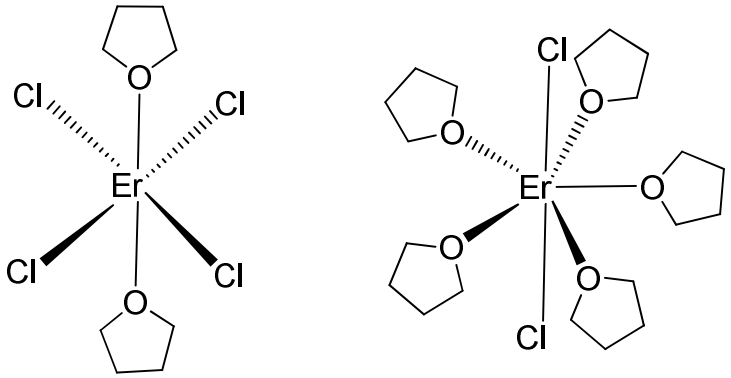

Scheme D-10: Structure of an ion-pair based erbium compound $[ErCl_2(THF)_5][ErCl_4(THF)_2]$.

In the anionic fragment ($[ErCl_4(THF)_2]^-$), the Er-Cl distances are about 2.6 Å and the Er-O (THF) distances are about 2.3 Å.[219] A similar system has been obtained by Anfang *et al.*,[220] by the reaction of erbium powder with trimethylchlorosilane. In both examples, the erbium center of the cationic fragment ($[ErCl_2(THF)_5]^+$) lies on a pentagonal bipyramid geometry, with axial positions occupied by the chlorine atoms.

D.3.3.3 Reactivity of L^1H_2-HgI_2 towards erbium chloride ($ErCl_3$): formation of an unexpected ion-pair

This reaction is conducted in THF by using two equivalents of **L^1H_2-HgI_2** and one equivalent of erbium chloride. Unfortunately, the reaction did not work as we expected. We isolated the heterobimetallic complex (**3**) as presented in the Scheme D-11 (the dithiolene ligand is not present in complex).

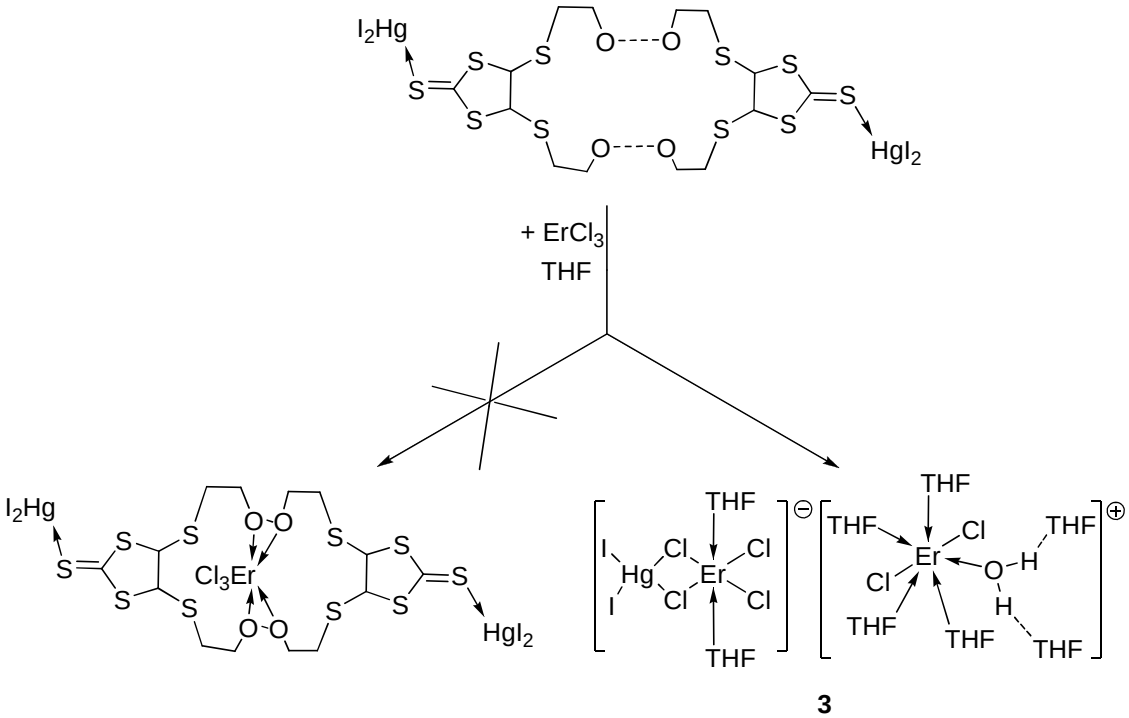

3

Scheme D-11: Attempts to access to heterometallic (5d-4f) complexes using a dithiolene template and the resulting unexpected complex (3).

It seems that a reaction between the HgI_2 and the $ErCl_3$ takes place instead of an insertion of $ErCl_3$ in the cavity of the **L^1H_2-HgI_2** (as expected). One possible

explanation of such a phenomenon could be related to the weak coordination of the thiocarbonyl function on mercury (in **L^1H_2-HgI_2**) which in solution goes through decomplexation. Another explanation can arise from the fact that compound **3** is more stable than the expected complex based on coordination bond.

D.3.3.4 Crystal structure description of complex 3

Pink crystals of **3** were grown from a concentrated THF/toluene solution of the reaction mixture. A crystal was isolated and a single crystal X-ray diffraction analysis was performed at 170 K. **3** crystallises in the triclinic system in the centrosymmetric space group $P\bar{1}$. The crystal structure of the complex **3** is shown in Figure D-6 and Table D-6 shows the crystallographical data and structure refinement for complex **3**.

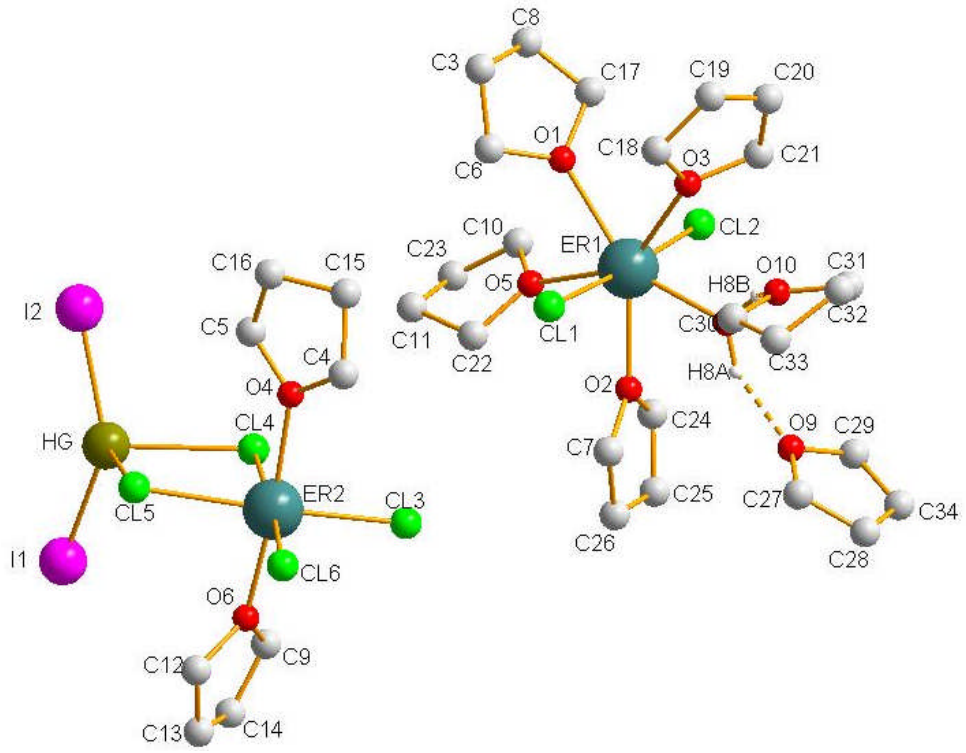

Figure D-6: Molecular structure of 3 (the hydrogen atoms of the THF molecules are omitted for clarity).

Table D-6: Crystal data and structure refinement for 3.

Compound	3
Identification code	sh2472
Empirical formula	$C_{32}H_{66}Cl_6Er_2HgI_2O_9$
Formula weight	1596.46
Temperature	170(2) K

Wavelength	0.71073 Å
Crystal system	Triclinic
Space group	$P\bar{1}$
Unit cell dimensions	a = 9.1770(3) Å α= 87.913(2)°.
	b = 15.7741(5) Å β= 75.2440(10)°.
	c = 17.9528(8) Å γ = 87.7110(10)°.
Volume	2510.19(16) $Å^3$
Z	2
Density (calculated)	2.112 Mg/m^3
Absorption coefficient	7.954 mm^{-1}
F(000)	1508
Crystal size	0.52 x 0.38 x 0.22 mm^3
Theta range for data collection	1.17 to 22.12°.
Index ranges	-9<=h<=9, -16<=k<=13, -18<=l<=18
Reflections collected	23683
Independent reflections	6137 [R(int) = 0.0339]
Completeness to theta = 22.12°	98.2 %
Absorption correction	Multiscan
Max. and min. transmission	0.2736 and 0.1040
Refinement method	Full-matrix least-squares on F^2
Data / restraints / parameters	6137 / 0 / 471
Goodness-of-fit on F^2	1.033
Final R indices [I>2sigma(I)]	R1 = 0.0314, wR2 = 0.0736
R indices (all data)	R1 = 0.0411, wR2 = 0.0782
Largest diff. peak and hole	0.695 and -1.852 $e.Å^{-3}$

Selected bond length and angles are reported on Table D-7.

Table D-7: Selected bond lengths [Å] and angles [°] for 3.

Er(1)-O(8)	2.289(6)	O(3)-Er(1)-Cl(2)	90.55(2)
Er(1)-O(2)	2.373(5)	O(8)-Er(1)-Cl(1)	91.55(2)
Er(1)-O(1)	2.379(5)	O(2)-Er(1)-Cl(1)	89.08(1)
Er(1)-O(5)	2.385(5)	O(6)-Er(2)-O(4)	173.7(2)
Er(1)-O(3)	2.388(5)	O(6)-Er(2)-Cl(6)	91.12(2)
Er(1)-Cl(2)	2.565(2)	O(4)-Er(2)-Cl(6)	93.43(2)
Er(1)-Cl(1)	2.572(2)	O(6)-Er(2)-Cl(3)	92.32(2)
Er(2)-O(6)	2.283(6)	O(4)-Er(2)-Cl(3)	91.61(2)
Er(2)-O(4)	2.307(6)	Cl(6)-Er(2)-Cl(3)	94.94(8)

Er(2)-Cl(6)	2.554(2)	O(6)-Er(2)-Cl(5)	88.33(2)
Er(2)-Cl(3)	2.556(2)	O(4)-Er(2)-Cl(5)	87.28(2)
Er(2)-Cl(5)	2.652(2)	Cl(6)-Er(2)-Cl(5)	90.61(7)
Er(2)-Cl(4)	2.653(2)	Cl(3)-Er(2)-Cl(5)	174.40(7)
Hg-I(2)	2.615(9)	O(6)-Er(2)-Cl(4)	88.81(2)
Hg-I(1)	2.619(8)	O(4)-Er(2)-Cl(4)	86.35(2)
Hg-Cl(4)	2.760(2)	Cl(6)-Er(2)-Cl(4)	175.97(7)
Hg-Cl(5)	2.761(2)	I(2)-Hg-I(1)	141.62(3)
		I(2)-Hg-Cl(4)	102.64(5)
O(5)-Er(1)-O(3)	143.81(2)	I(1)-Hg-Cl(4)	105.23(5)
O(8)-Er(1)-Cl(2)	92.59(2)	I(2)-Hg-Cl(5)	103.91(5)
O(2)-Er(1)-Cl(2)	92.95(1)	I(1)-Hg-Cl(5)	105.93(5)
O(1)-Er(1)-Cl(2)	89.26(1)	Cl(4)-Hg-Cl(5)	81.31(7)
O(5)-Er(1)-Cl(2)	86.32(2)		

The anionic fragment $[Er(THF)_2Cl_2(\mu\text{-}Cl)_2HgI_2]$- is mainly composed of HgI_2 and $Er(THF)_2Cl_4^-$ connected via two bridging chlorines (μ-Cl). The cationic fragment $[Er(THF)_4Cl_2(H_2O)(THF)_2]^+$, with a seven coordinated erbium ion is mainly composed of THF molecules. This structure remembers that of the ion–pairs reported by Willey *et al.*[219] and Anfang *et al.*[220]. The only difference between those systems and our complex **3** is the presence of the mercury in the anionic fragment. The two different erbium centers are separated by 8.016(2) Å.

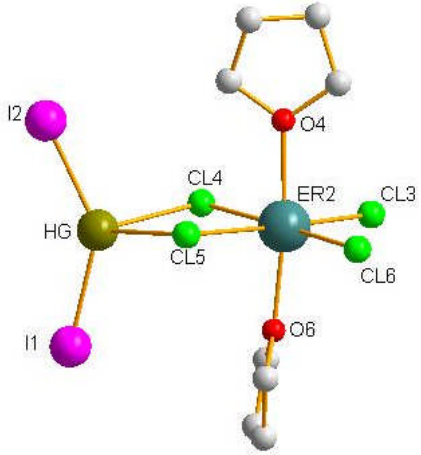

Figure D-7: Anionic fragment of the molecular structure of 3.

This structure represents the first Er-Hg system, containing Hg^{II} and Er^{III} ions linked through bridging chlorine atoms. In others reported Er-Hg systems, adjacent Er centers are linked via the ligand (**L^p**: propiolactam ligand) coordinated to the mercury (in the **$Hg(L^p)_2$** unit) and leading to polymeric arrays.[216, 217, 221] In the Er-Hg system of

Goodgame *et al*.[216], the ligand (**L^{p}**) ensures the connection between the Er centers. The structure of the anionic part of complex **3** matches closely to that obtained by Angang *et al.*[220] and Willey *et al.*[219] , therefore the following Scheme D-13 represents a structural comparison between the different systems.

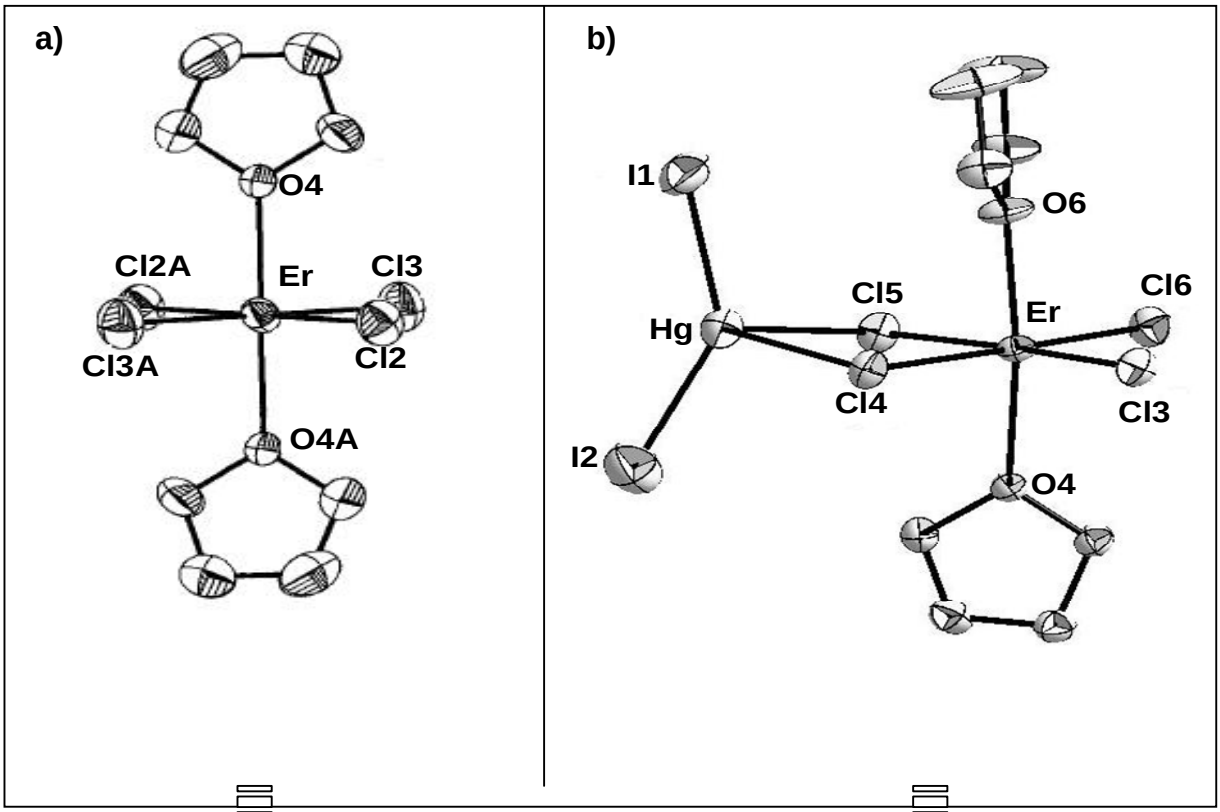

	from Ref. 217	from Ref. 216
	Distances in [Å]	
Er-Cl2	2.586(1)	2.593(3)
Er-Cl2A	2.586(1)	2.593(3)
Er-Cl3	2.598(1)	2.609(3)
Er-Cl3A	2.598(1)	2.609(3)
Er-O4	2.294(4)	2.313(9)
Er-O4A	2.294(4)	2.313(9)
	Angle O-Er-O in [°]	
O4-Er-O4A	180.0	180.0

from this work	
Distances in [Å]	
Er-Cl3	2.556(6)
Er-Cl5	2.652(2)
Er-Cl6	2.554(2)
Er-Cl4	2.653(2)
Er-O6	2.283(6)
Er-O4	2.30786)
Angle O-Er-O in [°]	
O4-Er-O6	173.7(2)

Scheme D-12: Comparison between:
a) Literature reports and b) this work.

In the anionic part of **3** (Scheme D-13: **b)**), the geometry around the Er^{III} ion is distorted square bipyramidal with the equatorial positions occupied by chlorine atoms and the axial positions by oxygen atoms (from THF molecules). The oxygen atoms

O4 and O6 are situated at almost equivalent distances of 2.307(6) and 2.283(6) Å respectively, from the Er^{III} center. The bridging chlorides, Cl4 and Cl5 which are situated at 2.653(2) and 2.652(2) Å, respectively, from the Er^{III} ion are slightly longer than the terminal ones Cl3 and Cl5 found at 2.556(2) and 2.554(2) Å, respectively.

The Er-Cl and Er-O lengths are in the same order than the reported values. But, contrarily to the reported examples, the D_{2h} symmetry found in example of Anfang *et al.* (Er-Cl2=Er-Cl2A, Er-Cl3=Er-Cl3A, and Er-O4=Er-O4A) is lost in **3**, since the Er-Cl bond lengths in equatorial positions and Er-O bond lengths in axial positions are no more equivalents *i.e.* Er-Cl3≠Er-Cl5, Er-Cl4≠Er-Cl6, and Er-O4≠Er-O6 (see table in Scheme D-13).

This distorted geometry around the erbium metal center in the anionic part of **3** is also a result of the coordination of the mercury which induces a lengthening of the Er-Cl distances (Cl4 and Cl5). Another proof of this distortion, is given by the O-Er-O angle of 173.7(2) ° in the anionic fragment of **3**, deviated from the linear O-Er-O angle (180.0°) reported by Anfang *et al.* [220]or willey *et al.* [219] The Er-Hg distance is about 4.024(2)Å in complex **3**.

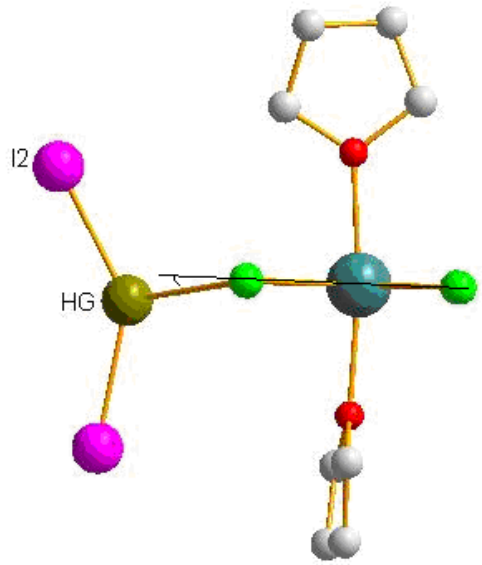

Figure D-8: Anionic fragment of the complex 3 showing the deviation of the Hg from the plan (black line) containing the Er and Cl atoms.

The mercury ion (Hg^{II}) is slightly deviated from the plane containing the Er^{III} and the four chlorine atoms (Figure D-8). A steric hindrance between the THF molecule and the iodine (I2) causes a rotation of one THF molecule about 90° around the O-Er-O axis. This complex is isolated in a 55 percent yield (from HgI_2), and the reaction was reproducible. An attempt to isolate this complex from a direct reaction between HgI_2

and $ErCl_3$ in THF was unsuccessful. However we failed in attempting to extend this result to others lanthanides (Nd^{III} and La^{III}).

D.4 Luminescent properties of the Ln^{3+}-dithiolene complexes

As explained at the beginning of this chapter, we are interested in luminescence studies. The results presented here are probably the first luminescent investigations devoted to Ln^{3+}-dithiolene complexes. These have been realised in collaboration with the group of Prof. C. Wickleder (Siegen, Germany) in the framework of the SPP 1166 project.

D.4.1 Measurement facility

The measurements have been performed on a JOBIN YVON Fluorolog 3 represented here.

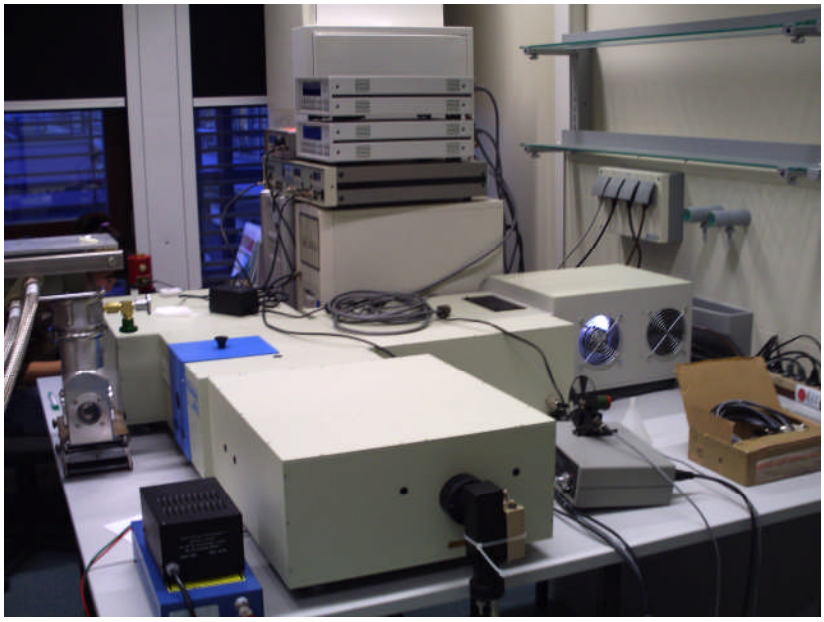

This is composed of a Xe lamp as light source, double monochromators, a sample chamber, detector, entrance slit and exit slit.

The samples were prepared in a quartz glass tube with 2 mm diameter and 2 cm height. The sample height was about 3 mm in the quartz glass tube.

D.4.2 Luminescent results and discussion

For commodity, this section will be divided in two parts depending on the emission region where the typical transitions are observed. The NIR (Near Infra red) emitting ions ($Nd^{3+}$and Er^{3+}) will be first described followed by the Vis (Visible) emitting ions ($Eu^{3+}$and Tb^{3+}).

D.4.2.1 Luminescent properties of Nd^{3+}-dithiolene complexes

Since the complexes are insoluble in common solvents only luminescence measurements in the solid state were performed. Excitation spectra of **$Nd_2(L^1)_3$** and **$Nd(L^2H)L^2$** are represented in Figure D-9 and D-10 respectively.

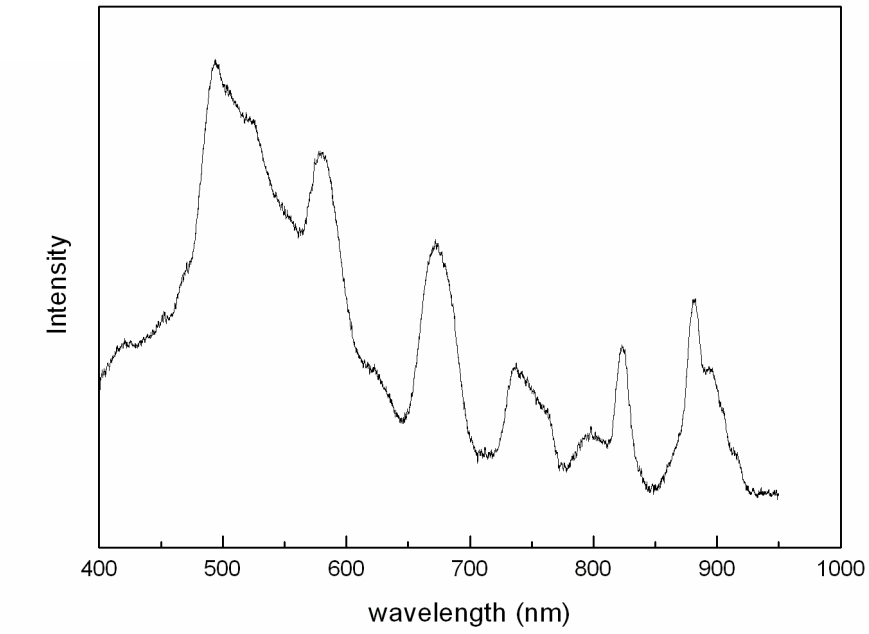

Figure D-9: Excitation spectrum of $Nd_2(L^1)_3$ (λ^{em} monitored 1080 nm).

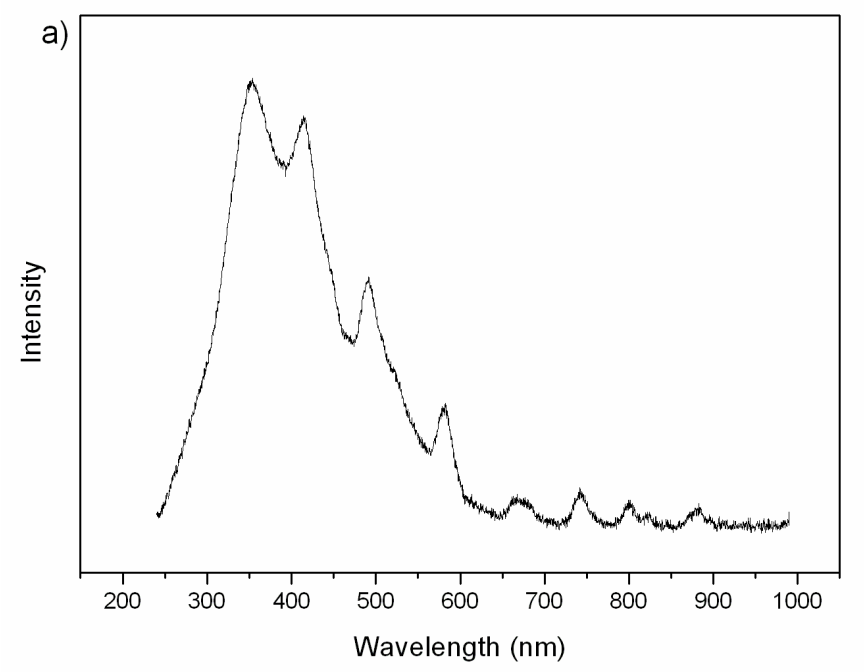

Figure D-10: Excitation spectrum of $Nd(L^2H)L^2$ (λ^{em} monitored 1064 nm).

The sharp peaks are attributed to f-f transition while the broad peaks are from the ligands. The f-f transitions are attributed using literature references since these transitions are not influenced by surrounding ligands. The assignments of the electronic transitions are listed in Table D-8 and for comparison the values found in the literature for neodymium doped in a bismuth triborate matrix ($BiB_3O_6:Nd^{3+}$)[222] are added.

Table D-8: Peaks depicted from the excitation spectra and their assignment to the corresponding f-f transitions.

	Wavelength (nm)		
Transitions	$Nd(L^2H)L^2$	$Nd_2(L^1)_3$	Nd^{3+} in matrix [a]
$^4I_{9/2} \rightarrow {}^4F_{3/2}$	886	880	872
$^4I_{9/2} \rightarrow {}^4F_{5/2}$	804	800	801
$^4I_{9/2} \rightarrow {}^4F_{7/2}$	747	740	745
$^4I_{9/2} \rightarrow {}^4F_{9/2}$	673	670	679
$^4I_{9/2} \rightarrow {}^2G_{7/2}$	582	580	583
$^4I_{11/2} \rightarrow {}^4G_{7/2}$	495	495	.

[a] : from ($BiB_3O_6:Nd^{3+}$) (see reference 222)

First of all, the recorded peaks for a given transition are found in similar positions independently of the composition of the complex or matrix. This observation states the fact that optical transitions within the f-subshell are not influenced by ligand environment.

The broadness of the ligand peak compared to f-f transitions arise from the absorption coefficient. In fact, f-f transitions are forbidden and are more or less forced while ligands transition are allowed (mostly $\pi-\pi^*$ transition).

Both complexes **Nd(L^2H)L^2** (Figure D-11) and **$Nd_2(L^1)_3$** (Figure D-12) exhibit NIR emission when they are excited at 360 and 495 nm respectively.

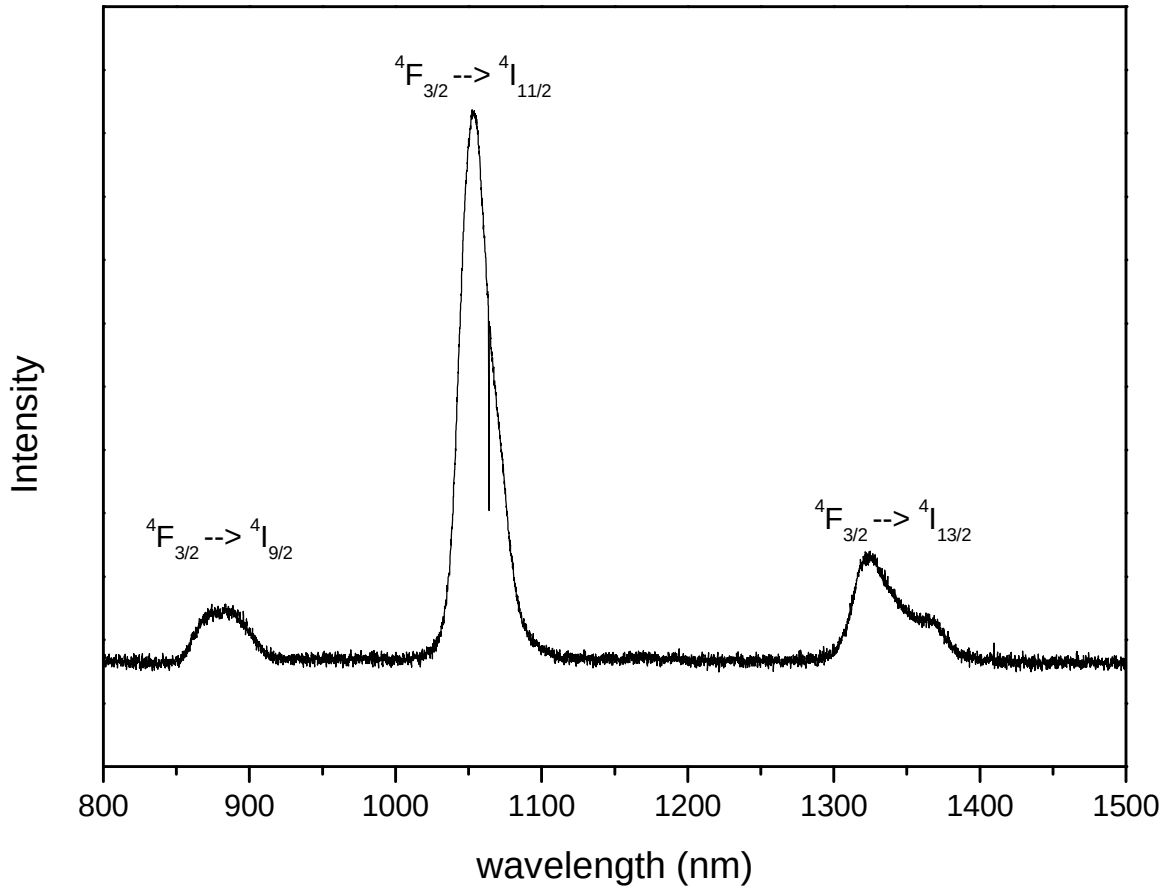

Figure D-11: Emission spectrum of Nd(L^2H)L^2 (λ^{ex} = 360 nm).

As depicted in Figure D-11, **Nd(L^2H)L^2** exhibits three bands characteristic of f-f transitions of Nd^{3+} species[75, 223, 224]at 880 nm ($^4F_{3/2} \rightarrow {}^4I_{9/2}$), 1060 nm ($^4F_{3/2} \rightarrow {}^4I_{11/2}$), and 1330 nm ($^4F_{3/2} \rightarrow 4I_{13/2}$). The ($^4F_{3/2} \rightarrow {}^4I_{11/2}$) transition (laser transition) dominates this spectrum. The ($^4F_{3/2} \rightarrow {}^4I_{13/2}$) transition presents a small shoulder probably due to splitting from crystal field effects.[224, 225]

This emission feature is obtained by excitation at 360 nm corresponding to the ligand band (or ligand absorption). The characteristic emission from the Nd^{3+} by excitation

on the ligand absorption (λ^{ex} = 360 nm) clearly demonstrates that the luminescence of **Nd(L^{2}H)L^2** is achieved by energy transfer from the ligand excited state to the neodymium excited state. In other words, we are dealing with a typical case of "antenna effect".[186] The much more intense excitation band of the ligands compared to those of the Nd^{3+} f-f transitions (Figure D-10) shows the efficiency of energy transfer in this case. The remaining OH group should be located outside of the first coordination sphere.

This effect is less pronounced in the case of **$Nd_2(L^1)_3$** where the ligand peaks present similar strength than those of the Nd^{3+}. However, as in **Nd(L^{2}H)L^2** , excitation at 495 nm produce the same NIR emission with similar Nd^{3+} characteristic transitions (Figure D-12).

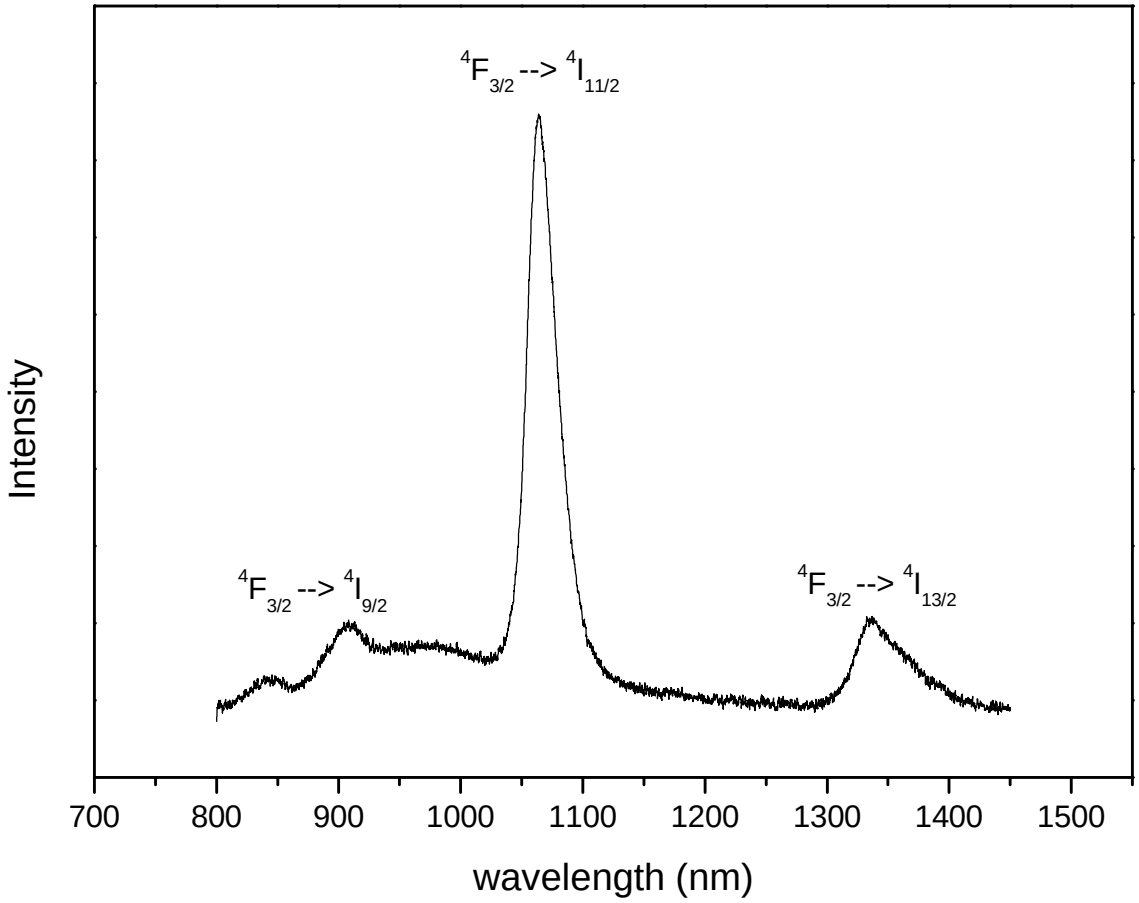

Figure D-12: Emission spectrum of $Nd_2(L^1)_3$ (λ^{ex} = 495 nm).

Another problem, which constrains us to rule out the existence of an energy transfer in this case, is the overlap between the ligand peak and Nd^{3+} peak at 495 nm ($^4I_{11/2} \rightarrow {}^4G_{7/2}$). The observation of two different absorption peaks (360 and 495 nm)

corresponding to two different ligands (**L^1H_2** and **L^2H_2**) suggests that these two ligands possess different excited states.

Since absorption of such ligands is mainly due to the presence of the DMIT unit (π-system), one could not expect that for the excitation such a large difference has to be used. A possible explanation of this difference could be in the ligand's excited states. **L^1H_2** and **L^2H_2** have probably different triplet excited states. The position of such ligand triplet states compared to the lowest luminescent states of the Nd^{3+} ($^4F_{3/2}$) is important for achieving the energy transfer process. Indeed, it is known that when the triplet-state energy of the ligand is at least greater than the energy gap between excited and ground states of the lanthanide ion (Ln^{3+}), an efficient luminescence could be obtained.

For lanthanides, two types of mechanism for energy transfer have been proposed: the Förster mechanism[226] or multipolar mechanism (mainly dipolar)[194] and the Dexter mechanism[227] or exchange mechanism.[194] These two mechanisms depend differently on the parameters of the studied system (spin of the ground and excited states, donor-acceptor distances etc.). The dipolar mechanism does not require contact between the donor (Ligand) and acceptor (Ln^{III} ion) while the exchange mechanism requires orbital overlap between the donor and acceptor. Since there is no physical contact between the π-system (DMIT) and the Nd^{3+} ion in both **$Nd_2(L^1)_3$** and **$Nd(L^2H)L^2$** , we can conclude that the energy transfer in the case of **$Nd(L^2H)L^2$** is predominantly dipolar in character (Förster mechanism).

D.4.2.2 Luminescent properties of Er^{3+}-dithiolene complexes

Similarly to the Nd^{3+}-dithiolene complexes, solid-state luminescence measurements have been performed for erbium complexes. The excitation and emission spectra for **$Er_2(L^1)_3$** are shown in Figure D-13.

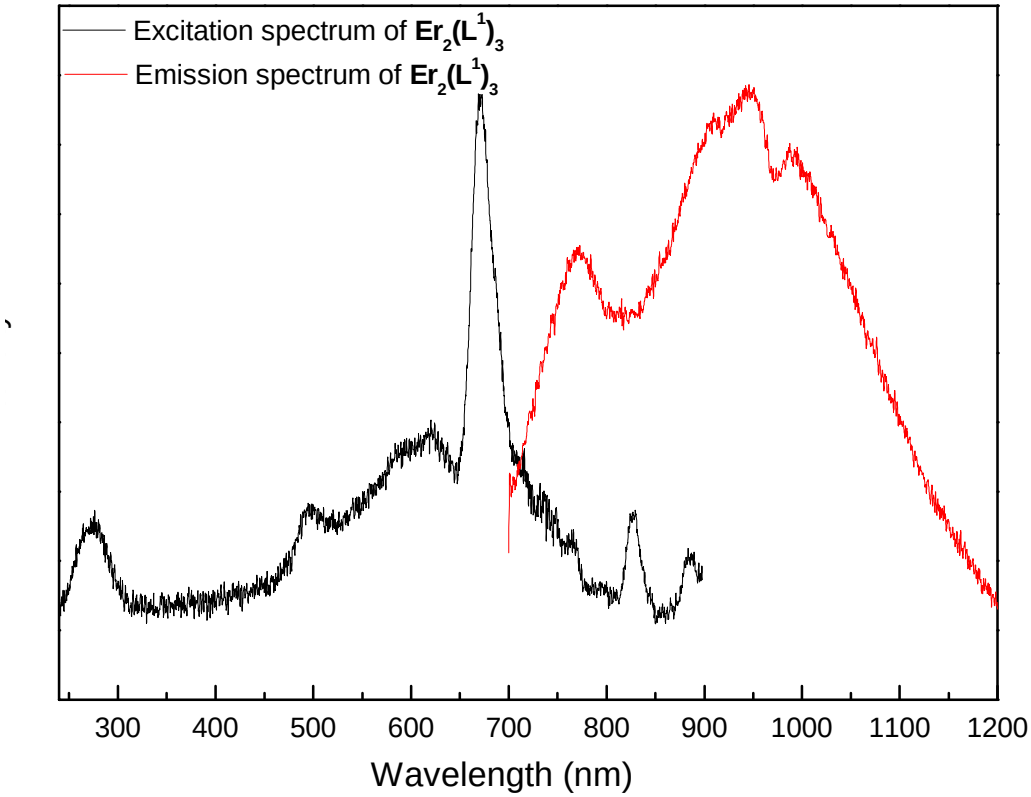

Figure D-13: Excitation (black) and emission (red) spectra for $Er_2(L^1)_3$ (λ^{ex}: 670 nm).

The excitation spectrum shows an intense peak at 670 nm and relative weak peaks at 270, 490 and 830 nm. The peaks at 670 and 490 nm could be attributed to $^4I_{15/2} \rightarrow {}^4F_{9/2}$ and $^4I_{15/2} \rightarrow {}^4F_{7/2}$ transitions respectively using literature data.[222, 224] However, the emission feature (peak around 900 nm) is not commonly observed in erbium complexes. The most observed luminescent transition, justifying the use of erbium in optical amplification, is localised around 1550 nm.[75, 224] Unfortunately, we could not localised this peak corresponding to the $^4I_{13/2} \rightarrow {}^4I_{15/2}$ even by excitation in the UV region.

Similar behaviour was observed in the case of **Er(L^2H)L^2** whose spectra are shown in Figure D-14.

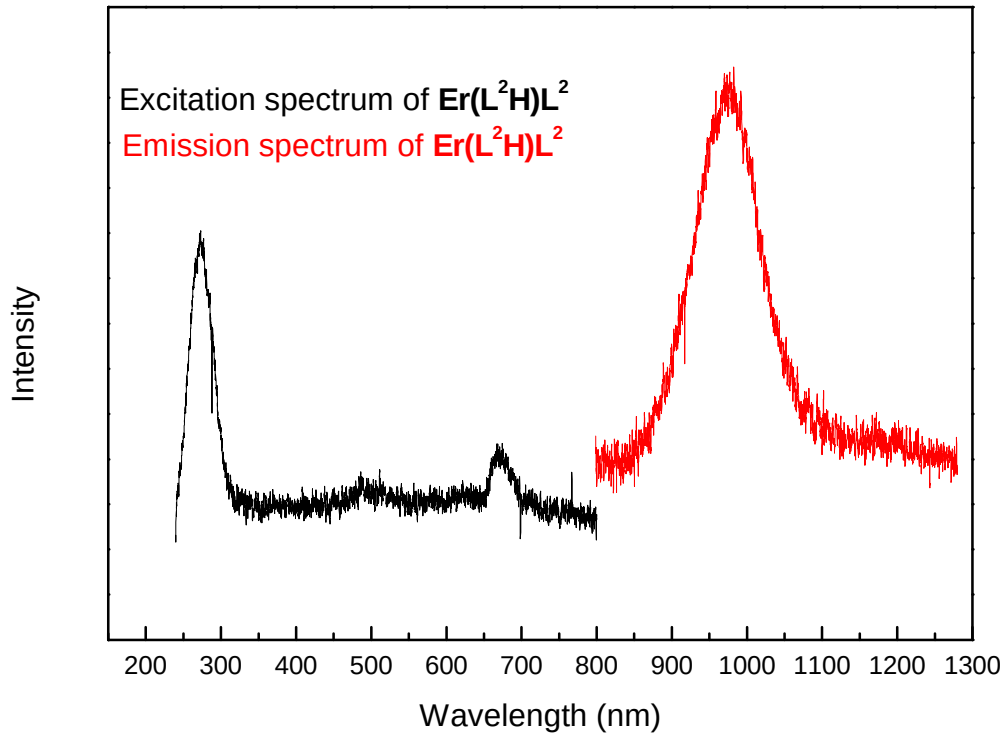

Figure D-14: Excitation (black) and emission (red) spectra for $Er(L^2H)L^2$ (λ^{ex}: 270 nm).

The excitation spectrum exhibits the same transitions as in **$Er_2(L^1)_3$**. The transition at 270 nm is more intensive than that at 670 nm. The emission spectrum remains unchanged. Once more, the main erbium transition around 1500 nm is not observed. These features are accounted for the low lying emissive states of erbium (Er^{3+}) compared to the ligands. The energy gap between the ligands excited states and a lanthanide emissive state is an important factor regarding sensitisation process.[186, 187] Another possibility, explaining this behaviour can arise from a deactivation process involving C-H or OH oscillators. This deactivation or quenching from oscillator is more pronounced in erbium complexes.[228]

D.4.2.3 Luminescent properties of Tb^{3+}-dithiolene complexes

Terbium is a potential ion for application in the visible domain because of its strong green emission and its relative longer lifetimes. As exhibited in Figure D-15, complex **$Tb(L^2H)L^2$** displays typical emission spectrum with expected luminescent transitions from the $^5D_4$ level to the $^7F_{6\text{-}0}$ levels. The spectrum is dominated by the $^5D_4 \rightarrow {}^7F_6$ transition, with maximum peak at 540 nm. **$Tb(L^2H)L^2$** shows an intense green

emission under irradiation with UV lamp, a typical feature for Tb^{3+} containing compounds.

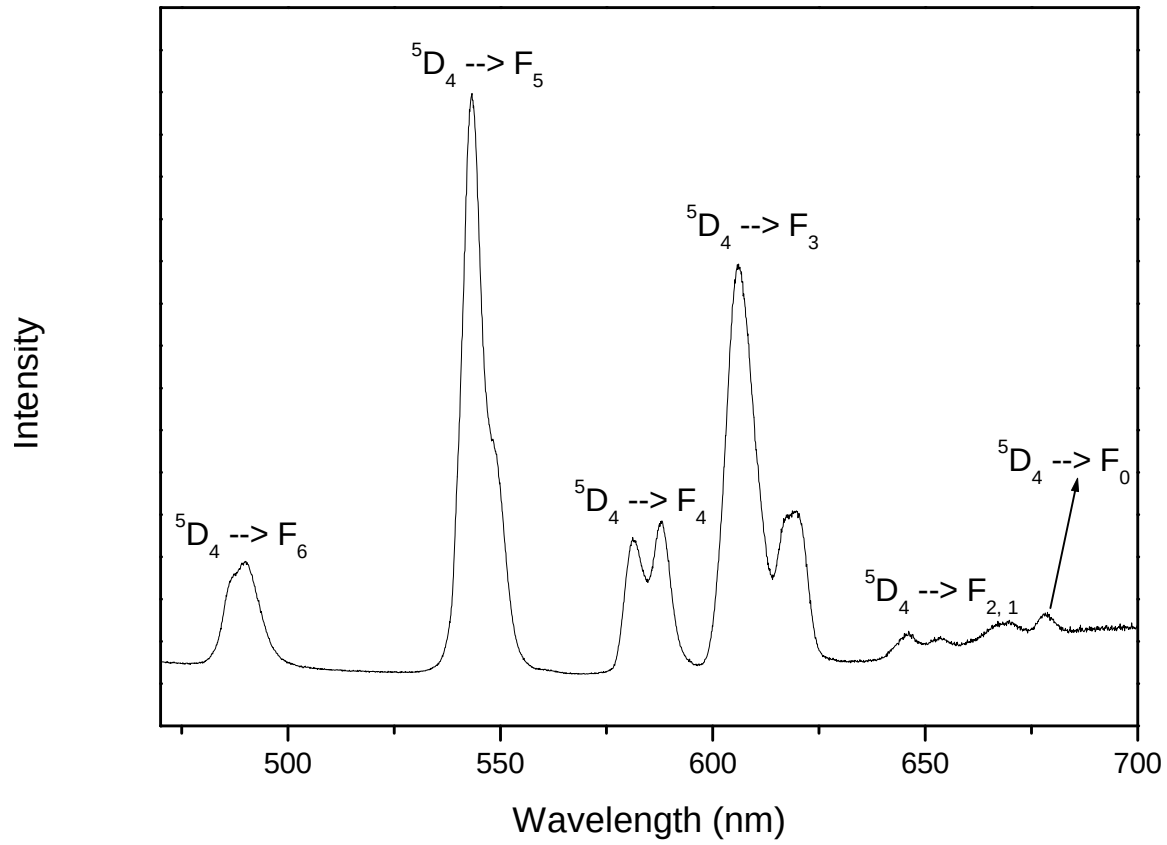

Figure D-15: Emission spectrum of $Tb(L^2H)L^2$ (λ^{ex} = 360 nm); peaks correspond to the $^5D_4 \rightarrow {}^7F_{6,5,4,3,2,1,0}$ transitions.

Apart from the $^5D_4 \rightarrow {}^7F_3$ transition, the relative intensities of the $^5D_4 \rightarrow {}^7F_J$ transitions fall in the same order than expected ($^7F_5 > {}^7F_6 > {}^7F_4 > {}^7F_3 > {}^7F_2$, $^7F_1$, $^7F_0$).[184] Such a relative intensity for the magnetic dipole transition $^5D_4 \rightarrow {}^7F_3$ over the electric dipole transition $^5D_4 \rightarrow {}^7F_6$ has been observed on Tb^{3+}-imidazole compounds.[229] However, the intensity ratio $I(^5D_4 \rightarrow {}^7F_6)/I(^5D_4 \rightarrow {}^7F_J)$ is much weaker than in the Tb^{3+}-imidazole compounds,[229] suggesting a poor color quality looking for application possibilities.

It is noteworthy that there is no apparent residual emission in the 550-700 nm region which should come from the ligand. This indicates that an efficient energy transfer from the ligand excited states to the Tb^{3+} excited states takes place.

D.4.2.4 Luminescent properties of Eu^{3+}-dithiolene complexes

The europium complex is of crucial importance for our investigations. Due to the polymer-like nature of the complexes, their characterisation by means of NMR or crystallography was not possible. But europium is the ion, per excellence, for probing the environment or symmetry of an ion in a complex (see Table D-2).

The excitation and emission spectra of **Eu(L^2H)L^2** are shown in Figure D-16 and D-17 respectively.

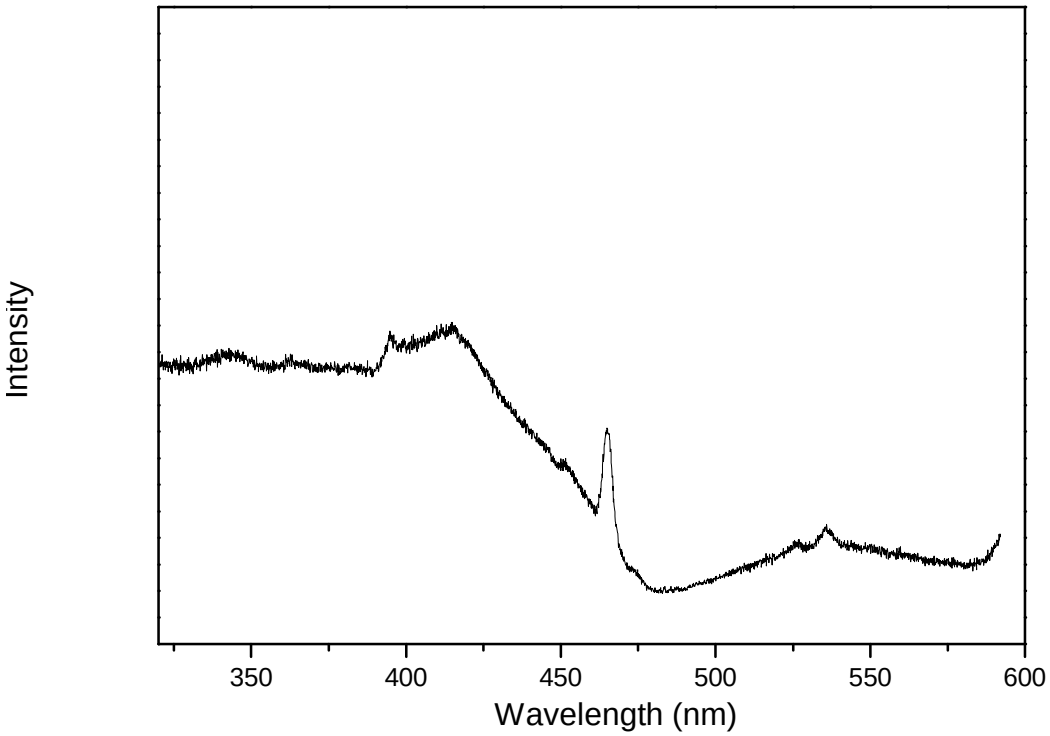

Figure D-16: Excitation spectrum of Eu(L^2H)L^2 (λ^{em} monitored 612 nm).

The excitation spectrum exhibits a broad band centered at 415nm (ligand peak) and some weak f-f contributions at 464 nm and 534 nm assigned respectively to $^5D_2 \leftarrow {}^7F_o$ and $^5D_1 \leftarrow {}^7F_o$ transitions.[230] The relative weak intensity of these Eu^{3+} peaks compared to the ligand peak suggests an energy transfer from the ligand to the europium ion.

Upon excitation at 415 nm, the **Eu(L^2H)L^2** complex shows typical peaks corresponding to the Eu^{3+}-centered $^5D_0 \rightarrow {}^7F_J$ transitions (Figure D-17). The

transitions $^5D_0 \rightarrow {}^7F_{1\text{-}6}$ are strong enough to be detectable, while a magnification of the 570-585 nm region was necessary to observe the magnetic dipole transition (see insets in Figure D-17).

No transitions arising from the $^5D_2$ and $^5D_1$ were observed although these states were populated according to the excitation spectrum. This can be explained by the small energy gap separating the $^5D_2$, $^5D_1$ and the $^5D_0$ level, leading to a fast relaxation populating the low lying luminescent state ($^5D_0$).

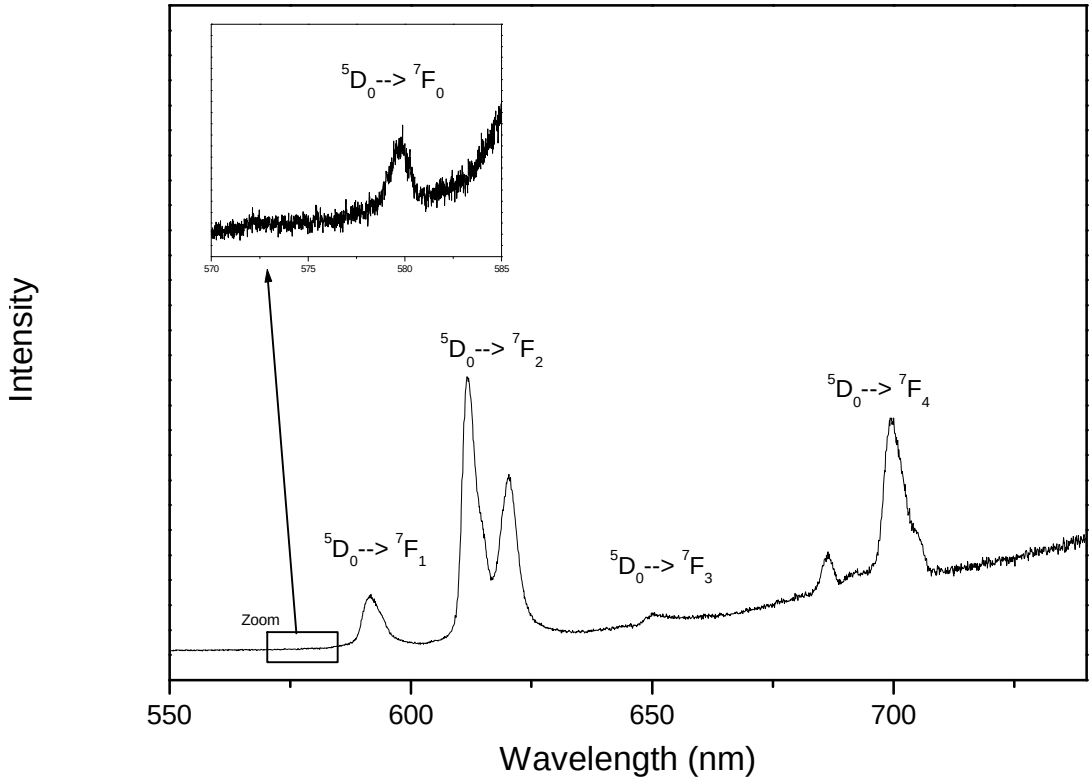

Figure D-17: Emission spectrum of Eu(L^2H)L^2 (λ^{ex} = 415 nm).

Here also, the absence of the ligand–based emission in the emission spectrum suggests that the luminescence of the complex is achieved via an energy transfer from the ligand to the europium center.

D.4.2.4.1 Analysis of the $^5D_0 \rightarrow {}^7F_J$ transitions in Eu(L^2H)L^2

The first information in our complex is provided by the analysis of the $^5D_0 \rightarrow {}^7F_o$ transition centered around 580 nm. The $^5D_0 \rightarrow {}^7F_o$ transition presents a single peak

centered at 580 nm. Since the $^7F_0$ of the Eu^{3+} is nondegenerate and can not be split by crystal field effect, we can assume that there is one europium (III) species in the complex. However, the broadness of this peak, illustrated by a width at half height (FWHM) of 36 cm^{-1}, traduces the presence of several closely related, chemical environments (polymeric nature) of the europium in the complex.

The second information is given by the intensity of the hypersensitive $^5D_0 \rightarrow {}^7F_2$ transition which is absent if the ion lies in a inversion center.[184] This peak centered at 612 nm, dominates the emission spectrum of the **Eu(L^{2}H)L^2** complex and indicates that the europium ion (Eu^{3+}) in the **Eu(L^{2}H)L^2** complex does not lie in an inversion center.

The third information, but less reliable in this case because of the lack of crystal structure, concerns the ratio $I(^5D_0 \rightarrow {}^7F_2)/I(^5D_0 \rightarrow {}^7F_1)$. The $^5D_0 \rightarrow {}^7F_1$ transition has a magnetic dipole character and is thus no sensitive to the metal environment contrary to the $^5D_0 \rightarrow {}^7F_2$ transition. The magnetic dipole transition ($^5D_0 \rightarrow {}^7F_1$) dominates in a centrosymmetric environment while an electric dipole transition (such as $^5D_0 \rightarrow {}^7F_2$) gain in intensity by distortion of the symmetry. Richardson *et al.*[231, 232] have established that this intensity ratio can be used to confirm the symmetry of the Eu^{3+} ion in a given structure.

The intensity ratio $I(^5D_0 \rightarrow {}^7F_2)/I(^5D_0 \rightarrow {}^7F_1)$ of about 4.9 indicates that the Eu^{3+} in **Eu(L^{2}H)L^2** do not occupy sites with high symmetry.[190, 233-238] The information provided by these observations on the f-f transitions, is in accordance with the proposed structure for Ln^{3+}-dithiolene carboxylate complexes (see Scheme D-8).

The hypersensitive $^5D_0 \rightarrow {}^7F_2$ transition presents peaks that are splitted and could be due to a crystal field effect. We have carried out time-dependent measurement to see this phenomenon in more details.

D.4.2.4.2 Temperature-dependent measurement for the Eu(L^{2}H)L^2 complex

The measurement have been realised using the same equipment adapted with a cryostat device (filled with helium). The measurements were performed between 10K and 313K and the emission spectra were recorded after temperature stabilisation within the same time interval, for consistency.

D.4.2.4.2.1 Information from the temperature-dependent measurement

The emission spectra for the RT, 160 K and 10 K are shown in Figure D-18. The first observation concerns the intensity of the $^5D_0 \rightarrow {}^7F_J$ which all increase significantly upon lowering the temperature.

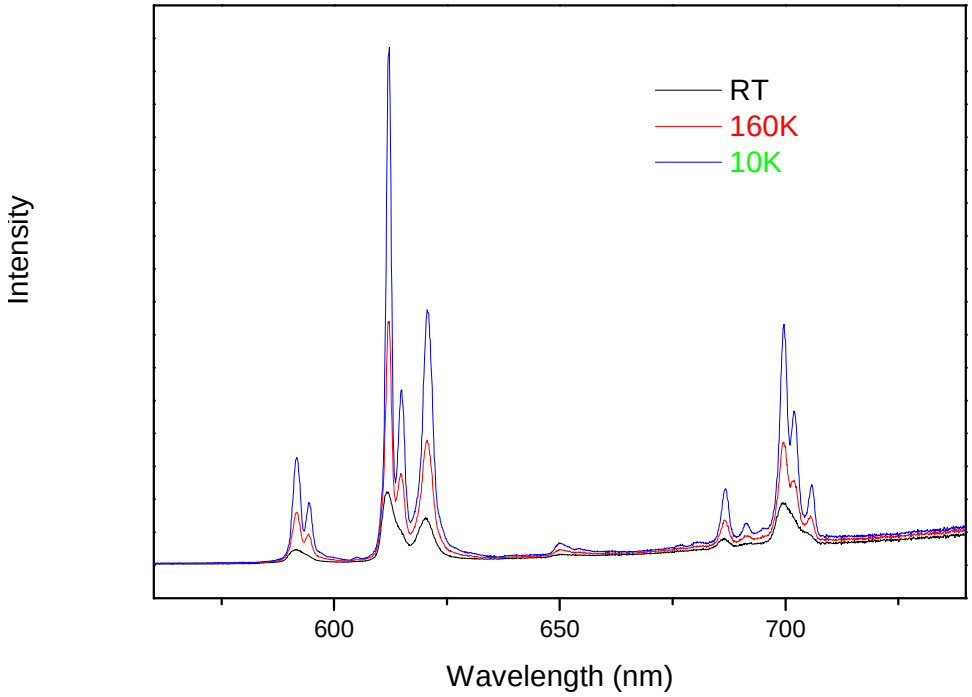

Figure D-18: Emission spectrum of Eu(L^2H)L^2 at RT, 160K and 10K (λ^{ex} = 415 nm).

This is expected since at low temperature, vibrations which are the main source of quenching are strongly reduced at low temperature and as a result the emission gains in intensity.

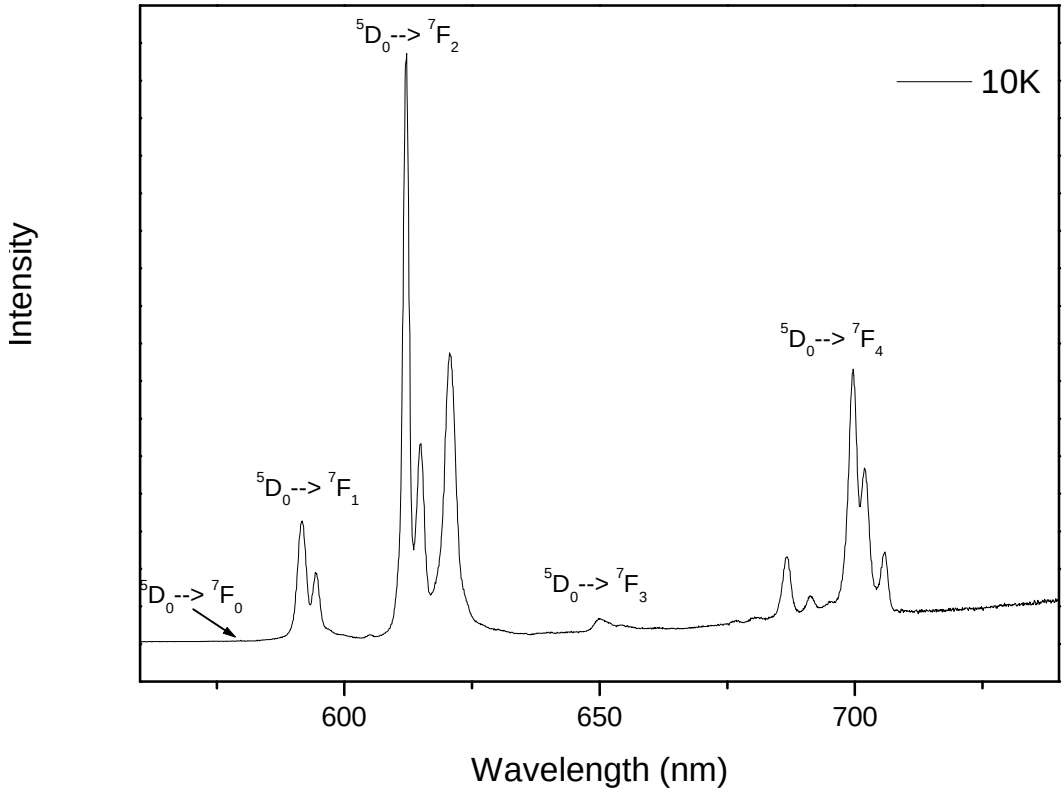

Figure D-19: Emission spectrum of Eu(L^2H)L^2 at 10K (λ^{ex} = 415 nm).

The second observation is related to the splitting of the $^5D_0 \rightarrow {}^7F_{1\text{-}4}$ transitions. This split is more visible at 10K and concerns only the $^5D_0 \rightarrow {}^7F_{1\text{-}4}$ transitions (Figure D-19). Such a splitting of the lanthanide (Ln^{3+} in general) line has been already observed and is well documented.[225, 239-241]

D.4.2.4.2.2 Approximation of the symmetry using the splitting pattern of the sublevels

The study of the intensity and splitting pattern of certain transitions in the fluorescence spectra of Eu^{3+} compounds can give information about the environment of the Eu^{3+} ion (symmetry). A classical example, illustrated this feature is the $[Eu(terpy)_3](ClO_4)_3$. The analysis of the luminescence spectrum of $[Eu(terpy)_3](ClO_4)_3$ suggested a D_3 geometry although no crystal structure was available at that time.[242] This symmetry was later confirmed by crystallographic details available some years after.

At low temperature, each band is splitted to several sublevels (Stark sublevels) due to crystal field effect. Thus we have 2 and 3 bands for the $^5D_0 \rightarrow {}^7F_1$ and the $^5D_0 \rightarrow {}^7F_2$ transitions respectively. About five bands for the $^5D_0 \rightarrow {}^7F_4$ transitions are also

detected, while those corresponding to the $^5D_0 \rightarrow {}^7F_3$ transitions are not strong enough to be countable. The different peaks are listed in Table D-9 and compared with literature data.[241]

Table D-9: Energy levels of the Eu^{3+} complex resulting from splitting due to crystal field and for the corresponding transitions; (comparison with values of reference 241).

Transitions	wavelength (nm)	Energy (cm^{-1})	Energy for Eu^{3+} in $LaCl_3$ (cm^{-1})[241]
$^5D_0 \rightarrow {}^7F_0$	580	17250	17267
$^5D_0 \rightarrow {}^7F_1$	591.7	16900	16912
	594.6	16818	16862
$^5D_0 \rightarrow {}^7F_2$	612.2	16334	16245
	614.7	16262	16239
	620.6	16113	16183
$^5D_0 \rightarrow {}^7F_3$	650 (v weak)	15384	a)
$^5D_0 \rightarrow {}^7F_4$	686.79	14560	14516
	691.2	14467	14434
	699.7	14291	14400
	701.9	14247	14364
	705.8	14168	14226

a) the reported value in reference[241] are not listed here because the corresponding peak is too weak in our case

However the intensity ratio $I(^5D_0 \rightarrow {}^7F_2)/I(^5D_0 \rightarrow {}^7F_1)$ remains unchanged with varying the temperature (4.9 at RT and 4.87 at 10K).

The number of Stark sublevels of a given transition can be correlated to the symmetry of a system.

Table D-10 gives the maximum of energy levels (Stark sublevels) generated in the various point groups.[184]

Table D-10: Number of J-sublevels in a given point symmetry *vs.* the quantum number J.[184]

Symmetry J:	0	1	2	3	4	5	6
Icosahedral	1	1	1	2	2	3	4
Cubic[1]	1	1	2	3	4	4	6
Hexagonal[2]	1	2	3	5	6	7	9
Pentagonal[3]	1	2	3	4	5	7	8
Tetragonal[4]	1	2	4	5	7	8	10
Low[5]	1	3	5	7	9	11	13

[1]: O_h, O, T_d,T_h,T

[2]: D_{6h}, D_6, C_{6v}, C_{6h}, C_6, D_{3h}, C_{3h}, D_{3d}, D_3, C_{3v}, S_6, C_3

[3]: D_{5h}, C_{5h}, C_{5v}, C_5, D_5

[4]: D_{4h}, D_4, C_{4v}, C_{4h}, C_4, D_{2d}, S_4

[5]: D_{2h}, D_2, C_{2v}, C_{2h}, C_2, C_s, S_2, C_1

From the **Eu(L^2H)L^2** spectrum recorded at 10K, we can identify the number of sublevels for the different transitions (1 sublevel for J=0, 2 sublevels for J=1, 3 sublevels for J=2 and 6 sublevels for J=4 (Table D-11)).

NB: For J=3, the weakness of the ($^5D_0 \rightarrow {}^7F_3$) transition do not allow us to identified the sublevels. The $^5D_0 \rightarrow {}^7F_5$ transition and the $^5D_0 \rightarrow {}^7F_6$ transition are generally seldom observed.

Table D-11: Number of Stark sublevels identified in the Eu(L^2H)L^2 complex

J:	0	1	2	3	4
Eu(L^2H)L^2 complex	1	2	3	-	6

From this observation and taking into account the information given in Table D-10, we can conclude that the **Eu(L^2H)L^2** complex possesses approximately a hexagonal symmetry which means that our system presents one of the following symmetry: D_{6h}, D_6, C_{6v}, C_{6h}, C_6, D_{3h}, C_{3h}, D_{3d}, D_3, C_{3v}, S_6, C_3.

And if we combine this information with that provided by the $^5D_0 \rightarrow {}^7F_2$ (most intensive peak) we can see that the D_{6h}, C_{6h}, D_{3d}, and S_6 symmetry are not possible (see character tables for chemically important symmetry groups[243]). Therefore we can reduce this group to the D_6, C_{6v}, C_6, D_{3h}, C_{3h}, D_3, C_{3v} and C_3 symmetry as the probable cases.

D.4.2.4.3 Lifetime measurement

The lifetime measurement of the **Eu(L^2H)L^2** complex was performed on the same spectrophotometer and was determined for the $^5D_0$ level. The excitation wavelength was chosen at 415 nm and the emission fixed at 612 nm. Figure D-20 represents the intensity decay of the **Eu(L^2H)L^2** and exhibits a mono-exponential decay illustrating the presence of one Eu^{3+} species.

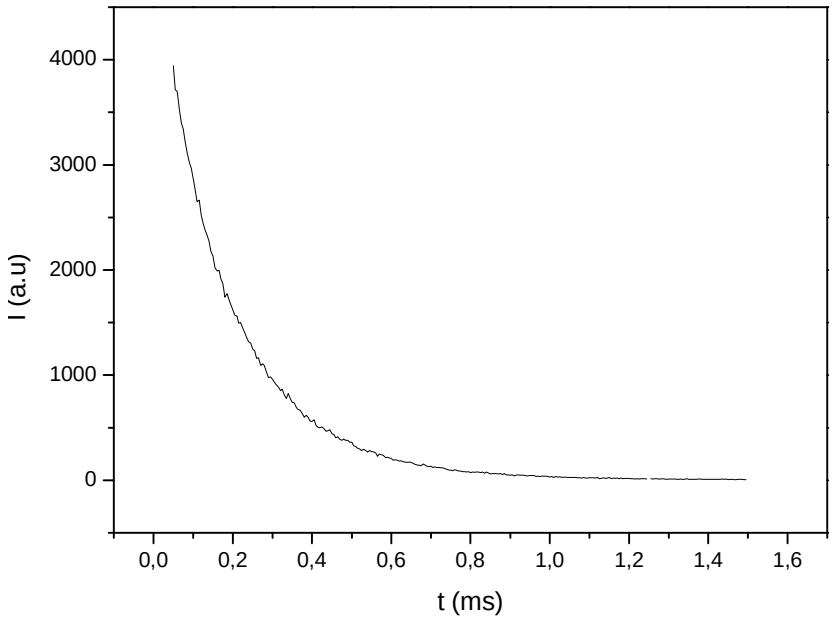

Figure D-20: Intensity decay of the $^5D_0$ level of the emission of Eu(L^2H)L^2 (λ^{ex} = 415 nm, λ^{em} = 612nm).

The emission decay profile of the **Eu(L^2H)L^2** complex in the solid state is plotted in Figure D-21 and corresponds to the logarithm of the exponential decay. The slope of this curve gives the value of the lifetime (τ) which is measured to be equal to 0.206 ms. This value of 0.206 ms is in the range of lifetimes reported for Eu^{3+} complexes in the solid-state but is slightly shorter than the known value which average sometime the milliseconds and more. It corresponds more to the lifetimes measured for europium species in H_20 solutions. However, this value (0.206 ms) is similar to those reported for europium (Eu^{3+}) species bearing imidazolecarboxylic acid moieties (0.178 ms[238] , 0.251 ms[236] and 0.256 ms[237]).

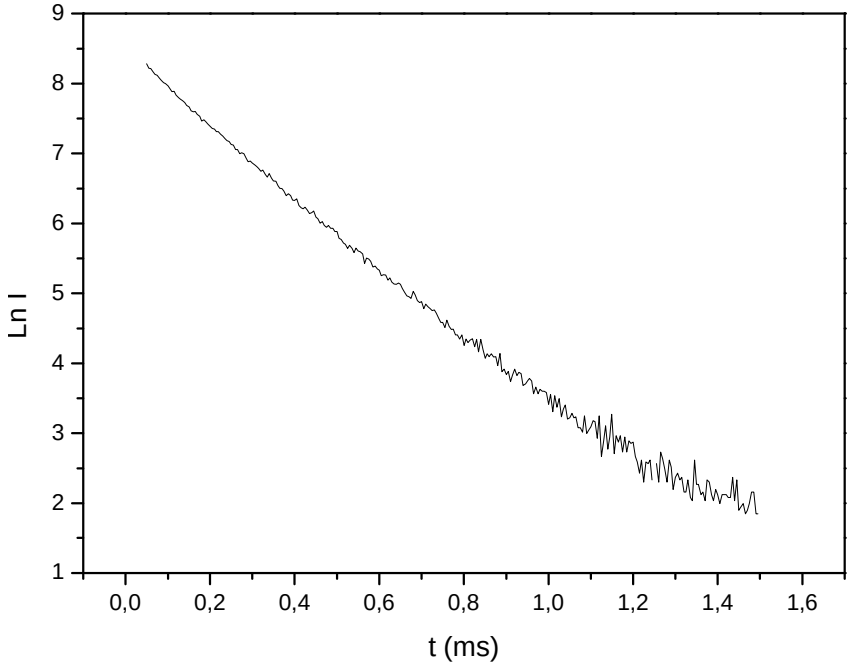

Figure D-21: Emission decay profile of the Eu(L^2H)L^2 complex in the solid state.

A possible explanation is that the remaining protonated carboxylate group (-COOH) on **Eu(L^2H)L^2** complex induces a quenching. However, this assumption is not plausible if we look at the intensity of the emission spectra, which seems to be correct in intensity. Indeed, we have previously assumed that surprisingly the OH function does not affect the luminescence in the **Nd(L^2H)L^2** complex and that it should be located outside of the first coordination sphere.

To get more insight into a possible quenching from the OH remaining group, we also have tried to prepare a derivative **Eu(L^2Na)L^2** where the remaining OH group is replaced by ONa.

D.4.2.4.4 Salt metathesis reactions between sodium carboxylate of L^2Na_2 and $EuCl_3$

Sodium carboxylate of L^2H_2 is prepared by adding MeONa to a methanol solution of L^2H_2. The resulting salt is then added to the methanol solution of $EuCl_3$. A precipitate is formed within a period of few minutes and the reaction mixture is stirred for additional 24h.

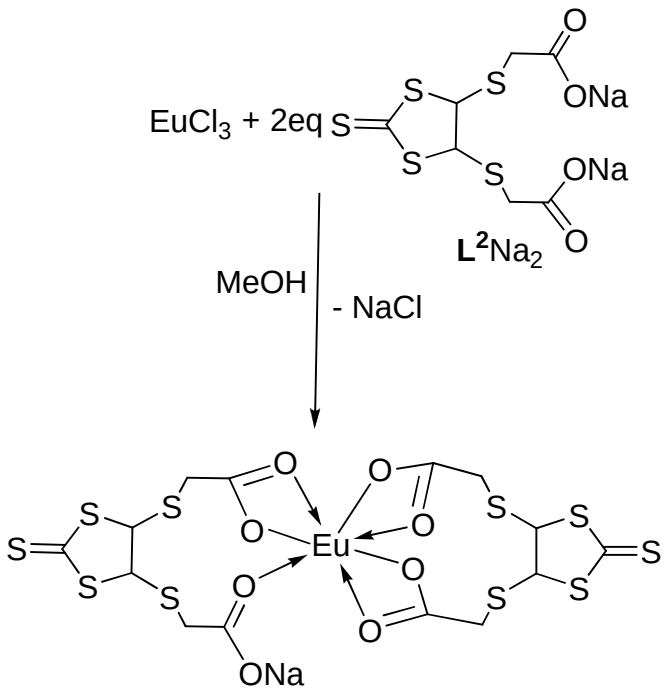

Eu(L^{2}Na)L^2

Scheme D-13: Metathesis reaction starting from the Sodium carboxylate of L^2H_2.

We should point out that, although this synthetic route is different from the silyl-amide route, the product of this reaction present similar behaviour (fast precipitation, insolubility). A polymeric nature of the product is, once again, the most reasonable explanation.

The emission spectra of the **Eu(L^{2}Na)L^2** salt exhibits the same features corresponding to the Eu^{3+}-centered $^5D_0 \rightarrow {}^7F_J$ transitions. Another difference is observed by examining the intensity ratio: $I(^5D_0 \rightarrow {}^7F_2)/I(^5D_0 \rightarrow {}^7F_1)$ amount 3.42 in the **Eu(L^{2}Na)L^2** instead of 4.9 in the **Eu(L^{2}H)L^2** complex**.** This difference indicates a little change in the environment of the Eu^{3+} ion, but does not alter the fact that the Eu^{III} ion does not possess an inversion center.[236, 237]

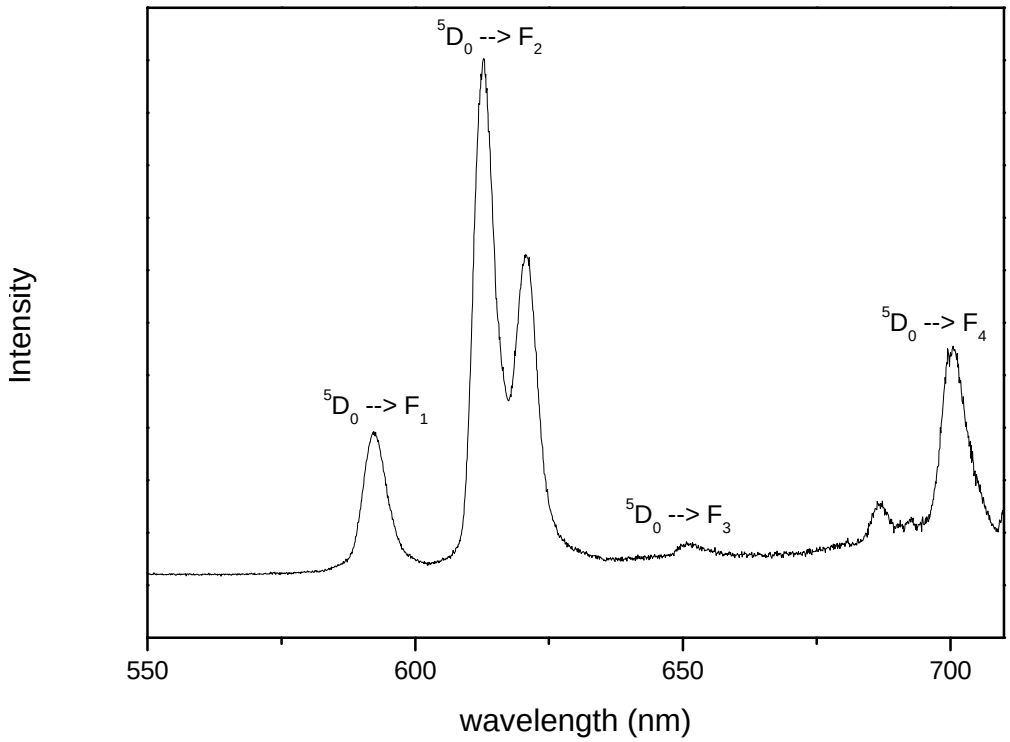

Figure D-22: Emission spectrum of Eu(L^2Na)L^2 at RT (λ^{ex} = 360 nm).

The emission decay profile of the **Eu(L^2Na)L^2** complex in the solid state is shown in Figure D-23 and corresponds to an exponential decay.

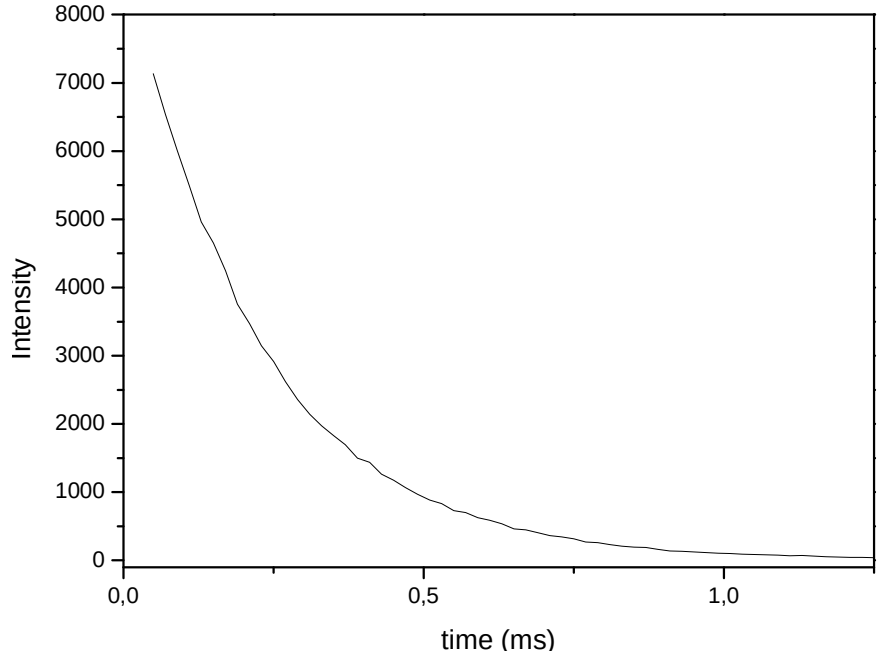

Figure D-23: Intensity decay of the $^5D_0$ level of the emission of Eu(L^2Na)L^2 (λ^{ex} = 360 nm, λ^{em} = 612nm).

The slope of this curve gives the value of the lifetime (τ), which is measured to be equal to 0.225 ms.

This lifetime value of 0.225 ms is slightly longer than the value measured for **Eu(L^{2}H)L^2** (0.206 ms). However, this value is not longer enough to state a quenching phenomenon but remains within the range of lifetimes recorded for Eu^{3+} complexes in the solid state.

According to the results obtained for the **Eu(L^{2}Na)L^2** complex, we can state that the OH group does not influence much the quenching process. This corroborated with our assumption that the OH is situated outside of the first coordination sphere.

D.5 Conclusion

We have synthesised Ln^{3+}-sulfur-rich system complexes using dithiolene-like neutral ligands functionalised with acid or alcohol groups. The synthetic approach is original in that way that it combined the versatility of dithiolene-functionalised ligands to isolate complexes (which were unfortunately insoluble). Their polymeric nature can be interpreted as resulting from additional coordination of the thiocarbonyl function (C=S). We have seen in this investigation that Ln^{3+}-dithiolene complexes are promising case for luminescent studies. The dithiolene ligands because of their π-system represent good chromophores suitable for achieving an energy transfer process. The efficiency of the transfer process could not be evaluated in this study because of the polymeric nature of the materials and the lack of device suitable for solid-state quantum yield measurement.

Nevertheless, we could see in the case of **Nd(L^{2}H)L^2** that an ***energy transfer*** from the ligand to the Nd^{III} center was at the origin of the luminescence. To get more information into the whole process, it should be helpful to measure the quantum yield and maybe deduce the efficiency of the energy transfer.

Investigating the europium compounds by low temperature measurement was a good idea since it has allowed us to have an idea of the symmetry of our system (without having the crystal structure).

- For example we could see by analysing the $^5D_0 \rightarrow {}^7F_2$ that our systems possess no *inversion center*.
- With the analysis of the J-splitting pattern at low temperature we have approximately identified a *hexagonal symmetry* group.

- One single peak for the $^5D_0 \rightarrow {}^7F_0$ at low temperature is an evidence for the presence of *one europium site*.
- And finally, the lifetime measurements have confirmed that, as predicted in the case of **Nd(L^{2}H)L^2**, the OH group is located *outside of the first coordination sphere* of the lanthanide center and do not contribute to quenching.

Of course, the absence of crystal structures makes the results difficult to be interpretable but the luminescence properties (especially those of europium compounds) of these polymer-like material bring the light into the unexplored domain of Ln^{3+}-dithiolene complexes. To the best of our knowledge, these are the first luminescence investigation on Ln^{3+}-dithiolene systems and need to be deeply investigated as future candidates for potential new luminescent materials.

CHAPTER E. SUMMARY AND PERSPECTIVES

E General Conclusion

Our objective in this study was to investigate on the physico-chemical properties of metal-dithiolene complexes. The dithiolene-like neutral ligands used are mainly dmit-derivatives while the metals used are transition metals and lanthanides.

We have used, in the chapter B, the functionalisation abilities of dithiolene ligands to access to supramolecular arrangement where the presence of non-covalent interactions was used to govern the solid-state organisation. We have seen that the presence of OH functional groups is a determinant factor, which can contribute to help a molecular system to self-organise in the solid state. Such functional groups are sensitive to the presence of a hydrogen bond donor or acceptor and tend to dominate the growth orientation by introducing new dimensionality.

In the chapter C we have played with the coordinative ability of such dithiolene ligands to soft metals center (mostly d^{10} electronic configuration metal center) to synthesise metallo-supramolecular systems which were stabilised by additional metal-metal interaction in addition to the non-covalent interactions observed between ligands in chapter B. In such metal organic framework (MOF), the combination of π–π, metal-ligand, metal-metal (in some cases) and hydrogen bonding interactions were found to be systematically at the origin of the solid state organisation. Nevertheless, we could not conclude on the relative strength of one interaction over the others.

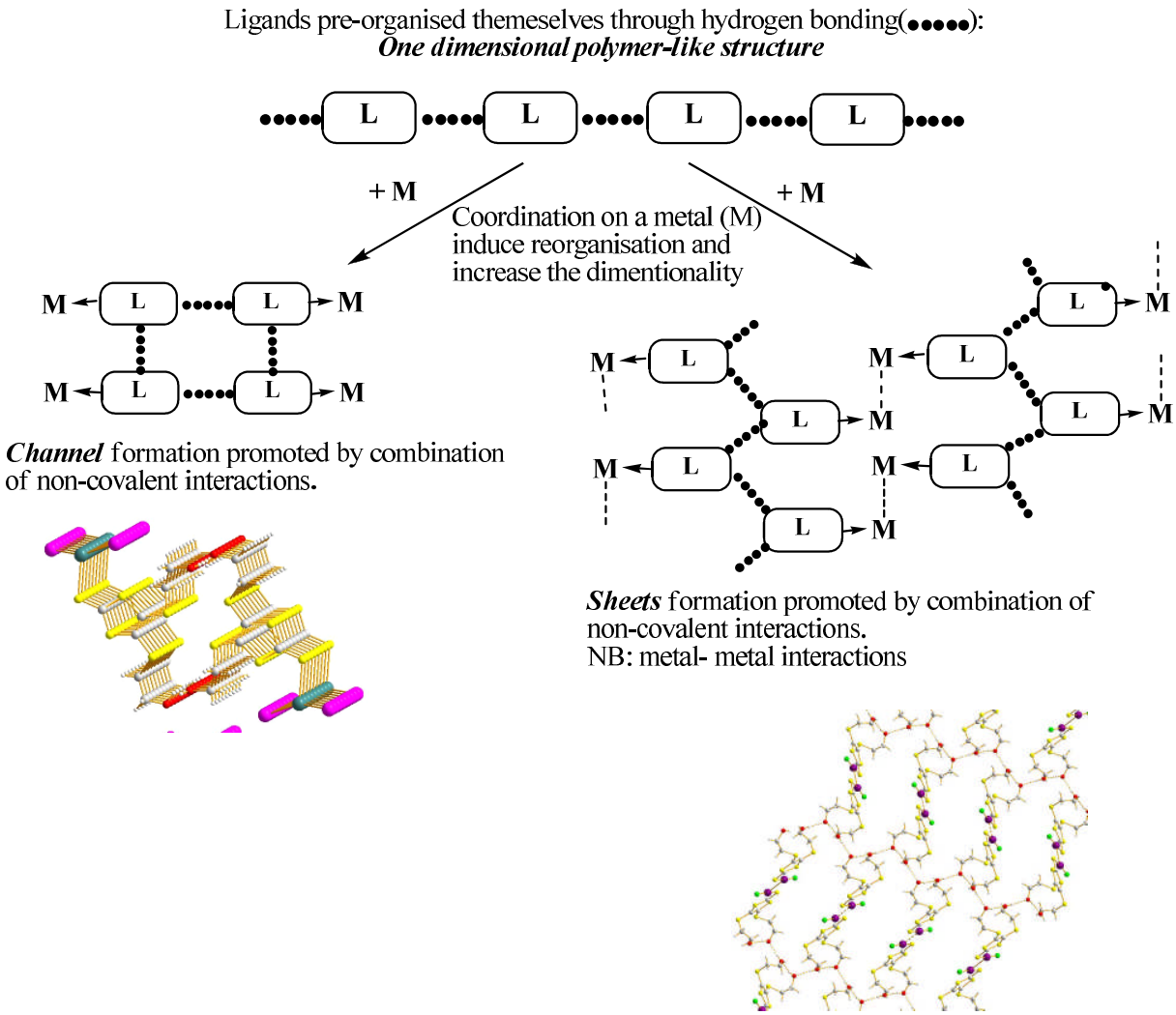

Their luminescent properties were investigated as well, and the results presented here show that they all present luminescent properties which are centered on ligands (intraligand transitions) or take their origin in the metal-ligands centered transitions.

The third and last chapter (chapter D) was devoted to an unexplored field which concerns the Ln^{3+}-dithiolene complexes. Here again, we have used the versality (different reaction sites) of dithiolene-like neutral ligands to set up a synthetical approach using the reactivity of the functional groups. The polymeric nature of the synthesised complexes limited the characterisation possibilities, but the luminescent measurement showed remarquable ability of the dithiolene moiety regarding the luminescence of the resulting lanthanide complexes. In fact, these ligands play a predominant role acting as chromophore to sensitise the lanthanide's luminescence (see below).

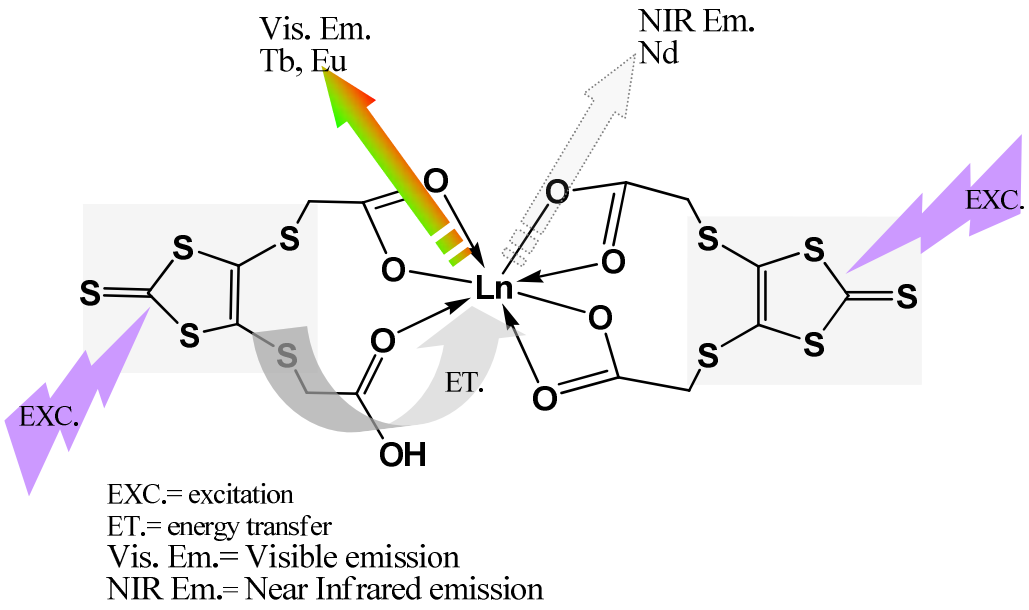

For Near Infrared-emitting ions (such as Nd^{3+}) as well as for Visible-emitting ions (Eu^{3+} and Tb^{3+}), an energy transfer from the ligand to the lanthanide ions seems to govern the luminescence observed; a typical “antenna effect”. Photophysical studies need to be undertaken for a better quantification of these systems and for potential application.

CHAPTER F. EXPERIMENTAL SECTION

F Experimental Part

F.1 General

All reactions were carried out under N_2 atmosphere using a modified “Stock vacuum apparatus” adapted with a N_2 input. The necessary vacuum was obtained with a rotary vane pump of the Vacuumbrand company (model R75, 5.4 m^3/h, $4*10^{-4}$mbar). The solvents (THF, Toluene, Hexane, and Ether) were dried and distilled from sodium-benzophenone and keep under N_2 atmosphere.

F.2 Elemental analysis

Elemental analysis (C and H) were performed on a LECO CHN 900 elemental analyzer. The lanthanide (Nd, Eu, Tb and Er) content was obtained by complexometry and titration method using EDTA as complexing agent. Calculation of the theoretical molar mass was done with relative atomic mass obtained from IUPAC tables.

F.3 Spectroscopic methods

F.3.1 Nuclear magnetic Resonance

The NMR spectra were recorded on Bruker 200 ACF NMR spectrometer operating at 200.13 MHz and 50.3 MHz for ^1H and ^{13}C, respectively. Samples were prepared by dissolving small amount of compounds in appropriate deuterated solvents ($CDCl_3$, C_6D_6 and DMSO-d6). Chemical shifts are given according to δ-scale in ppm. For the assignment of the peaks the following abbreviations are used: s=singlet, d=doublet, t=triplet and br=broad.

F.3.2 Infrared

ATR-IR spectra were performed using a Varian 2000 FT-IR (Scimitar 2000) equipped with a Golden Gate. Measurements were performed in the solid state and the

chamber clean by N_2 flow before the measurement. The assignment of the bands was done with subjective appreciation: s (strong) , w (weak) and br (broad).

F.3.3 UV-Vis (Ultraviolet-visible)

UV-Vis spectra were performed on a Lambda 35 UV-Vis spectrometer (Perkin Elmer Instruments) operating between 200 and 800 nm. Solutions with concentrations ranging from 10^{-4} to 10^{-5} Mol.L^{-1} were prepared for the measurements.

F.3.4 Photoluminescence measurement

The solid-state emission spectra for the ligands and the transition metal complexes were recorded at room temperature on a Jobin-Yvon Fluorolog-3 spectrometer using a cylindrical 0.5 cm diameter quartz capillary with a scan speed of 1 nm/s. Intensity scales are presented in arbitrary units.

Photoluminescence measurements for lanthanide complexes, at room temperature, were recorded on a Jobin-Yvon fluorescence spectrometer (Fluorolog 3) equipped with two 0.22 m double monochromators (SPEX, 1680) and a 450 W xenon lamp. The emission spectra were corrected for photomultiplier sensitivity, the excitation spectra for lamp intensity, and both for the transmission of the monochromators. Temperature-dependent measurements were achieved by using a Helium cryostat operating from 10 K to RT.

F.4 Crystals structure determination

The single crystal X-ray diffraction analysis was performed on a Stoe imaging plate diffractometer (IPDS) at -70 °C and 25°C for **L^1H_2-HgI_2** and **L^1H_2-AuCl** respectively and a BrukerAxs X8 ApexII diffractometer at -170°C (for **L^1H_2**, **L^2H_2** and **L^2H_2.THF**), using graphite monochromated Mo Kα X-ray radiation (λ = 0.71073 Å). The crystal structures were solved by direct methods and refined by full-matrix least squares on F^2 using the SHELX software package for crystal structure solution and refinement[90]

All non-hydrogen atoms were refined with anisotropic thermal parameters in the later cycles of refinement. For **L^1H_2-HgI_2**, the hydrogen atoms were placed in idealized positions and refined using the riding model with general isotropic temperature factors.

F.5 Starting materials

The following compounds were prepared using literature procedure. In some case the proposed method were modified for improving the yield or isolating crystals if necessary.

Compounds	Reference
$[Zn(Dmit)_2](Et_4N)_2$	42
DmitCOPh (L_0)	42
$Ln(N(SiMe_3)_2)_3$ (Ln= Nd, Eu, Tb, Er)	210
Au(THT)Cl	156

F.6 Synthesis

F.6.1 Synthesis of 4,5-bis[(2´-hydroxyethyl)thio]1,3-dithiole-2-thione (L^1H_2)

Ligand **L^1H_2** was synthesised following the report of *Hansen* [Ref. 47], for this reason, only the way to obtain crystals will be reported here. The yellow plates (obtained according to reference 47) were dissolved in THF and filtrated. The filtrate was reduced by slow evaporation of the solvent and after cooling **L^1H_2** was obtained as yellow crystals suitable for X-ray measurement.

m.p: 58-60 °C (65-67 °C [Ref 47]).

NMR ($CDCl_3$): δ(ppm)= 2.80 (2H, s); 3.06 (4H, t, J= 5.5 Hz); 3.63 (4H, t, J= 5.5Hz).

(NMR (DMSO-d6): δ (ppm)= 3.04 (4H, t, J= 6.17 Hz); 3.63 (4H, t, J= 6.17Hz); 5.05 (2H, s).

NMR ($CDCl_3$), [from Ref. 47]: δppm= 3.05 (4H, t, J= 6 Hz); 3.63 (4H, q, J= 6 Hz); 5.06 (2H, t, 6 Hz).

ATR-IR: ν(OH) 3272 (br.), ν(CH) 2920, ν (C=S) 1074(s), ν (C-S) 796 cm^{-1}.

El.An: $C_7H_{10}S_5O_2$ (Mw=286 g.mol^{-1}): found (calc.) C, 28.55 (29.37); H, 3.31 (3.57)%.
UV-Vis (CH_2Cl_2) : λ_{max}(nm) (ε, M^{-1}cm^{-1}) = 272 (22400), 380 (47820).

F.6.2 Synthesis of 4,5-bis[carboxymethylthio]-1,3-dithiol-2-thione (L^2H_2)

In a 2.1 g (2.9mmol) solution of Bis(tetraethyl ammonium) bis(1,3-dithiol-2-thione-4,5-dithiolate)-zincate dissolved in 50 ml acetone were added a mixture of 2.08 g (22mmol) of $ClCH_2COOH$, 0.88 g (22 mmol) of NaOH and 20 ml H_2O. The mixture was heated under reflux for 1 day resulting in a colour change from deep-red to orange. The solvents were then removed in *vacuum* and HCl (50%) was added with cooling to give yellow precipitate. After filtration the precipitate was then dissolved in diethyl ether. The organic phase was then filtrated after decantation, and dried under $MgSO_4$. Slow evaporation of this solution allowed for isolation of yellow crystals (1.53 g, 84%) suitable for X-ray analysis.
NMR (DMSO-d6/TMS, δ, ppm): ^{1}H, 3.87 (4H, s), 4.27 (2H, broad); ^{13}C, 211.16 (C=S), 169.72 (C=O), 136.51 (C=C), 37.59 (CH_2).
El.An: $C_7H_6S_5O_4$ (Mw=314.42 g.mol^{-1}): calc.(found) C 26.75 (26.62); H 2.22 (2.18) %.
UV-Vis (THF): λ_{max}(nm) (ε, M^{-1}cm^{-1}) = 265.7 (27900), 378.6 (40560).
ATR-IR: ν(OH) 3273-2800 (br.), ν(CH) 2970, ν(C=O) 1738 (m) and 1692(s), ν (C=S) 1065(s) cm^{-1}.

F.6.3 Synthesis of 4,5-bis[carboxymethylthio]-1,3-dithiol-2-thione.THF (L^2H_2.THF)

In a 2.1 g (2.9mmol) solution of Bis(tetraethyl ammonium) bis(1,3-dithiol-2-thione-4,5-dithiolate)-zincate dissolved in 50 ml acetone were added a mixture of 2.08 g (22mmol) of $ClCH_2COOH$, 0.88 g (22 mmol) of NaOH and 20 ml H_2O. The mixture was heated under reflux for 1 day resulting in a colour change from deep-red to orange. The solvent were then removed in *vacuum* and HCl (50%) was added with cooling to give yellow precipitate. After filtration the precipitate was then dissolved in THF and heated for half an hour. The solution was then filtrated and dried under

$MgSO_4$. Slow evaporation of this solution allowed for isolation of yellow crystals (1.59 g, 71%) suitable for X-ray analysis.

NMR (DMSO-d6/TMS, δ, ppm): ^{1}H, 3.87 (4H, s), 4.27 (2H, broad); ^{13}C, 211.16 (C=S), 169.72 (C=O), 136.51 (C=C), 37.59 (CH_2).

Additional peaks corresponding to THF were found in the NMR spectra. [^{1}H, 1.74 (4H, m), 3.54 (4H, m); ^{13}C 25.16 (CH_2), 66.72 (CH_2O)].

El.An: $C_{11}H_{14}S_5O_5$ (Mw=386.42 g.mol^{-1}): calc.(found) C 34.16 (33.92); H 3.60 (3.28) %.

UV-Vis (THF): λ_{max}(nm) (ε, M^{-1}cm^{-1}) = 265.7 (27900), 378.6 (40560).

ATR-IR: ν(OH) 3400-2200 (br.), ν(CH) 2889, ν(C=O) 1693(s), ν (C=S) 1051(s) cm^{-1}.

F.6.4 Synthesis of 4,5-bis[benzoylthio]-1,3-dithiol-2-thione (L_0)

In a 8 g (11 mmol) solution of Bis(tetraethyl ammonium) bis(1,3-dithiol-2-thione-4,5-dithiolate)-zincate dissolved in 200 ml acetone were added dropwisely 20mL (17mmol) of benzoyl chloride (ClCOPh) and with stirring over a period of 2h. The reaction mixture was allowed to stand overnight at room temperature resulting in a colour change from deep-red to orange with formation of a yellow/light brown precipitate. This precipitate was then filtered at the pump, and successively washed on the filter with H_2O (100 mL) and acetone (100 mL). The crude material was dissolved in $CHCl_3$ (100 mL), refluxed for 10 min with decolourising charcoal, and filtered hot on a fluted filter paper. The $CHCl_3$ solution was reduced to 50 mL in vacuum, MeOH was added portionwise with shaking, and the solution was left in the refrigerator. Large yellow air-stable crystals, suitable for X-ray analysis, were obtained after filtering off and air-drying (7.22 g, 79%).

NB: The crystals could also be obtained from pure $CHCl_3$ solution of **L_0**.

NMR ($CDCl_3$/TMS, δ, ppm): ^{1}H, 7.50 (4H, t), 7.66 (2H, t), 7.95 (4H, d); ^{13}C, 212.49 (C=S), 185.59 (C=O), 135.02 (C=C dmit-ring), 129,128 ect. (C=C Ph-ring).

El.An: $C_{17}H_{10}S_5O_2$ (Mw=406.14 g.mol^{-1}): found (calc.) C 50.22 (51.62); H 2.46 (2.10) %.

UV-Vis (CH_3CN): λ_{max}(nm) (ε, M^{-1}cm^{-1}) = 366.6 (36333) nm.

ATR-IR: ν(C-H) 3046 (w), ν(C=O) 1686 (s) and 1670, ν (C=S) 1056(s) cm^{-1}, ν (C-S) 878 cm^{-1}.

F.6.5 Synthesis of complex L_0-CuI

Copper iodide (0.140 g; 0.739 mmol) was dried under vacuum at room temperature (45 min) and dissolved in acetonitrile (15 mL). A solution of ligand **L_0** (4,5-di(benzyolthio)-1,3-dithiole-2-thione) (0.300 g 0.739 mmol) dissolved in THF (10 mL) was added to the copper solution at room temperature. The clear solution turned immediately to deep red after addition of the ligand. The resulting red solution was stirring during 1h and then filtrated. The filtrate was then reduced to *ca* 10 mL and cooled to allow the formation of red crystals of **L_0-CuI** (65% yield) suitable for X-ray measurement.

ATR-IR: ν(CH) 3060 , ν(C=O) 1698 and 1668(s), ν (C=S) 1026(s), ν (C-S) 877 cm^{-1}.

El.An: $C_{68}H_{40}S_{20}O_8Cu_2I_2$ (Mw=2005.46 $g.mol^{-1}$): found (calc.) C 40.52 (40.69); H1.92 (1.99)%.

UV-Vis (CH_3CN) : λ_{max}(nm) (ε, $M^{-1}cm^{-1}$) = 366 (27599).

F.6.6 Synthesis of complex L^1H_2-CuI

Copper iodide (0.0665 g; 0.349 mmol) was dried under vacuum at room temperature (45 min) and dissolved in acetonitrile (15 mL). A solution of ligand **L^1H_2** (4,5-di(hydroxyethylthio)-1,3-dithiole-2-thione) (0.200 g; 0.699 mmol) dissolved in THF (10 mL) was added to the copper solution at room temperature. The clear resulting yellow solution turned trouble 2 minutes after addition of the ligand. The resulting yellow-orange solution was stirring during 1h and then filtrated. The filtrate was then reduced to *ca* 10 mL to allow formation of yellow-red powder of **L^1H_2-CuI** (65% yield). All attempts to crystals growth were unsuccessful.

ATR-IR: ν(OH) 3245, ν(CH) 2917, ν (C=S) 1033 and 1004(s), ν (C-S) 842 cm^{-1}.

El.An: $C_{28}H_{40}O_8S_{20}Cu_2I_2$ (Mw=1526.83 $g.mol^{-1}$): found (calc.) C 20.3 (22.03); H 2.48 (2.64)%.

UV-Vis (CH_2Cl_2) : λ_{max}(nm) (ε, $M^{-1}cm^{-1}$) = 380 (24840).

NMR (DMSO-D6, δ ppm)= 3.05 (4H, t, J= 6.17 Hz); 3.62 (4H, q, J= 6.17Hz);
5.07 (2H, t).

F.6.7 Synthesis of L^2H_2-CuI complex

Copper iodide (0.100 g; 0.525 mmol) was dried under vacuum at room temperature (45 min) and dissolved in acetonitrile (12 mL). A solution of ligand **L^2H_2** (4,5-di(carboxymethylthio)-1,3-dithiole-2-thione) (0.082 g 0.262 mmol) dissolved in acetonitrile (10 mL) was added to the copper solution at room temperature. The clear solution turned immediately to deep red after addition of the ligand. The resulting red solution was stirring during 1h and then filtrated. The filtrate was then reduced to *ca* 15 mL to allow for formation of red-brown crystals of **L^2H_2-CuI** (54% yield).

NB: the crystals should be grown by room temperature; cooling the filtrate overnight gives aggregated which are not measurable by X-Ray diffraction.

ATR-IR : ν(OH) 3273-2800 (br.), ν(CH) 2888, ν(C=O) 1685 (s), ν (C=S) 1028(s) cm^{-1}.

El.An: $C_{28}H_{24}S_{20}O_{16}Cu_2I_2$ (Mw=1638.7 $g.mol^{-1}$): found (calc.) C 16.52 (20.52); H 1.92 (1.48)%.

UV-Vis (CH_3CN) : λ_{max}(nm) (ε, $M^{-1}cm^{-1}$) = 376 (9090).

F.6.8 Synthesis of complex L^1H_2-HgI_2 and L^1H_2-$HgCl_2$ • 0.25 THF

Synthesis of complex **L^1H_2-HgI_2**:

Mercury iodide (0.160 g; 0.349 mmol) was dried under vacuum at room temperature (45 min) and dissolved in hot toluene (15 mL). A solution of 4,5-bis[(2´-hydroxyethyl)thio]1,3-dithiole-2-thione (0.100 g 0.349 mmol) dissolved in THF (5 mL) was added to the mercury solution while a temperature of 60 °C was maintained. The resulting clear yellow solution was stirring during 45 min and then filtrated. The filtrate was then reduced to *ca* 10 mL and cooled to allow formation of yellow crystals (0.169 g; 65% yield) suitable for X-ray measurement.

m.p: 72-74 °C

El.An: $C_7H_{10}S_5O_2HgI_2$ (Mw=740 $g.mol^{-1}$): found (calc.) C 11.18 (11.35); H 1.30 (1.35)%.

UV-Vis (in CH_2Cl_2): λ_{max}(nm) (ε, $M^{-1}cm^{-1}$)= 270 (15400), 380 (11820) nm.

ATR-IR: ν(OH) 3240, ν (CH) 2964, ν (C=S) 1031, ν (C-S) 796 cm^{-1}.

Synthesis of complex **L^1H_2-$HgCl_2$ • 0.25 THF**:

Complex **L^1H_2-$HgCl_2$ • 0.25 THF** was synthesized in a similar manner as described for **L^1H_2-HgI_2** from **L^1H_2** and equimolar $HgCl_2$ (0.094 g; 0.349 mmol). **L^1H_2-HgI_2** was isolated as yellow material (0.137 g; 68% yield). However we failed in growing crystals suitable for X-ray measurements.

m.p: 68-70 °C

El.An: $C_8H_{12}S_5O_{2.25}HgCl_2$ (Mw=575 $g.mol^{-1}$): calc. (found) C 16.92 (16.70); H 2.20 (2.10)%.

UV-Vis (CH_2Cl_2): λ_{max}(nm) (ε, $M^{-1}cm^{-1}$)= 274 (6530), 380 (7280).

ATR-IR: ν (OH) 3229, ν (CH) 2934, ν (C=S) 1015cm^{-1}.

F.6.9 Synthesis of complex L^1H_2-AuCl

Chloro(tetrahydrothiophene)gold(I) (0.112 g; 0.349 mmol) (Au(THT)Cl) was dissolved in acetone (8 mL). A solution of 4,5-bis[(2´-hydroxyethyl)thio]1,3-dithiole-2-thione (0.100 g 0.349 mmol) dissolved in acetone (7 mL) was added to the clear gold solution at room temperature. The resulting clear yellow-orange solution was stirring during 1h and then filtrated. The filtrate was then reduced to *ca* 7 mL and cooled to allow formation of yellow crystals (0.105 g; 58% yield) suitable for X-ray measurement.

NMR (DMSO-d6): δ (ppm) = 3.12 (4H, t, J= 6.17 Hz); 3.63 (4H, t, J= 6.17Hz);
5.12 (2H, s).

El.An: $C_7H_{10}S_5O_2AuCl$ (Mw=518.5 $g.mol^{-1}$); found (calc): C 16.15 (16.20); H 1.84 (1.92) %.

UV-Vis (THF): λ_{max}(nm) (ε, $M^{-1}cm^{-1}$) = 315 (5800), 424 (12780) nm.

ATR-IR: ν(OH) 3252, ν (CH) 2960, ν (C=S) 1008, ν (C-S) 806 cm^{-1}.

F.6.10 Synthesis of complex L^2H_2-AuCl

Chloro(tetrahydrothiophene)gold(I) (0.100 g; 0.312 mmol) was dissolved in acetone (15 mL). A solution of 4,5-bis[carboxymethylthio]1,3-dithiole-2-thione **L^2H_2** (0.098 g 0.312 mmol) dissolved in acetone (15 mL) was added to the clear gold solution at room temperature. The resulting clear yellow solution turned to deep orange within a period of few seconds. The mixture was stirring during 1h and then filtrated. The filtrate was then reduced to *ca* 10 mL and cooled to allow formation of yellow crystals (0.092 g; 54.11 % yield) suitable for X-ray measurement. (NB: 2 acetone molecules were found in the crystal structure (in the dimer)).

NMR (DMSO-d6): δ (ppm)= 3.72 (4H, s); 3.26 (2H, s, br).

El.An: $C_{26}H_{38}S_{10}O_{12}Au_2Cl_2$ (Mw=1324.5 g.mol^{-1}); found (calc): C 21.15 (23.56); H 1.14 (2.70) %.

UV-Vis (in THF): λ_{max}(nm) (ε, M^{-1}cm^{-1}) = 320 (6200), 416 (12820) nm.

ATR-IR: ν(OH) 3377, ν (CH) 2951, ν (C=O) 1694, ν (C=S) 1013, ν (C-S) 784 cm^{-1}.

F.6.11 Synthesis of lanthanides silyl-amide ($M[N(SiMe_3)_2]_3$, M= Ce, Nd, Eu, Tb, Er)

Cerium, neodymium and erbium silyl amides (formula $M[N(SiMe_3)_2]_3$, where M= Ce, Nd, Eu, Tb, Er) were synthesised by respective reaction between metal chlorides (2.5 g, 10.14 mmol of $CeCl_3$; 2.16 g, 8.6 mmol of $NdCl_3$; 0.32 g, 1.2 mmol of $EuCl_3$; 1.4 g, 5.27 mmol of $TbCl_3$; and 2.13 g, 7.78 mmol of $ErCl_3$) and three equivalents of Li-$N(SiMe_3)_2$ (5.09 g, 30.42 mmol; 4.33 g, 25.8 mmol; 0.622 g, 3.7 mmol; 2.64 g, 15.8 mmol; and 3.91 g, 23.3 mmol, respectively). The metal chlorides were dried in a dynamic vacuum at 130 °C for 2h and dissolved in 25 mL THF (the flask was cooled with liquid nitrogen because of the strongly exothermal reaction). The stoichiometric amount of Li-$N(SiMe_3)_2$ was dissolved in toluene and added to the THF solution containing the metal salts. The reaction mixture was stirred and heated at 60 °C for 48 h. The resulting white precipitate (LiCl) was removed by filtration and the formed lanthanide silyl amides were sublimed at 100 °C (10^{-2} Torr). The Ce, Nd, Er silyl amides were obtained as yellow-brown, blue, and pink solid powders, respectively.

El.An: Calculated (found)%.

$Ce[N(SiMe_3)_2]_3$: 4.712 g, 76 %; $C_{18}H_{54}N_3Si_6Ce$ (Mw=621.32 $g.mol^{-1}$); C 34.79 (29.7); H 8.78 (5.9); N 6.76 (3.9) %. (Pyrophoric compound)

$Nd[N(SiMe_3)_2]_3$: 4.02 g, 75 %; $C_{18}H_{54}N_3Si_6Nd$ (Mw=624.24 $g.mol^{-1}$); C 34.6 (31.87); H 8.65 (9.6); N 6.73 (6.29) %.

$Eu[N(SiMe_3)_2]_3$: 0.535 g, 70.5 %; $C_{18}H_{54}N_3Si_6Eu$ (Mw=631.96 $g.mol^{-1}$); C 34.18 (30.92); H 8.54 (8.62); N 6.64 (6.17) %.

$Tb[N(SiMe_3)_2]_3$: 1.76 g, 52%; $C_{18}H_{54}N_3Si_6Tb$ (Mw=638.72 $g.mol^{-1}$); C 33.81 (32.03); H 8.45 (8.95); N 6.58 (5.93) %.

$Er[N(SiMe_3)_2]_3$: 3.52 g, 70 %; $C_{18}H_{54}N_3Si_6Er$ (Mw=647.26 $g.mol^{-1}$); C 33.38 (31.85); H 8.34 (8.70); N 6.49 (6.32) %.

F.6.12 Synthesis of Ln^{3+}-dithiolene complexes

F.6.12.1 Synthesis of $Ln_2(L^1)_3$ complexes

Lanthanide silyl amides ($Ln[N(SiMe_3)_2]_3$; Ln= **Nd** (0.5 g, 0.8 mmol); **Er** (0.52 g, 0.8 mmol)) was dissolved in freshly distilled THF under stirring. The resulting solution was degassed with a N_2 flow to avoid any trace of moisture. 0.456 g (1.6 mmol) of $\mathbf{L^1}H_2$ (4,5-bis[hydroxyl-ethylthio]-1,3-dithiol-2-thione) dissolved in THF was then dropwisely added to lanthanide silyl amides solution giving rise to a rapid precipitation of a yellow solid. The reaction was left 1h after complete addition of the ligand, filtrated and washed twice with pentane to remove any rest of lanthanide silyl-amide. The complexes were then obtained after drying the resulting yellow solid under vacuum and characterised as followed:

- $Nd_2(L^1)_3$

Yield 60% (0.547 g); El.An: $C_{21}H_{24}S_{15}O_6Nd_2$ (Mw=1140.48 $g.mol^{-1}$): found (calc.) C 21.06 (22.09); H 2.23 (2.10); Nd 25.51 (25.29) %.

ATR-IR: ν (CH) 2920, ν (C=S) 1051, ν (C-S) 879 cm^{-1}.

- $Er_2(L^1)_3$

Yield 51%; El.An: $C_{21}H_{24}S_{15}O_6Er_2$ (Mw=1187.96 $g.mol^{-1}$): found (calc.) C 20.62 (21.21); H 2.34 (2.02); Er 27.31 (28.16) %.

ATR-IR: ν (CH) 2965, ν (C=S) 1060, ν (C-S) 798 cm^{-1}.

NB: all attempts to dissolve these products in common solvents were unsuccessful.

F.6.12.2 Synthesis of Nd(L^2H)L^2 complexes

One equivalent of lanthanide silyl amide ($Ln[N(SiMe_3)_2]_3$; Ln= **Nd** (1.49 g, 2.38 mmol); **Eu** (1.51 g, 2.38 mmol); **Tb** (1.52 g, 2.38 mmol); **Er** (1.54 g, 2.38 mmol)) was dissolved in freshly distilled THF under stirring. The resulting solution was degassed with a N_2 flow to avoid any trace of moisture.1.50 g (4.77 mmol) of **L^2H_2** (4,5-bis[carboxymethylthio]-1,3-dithiol-2-thione) dissolved in THF was then dropwisely added to lanthanide solution giving rise to a rapid precipitation of a yellow solid. The reaction was left 1h after complete addition of the ligand, filtrated and washed twice with pentane to remove any rest of lanthanide silyl-amide. The complexes were then obtained after drying the resulting yellow solid under vacuum and characterised as followed:

- **Nd(L^2H)L^2**

Yield 66%; El.An: $C_{14}H_9S_{10}O_8Nd$ (Mw=770.12 $g.mol^{-1}$): calc.(found) C 21.83 (21.11); H 1.18 (1.35); Nd 18.73 (18.50) %.

ATR-IR: ν(OH) 3240 (s), ν(CH) 2964, ν (C=O) 1649, ν (C=S) 1051, ν (C-S) 796 cm^{-1}.

- **Eu(L^2H)L^2**

Yield 44%; El.An: $C_{14}H_9S_{10}O_8Eu$ (Mw=777.84 $g.mol^{-1}$): calc.(found) C 21.62 (20.01); H 1.17 (1.03); Eu 19.54 (19.76) %.

ATR-IR: ν(OH) 3334 (s), ν (CH) 2965, ν (C=O) 1647, ν (C=S) 1061, ν (C-S) 794 cm^{-1}.

- **Tb(L^2H)L^2**

Yield 54%, $C_{14}H_9S_{10}O_8Tb$ (Mw=784.8 $g.mol^{-1}$): calc.(found) C 21.43 (C 20.14); H 1.16 (1.45); Tb 20.25 (19.38) %.

ATR-IR: ν(OH) 3240 (s), ν (CH) 2965, ν (C=O) 1643, ν (C=S) 1056, ν (C-S) 801 cm^{-1}.

- **Er(L^2H)L^2**

Yield 60%, $C_{14}H_9S_{10}O_8Er$ (Mw=792.26 $g.mol^{-1}$): calc.(found) C 21.20 (19.11); H 1.13 (1.25); Er 21.11 (16.19) %.

ATR-IR: ν(OH) 3500-2800 (br), ν (CH) 2962, ν (C=O) 1645, ν (C=S) 1056, ν (C-S) 882 cm^{-1}.

NB: all attempts to dissolve these products in common solvents were unsuccessful.

F.6.12.3 Synthesis of Eu(L^2Na)L^2

0.351 g (1.36 mmol) of europium chloride was dissolved in freshly distilled methanol under stirring. The resulting white suspension was degassed with a N_2 flow to avoid any trace of moisture. 0.853 g (2.72 mmol) of $\mathbf{L^2}H_2$ (4,5-bis[carboxymethylthio]-1,3-dithiol-2-thione) in methanol was treated with MeONa (2 equivalents) and the resulting carboxylate solution was then dropwisely added to the europium solution, giving rise to a rapid precipitation of a yellow solid. The reaction was left 1 week, in which a yellowish mixture was obtained. The resulting precipitate was filtered off and washed several times with alkohol to eliminate the NaCl. **Eu(L^2Na)L^2** was isolate as an amorphous yellow powder in a 61% yield (1.36 g) after drying.

NB: all attempts to dissolve this product in common solvents were unsuccessful.

El.An: $C_{14}H_8S_{10}O_8EuNa$ (Mw=799.82 g.mol^{-1}): calc.(found) C 21.02 (C 20.61); H 1.01 (H 0.95); Eu 19.00 (19.50) %.

ATR-IR: ν (CH) 2970, ν (C=O) 1615, ν (C=S) 1063, ν (C-S) 792 cm^{-1}.

F.6.12.4 Synthesis of Er-Hg heterobimetallic complex

In a THF/Toluene (5 mL/10 mL) solution of $\mathbf{L^1}H_2$**-HgI_2** (0.309g, 0.418mmol) was added dropwisely a THF (10 mL) solution of $ErCl_3$ (0.057g, 0.208mmol). The resulting yellow solution turns turbid. The mixture is stirred during one day at 60°C. The resulting clear yellow solution was then filtrated and the filtrate reduced to 10 mL. Pink crystals of **Er-Hg** were obtained after cooling at -5 °C within a period of one week. Yield (from HgI_2): 55%.

CHAPTER G

G References

1. Davison, A.; Edelstein, N.; Holm, R. H.; Maki, A. H., *J. Am. Chem. Soc.* **1963,** 85, 2029-2030.
2. Williams, R.; Billig, E.; Waters, J. H.; Gray, H. B., *J. Am. Chem. Soc.* **1966,** 88, 43-50.
3. Schrauzer, G. N.; Mayweg, V., *J. Am. Chem. Soc.* **1962,** 84, 3221-3221.
4. Fourmigue, M., *Acc. Chem. Res.* **2004,** 37, 179-186.
5. Stiefel, E. I., *Dithiolene Chemistry: Synthesis, Properties and Applications*. Wiley: 2004; Vol. 52.
6. Kajitani, M.; Hagino, G.; Tamada, M.; Fujita, T.; Sakurada, M.; Akiyama, T.; Sugimori, A., *J. Am. Chem. Soc.* **1996,** 118, 489-490.
7. Holloway, G. A.; Klausmeyer, K. K.; Wilson, S. R.; Rauchfuss, T. B., *Organometallics* **2000,** 19, 5370-5375.
8. Lim, B. S.; Sung, K. M.; Holm, R. H., *J. Am. Chem. Soc.* **2000,** 122, 7410-7411.
9. Lim, B. S.; Holm, R. H., *J. Am. Chem. Soc.* **2001,** 123, 1920-1930.
10. Lim, B. S.; Willer, M. W.; Miao, M.; Holm, R. H., *J. Am. Chem. Soc.* **2001,** 123, 8343-8349.
11. Rauchfuss, T. B.; Contakes, S. M.; Hsu, S. C. N.; Reynolds, M. A.; Wilson, S. R., *J. Am. Chem. Soc.* **2001,** 123, 6933-6934.
12. Wudl, F.; Smith, G. M.; Hufnagel, E. J., *J. Chem. Soc. Chem. Comm.* **1970**, 1453-1454.
13. Schrauzer, G. N., *Acc. Chem. Res.* **1969,** 2, 72-80.
14. McCleverty, J. A., *Prog. Inorg. Chem.* **1968,** 10, 49.
15. Jeppesen, J. O.; Becher, J., *Eur.J. Org. Chem.* **2003,** 2003, 3245-3266.
16. Jeppesen, J. O.; Nielsen, M. B.; Becher, J., *Chem. Rev.* **2004,** 104, 5115-5132.
17. Faulmann, C.; Cassoux, P., Solid-State Properties (Electronic, Magnetic, Optical) of Dithiolene Complex-Based Compounds. In *Dithiolene Chemistry*, Edward, I. S., Ed. 2004; pp 399-489.
18. Pullen, A. E.; Olk, R.-M., *Coord. Chem. Rev.* **1999,** 188, 211-262.
19. Bousseau, M.; Valade, L.; Legros, J. P.; Cassoux, P.; Garbauskas, M.; Interrante, L. V., *J. Am. Chem. Soc.* **1986,** 108, 1908-1916.
20. Cassoux, P.; Valade, L.; Kobayashi, H.; Kobayashi, A.; Clark, R. A.; Underhill, A. E., *Coord. Chem. Rev.* **1991,** 110, 115-160.
21. Cassoux, P., *Coord. Chem. Rev.* **1999,** 185-186, 213-232.
22. Olk, R.-M.; Olk, B.; Dietzsch, W.; Kirmse, R.; Hoyer, E., *Coord. Chem. Rev.* **1992,** 117, 99-131.
23. Faulmann, C.; Jacob, K.; Dorbes, S.; Lampert, S.; Malfant, I.; Doublet, M. L.; Valade, L.; Real, J. A., *Inorg. Chem.* **2007,** 46, 8548-8559.
24. Faulmann, C.; Dorbes, S.; Lampert, S.; Jacob, K.; Garreau de Bonneval, B.; Molnar, G.; Bousseksou, A.; Real, J. A.; Valade, L., *Inorg. Chim. Acta* **2007,** 360, 3870-3878.
25. Nishihara, S.; Akutagawa. T.; Sato. D.; Takeda. S.; Noro. S-i.; Nakamura, T. *Chemistry - An Asian Journal* **2007,** 2, 1083-1090.
26. Sato, D.; Akutagawa, T.; Takeda, S.; Noro, S. i.; Nakamura, T., *Inorg. Chem.* **2007,** 46, 363-365.

27. Savy, J. P.; Caro, D. d.; Valade, L.; Legros, J. P.; Auban-Senzier, P.; Pasquier, C. R.; Fraxedas, J.; Senocq, F., *Europhys. Lett.* **2007,** 78, 37005.
28. De Caro, D.; Fraxedas, J.; Faulmann, C.; Malfant, I.; Milon, J.; Lamère, J. F.; Collière, V.; Valade, L., *Adv. Mater.* **2004,** 16, 835-838.
29. Jeannin, O.; Clérac, R.; Cauchy, T.; Fourmigué, M., *Inorg. Chem.* **2008,** 47, 10656-10661.
30. Fourmigué, M.; Domercq, B.; Jourdain, I. V.; Molinié, P.; Guyon, F.; Amaudrut, J., *Chem. Eur. J.* **1998,** 4, 1714-1723.
31. Jourdain, I. V.; Fourmigue, M.; Guyon, F.; Amaudrut, J., *Organometallics* **1999,** 18, 1834-1839.
32. Guyon, F.; Lucas, D.; Jourdain, I. V.; Fourmigue, M.; Mugnier, Y.; Cattey, H., *Organometallics* **2001,** 20, 2421-2424.
33. Guyon, F.; Jourdain, I. V.; Knorr, M.; Lucas, D.; Monzon, T.; Mugnier, Y.; Avarvari, N.; Fourmigue, M., *Eur. J. Inorg. Chem.* **2002**, 2026-2033.
34. Harris, H. A.; Rae, A. D.; Dahl, L. F., *J. Am. Chem. Soc.* **1987,** 109, 4739-4741.
35. Arliguie, T.; Thuery, P.; Fourmigue, M.; Ephritikhine, M., *Organometallics* **2003,** 22, 3000-3003.
36. Arliguie, T.; Thuéry, P.; Fourmigué, M.; Ephritikhine, M., *Eur.J. Inorg. Chem.* **2004,** 2004, 4502-4509.
37. Roger, M.; Belkhiri, L.; Thuery, P.; Arliguie, T.; Fourmigue, M.; Boucekkine, A.; Ephritikhine, M., *Organometallics* **2005,** 24, 4940-4952.
38. Nam, H. J.; Lee, H.-J.; Noh, D.-Y., *Polyhedron* **2004,** 23, 115-123.
39. Schukat, G.; Richter, A. M.; Fanghänel, E., *Sulfur Reports* **1987,** 7, 155-240.
40. Steimecke, G.; Sieler, H.-J.; Kirmse, R.; Hoyer, E., *Phosphorus, Sulfur, and Silicon and the Related Elements* **1978,** 7, 49 - 55.
41. Wang, C.; Batsanov, A. S.; Bryce, M. R.; Howard, J. A. K., *Synthesis* **1998**, 1615-1618.
42. Svenstrup, N.; Becher, J., *Synthesis* **1995**, 215-235.
43. Breitzer, J. G.; Rauchfuss, T. B., *Polyhedron* **2000,** 19, 1283-1291.
44. Segura, J. L.; Martín, N., *Angew. Chem. Int. Ed.* **2001,** 40, 1372-1409.
45. Heuzé, K.; Fourmigué, M.; Batail, P., *J. Mater. Chem.* **1999,** 9, 2373 - 2379.
46. Hu, P.-Z.; Wang, J.-G.; Wang, L.; Chen, J.-Q.; Zhao, B.-T., *Acta Crystallogr. E* **2006,** 62, o2059-o2061.
47. Hansen, T. K.; Joergensen, T.; Jensen, F.; Thygesen, P. H.; Christiansen, K.; Hursthouse, M. B.; Harman, M. E.; Malik, M. A.; Girmay, B.; et al., *J. Org. Chem.* **1993,** 58, 1359-1366.
48. Moore, A. J.; Bryce, M. R.; Cooke, G.; Marshallsay, G. J.; Skabara, P. J.; Batsanov, A. S.; Howard, J. A. K.; Daley, S. T. A. K., *J. Chem. Soc. Perkin Trans. 1* **1993**, 1403-1410.
49. Moore, A. J.; Goldenberg, L. M.; Bryce, M. R.; Petty, M. C.; Moloney, J.; Howard, J. A. K.; Joyce, M. J.; Port, S. N., *J. Org. Chem.* **2000,** 65, 8269-8276.
50. Baudron, S. A.; Avarvari, N.; Canadell, E.; Auban-Senzier, P.; Batail, P., *Chem. Eur. J.* **2004,** 10, 4498-4511.
51. Baudron, S. A.; Avarvari, N.; Batail, P., *Inorg. Chem.* **2005,** 44, 3380-3382.
52. Baudron, S. A.; Avarvari, N.; Batail, P.; Coulon, C.; Clerac, R.; Canadell, E.; Auban-Senzier, P., *J. Am. Chem. Soc.* **2003,** 125, 11583-11590.
53. Brammer, L.; Rivas, J. C. M.; Atencio, R.; Fang, S.; Pigge, F. C., *J. Chem. Soc. Dalton Trans.* **2000**, 3855-3867.
54. Brammer, L., *Chem. Soc. Rev.* **2004,** 33, 476-489.
55. Jeannin, O.; Delaunay, J.; Barriere, F.; Fourmigue, M., *Inorg. Chem.* **2005,** 44, 9763-9770.

56. Cotton, S., *Lanthanide and actinide chemistry*. John Wiley and Sons LTd: England, 2006; Vol. 2 Rev Ed edition.
57. http://antoine.frostburg.edu/chem/senese/101/electrons/faq/f-orbital-shapes.shtml, In.
58. Greenwood, N.N.; Earnshaw, A., *Chemistry of the Elements (2nd Edition)*. . 1998; Vol. 2nd Edition.
59. Kobayashi, S., *Lanthanides: Chemistry and Use in Organic Synthesis*. Springer-Verlag Heidelberg 1999; Vol. 2, p 307.
60. Cotton, S. A., *C. R. Chimie* **2005,** 8, 129-145.
61. Cotton, S. , *Lanthanide and actinide chemistry*. John Wiley and Sons LTd: England, 2006; Vol. 2 Rev Ed edition.
62. Stein, G.; Wurzberg, E., *J. Chem. Phys.* **1975,** 62, 208-213.
63. Carnall, W. T.; Fields, P. R.; Rajnak, K., *J. Chem. Phys.* **1968,** 49, 4424-4442.
64. Carnall, W. T.; Fields, P. R.; Rajnak, K., *J. Chem. Phys.* **1968,** 49, 4443-4446.
65. Carnall, W. T.; Fields, P. R.; Rajnak, K., *J. Chem. Phys.* **1968,** 49, 4447-4449.
66. Carnall, W. T.; Fields, P. R.; Rajnak, K., *J. Chem. Phys.* **1968,** 49, 4450-4455.
67. Dieke, G. H.; Crosswhite, H. M., *Appl. Opt.* **1963,** 2, 675-686.
68. Wegh, R. T.; Meijerink, A.; Lamminmäki, R.-J.; Jorma, H., *J. Lumin.* **2000,** 87-89, 1002-1004.
69. Bunzli, J. C. G.; Choppin, G. R., *Lanthanide Probes in Life, Chemical and Earth Sciences: Theory and Practice* Elsevier Science Ltd The Netherlands, 1989.
70. Bunzli, J.-C. G.; Piguet, C., *Chem. Soc. Rev.* **2005,** 34, 1048-1077.
71. Maas, H.; Currao, A.; Calzaferri, G., *Angew. Chem. Int. Ed.* **2002,** 41, 2495-2497.
72. Conde-Gallardo, A.; Garcia-Rocha, M.; Hernandez-Calderon, I.; Palomino-Merino, R., *Appl. Phys. Lett.* **2001,** 78, 3436-3438.
73. Jüstel, T.; Nikol, H.; Ronda, C., *Angew. Chem. Int. Ed.* **1998,** 37, 3084-3103.
74. Thornton, W. A., *J Opt Soc Amer* **1971,** 61, 1155-1163.
75. Comby, S.; Bünzli, J.-C. G.; Karl A. Gschneidner, J. J.-C. B.; Vitalij, K. P., Chapter 235 Lanthanide Near-Infrared Luminescence in Molecular Probes and Devices. In *Handbook on the Physics and Chemistry of Rare Earths*, Elsevier: 2007; Vol. Volume 37, pp 217-470.
76. Stiefel, E. I., *Dithiolene Chemistry: Synthesis, Properties and Applications* wiley ed.; Wiley: New York, 2004; Vol. 52, p 738.
77. Zheng, H.; Zhang, R.; Shen, J., *Supramolecular Science* **1998,** 5, 627-629.
78. Fourmigué, M.; Batail, P., *Chem. Rev.* **2004,** 104, 5379-5418.
79. Russell, V. A.; Ward, M. D., *Chem. Mater.* **1996,** 8, 1654-1666.
80. Aakeroy, C. B.; Schultheiss, N.; Desper, J.; Moore, C., *New J. Chem.* **2006,** 30, 1452-1460.
81. Kim, H.; Kobayashi, A.; Sasaki, Y.; Kato, R.; Kobayashi, H., *Chem. Lett.* **1987,** 16, 1799-1802.
82. Delhaes, P., *Graphite and Precursors*. CRC Press: 2001.
83. Novoa, J. J.; Carme Rovira, M.; Rovira, C.; Veciana, J.; Tarrés, J., *Adv. Mater.* **1995,** 7, 233-237.
84. Blackman, A.; Bottle, S.; Schmid, S.; Mocerino, M.; Wille, U., *Chemistry*. John Wiley and sons ed.; John Wliey and sons: 2007.
85. Batsanov, A. S.; Svenstrup, N.; Lau, J.; Becher, J.; Bryce, M. R.; Howard, J. A. K., *J. Chem. Soc., Chem. Commun.* **1995**, 1201-1202.
86. Jeffrey, G. A., *Hydrogen bonding in biological structures*. Springer: Berlin ; Heidelberg [u.a.], 1991.
87. Lehn, J.-M., *Angew. Chem. Int. Ed.* **1990,** 29, 1304-1319.
88. Aakeröy, C. B.; Seddon, K. R., *Chem. Soc. Rev.* **1993,** 22, 397 - 407.
89. Emsley, J., *Chem. Soc. Rev.* **1980,** 9, 91-124.

90. Sheldrick, G. M., *SHELX-97, Progam for refinement of crystal structures, University of Göttingen, Germany,*
1997.
91. Dolbecq, A.; Fourmigue, M.; Batail, P., *Acta Crystallogr. C* **1996,** 52, 1543-1545.
92. Legros, J.-P.; Dahan, F.; Binet, L.; Carcel, C.; Fabre, J.-M., *J. Mater. Chem.* **2000,** 10, 2685-2691.
93. Wang, C.; Bryce, M. R.; Batsanov, A. S.; Stanley, C. F.; Beeby, A.; Howard, J. A. K., *J. Chem. Soc., Perkin Trans. 2* **1997**, 1671 - 1678.
94. Taylor, R.; Kennard, O., *Acc. Chem. Res.* **1984,** 17, 320-326.
95. Steiner, T., *Angew. Chem. Int. Ed.* **2002,** 41, 48-76.
96. Ndiaye, A. L. ; Guyon, F.; Knorr, M.; Huch, V.; Veith, M., *Z. Anorg. Allg. Chem.* **2007,** 633, 1959-1963.
97. Bertolasi, V.; Gilli, P.; Ferretti, V.; Gilli, G., *J. Chem. Soc. Perkin Trans. 2* **1997**, 945-952.
98. Etter, M. C., *Acc. Chem. Res.* **1990,** 23, 120-126.
99. Allen, F. H.; Motherwell, W. D. S.; Raithby, P. R.; Shields, G. P.; Taylor, R., *New J. Chem.* **1999,** 23, 25-34.
100. Solans, X.; Font-Bardia, M.; Font-Altaba, M.; Vicente, R.; Segui, A., *Acta. Crystallogr. C* **1987,** 43, 1415-1417.
101. Cox, P. J.; Doidge-Harrison, S. M. S. V., *Acta. Crystallogr. C* **1996,** 52, 720-722.
102. Zmolek, P. B.; Sohn, H.; Gantzel, P. K.; Trogler, W. C., *J. Am. Chem. Soc.* **2001,** 123, 1199-1207.
103. Gautam, R. D., *Angew. Chem. Int. Ed.* **1995,** 34, 2311-2327.
104. Pyykko, P., *Chem. Rev.* **1997,** 97, 597-636.
105. Liu, X. M.; Mu, X. Y.; Xia, H.; Ye, L.; Gao, W.; Wang, H. Y.; Mu, Y., *Eur.J. Inorg. Chem.* **2006**, 4317-4323.
106. Miller, A. J. M.; Dempsey, J. L.; Peters, J. C., *Inorg. Chem.* **2007,** 46, 7244-7246.
107. Hu, T.-L.; Zou, R.-Q.; Li, J.-R.; Bu, X.-H., *Dalton Trans.* **2008**, 1302-1311.
108. Barbieri, A.; Accorsi, G.; Armaroli, N., *Chem. Comm.* **2008**, 2185-2193.
109. Schmidbaur, H., *Gold. Bull.* **1990,** 23, 11-21.
110. Jansen, M.; Bortz, M.; Heidebrecht, K., *J. Less-Common Met.* **1990,** 161, 17-24.
111. Anders Byström; Lars Evers, *Acta. Chem. Scand.* **1950,** 4, 613-627.
112. Luth, M. S.; Freisinger, E.; Glahe, F.; Lippert, B., *Inorg. Chem.* **1998,** 37, 5044-5045.
113. Hitchcock, P., *Acta Crystallogr. B* **1979,** 35, 746-747.
114. Faville, S. J.; Henderson, W.; Mathieson, T. J.; Nicholson, B. K., *J. Organomet. Chem.* **1999,** 580, 363-369.
115. Scherbaum, F.; Grohmann, A.; Huber, B.; Krüger, C.; Schmidbaur, H., *Angew. Chem. Int. Ed.* **1988,** 27, 1544-1546.
116. Bodensieck, U.; Braunstein, P.; Knorr, M.; Strampfer, M.; Bénard, M.; Strohmann, C., *Angew. Chem. Int. Ed.* **1997,** 36, 2758-2761.
117. Wang, S.; Fackler, J. P., *Organometallics* **1988,** 7, 2415-2417.
118. Manojlovic-Muir, L.; Muir, K. W.; Grossel, M. C.; Brown, M. P.; Nelson, C. D.; Yavari, A.; Kallas, E.; Moulding, R. P.; Seddon, K. R., *J. Chem. Soc. Dalton Trans.* **1986**, 1955-1963.
119. Carvajal, M. A.; Alvarez, S.; Novoa, J. J., *Chem. Eur. J.* **2004,** 10, 2117-2132.
120. Merz, K. M.; Hoffmann, R., *Inorg. Chem.* **1988,** 27, 2120-2127.
121. Yam, V. W. W.; Lo, K. K. W., *Chem. Soc. Rev.* **1999,** 28, 323-334.
122. Zheng, S-L.; Zhang, J-P.; Chen, X-M; Huang, Z-L; Lin, Z-Y.; Wong, W-T., *Chem. Eur. J.* **2003,** 9, 3888-3896.
123. Ziolo, R. F.; Lipton, S.; Dori, Z., *J. Chem. Soc.D , Chem. Comm.* **1970**, 1124-1125.
124. Kutal, C., *Coord. Chem. Rev.* **1990,** 99, 213-252.

125. Robert S. Pilato, K. A. v. H., Metal Dithiolene Complexes in Detection: Past, Present, and Future. In *Dithiolene Chemistry*, Edward, I. S., Ed. 2004; pp 369-397.
126. Dias, H. V. R.; Diyabalanage, H. V. K.; Eldabaja, M. G.; Elbjeirami, O.; Rawashdeh-Omary, M. A.; Omary, M. A., *J. Am. Chem. Soc.* **2005,** 127, 7489-7501.
127. Thebault, F.; Barnett, S. A.; Blake, A. J.; Wilson, C.; Champness, N. R.; Schroder, M., *Inorg. Chem.* **2006,** 45, 6179-6187.
128. Bondi, A., *J. Phys. Chem.* **1964,** 68, 441-451.
129. King, R. B., *J. Chem. Inf. Comput. Sci.* **1994,** 34, 410-417.
130. Peindy, H. N.; Guyon, F.; Khatyr, A.; Knorr, M.; Strohmann, C., *Eur. J. Inorg. Chem.* **2007,** 2007, 1823-1828.
131. Wang, X.-Q.; Cheng, J.-K.; Wen, Y.-H.; Zhang, J.; Li, Z.-J.; Yao, Y.-G., *Inorg. Chem. Comm.* **2005,** 8, 897-899.
132. Dai, J.; Munakata, M.; Wu, L. P.; Kuroda-Sowa, T.; Suenaga, Y., *Inorg. Chim. Acta* **1997,** 258, 65-69.
133. Dai, J.; Yang, W.; Ren, Z.-G.; Zhu, Q.-Y.; Jia, D.-X., *Polyhedron* **2004,** 23, 1447-1451.
134. Raston, C. L.; White, A. H., *J. Chem. Soc. Dalton Trans.* **1976**, 2153-2156.
135. DeAngelis, F.; Fantacci, S.; Sgamellotti, A.; Cariati, E.; Ugo, R.; Ford, P. C., *Inorg. Chem.* **2006,** 45, 10576-10584.
136. Rath, N. P.; Holt, E. M.; Tanimura, K., *Inorg. Chem.* **1985,** 24, 3934-3938.
137. Churchill, M. R.; DeBoer, B. G.; Mendak, S. J., *Inorg. Chem.* **1975,** 14, 2041-2047.
138. Hu, G.; Mains, G. J.; Holt, E. M., *Inorg. Chim. Acta* **1995,** 240, 559-565.
139. Ford, P. C.; Cariati, E.; Bourassa, J., *Chem. Rev.* **1999,** 99, 3625-3648.
140. Hardt, H. D.; Stoll, H. J., *Z. Anorg. Allg. Chem.* **1981,** 480, 193-198.
141. Hesse, M.; Meier, H.; Zeeh, B., *Spektroskopische Methoden in der Organischen Chemie*. thieme ed.; Thieme: stuttgart, 2005; Vol. 7.
142. Hameau, A.; Guyon, F.; Knorr, M.; Enescu, M.; Strohmann, C., *Monatsh. Chem.* **2006,** 137, 545-555.
143. Dai, J.; Megumu, M.; Bian, G.-q.; Takayoshi, K.-S.; Masahiko, M., *Polyhedron* **1998,** 17, 2267-2270.
144. Dai, J.; Wang, X.; Bian, G.-Q.; Zhang, J.-S.; Guo, L.; Munakata, M., *J. Mol. Struc.* **2004,** 690, 115-119.
145. Gade, L. H., *Angew. Chem. Int. Ed.* **1997,** 36, 1171-1173.
146. Peter J. Sadler; Sue, R. E., *Metal-Based Drugs* **1994,** 1, 107-144.
147. Pyykko, P.; Desclaux, J. P., *Acc. Chem. Res.* **1979,** 12, 276-281.
148. Schmidbaur, H.; Cronje, S.; Djordjevic, B.; Schuster, O., *Chem. Phys.* **2005,** 311, 151-161.
149. Hollatz, C.; Schier, A.; Schmidbaur, H., *J. Am. Chem. Soc.* **1997,** 119, 8115-8116.
150. Schmidbaur, H.; Graf, W.; Müller, G., *Angew. Chem. Int. Ed.* **1988,** 27, 417-419.
151. Schmidbaur, H.; Dziwok, K.; Grohmann, A.; Müller, G., *Chem. Ber.* **1989,** 122, 893-895.
152. Harwell, D. E.; Mortimer, M. D.; Knobler, C. B.; Anet, F. A. L.; Hawthorne, M. F., *J. Am. Chem. Soc.* **1996,** 118, 2679-2685.
153. Narayanaswamy, R.; Young, M. A.; Parkhurst, E.; Ouellette, M.; Kerr, M. E.; Ho, D. M.; Elder, R. C.; Bruce, A. E.; Bruce, M. R. M., *Inorg. Chem.* **1993,** 32, 2506-2517.
154. Dziwok, K.; Lachmann, J.; Wilkinson, D. L.; Müller, G.; Schmidbaur, H., *Chem. Ber.* **1990,** 123, 423-431.
155. Hunks, W. J.; Jennings, M. C.; Puddephatt, R. J., *Inorg. Chem.* **2002,** 41, 4590-4598.
156. Uson, R.; Laguna, A.; Laguna, M., *Inorg. Synth.* **1989,** 26, 85-91.
157. Bachman, R. E.; Fioritto, M. S.; Fetics, S. K.; Cocker, T. M., *J. Am. Chem. Soc.* **2001,** 123, 5376-5377.

158. Raubenheimer, H. G.; Otte, R.; Linford, L.; Van Zyl, W. E.; Lombard, A.; Kruger, G. J., *Polyhedron* **1992,** 11, 893-900.
159. Mohr, F.; Jennings, M. C.; Puddephatt, R. J., *Eur. J. Inorg. Chem.* **2003,** 2003, 217-223.
160. Pyykkö, P.; Li, J.; Runeberg, N., *Chem. Phys. Lett.* **1994,** 218, 133-138.
161. Nunokawa, K.; Okazaki, K.; Onaka, S.; Ito, M.; Sunahara, T.; Ozeki, T.; Imai, H.; Inoue, K., *J. Organomet. Chem.* **2005,** 690, 1332-1339.
162. Zang, S.; Su, Y.; Li, Y.; Ni, Z.; Meng, Q., *Inorg. Chem.* **2006,** 45, 174-180.
163. Chen, C. H.; Jianmin, S., *Coord. Chem. Rev.* **1998,** 171, 161-174.
164. Wang, S., *Coord. Chem. Rev.* **2001,** 215, 79-98.
165. Tsuboyama, A.; Kuge, K.; Furugori, M.; Okada, S.; Hoshino, M.; Ueno, K., *Inorg. Chem.* **2007,** 46, 1992-2001.
166. Teets, T. S.; Partyka, D. V.; Esswein, A. J.; Updegraff, J. B.; Zeller, M.; Hunter, A. D.; Gray, T. G., *Inorg. Chem.* **2007,** 46, 6218-6220.
167. Araki, H.; Tsuge, K.; Sasaki, Y.; Ishizaka, S.; Kitamura, N., *Inorg. Chem.* **2007,** 46, 10032-10034.
168. Lo, W. Y.; Lam, C. H.; Yam, V. W. W.; Zhu, N.; Cheung, K. K.; Fathallah, S.; Messaoudi, S.; LeGuennic, B.; Kahlal, S.; Halet, J. F., *J. Am. Chem. Soc.* **2004,** 126, 7300-7310.
169. Wong, W-Y.; Liu, L.; Shi, J.-X., *Angew. Chem. Int. Ed.* **2003,** 42, 4064-4068.
170. Fernàndez, A.; Kisch, H., *Chem. Ber.* **1984,** 117, 3102-3111.
171. Riva, H. d. l.; Pintado-Alba, A.; Nieuwenhuyzen, M.; Hardacre, C.; Lagunas, M. C., *Chem. Commun.* **2005**, 4970-4972.
172. Lagunas, M C.; Fierro, C. M.; Pintado Alba, A.; de la Riva, H.; Betanzos-Lara, S., *Gold. Bull.* **2007,** 40, 135-141.
173. Jones, W. B.; Yuan, B. J.; Narayanaswamy, R.; Young, M. A.; Elder, R. C.; Bruce, A. E.; Bruce, M. R. M., *Inorg. Chem.* **1995,** 34, 1996-2001.
174. King, C.; Khan, M. N. I.; Staples, R. J.; Fackler, J. P., *Inorg. Chem.* **1992,** 31, 3236-3238.
175. McCleskey, T. M.; Gray, H. B., *Inorg. Chem.* **1992,** 31, 1733-1734.
176. Forward, J. M.; Bohmann, D.; Fackler, J. P.; Staples, R. J., *Inorg. Chem.* **1995,** 34, 6330-6336.
177. Yam, V. W-W.; Li, C-K.; Chan, C-L., *Angew. Chem. Int. Ed.* **1998,** 37, 2857-2859.
178. Balch, A. L., Remarkable Luminescence Behaviors and Structural Variations of Two-Coordinate Gold(I) Complexes. In *Struct. Bond.*, Springer, Ed. Springer-verlag: Berlin Heidelberg, 2007; Vol. 123, pp 1-40.
179. Zhang, H-X.; Che, C.-M., *Chem. Eur. J.* **2001,** 7, 4887-4893.
180. Fernandez, E. J.; Laguna, A.; Lopez-de-Luzuriaga, J. M.; Monge, M.; Montiel, M.; Olmos, M. E.; Rodriguez-Castillo, M., *Dalton Trans.* **2006**, 3672-3677.
181. Assefa, Z.; McBurnett, B. G.; Staples, R. J.; Fackler, J. P., *Inorg. Chem.* **1995,** 34, 4965-4972.
182. Spanget-Larsen, J.; Gleiter, R.; Kobayashi, M.; Engler, E. M.; Shu, P.; Cowan, D. O., *J. Am. Chem. Soc.* **1977,** 99, 2855-2865.
183. Guyon, F.; Hameau, A.; Khatyr, A.; Knorr, M.; Amrouche, H.; Fortin, D.; Harvey, P. D.; Strohmann, C.; Ndiaye, A. L.; Huch, V.; Veith, M.; Avarvari, N., *Inorg. Chem.* **2008,** 47, 7483-7492.
184. Bunzli, J. C. G.; Choppin, G. R., *Lanthanide Probes in Life, Chemical and Earth Sciences: Theory and Practice* Elsevier Science Ltd The Netherlands, 1989.
185. Weissman, S. I., *J. Chem. Phys.* **1942,** 10, 214-217.
186. Bunzli, J.-C. G., *J. Alloys Compds* **2006,** 408-412, 934-944.

187. Petoud, S.; Bunzli, J.-C. G.; Glanzman, T.; Piguet, C.; Xiang, Q.; Thummel, R. P., *J. Lumin.* **1999,** 82, 69-79.
188. Zhu, W. H.; Wang, Z. M.; Gao, S., *Inorg. Chem.* **2007,** 46, 1337-1342.
189. Parker, D.; Williams, J. A. G., *J. Chem. Soc., Perkin Trans. 2* **1996**, 1581-1586.
190. Klink, S. I.; Hebbink, G. A; Grave, L.; Peters, F. G. A; Van Veggel, F. C. J. M; Reinhoudt, D. N.; Hofstraat, J. W., *Eur.J. Org. Chem.* **2000,** 2000, 1923-1931.
191. Sabbatini, N.; Guardigli, M.; Lehn, J.-M., *Coord. Chem. Rev.* **1993,** 123, 201-228.
192. Klink, S. I.; Grave, L.; Reinhoudt, D. N.; van Veggel, F. C. J. M.; Werts, M. H. V.; Geurts, F. A. J.; Hofstraat, J. W., *J. Phys. Chem. A* **2000,** 104, 5457-5468.
193. Marchal, C.; Filinchuk, Y.; Imbert, D.; Bunzli, J. C. G.; Mazzanti, M., *Inorg. Chem.* **2007,** 46, 6242-6244.
194. de Sa, G. F.; Malta, O. L.; de Mello Donega, C.; Simas, A. M.; Longo, R. L.; Santa-Cruz, P. A.; da Silva, E. F., *Coord. Chem. Rev.* **2000,** 196, 165-195.
195. Wrighton, M. S.; Ginley, D. S.; Morse, D. L., *J. Phys. Chem.* **1974,** 78, 2229-2233.
196. de Mello, J. C.; Wittmann, H. F.; Friend, R. H., *Adv. Mater.* **1997,** 9, 230-232.
197. Senegas, J. M.; Bernardinelli, G.; Imbert, D.; Bunzli, J. C. G.; Morgantini, P. Y.; Weber, J.; Piguet, C., *Inorg. Chem.* **2003,** 42, 4680-4695.
198. Comby, S.; Imbert, D.; Chauvin, A. S.; Bunzli, J. C. G.; Charbonniere, L. J.; Ziessel, R. F., *Inorg. Chem.* **2004,** 43, 7369-7379.
199. Weber, M. J., *Phys. Rev.* **1968,** 171, 283.
200. Li, H. X.; Ren, Z. G.; Zhang, Y.; Zhang, W. H.; Lang, J. P.; Shen, Q., *J. Am. Chem. Soc.* **2005,** 127, 1122-1123.
201. Lee, J.; Freedman, D.; Melman, J. H.; Brewer, M.; Sun, L.; Emge, T. J.; Long, F. H.; Brennan, J. G., *Inorg. Chem.* **1998,** 37, 2512-2519.
202. Lee, J.; Brewer, M.; Berardini, M.; Brennan, J. G., *Inorg. Chem.* **1995,** 34, 3215-3219.
203. Melman, J. H.; Emge, T. J.; Brennan, J. G., *Chem. Commun.* **1997**, 2269-2270.
204. Aspinall, H. C.; Cunningham, S. A.; Maestro, P.; Macaudiere, P., *Inorg. Chem.* **1998,** 37, 5396-5398.
205. Tang, Y.; Gan, X.; Tan, M.; Zheng, X., *Polyhedron* **1998,** 17, 429-432.
206. Roger, M.; Arliguie, T.; Thuery, P.; Fourmigue, M.; Ephritikhine, M., *Inorg. Chem.* **2005,** 44, 584-593.
207. Gromada, J.; Mortreux, A.; Chenal, T.; Ziller, J. W.; Leising, F.; Carpentier, J-F., *Chem. Eur. J.* **2002,** 8, 3773-3788.
208. Barnhart, D. M.; Clark, D. L.; Gordon, J. C.; Huffman, J. C.; Vincent, R. L.; Watkin, J. G.; Zwick, B. D., *Inorg. Chem.* **1994,** 33, 3487-3497.
209. Schuetz, S. A.; Day, V. W.; Sommer, R. D.; Rheingold, A. L.; Belot, J. A., *Inorg. Chem.* **2001,** 40, 5292-5295.
210. Bradley, D. C.; Ghotra, J. S.; Hart, F. A., *Journal of the Chemical Society, Dalton Transactions* **1973**, 1021-1023.
211. Monga, V.; Patrick, B. O.; Orvig, C., *Inorg. Chem.* **2005,** 44, 2666-2677.
212. Ward, M. D., *Coord. Chem. Rev.* **2007,** 251, 1663-1677.
213. Wu, G.; Hewitt, I. J.; Mameri, S.; Lan, Y.; Clerac, R.; Anson, C. E.; Qiu, S.; Powell, A. K., *Inorg. Chem.* **2007,** 46, 7229-7231.
214. Liu, B.; Li, B. L.; Li, Y. Z.; Chen, Y.; Bao, S. S.; Zheng, L. M., *Inorg. Chem.* **2007,** 46, 8524-8532.
215. Zhao, B.; Chen, X. Y.; Cheng, P.; Liao, D. Z.; Yan, S. P.; Jiang, Z. H., *J. Am. Chem. Soc.* **2004,** 126, 15394-15395.
216. Goodgame, D. M. L.; Khaled, A. M.; O'Mahoney, C. A.; Williams, D. J., *J. Chem. Soc. Chem. Comm.* **1990**, 851-853.
217. Goodgame, D. M. L.; Hill, S. P. W.; Lincoln, R.; Quiros, M.; Williams, D. J., *Polyhedron* **1993,** 12, 2753-2762.

218. Chen, W-T.; Xu, Y-P.; Luo, Q-Y.; Fang, X-N.; Chen, H-L, *Z. Anorg. Allg. Chem.* **2008,** 634, 529-533.
219. Willey, G. R.; Woodman, T. J.; Errington, W., *J. Indian Chem. Soc.* **1998,** 75, 435-438.
220. Anfang, S.; Karl, M.; Faza, N.; Massa, W.; Dehnicke, K.; Magull, J., *Z. Anorg. Allg. Chem.* **1997,** 623, 1425-1432.
221. Goodgame, D. M. L.; Khaled, A. M.; Williams, D. J., *Polyhedron* **1991,** 10, 1079-1083.
222. Becker, P., Wickleder, C., *Crystal Research and Technology* **2001,** 36, 27-37.
223. Quici, S.; Cavazzini, M.; Marzanni, G.; Accorsi, G.; Armaroli, N.; Ventura, B.; Barigelletti, F., *Inorg. Chem.* **2005,** 44, 529-537.
224. Sun, L-N.; Yu, J-B.; Zheng, G-L.; Zhang, H-J.; Meng, Q-G.; Peng, C-Y.; Fu, L-S.; Liu, F-Y.; Yu, Y-N., *Eur. J. Inorg. Chem.* **2006**, 3962-3973.
225. Shen, Y. L.; Jiang, H. L.; Xu, J.; Mao, J. G.; Cheah, K. W., *Inorg. Chem.* **2005,** 44, 9314-9321.
226. Förster, T., *Annalen der Physik* **1948,** 437, 55-75.
227. Dexter, D. L., *J. Chem. Phys.* **1953,** 21, 836-850.
228. Chen, B.; Yang, Y.; Zapata, F.; Qian, G.; Luo, Y.; Zhang, J.; Lobkovsky, E. B., *Inorg. Chem.* **2006,** 45, 8882-8886.
229. Muller-Buschbaum, K.; Gomez-Torres, S.; Larsen, P.; Wickleder, C., *Chem. Mater.* **2007,** 19, 655-659.
230. Eliseeva, S. V.; Ryazanov, M.; Gumy, F.; Troyanov, S. I.; Lepnev, L. S.; Bünzli, J-C. G.; Kuzmina, N. P., *Eur.J. Inorg. Chem.* **2006,** 2006, 4809-4820.
231. Kirby, A. F.; Foster, D.; Richardson, F. S., *Chem. Phys. Lett.* **1983,** 95, 507-512.
232. Kirby, A. F.; Richardson, F. S., *J. Phys. Chem.* **1983,** 87, 2544-2556.
233. Cheng, J. W.; Zheng, S. T.; Ma, E.; Yang, G. Y., *Inorg. Chem.* **2007,** 46, 10534-10538.
234. Gu, X.; Xue, D., *Inorg. Chem.* **2006,** 45, 9257-9261.
235. Zhang, Z. H.; Song, Y.; Okamura, T. a.; Hasegawa, Y.; Sun, W. Y.; Ueyama, N., *Inorg. Chem.* **2006,** 45, 2896-2902.
236. Sun, Y.-Q.; Zhang, J.; Chen, Y.-M.; Yang, G.-Y., *Angew. Chem. Int. Ed.* **2005,** 44, 5814-5817.
237. Sun, Y.-Q.; Zhang, J.; Yang, G.-Y., *Chem. Commun.* **2006**, 1947-1949.
238. Sun, Y.-Q.; Zhang, J.; Yang, G.-Y., *Chem. Commun.* **2006**, 4700-4702.
239. Yersin, H.; Trumbach, D.; Strasser, J.; Patterson, H. H.; Assefa, Z., *Inorg. Chem.* **1998,** 37, 3209-3216.
240. Richardson, F. S.; Reid, M. F.; Dallara, J. J.; Smith, R. D., *J. Chem. Phys.* **1985,** 83, 3813-3830.
241. Dieke, G. H., *Spectra and Energy levels of Rare Earth Ions in Crystals* Wiley-Interscience Publishers: New York, 1968.
242. Durham, D. A.; Frost, G. H.; Hart, F. A., *J. Inorg. Nucl. Chem.* **1969,** 31, 833-838.
243. Vincent, A., *Molecular Symmetry and Group Theory : A Programmed Introduction to Chemical Applications, 2nd Edition*. John Wiley & Sons: 2000.

CHAPTER H: Appendix

H Annexes: additional crystallographical data

4,5-bis[(2´-hydroxyethyl)thio]1,3-dithiole-2-thione ($\underline{L^1H_2}$)

Table 1. Crystal data and structure refinement for $\underline{L^1H_2}$.

Identification code	sh2250	
Empirical formula	C7 H10 O2 S5	
Formula weight	286.45	
Temperature	103(2) K	
Wavelength	0.71073 Å	
Crystal system	Monoclinic	
Space group	P2(1)/n	
Unit cell dimensions	a = 5.2765(5) Å	α= 90°.
	b = 25.853(3) Å	β= 105.124(6)°.
	c = 8.6152(10) Å	γ = 90°.
Volume	1134.5(2) Å^3	
Z	4	
Density (calculated)	1.677 Mg/m^3	
Absorption coefficient	0.991 mm^{-1}	
F(000)	592	
Crystal size	0.5 x 0.4 x 0.2 mm^3	
Theta range for data collection	1.58 to 29.46°.	
Index ranges	-7<=h<=7, -34<=k<=35, -11<=l<=10	
Reflections collected	13208	
Independent reflections	3138 [R(int) = 0.0406]	
Completeness to theta = 29.46°	99.7 %	
Absorption correction	None	
Refinement method	Full-matrix least-squares on F^2	
Data / restraints / parameters	3138 / 0 / 167	
Goodness-of-fit on F^2	1.008	
Final R indices [I>2sigma(I)]	R1 = 0.0296, wR2 = 0.0568	
R indices (all data)	R1 = 0.0475, wR2 = 0.0633	
Largest diff. peak and hole	0.445 and -0.312 e.Å^{-3}	

Table 2. Atomic coordinates (x 10^4) and equivalent isotropic displacement parameters ($Å^2$x 10^3) for sh2250. U(eq) is defined as one third of the trace of the orthogonalized U^{ij} tensor.

_	x	y	z	U(eq)
S(1)	220(1)	-276(1)	2949(1)	18(1)
S(2)	3292(1)	656(1)	4468(1)	16(1)
S(3)	3554(1)	322(1)	1325(1)	14(1)
S(4)	7435(1)	1160(1)	1002(1)	16(1)
S(5)	6974(1)	1551(1)	4651(1)	17(1)
C(1)	2207(3)	213(1)	2927(2)	13(1)
C(2)	5413(3)	871(1)	2086(2)	13(1)
C(3)	5280(3)	1026(1)	3555(2)	14(1)
C(4)	5378(4)	1135(1)	-1058(2)	15(1)
C(5)	2949(4)	1470(1)	-1354(2)	15(1)
C(6)	4243(4)	2004(1)	4435(2)	18(1)
C(7)	2972(4)	2164(1)	2726(3)	18(1)
O(1)	3698(3)	1999(1)	-1029(2)	18(1)
O(2)	4782(3)	2434(1)	2032(2)	18(1)

Table 3. Bond lengths [Å] and angles [°] for sh2250.

S(1)-C(1)	1.6442(2)
S(2)-C(1)	1.7343(2)
S(2)-C(3)	1.7509(2)
S(3)-C(1)	1.7330(2)
S(3)-C(2)	1.7525(2)
S(4)-C(2)	1.7564(2)
S(4)-C(4)	1.824(2)
S(5)-C(3)	1.7571(2)
S(5)-C(6)	1.829(2)
C(2)-C(3)	1.347(3)
C(4)-C(5)	1.512(3)
C(5)-O(1)	1.431(2)
C(6)-C(7)	1.508(3)
C(7)-O(2)	1.433(2)

C(1)-S(2)-C(3)	97.72(9)
C(1)-S(3)-C(2)	98.08(9)
C(2)-S(4)-C(4)	102.28(9)
C(3)-S(5)-C(6)	99.41(9)
S(1)-C(1)-S(3)	122.02(1)
S(1)-C(1)-S(2)	125.65(1)
S(3)-C(1)-S(2)	112.29(1)
C(3)-C(2)-S(3)	115.53(1)
C(3)-C(2)-S(4)	124.16(1)
S(3)-C(2)-S(4)	120.19(1)
C(2)-C(3)-S(2)	116.36(1)
C(2)-C(3)-S(5)	126.18(1)
S(2)-C(3)-S(5)	117.43(1)
C(5)-C(4)-S(4)	114.02(1)
O(1)-C(5)-C(4)	109.60(2)
C(7)-C(6)-S(5)	114.39(1)
O(2)-C(7)-C(6)	111.45(2)

Table 4. Anisotropic displacement parameters ($Å^2 x\ 10^3$) for sh2250. The anisotropic displacement factor exponent takes the form: $-2\pi^2[\ h^2\ a^{*2} U^{11} + ... + 2\ h\ k\ a^*\ b^*\ U^{12}\ ]$

	U^{11}	U^{22}	U^{33}	U^{23}	U^{13}	U^{12}
S(1)	18(1)	17(1)	18(1)	-1(1)	4(1)	-7(1)
S(2)	19(1)	17(1)	12(1)	0(1)	4(1)	-6(1)
S(3)	14(1)	14(1)	15(1)	-1(1)	6(1)	0(1)
S(4)	11(1)	20(1)	17(1)	5(1)	4(1)	-1(1)
S(5)	15(1)	17(1)	16(1)	1(1)	-1(1)	-5(1)
C(1)	11(1)	13(1)	13(1)	1(1)	1(1)	1(1)
C(2)	9(1)	13(1)	18(1)	4(1)	2(1)	0(1)
C(3)	12(1)	13(1)	16(1)	3(1)	1(1)	-2(1)
C(4)	17(1)	14(1)	16(1)	1(1)	6(1)	2(1)
C(5)	13(1)	15(1)	14(1)	0(1)	1(1)	-2(1)
C(6)	20(1)	18(1)	17(1)	-3(1)	6(1)	-5(1)
C(7)	16(1)	18(1)	20(1)	-2(1)	3(1)	0(1)
O(1)	20(1)	13(1)	20(1)	2(1)	0(1)	2(1)
O(2)	24(1)	15(1)	15(1)	-1(1)	3(1)	-4(1)

Table 5. Hydrogen coordinates (x 10^4) and isotropic displacement parameters ($Å^2$x 10^3) for sh2250.

	x	y	z	U(eq)
H(7)	2270(40)	1870(8)	2040(20)	10(5)
H(3)	1810(40)	1352(8)	-650(30)	15(5)
H(2)	6610(40)	1249(8)	-1670(30)	16(5)
H(5)	2810(40)	1841(9)	4900(30)	21(6)
H(4)	1920(40)	1424(9)	-2500(30)	21(6)
H(8)	1520(50)	2393(10)	2760(30)	36(7)
H(1)	4910(40)	785(9)	-1380(30)	23(6)
H(9)	2530(50)	2167(11)	-1590(30)	40(8)
H(6)	5010(40)	2294(9)	5060(30)	20(6)
H(10)	4760(50)	2306(10)	1230(30)	29(8)

4,5-bis[carboxymethylthio]-1,3-dithiol-2-thione (L^{2}H$_2$)

Table 1. Crystal data and structure refinement for **L^2**H$_2$.

Identification code	sh2498	
Empirical formula	C7 H6 O4 S5	
Formula weight	314.42	
Temperature	200(2) K	
Wavelength	0.71073 Å	
Crystal system	Triclinic	
Space group	$P\bar{1}$	
Unit cell dimensions	a = 5.1049(10) Å	α= 108.07(3)°.
	b = 10.755(2) Å	β= 101.06(3)°.
	c = 11.638(2) Å	γ = 91.18(3)°.
Volume	594.0(2) $Å^3$	
Z	2	
Density (calculated)	1.758 Mg/m^3	
Absorption coefficient	0.968 mm^{-1}	
F(000)	320	

Crystal size	0.6 x 0.44 x 0.2 mm^3
Theta range for data collection	3.15 to 27.93°.
Index ranges	-6<=h<=6, -13<=k<=13, -15<=l<=15
Reflections collected	5383
Independent reflections	2612 [R(int) = 0.0476]
Completeness to theta = 27.93°	91.6 %
Absorption correction	None
Refinement method	Full-matrix least-squares on F^2
Data / restraints / parameters	2612 / 0 / 169
Goodness-of-fit on F^2	0.784
Final R indices [I>2sigma(I)]	R1 = 0.0334, wR2 = 0.0608
R indices (all data)	R1 = 0.0720, wR2 = 0.0677
Largest diff. peak and hole	0.361 and -0.322 e.$Å^{-3}$

Table 2. Atomic coordinates (x 10^4) and equivalent isotropic displacement parameters ($Å^2$x 10^3) for sh2498. U(eq) is defined as one third of the trace of the orthogonalized U^{ij} tensor.

	x	y	z	U(eq)
S(1)	11621(1)	219(1)	8944(1)	23(1)
S(2)	7767(1)	2330(1)	9632(1)	26(1)
S(3)	5750(2)	1694(1)	6545(1)	35(1)
S(4)	9468(2)	-470(1)	6317(1)	32(1)
S(5)	13729(2)	-2018(1)	7200(1)	39(1)
O(1)	4165(4)	3730(2)	5481(2)	31(1)
O(2)	8180(4)	4876(2)	5917(2)	37(1)
O(3)	12185(3)	4079(2)	9401(2)	26(1)
O(4)	14367(4)	4653(2)	11388(2)	30(1)
C(1)	11735(5)	-818(3)	7466(2)	25(1)
C(2)	9126(5)	1179(3)	8510(2)	22(1)
C(3)	8159(5)	865(3)	7262(2)	27(1)
C(4)	8051(6)	2991(3)	6516(3)	28(1)
C(5)	6596(6)	3908(3)	5919(2)	24(1)
C(6)	10687(6)	3098(3)	10807(3)	24(1)
C(7)	12461(5)	3998(3)	10447(2)	20(1)

Table 3. Bond lengths [Å] and angles [°] for sh2498.

S(1)-C(1)	1.749(3)
S(1)-C(2)	1.753(3)
S(2)-C(2)	1.761(3)
S(2)-C(6)	1.800(3)
S(3)-C(3)	1.766(3)
S(3)-C(4)	1.818(3)
S(4)-C(1)	1.732(3)
S(4)-C(3)	1.749(3)
S(5)-C(1)	1.651(3)
O(1)-C(5)	1.234(3)
O(2)-C(5)	1.305(3)
O(3)-C(7)	1.228(3)
O(4)-C(7)	1.314(3)
C(2)-C(3)	1.371(4)
C(4)-C(5)	1.505(4)
C(6)-C(7)	1.514(4)
C(1)-S(1)-C(2)	97.94(1)
C(2)-S(2)-C(6)	102.69(1)
C(3)-S(3)-C(4)	97.03(1)
C(1)-S(4)-C(3)	97.94(1)
S(5)-C(1)-S(4)	123.84(2)
S(5)-C(1)-S(1)	123.64(2)
S(4)-C(1)-S(1)	112.51(2)
C(3)-C(2)-S(1)	115.3(2)
C(3)-C(2)-S(2)	123.7(2)
S(1)-C(2)-S(2)	120.70(1)
C(2)-C(3)-S(4)	116.3(2)
C(2)-C(3)-S(3)	125.6(2)
S(4)-C(3)-S(3)	118.06(2)
C(5)-C(4)-S(3)	111.1(2)
O(1)-C(5)-O(2)	125.2(2)
O(1)-C(5)-C(4)	122.1(3)
O(2)-C(5)-C(4)	112.7(2)
C(7)-C(6)-S(2)	114.0(2)
O(3)-C(7)-O(4)	124.6(3)
O(3)-C(7)-C(6)	124.2(2)

O(4)-C(7)-C(6)	111.3(2)

Table 4. Anisotropic displacement parameters ($Å^2 x\ 10^3$) for sh2498. The anisotropic displacement factor exponent takes the form: $-2\pi^2[\ h^2\ a^{*2} U^{11} + ... + 2\ h\ k\ a^*\ b^*\ U^{12}\ ]$

	U^{11}	U^{22}	U^{33}	U^{23}	U^{13}	U^{12}
S(1)	23(1)	24(1)	23(1)	10(1)	2(1)	7(1)
S(2)	18(1)	21(1)	37(1)	7(1)	4(1)	2(1)
S(3)	28(1)	33(1)	46(1)	25(1)	-10(1)	0(1)
S(4)	42(1)	32(1)	22(1)	12(1)	1(1)	5(1)
S(5)	43(1)	41(1)	36(1)	10(1)	13(1)	20(1)
O(1)	31(1)	30(2)	34(1)	16(1)	2(1)	9(1)
O(2)	35(1)	36(2)	47(1)	29(1)	0(1)	3(1)
O(3)	21(1)	32(1)	24(1)	10(1)	3(1)	-2(1)
O(4)	29(1)	32(2)	26(1)	10(1)	-1(1)	-9(1)
C(1)	24(1)	26(2)	30(2)	14(1)	9(1)	3(1)
C(2)	20(1)	19(2)	29(1)	13(1)	2(1)	0(1)
C(3)	26(1)	26(2)	29(2)	15(1)	-2(1)	-1(1)
C(4)	30(2)	28(2)	28(2)	13(2)	2(1)	6(1)
C(5)	29(2)	25(2)	20(1)	9(1)	5(1)	7(1)
C(6)	25(2)	17(2)	28(2)	6(1)	1(1)	-1(1)
C(7)	17(1)	15(2)	25(1)	2(1)	5(1)	5(1)

Table 5. Hydrogen coordinates ($x\ 10^4$) and isotropic displacement parameters ($Å^2 x\ 10^3$) for sh2498.

	x	y	z	U(eq)
H(1)	7250(80)	5330(50)	5510(40)	86(15)
H(2)	15290(60)	5070(30)	11140(30)	30(10)
H(4A)	8870(60)	3450(30)	7300(30)	34(9)
H(4B)	9340(60)	2670(30)	6070(30)	35(9)
H(6A)	11720(60)	2460(40)	11050(30)	40(9)
H(6B)	10120(60)	3600(30)	11470(30)	39(9)

4,5-bis[carboxymethylthio]-1,3-dithiol-2-thione.THF (L^2H_2.THF)

Table 1. Crystal data and structure refinement for **L^2H_2.THF.**

Identification code	sh2594	
Empirical formula	C11 H14 O5 S5	
Formula weight	386.52	
Temperature	180(2) K	
Wavelength	0.71073 Å	
Crystal system	Orthorhombic	
Space group	Pnna	
Unit cell dimensions	a = 7.9656(4) Å	α= 90°.
	b = 21.0885(11) Å	β= 90°.
	c = 9.5192(5) Å	γ = 90°.
Volume	1599.06(14) $Å^3$	
Z	4	
Density (calculated)	1.606 Mg/m^3	
Absorption coefficient	0.740 mm^{-1}	
F(000)	800	
Crystal size	0.66 x 0.40 x 0.30 mm^3	
Theta range for data collection	1.93 to 27.32°.	
Index ranges	-10<=h<=10, -27<=k<=27, -12<=l<=12	
Reflections collected	28804	
Independent reflections	1800 [R(int) = 0.0520]	
Completeness to theta = 27.32°	99.9 %	
Absorption correction	Multiscan	
Max. and min. transmission	0.8085 and 0.6409	
Refinement method	Full-matrix least-squares on F^2	
Data / restraints / parameters	1800 / 0 / 125	
Goodness-of-fit on F^2	1.080	
Final R indices [I>2sigma(I)]	R1 = 0.0302, wR2 = 0.0585	
R indices (all data)	R1 = 0.0420, wR2 = 0.0619	
Largest diff. peak and hole	0.257 and -0.258 $e.Å^{-3}$	

Table 2. Atomic coordinates (x 10^4) and equivalent isotropic displacement parameters ($Å^2$x 10^3) for sh2594. U(eq) is defined as one third of the trace of the orthogonalized U^{ij} tensor.

	x	y	z	U(eq)
S(1)	1555(1)	4266(1)	6792(1)	25(1)
S(2)	1726(1)	4384(1)	9928(1)	26(1)
S(3)	2500	5000	12674(1)	37(1)
O(1)	4240(2)	3405(1)	8111(1)	37(1)
O(2)	7736(2)	2500	7500	33(1)
O(3)	5803(2)	3337(1)	6167(2)	41(1)
C(1)	2500	5000	10937(3)	25(1)
C(2)	2150(2)	4709(1)	8281(2)	21(1)
C(3)	4532(2)	3562(1)	6927(2)	27(1)
C(4)	10541(3)	2418(1)	6730(2)	42(1)
C(5)	3581(2)	4050(1)	6087(2)	27(1)
C(6)	8814(3)	2162(1)	6502(2)	43(1)

Table 3. Bond lengths [Å] and angles [°] for sh2594.

S(1)-C(2)	1.762(2)
S(1)-C(5)	1.806(2)
S(2)-C(1)	1.730(1)
S(2)-C(2)	1.744(2)
S(3)-C(1)	1.653(3)
O(1)-C(3)	1.198(2)
O(2)-C(6)#1	1.466(2)
O(2)-C(6)	1.466(2)
O(3)-C(3)	1.331(2)
C(1)-S(2)#2	1.730(1)
C(2)-C(2)#2	1.350(3)
C(3)-C(5)	1.507(3)
C(4)-C(6)	1.493(3)
C(4)-C(4)#1	1.507(4)
C(2)-S(1)-C(5)	101.09(8)
C(1)-S(2)-C(2)	97.74(9)
C(6)#1-O(2)-C(6)	108.3(2)

S(3)-C(1)-S(2)#2	123.73(7)
S(3)-C(1)-S(2)	123.73(7)
S(2)#2-C(1)-S(2)	112.55(1)
C(2)#2-C(2)-S(2)	115.98(6)
C(2)#2-C(2)-S(1)	126.40(6)
S(2)-C(2)-S(1)	117.57(1)
O(1)-C(3)-O(3)	124.11(2)
O(1)-C(3)-C(5)	126.16(2)
O(3)-C(3)-C(5)	109.70(2)
C(6)-C(4)-C(4)#1	102.98(1)
C(3)-C(5)-S(1)	115.12(1)
O(2)-C(6)-C(4)	105.65(2)

Symmetry transformations used to generate equivalent atoms:
#1 x,-y+1/2,-z+3/2 #2 -x+1/2,-y+1,z

Table 4. Anisotropic displacement parameters ($Å^2 x\ 10^3$) for sh2594. The anisotropic displacement factor exponent takes the form: $-2\pi^2[\ h^2\ a^{*2} U^{11} + ... + 2\ h\ k\ a^*\ b^*\ U^{12}\ ]$

	U^{11}	U^{22}	U^{33}	U^{23}	U^{13}	U^{12}
S(1)	22(1)	29(1)	25(1)	-5(1)	-3(1)	-1(1)
S(2)	26(1)	29(1)	23(1)	3(1)	2(1)	-1(1)
S(3)	31(1)	60(1)	19(1)	0	0	1(1)
O(1)	36(1)	48(1)	27(1)	5(1)	4(1)	8(1)
O(2)	27(1)	34(1)	39(1)	-8(1)	0	0
O(3)	42(1)	45(1)	36(1)	0(1)	10(1)	17(1)
C(1)	18(1)	36(1)	22(1)	0	0	6(1)
C(2)	18(1)	27(1)	18(1)	0(1)	1(1)	2(1)
C(3)	25(1)	27(1)	28(1)	-8(1)	0(1)	-1(1)
C(4)	37(1)	47(1)	43(1)	12(1)	9(1)	12(1)
C(5)	27(1)	32(1)	21(1)	-5(1)	2(1)	0(1)
C(6)	44(1)	48(1)	38(1)	-16(1)	-5(1)	15(1)

Table 5. Hydrogen coordinates (x 10^4) and isotropic displacement parameters ($Å^2$x 10^3) for sh2594.

	x	y	z	U(eq)
H(1)	6340(30)	3063(13)	6620(30)	68(9)
H(2)	4250(20)	4409(9)	5990(20)	28(5)
H(3)	3370(30)	3903(9)	5240(20)	36(6)
H(4)	8690(30)	3296(11)	8230(20)	43(6)
H(5)	11410(30)	2908(12)	8530(20)	58(7)
H(6)	10720(30)	2192(11)	8800(20)	48(6)
H(7)	8390(30)	2759(11)	9430(30)	59(7)

L_0-CuI complex

Table 1. Crystal data and structure refinement for **L_0-CuI**.

Identification code	sh2465	
Empirical formula	C74 H40 Cu2 I2 O8 S20	
Formula weight	2079.14	
Temperature	170(2) K	
Wavelength	0.71073 Å	
Crystal system	Triclinic	
Space group	$P\bar{1}$	
Unit cell dimensions	a = 12.1861(6) Å	α= 62.198(2)°.
	b = 13.5080(6) Å	β= 84.796(2)°.
	c = 13.5835(6) Å	γ = 87.493(2)°.
Volume	1969.71(16) $Å^3$	
Z	1	
Density (calculated)	1.753 Mg/m^3	
Absorption coefficient	1.909 mm^{-1}	
F(000)	1032	
Crystal size	0.6 x 0.3 x 0.15 mm^3	
Theta range for data collection	1.68 to 36.34°.	
Index ranges	-20<=h<=18, -20<=k<=22, -22<=l<=22	
Reflections collected	55470	
Independent reflections	18876 [R(int) = 0.0280]	

Completeness to theta = 36.34°	98.7 %
Absorption correction	None
Refinement method	Full-matrix least-squares on F^2
Data / restraints / parameters	18876 / 0 / 463
Goodness-of-fit on F^2	0.967
Final R indices [I>2sigma(I)]	R1 = 0.0347, wR2 = 0.0844
R indices (all data)	R1 = 0.0618, wR2 = 0.0969
Largest diff. peak and hole	1.438 and -0.681 e.$Å^{-3}$

Table 2. Atomic coordinates (x 10^4) and equivalent isotropic displacement parameters ($Å^2$x 10^3) for sh2465. U(eq) is defined as one third of the trace of the orthogonalized U^{ij} tensor.

	x	y	z	U(eq)
C(1)	2381(1)	2149(1)	2985(1)	21(1)
C(2)	1278(1)	3998(1)	1978(1)	22(1)
C(3)	2324(2)	4304(1)	1982(2)	23(1)
C(4)	2365(2)	6138(2)	2351(2)	28(1)
C(5)	2837(2)	7224(2)	2114(2)	28(1)
C(6)	3774(2)	7666(2)	1400(2)	39(1)
C(7)	4182(2)	8684(2)	1228(2)	48(1)
C(8)	3660(3)	9245(2)	1759(2)	52(1)
C(9)	2734(3)	8815(2)	2457(3)	56(1)
C(10)	2311(2)	7797(2)	2639(2)	44(1)
C(11)	-906(2)	4253(2)	1477(2)	27(1)
C(12)	-1910(2)	4949(2)	1076(2)	26(1)
C(13)	-2914(2)	4397(2)	1349(2)	36(1)
C(14)	-3875(2)	5000(2)	973(2)	43(1)
C(15)	-3831(2)	6148(2)	340(2)	42(1)
C(16)	-2834(2)	6710(2)	67(2)	38(1)
C(17)	-1868(2)	6108(2)	436(2)	31(1)
C(18)	6815(2)	1243(1)	2199(2)	25(1)
C(19)	8872(2)	953(1)	1761(2)	24(1)
C(20)	8702(2)	452(2)	2889(2)	26(1)
C(21)	10045(2)	1662(2)	-312(2)	29(1)
C(22)	11054(2)	1683(2)	-1007(2)	29(1)
C(23)	11894(2)	900(2)	-616(2)	34(1)

C(24)	12825(2)	988(2)	-1319(2)	42(1)
C(25)	12927(2)	1864(2)	-2393(2)	50(1)
C(26)	12089(2)	2648(2)	-2779(2)	51(1)
C(27)	11149(2)	2559(2)	-2099(2)	39(1)
C(28)	9319(2)	-1619(2)	4446(2)	27(1)
C(29)	10198(2)	-2440(2)	4984(2)	25(1)
C(30)	9972(2)	-3562(2)	5323(2)	34(1)
C(31)	10770(2)	-4367(2)	5802(2)	41(1)
C(32)	11781(2)	-4065(2)	5960(2)	43(1)
C(33)	12003(2)	-2946(2)	5642(2)	40(1)
C(34)	11216(2)	-2136(2)	5145(2)	32(1)
Cu(2)	4593(1)	687(1)	3840(1)	29(1)
I(1)	5058(1)	1499(1)	5175(1)	29(1)
O(1)	1706(2)	5598(1)	3114(1)	44(1)
O(2)	-889(1)	3250(1)	1849(2)	41(1)
O(3)	9210(1)	2170(2)	-674(1)	49(1)
O(4)	8383(1)	-1853(1)	4436(2)	44(1)
S(1)	2733(1)	807(1)	3613(1)	26(1)
S(2)	1054(1)	2553(1)	2602(1)	22(1)
S(3)	3261(1)	3237(1)	2654(1)	25(1)
S(4)	283(1)	5034(1)	1388(1)	27(1)
S(5)	2839(1)	5670(1)	1322(1)	25(1)
S(6)	5488(1)	1583(1)	2061(1)	30(1)
S(7)	7729(1)	1623(1)	1036(1)	27(1)
S(8)	7376(1)	507(1)	3447(1)	30(1)
S(9)	10180(1)	864(1)	1152(1)	35(1)
S(10)	9776(1)	-165(1)	3755(1)	30(1)
C(35)	4123(6)	4733(6)	4755(6)	136(2)
C(36)	4307(7)	4476(7)	5785(8)	167(3)
C(37)	4983(8)	5124(8)	3810(8)	225(3)

Table 3. Bond lengths [Å] and angles [°] for sh2465.

C(1)-S(1)	1.6602(2)
C(1)-S(3)	1.7154(2)
C(1)-S(2)	1.7305(2)
C(2)-C(3)	1.359(2)
C(2)-S(4)	1.7474(2)

C(2)-S(2)	1.7504(2)
C(3)-S(3)	1.7407(2)
C(3)-S(5)	1.7493(2)
C(4)-O(1)	1.202(2)
C(4)-C(5)	1.479(3)
C(4)-S(5)	1.825(2)
C(5)-C(10)	1.382(3)
C(5)-C(6)	1.385(3)
C(6)-C(7)	1.390(3)
C(7)-C(8)	1.372(4)
C(8)-C(9)	1.364(4)
C(9)-C(10)	1.392(3)
C(11)-O(2)	1.205(2)
C(11)-C(12)	1.490(2)
C(11)-S(4)	1.793(2)
C(12)-C(13)	1.389(3)
C(12)-C(17)	1.392(3)
C(13)-C(14)	1.391(3)
C(14)-C(15)	1.379(4)
C(15)-C(16)	1.388(4)
C(16)-C(17)	1.394(3)
C(18)-S(6)	1.664(2)
C(18)-S(8)	1.705(2)
C(18)-S(7)	1.725(2)
C(19)-C(20)	1.355(2)
C(19)-S(7)	1.743(2)
C(19)-S(9)	1.753(2)
C(20)-S(8)	1.734(2)
C(20)-S(10)	1.750(2)
C(21)-O(3)	1.209(2)
C(21)-C(22)	1.474(3)
C(21)-S(9)	1.785(2)
C(22)-C(23)	1.389(3)
C(22)-C(27)	1.399(3)
C(23)-C(24)	1.386(3)
C(24)-C(25)	1.383(4)
C(25)-C(26)	1.387(4)
C(26)-C(27)	1.378(4)
C(28)-O(4)	1.199(2)

C(28)-C(29)	1.481(3)
C(28)-S(10)	1.825(2)
C(29)-C(34)	1.389(3)
C(29)-C(30)	1.396(3)
C(30)-C(31)	1.383(3)
C(31)-C(32)	1.380(4)
C(32)-C(33)	1.397(4)
C(33)-C(34)	1.381(3)
Cu(2)-S(1)	2.304(5)
Cu(2)-S(6)	2.325(6)
Cu(2)-I(1)	2.627(3)
Cu(2)-I(1)#1	2.645(3)
Cu(2)-Cu(2)#1	3.051(5)
I(1)-Cu(2)#1	2.645(3)
C(35)-C(36)	1.314(9)
C(35)-C(37)	1.483(1)
C(36)-C(37)#2	1.322(1)
C(37)-C(36)#2	1.322(1)

S(1)-C(1)-S(3)	124.56(1)
S(1)-C(1)-S(2)	120.90(1)
S(3)-C(1)-S(2)	114.54(9)
C(3)-C(2)-S(4)	119.22(1)
C(3)-C(2)-S(2)	115.09(1)
S(4)-C(2)-S(2)	125.68(1)
C(2)-C(3)-S(3)	117.23(1)
C(2)-C(3)-S(5)	126.12(1)
S(3)-C(3)-S(5)	116.58(1)
O(1)-C(4)-C(5)	125.73(2)
O(1)-C(4)-S(5)	120.77(2)
C(5)-C(4)-S(5)	113.46(1)
C(10)-C(5)-C(6)	120.17(2)
C(10)-C(5)-C(4)	117.51(2)
C(6)-C(5)-C(4)	122.32(2)
C(5)-C(6)-C(7)	119.3(2)
C(8)-C(7)-C(6)	120.3(2)
C(9)-C(8)-C(7)	120.5(2)
C(8)-C(9)-C(10)	120.1(3)
C(5)-C(10)-C(9)	119.6(2)

O(2)-C(11)-C(12)	123.62(2)
O(2)-C(11)-S(4)	122.26(1)
C(12)-C(11)-S(4)	114.11(1)
C(13)-C(12)-C(17)	120.00(2)
C(13)-C(12)-C(11)	117.43(2)
C(17)-C(12)-C(11)	122.56(2)
C(12)-C(13)-C(14)	120.0(2)
C(15)-C(14)-C(13)	119.9(2)
C(14)-C(15)-C(16)	120.64(2)
C(15)-C(16)-C(17)	119.7(2)
C(12)-C(17)-C(16)	119.8(2)
S(6)-C(18)-S(8)	124.52(1)
S(6)-C(18)-S(7)	120.41(1)
S(8)-C(18)-S(7)	115.06(1)
C(20)-C(19)-S(7)	115.44(1)
C(20)-C(19)-S(9)	118.99(1)
S(7)-C(19)-S(9)	125.56(1)
C(19)-C(20)-S(8)	117.08(1)
C(19)-C(20)-S(10)	121.98(2)
S(8)-C(20)-S(10)	120.87(1)
O(3)-C(21)-C(22)	124.41(2)
O(3)-C(21)-S(9)	121.88(2)
C(22)-C(21)-S(9)	113.63(1)
C(23)-C(22)-C(27)	120.3(2)
C(23)-C(22)-C(21)	123.05(2)
C(27)-C(22)-C(21)	116.67(2)
C(24)-C(23)-C(22)	119.5(2)
C(25)-C(24)-C(23)	120.3(2)
C(24)-C(25)-C(26)	120.1(2)
C(27)-C(26)-C(25)	120.3(2)
C(26)-C(27)-C(22)	119.5(2)
O(4)-C(28)-C(29)	125.03(2)
O(4)-C(28)-S(10)	120.94(2)
C(29)-C(28)-S(10)	114.03(1)
C(34)-C(29)-C(30)	120.02(2)
C(34)-C(29)-C(28)	123.09(2)
C(30)-C(29)-C(28)	116.88(2)
C(31)-C(30)-C(29)	119.7(2)
C(32)-C(31)-C(30)	120.2(2)

C(31)-C(32)-C(33)	120.2(2)
C(34)-C(33)-C(32)	119.9(2)
C(33)-C(34)-C(29)	120.0(2)
S(1)-Cu(2)-S(6)	106.626(2)
S(1)-Cu(2)-I(1)	111.146(2)
S(6)-Cu(2)-I(1)	114.295(2)
S(1)-Cu(2)-I(1)#1	102.49(1)
S(6)-Cu(2)-I(1)#1	112.34(2)
I(1)-Cu(2)-I(1)#1	109.29(1)
S(1)-Cu(2)-Cu(2)#1	119.88(2)
S(6)-Cu(2)-Cu(2)#1	133.14(2)
I(1)-Cu(2)-Cu(2)#1	54.92(9)
I(1)#1-Cu(2)-Cu(2)#1	54.37(8)
Cu(2)-I(1)-Cu(2)#1	70.708(1)
C(1)-S(1)-Cu(2)	108.40(6)
C(1)-S(2)-C(2)	96.70(8)
C(1)-S(3)-C(3)	96.33(8)
C(2)-S(4)-C(11)	103.22(8)
C(3)-S(5)-C(4)	100.55(9)
C(18)-S(6)-Cu(2)	106.60(6)
C(18)-S(7)-C(19)	96.18(9)
C(18)-S(8)-C(20)	96.15(9)
C(19)-S(9)-C(21)	103.84(9)
C(20)-S(10)-C(28)	99.58(9)
C(36)-C(35)-C(37)	124.3(8)
C(35)-C(36)-C(37)#2	131.6(9)
C(36)#2-C(37)-C(35)	98.6(8)

Symmetry transformations used to generate equivalent atoms:
#1 -x+1,-y,-z+1 #2 -x+1,-y+1,-z+1

Table 4. Anisotropic displacement parameters ($Å^2 x\ 10^3$) for sh2465. The anisotropic displacement factor exponent takes the form: $-2\pi^2[\ h^2\ a^{*2} U^{11} + ... + 2\ h\ k\ a^*\ b^*\ U^{12}\ ]$

	U^{11}	U^{22}	U^{33}	U^{23}	U^{13}	U^{12}
C(1)	19(1)	20(1)	25(1)	-11(1)	-1(1)	0(1)
C(2)	22(1)	18(1)	26(1)	-11(1)	-4(1)	1(1)

C(3)	23(1)	18(1)	28(1)	-11(1)	-3(1)	0(1)
C(4)	30(1)	24(1)	31(1)	-14(1)	1(1)	-5(1)
C(5)	31(1)	24(1)	29(1)	-13(1)	-3(1)	-5(1)
C(6)	33(1)	33(1)	53(1)	-22(1)	4(1)	-9(1)
C(7)	41(1)	36(1)	64(2)	-21(1)	3(1)	-18(1)
C(8)	73(2)	30(1)	56(2)	-21(1)	-12(1)	-15(1)
C(9)	86(2)	39(1)	56(2)	-34(1)	5(2)	-13(1)
C(10)	58(2)	39(1)	45(1)	-30(1)	8(1)	-13(1)
C(11)	22(1)	26(1)	33(1)	-14(1)	-6(1)	3(1)
C(12)	21(1)	30(1)	30(1)	-17(1)	-6(1)	5(1)
C(13)	26(1)	39(1)	43(1)	-19(1)	-5(1)	2(1)
C(14)	22(1)	57(1)	51(1)	-26(1)	-5(1)	4(1)
C(15)	32(1)	55(1)	45(1)	-29(1)	-12(1)	20(1)
C(16)	40(1)	36(1)	39(1)	-18(1)	-12(1)	16(1)
C(17)	31(1)	30(1)	35(1)	-17(1)	-9(1)	7(1)
C(18)	24(1)	23(1)	25(1)	-8(1)	-2(1)	0(1)
C(19)	21(1)	22(1)	25(1)	-8(1)	-2(1)	1(1)
C(20)	21(1)	25(1)	26(1)	-7(1)	-3(1)	0(1)
C(21)	29(1)	26(1)	29(1)	-10(1)	0(1)	-2(1)
C(22)	29(1)	28(1)	31(1)	-15(1)	3(1)	-3(1)
C(23)	29(1)	32(1)	40(1)	-17(1)	3(1)	-2(1)
C(24)	32(1)	45(1)	54(1)	-27(1)	5(1)	0(1)
C(25)	43(1)	57(2)	52(1)	-30(1)	18(1)	-8(1)
C(26)	55(2)	52(1)	36(1)	-15(1)	14(1)	-4(1)
C(27)	43(1)	39(1)	31(1)	-14(1)	5(1)	2(1)
C(28)	25(1)	26(1)	29(1)	-12(1)	1(1)	-3(1)
C(29)	24(1)	25(1)	24(1)	-10(1)	3(1)	-1(1)
C(30)	36(1)	27(1)	34(1)	-11(1)	0(1)	-2(1)
C(31)	49(1)	28(1)	39(1)	-10(1)	-4(1)	6(1)
C(32)	43(1)	40(1)	36(1)	-11(1)	-4(1)	13(1)
C(33)	29(1)	43(1)	40(1)	-11(1)	-5(1)	4(1)
C(34)	27(1)	30(1)	33(1)	-10(1)	-2(1)	-2(1)
Cu(2)	22(1)	27(1)	34(1)	-12(1)	-1(1)	2(1)
I(1)	30(1)	23(1)	36(1)	-14(1)	-5(1)	2(1)
O(1)	52(1)	40(1)	43(1)	-24(1)	19(1)	-22(1)
O(2)	28(1)	26(1)	67(1)	-19(1)	-15(1)	2(1)
O(3)	36(1)	60(1)	31(1)	-6(1)	0(1)	17(1)
O(4)	27(1)	33(1)	66(1)	-18(1)	-7(1)	-3(1)
S(1)	21(1)	18(1)	36(1)	-11(1)	-4(1)	1(1)

S(2)	19(1)	18(1)	30(1)	-11(1)	-3(1)	0(1)
S(3)	19(1)	20(1)	34(1)	-11(1)	-5(1)	0(1)
S(4)	23(1)	20(1)	37(1)	-13(1)	-8(1)	3(1)
S(5)	26(1)	19(1)	29(1)	-11(1)	2(1)	-3(1)
S(6)	22(1)	32(1)	29(1)	-8(1)	-4(1)	5(1)
S(7)	24(1)	27(1)	23(1)	-6(1)	-2(1)	3(1)
S(8)	24(1)	37(1)	23(1)	-9(1)	-1(1)	1(1)
S(9)	24(1)	46(1)	27(1)	-11(1)	-1(1)	6(1)
S(10)	25(1)	27(1)	29(1)	-5(1)	-8(1)	-4(1)

Table 5. Hydrogen coordinates (x 10^4) and isotropic displacement parameters (Å^{2}x 10^3) for sh2465.

	x	y	z	U(eq)
H(6)	4134	7277	1032	47
H(7)	4824	8993	741	57
H(8)	3947	9939	1640	62
H(9)	2376	9210	2819	67
H(10)	1663	7499	3123	52
H(13)	-2944	3607	1792	43
H(14)	-4561	4623	1153	52
H(15)	-4490	6559	87	50
H(16)	-2810	7501	-370	46
H(17)	-1182	6487	252	37
H(23)	11832	308	127	41
H(24)	13394	445	-1062	51
H(25)	13573	1928	-2867	60
H(26)	12164	3249	-3517	61
H(27)	10570	3089	-2369	47
H(30)	9272	-3773	5226	41
H(31)	10622	-5129	6022	49
H(32)	12328	-4620	6285	51
H(33)	12693	-2742	5767	48
H(34)	11370	-1373	4914	38

L^1H_2-HgI_2 complex

Table 1. Crystal data and structure refinement for sh2303.

Identification code	sh2303	
Empirical formula	C7 H10 Hg I2 O2 S5	
Formula weight	740.84	
Temperature	200(2) K	
Wavelength	0.71073 Å	
Crystal system	Triclinic	
Space group	$P\bar{1}$	
Unit cell dimensions	a = 4.4760(10) Å	α= 116.30(3)°.
	b = 13.973(3) Å	β= 92.86(3)°.
	c = 14.900(3) Å	γ = 93.97(3)°.
Volume	830.0(3) $Å^3$	
Z	2	
Density (calculated)	2.964 Mg/m^3	
Absorption coefficient	13.607 mm^{-1}	
F(000)	668	
Crystal size	0.4 x 0.2 x 0.18 mm^3	
Theta range for data collection	2.75 to 24.00°.	
Index ranges	-4<=h<=5, -15<=k<=15, -16<=l<=16	
Reflections collected	5130	
Independent reflections	2394 [R(int) = 0.0464]	
Completeness to theta = 24.00°	92.0 %	
Absorption correction	Numerical	
Refinement method	Full-matrix least-squares on F^2	
Data / restraints / parameters	2394 / 0 / 156	
Goodness-of-fit on F^2	1.027	
Final R indices [I>2sigma(I)]	R1 = 0.0248, wR2 = 0.0627	
R indices (all data)	R1 = 0.0273, wR2 = 0.0637	
Largest diff. peak and hole	1.374 and -1.154 $e.Å^{-3}$	

Table 2. Atomic coordinates (x 10^4) and equivalent isotropic displacement parameters ($Å^2$x 10^3) for sh2303. U(eq) is defined as one third of the trace of the orthogonalized U^{ij} tensor.

	x	y	z	U(eq)
Hg	878(1)	3507(1)	1825(1)	54(1)
I(1)	-1502(1)	4178(1)	3556(1)	43(1)
I(2)	4696(1)	3673(1)	582(1)	39(1)
S(1)	-1210(5)	1312(1)	877(1)	53(1)
S(2)	2237(4)	1511(1)	2739(1)	37(1)
S(3)	-1809(4)	-391(1)	1557(1)	42(1)
S(4)	-637(4)	-1415(1)	2932(1)	38(1)
S(5)	3991(4)	750(1)	4314(1)	45(1)
O(1)	825(10)	-3762(3)	2609(3)	42(1)
O(2)	3839(10)	3078(3)	6232(3)	44(1)
C(1)	-287(13)	834(4)	1690(4)	33(1)
C(2)	1965(13)	548(3)	3191(4)	29(1)
C(3)	126(14)	-347(4)	2630(4)	34(1)
C(4)	1148(14)	-2470(4)	1916(4)	37(1)
C(5)	-6(14)	-3569(4)	1774(4)	36(1)
C(6)	6247(14)	2030(4)	4720(4)	38(1)
C(7)	4691(14)	3018(4)	5311(4)	36(1)

Table 3. Bond lengths [Å] and angles [°] for sh2303.

Hg-I(1)	2.633(9)
Hg-I(2)	2.655(8)
Hg-S(1)	2.812(2)
S(1)-C(1)	1.669(5)
S(2)-C(1)	1.727(6)
S(2)-C(2)	1.751(5)
S(3)-C(1)	1.720(5)
S(3)-C(3)	1.754(6)
S(4)-C(3)	1.757(5)
S(4)-C(4)	1.846(5)
S(5)-C(2)	1.759(6)

S(5)-C(6)	1.821(6)
O(1)-C(5)	1.423(6)
O(2)-C(7)	1.410(6)
C(2)-C(3)	1.343(8)
C(4)-C(5)	1.503(7)
C(6)-C(7)	1.511(8)

I(1)-Hg-I(2)	154.07(2)
I(1)-Hg-S(1)	102.10(5)
I(2)-Hg-S(1)	102.81(5)
C(1)-S(1)-Hg	106.18(2)
C(1)-S(2)-C(2)	97.2(2)
C(1)-S(3)-C(3)	97.1(3)
C(3)-S(4)-C(4)	99.7(2)
C(2)-S(5)-C(6)	104.2(3)
S(1)-C(1)-S(3)	122.5(3)
S(1)-C(1)-S(2)	123.9(3)
S(3)-C(1)-S(2)	113.5(3)
C(3)-C(2)-S(2)	116.0(4)
C(3)-C(2)-S(5)	122.4(4)
S(2)-C(2)-S(5)	121.6(3)
C(2)-C(3)-S(4)	125.1(4)
C(2)-C(3)-S(3)	116.1(4)
S(4)-C(3)-S(3)	118.6(3)
C(5)-C(4)-S(4)	111.2(4)
O(1)-C(5)-C(4)	113.3(5)
C(7)-C(6)-S(5)	115.8(4)
O(2)-C(7)-C(6)	112.8(4)

Symmetry transformations used to generate equivalent atoms:

Table 4. Anisotropic displacement parameters ($Å^2 x\ 10^3$) for sh2303. The anisotropic displacement factor exponent takes the form: $-2\pi^2[\ h^2\ a^{*2} U^{11} + ...\ + 2\ h\ k\ a^*\ b^*\ U^{12}\ ]$

	U^{11}	U^{22}	U^{33}	U^{23}	U^{13}	U^{12}
Hg	65(1)	69(1)	46(1)	37(1)	25(1)	19(1)
I(1)	59(1)	39(1)	34(1)	17(1)	16(1)	9(1)

I(2)	35(1)	54(1)	36(1)	26(1)	6(1)	3(1)
S(1)	97(2)	34(1)	32(1)	20(1)	1(1)	5(1)
S(2)	50(1)	26(1)	37(1)	18(1)	5(1)	0(1)
S(3)	62(1)	31(1)	34(1)	17(1)	0(1)	-5(1)
S(4)	57(1)	26(1)	34(1)	17(1)	12(1)	0(1)
S(5)	64(1)	33(1)	42(1)	21(1)	-6(1)	3(1)
O(1)	47(3)	53(2)	40(2)	30(2)	12(2)	15(2)
O(2)	45(3)	55(2)	38(2)	26(2)	13(2)	7(2)
C(1)	42(4)	28(2)	30(3)	11(2)	8(3)	8(2)
C(2)	38(3)	22(2)	30(2)	12(2)	9(2)	9(2)
C(3)	46(4)	27(2)	32(3)	15(2)	9(3)	5(2)
C(4)	46(4)	35(3)	37(3)	21(2)	13(3)	5(2)
C(5)	49(4)	30(3)	30(3)	13(2)	6(3)	9(2)
C(6)	33(3)	44(3)	34(3)	16(2)	3(3)	2(2)
C(7)	47(4)	32(3)	31(3)	16(2)	8(3)	-5(2)

L^1H_2-AuCl complex

Table 1. Crystal data and structure refinement for **L^1H_2-AuCl**.

Identification code	sh2566	
Empirical formula	C14 H20 Au2 Cl2 O4 S10	
Formula weight	1037.73	
Temperature	293(2) K	
Wavelength	0.71073 Å	
Crystal system	Monoclinic	
Space group	P2(1)/n	
Unit cell dimensions	a = 5.4398(11) Å	α= 90°.
	b = 30.511(6) Å	β= 105.49(3)°.
	c = 8.6704(17) Å	γ = 90°.
Volume	1386.8(5) $Å^3$	
Z	2	
Density (calculated)	2.485 Mg/m^3	
Absorption coefficient	11.535 mm^{-1}	
F(000)	976	
Crystal size	0.7 x 0.1 x 0.05 mm^3	
Theta range for data collection	2.53 to 27.98°.	
Index ranges	-6<=h<=6, -40<=k<=39, -11<=l<=11	

Reflections collected	12410
Independent reflections	3107 [R(int) = 0.0798]
Completeness to theta = 27.98°	92.9 %
Absorption correction	Numerical
Refinement method	Full-matrix least-squares on F^2
Data / restraints / parameters	3107 / 0 / 148
Goodness-of-fit on F^2	1.034
Final R indices [I>2sigma(I)]	R1 = 0.0270, wR2 = 0.0629
R indices (all data)	R1 = 0.0396, wR2 = 0.0674
Largest diff. peak and hole	1.074 and -1.219 e.$Å^{-3}$

Table 2. Atomic coordinates (x 10^4) and equivalent isotropic displacement parameters ($Å^2$x 10^3) for sh2566. U(eq) is defined as one third of the trace of the orthogonalized U^{ij} tensor.

	x	y	z	U(eq)
Au	12958(1)	341(1)	89(1)	26(1)
Cl	13399(3)	560(1)	-2353(2)	36(1)
S(1)	12263(3)	193(1)	2531(2)	29(1)
S(2)	8943(3)	955(1)	1076(2)	29(1)
S(3)	8656(3)	618(1)	4134(2)	29(1)
S(4)	5289(3)	1702(1)	983(2)	32(1)
S(5)	5080(3)	1328(1)	4674(2)	32(1)
C(1)	10047(11)	583(1)	2582(6)	26(1)
C(3)	7003(11)	1251(2)	2023(6)	26(1)
C(2)	6901(11)	1097(2)	3469(6)	26(1)
C(4)	7894(13)	2079(2)	1024(7)	36(1)
C(6)	7361(12)	1307(2)	6669(6)	30(1)
C(5)	9393(13)	2225(2)	2690(7)	35(1)
C(7)	9670(12)	1597(2)	6834(7)	33(1)
O(2)	9083(9)	2054(1)	6746(5)	37(1)
O(1)	7853(10)	2395(1)	3636(5)	38(1)

Table 3. Bond lengths [Å] and angles [°] for sh2566.

Au-S(1)	2.2928(2)
Au-Cl	2.2932(2)
Au-Au#1	3.0778(6)
S(1)-C(1)	1.702(5)
S(2)-C(1)	1.714(5)
S(2)-C(3)	1.752(6)
S(3)-C(1)	1.714(6)
S(3)-C(2)	1.758(5)
S(4)-C(3)	1.768(5)
S(4)-C(4)	1.818(7)
S(5)-C(2)	1.767(6)
S(5)-C(6)	1.840(6)
C(3)-C(2)	1.353(8)
C(4)-C(5)	1.523(8)
C(6)-C(7)	1.513(8)
C(5)-O(1)	1.419(8)
C(7)-O(2)	1.427(6)
S(1)-Au-Cl	173.59(5)
S(1)-Au-Au#1	102.27(4)
Cl-Au-Au#1	84.00(4)
C(1)-S(1)-Au	100.30(2)
C(1)-S(2)-C(3)	96.7(3)
C(1)-S(3)-C(2)	96.3(3)
C(3)-S(4)-C(4)	100.4(3)
C(2)-S(5)-C(6)	101.4(3)
S(1)-C(1)-S(2)	123.4(3)
S(1)-C(1)-S(3)	121.9(3)
S(2)-C(1)-S(3)	114.7(3)
C(2)-C(3)-S(2)	115.7(4)
C(2)-C(3)-S(4)	126.6(4)
S(2)-C(3)-S(4)	117.6(3)
C(3)-C(2)-S(3)	116.1(4)
C(3)-C(2)-S(5)	125.3(4)
S(3)-C(2)-S(5)	118.6(3)
C(5)-C(4)-S(4)	114.8(4)
C(7)-C(6)-S(5)	113.7(4)

O(1)-C(5)-C(4)	114.0(5)
O(2)-C(7)-C(6)	113.5(5)

Symmetry transformations used to generate equivalent atoms: #1 -x+3,-y,-z

Table 4. Anisotropic displacement parameters ($Å^2 x\ 10^3$) for sh2566. The anisotropic displacement factor exponent takes the form: $-2\pi^2[\ h^2\ a^{*2} U^{11} + ... + 2\ h\ k\ a^*\ b^*\ U^{12}\ ]$

	U^{11}	U^{22}	U^{33}	U^{23}	U^{13}	U^{12}
Au	24(1)	23(1)	31(1)	-2(1)	5(1)	0(1)
Cl	33(1)	37(1)	36(1)	9(1)	8(1)	3(1)
S(1)	26(1)	26(1)	34(1)	2(1)	6(1)	1(1)
S(2)	33(1)	30(1)	23(1)	1(1)	6(1)	5(1)
S(3)	31(1)	28(1)	27(1)	3(1)	7(1)	0(1)
S(4)	28(1)	33(1)	30(1)	-2(1)	-2(1)	7(1)
S(5)	23(1)	43(1)	31(1)	-6(1)	7(1)	-2(1)
C(1)	25(3)	21(2)	28(3)	-6(2)	3(2)	-5(2)
C(3)	24(3)	26(2)	22(2)	-6(2)	-1(2)	1(2)
C(2)	20(3)	30(2)	25(2)	-6(2)	1(2)	-5(2)
C(4)	44(4)	31(3)	33(3)	5(2)	11(3)	7(2)
C(6)	34(4)	37(3)	21(2)	0(2)	9(2)	-3(2)
C(5)	37(4)	30(2)	34(3)	4(2)	3(3)	-3(2)
C(7)	32(4)	35(3)	28(3)	-7(2)	4(2)	-3(2)
O(2)	44(3)	34(2)	28(2)	-4(2)	4(2)	-4(2)
O(1)	49(3)	31(2)	30(2)	1(2)	3(2)	8(2)

Table 5. Hydrogen coordinates ($x\ 10^4$) and isotropic displacement parameters ($Å^2 x\ 10^3$) for sh2566.

	x	y	z	U(eq)
H(4A)	9061	1940	502	43
H(4B)	7204	2337	405	43
H(6A)	6491	1393	7462	36
H(6B)	7929	1006	6896	36

H(5A)	10346	1976	3243	42
H(5B)	10614	2447	2585	42
H(7A)	10890	1537	7852	39
H(7B)	10473	1524	5993	39
H(2)	8528	2126	5806	27(16)
H(1)	6731	2551	3079	57

L^2H_2-AuCl complex

Table 1. Crystal data and structure refinement for **L^2H_2-AuCl**.

Identification code	sh2793	
Empirical formula	C13 H18 Au Cl O6 S5	
Formula weight	662.99	
Temperature	153(2) K	
Wavelength	0.71073 Å	
Crystal system	Triclinic	
Space group	$P\bar{1}$	
Unit cell dimensions	a = 5.6607(3) Å	α= 71.359(2)°.
	b = 14.1790(6) Å	β= 88.234(3)°.
	c = 14.3137(6) Å	γ = 85.486(3)°.
Volume	1085.20(9) $Å^3$	
Z	2	
Density (calculated)	2.029 Mg/m^3	
Absorption coefficient	7.408 mm^{-1}	
F(000)	640	
Crystal size	1.21 x 0.09 x 0.06 mm^3	
Theta range for data collection	1.50 to 32.41°.	
Index ranges	-8<=h<=8, -17<=k<=21, -19<=l<=21	
Reflections collected	25482	
Independent reflections	7708 [R(int) = 0.0552]	
Completeness to theta = 32.41°	98.8 %	
Absorption correction	Multiscan	
Max. and min. transmission	0.6818 and 0.0403	
Refinement method	Full-matrix least-squares on F^2	
Data / restraints / parameters	7708 / 0 / 235	
Goodness-of-fit on F^2	1.054	
Final R indices [I>2sigma(I)]	R1 = 0.0448, wR2 = 0.0915	

R indices (all data)	R1 = 0.0691, wR2 = 0.0995
Largest diff. peak and hole	1.801 and -3.112 e.Å^{-3}

Table 2. Atomic coordinates (x 10^4) and equivalent isotropic displacement parameters (Å^{2}x 10^3) for sh2793. U(eq) is defined as one third of the trace of the orthogonalized U^{ij} tensor.

	x	y	z	U(eq)
Au(1)	2418(1)	4267(1)	88(1)	25(1)
S(1)	3091(2)	4358(1)	1607(1)	27(1)
S(3)	7250(2)	3057(1)	1252(1)	24(1)
S(2)	6641(2)	3356(1)	3139(1)	26(1)
S(4)	11018(2)	2040(1)	4012(1)	27(1)
S(5)	11721(2)	1735(1)	1789(1)	31(1)
Cl(1)	1751(2)	4068(1)	-1394(1)	35(1)
C(1)	5599(8)	3603(4)	1966(4)	23(1)
C(4)	8960(9)	1695(4)	5038(4)	26(1)
C(5)	7247(9)	944(4)	4982(3)	24(1)
C(2)	9051(8)	2557(4)	3030(4)	22(1)
C(3)	9339(8)	2422(4)	2143(4)	24(1)
C(6)	10932(9)	491(4)	2454(4)	31(1)
C(7)	8745(10)	185(4)	2095(4)	30(1)
O(1)	7410(6)	477(3)	4401(3)	30(1)
O(2)	5578(7)	866(3)	5650(3)	30(1)
O(4)	8230(8)	-717(3)	2662(3)	38(1)
O(3)	7543(10)	673(3)	1413(4)	64(2)
O(5)	4571(8)	8566(4)	2084(3)	48(1)
C(9)	4502(10)	8358(4)	1315(5)	36(1)
C(8)	6294(11)	8675(5)	516(4)	40(1)
C(10)	2580(13)	7756(6)	1175(6)	58(2)
O(6A)	2810(20)	6198(9)	4760(8)	53(3)
C(11A)	1810(30)	5214(11)	3686(10)	48(3)
C(12A)	980(20)	5931(9)	4216(9)	35(2)
C(13A)	-1530(30)	6469(12)	3909(12)	59(4)
O(6B)	1935(18)	6049(7)	4908(7)	41(2)
C(12B)	4130(30)	6093(12)	4112(12)	60(4)
C(13B)	-3580(50)	6600(20)	3909(19)	110(8)
C(11B)	3220(30)	5410(13)	3541(12)	61(4)

Table 3. Bond lengths [Å] and angles [°] for sh2793.

Au(1)-S(1)	2.264(1)
Au(1)-Cl(1)	2.274(1)
Au(1)-Au(1)#1	3.270(4)
S(1)-C(1)	1.697(5)
S(3)-C(1)	1.688(5)
S(3)-C(3)	1.740(5)
S(2)-C(1)	1.715(5)
S(2)-C(2)	1.739(5)
S(4)-C(2)	1.750(5)
S(4)-C(4)	1.810(5)
S(5)-C(3)	1.758(5)
S(5)-C(6)	1.800(6)
C(4)-C(5)	1.517(7)
C(5)-O(1)	1.214(6)
C(5)-O(2)	1.309(6)
C(2)-C(3)	1.348(7)
C(6)-C(7)	1.501(8)
C(7)-O(3)	1.196(7)
C(7)-O(4)	1.327(7)
O(5)-C(9)	1.230(7)
C(9)-C(8)	1.487(9)
C(9)-C(10)	1.489(9)
O(6A)-C(12A)	1.457(2)
C(11A)-C(12A)	1.492(2)
C(12A)-C(13A)	1.562(2)
O(6B)-C(12B)	1.649(2)
C(12B)-C(13B)#2	1.51(3)
C(12B)-C(11B)	1.58(2)
C(13B)-C(12B)#3	1.51(3)
S(1)-Au(1)-Cl(1)	176.37(5)
S(1)-Au(1)-Au(1)#1	90.30(3)
Cl(1)-Au(1)-Au(1)#1	91.74(4)
C(1)-S(1)-Au(1)	103.24(2)
C(1)-S(3)-C(3)	96.7(2)
C(1)-S(2)-C(2)	96.3(2)

C(2)-S(4)-C(4)	100.7(2)
C(3)-S(5)-C(6)	99.4(2)
S(3)-C(1)-S(1)	125.4(3)
S(3)-C(1)-S(2)	115.0(3)
S(1)-C(1)-S(2)	119.6(3)
C(5)-C(4)-S(4)	114.5(3)
O(1)-C(5)-O(2)	124.7(5)
O(1)-C(5)-C(4)	124.7(5)
O(2)-C(5)-C(4)	110.5(4)
C(3)-C(2)-S(2)	115.7(4)
C(3)-C(2)-S(4)	123.9(4)
S(2)-C(2)-S(4)	120.3(3)
C(2)-C(3)-S(3)	116.2(4)
C(2)-C(3)-S(5)	125.9(4)
S(3)-C(3)-S(5)	117.8(3)
C(7)-C(6)-S(5)	115.1(4)
O(3)-C(7)-O(4)	122.6(6)
O(3)-C(7)-C(6)	126.6(6)
O(4)-C(7)-C(6)	110.7(5)
O(5)-C(9)-C(8)	122.3(6)
O(5)-C(9)-C(10)	119.4(6)
C(8)-C(9)-C(10)	118.3(6)
O(6A)-C(12A)-C(11A)	114.8(1)
O(6A)-C(12A)-C(13A)	128.5(1)
C(11A)-C(12A)-C(13A)	115.0(1)
C(13B)#2-C(12B)-C(11B)	125.6(2)
C(13B)#2-C(12B)-O(6B)	134.3(2)
C(11B)-C(12B)-O(6B)	100.1(1)

Symmetry transformations used to generate equivalent atoms: #1 -x,-y+1,-z #2 x+1,y,z #3 x-1,y,z

Table 4. Anisotropic displacement parameters ($Å^2 x\ 10^3$) for sh2793. The anisotropic displacement factor exponent takes the form: $-2\pi^2[\ h^2\ a^{*2} U^{11} + ... + 2\ h\ k\ a^*\ b^*\ U^{12}\ ]$

	U^{11}	U^{22}	U^{33}	U^{23}	U^{13}	U^{12}
Au(1)	25(1)	20(1)	29(1)	-4(1)	-4(1)	-3(1)

S(1)	26(1)	24(1)	31(1)	-9(1)	-3(1)	1(1)
S(3)	27(1)	23(1)	23(1)	-7(1)	0(1)	-3(1)
S(2)	27(1)	26(1)	25(1)	-10(1)	-2(1)	2(1)
S(4)	23(1)	29(1)	29(1)	-7(1)	-5(1)	-4(1)
S(5)	29(1)	28(1)	36(1)	-12(1)	9(1)	-2(1)
Cl(1)	37(1)	32(1)	38(1)	-14(1)	-11(1)	1(1)
C(1)	19(2)	21(2)	29(2)	-8(2)	1(2)	-5(2)
C(4)	28(2)	25(3)	26(2)	-8(2)	-3(2)	-5(2)
C(5)	25(2)	23(3)	23(2)	-8(2)	-5(2)	2(2)
C(2)	22(2)	19(2)	26(2)	-5(2)	-1(2)	-5(2)
C(3)	17(2)	27(3)	27(2)	-8(2)	0(2)	-3(2)
C(6)	28(3)	29(3)	35(3)	-12(2)	-2(2)	3(2)
C(7)	39(3)	23(3)	31(3)	-14(2)	-4(2)	0(2)
O(1)	30(2)	33(2)	32(2)	-15(2)	3(2)	-10(2)
O(2)	30(2)	33(2)	32(2)	-14(2)	5(2)	-11(2)
O(4)	42(2)	35(2)	36(2)	-10(2)	-5(2)	-8(2)
O(3)	87(4)	32(3)	68(3)	-6(2)	-49(3)	-6(2)
O(5)	47(3)	56(3)	54(3)	-35(2)	8(2)	-14(2)
C(9)	28(3)	33(3)	53(4)	-23(3)	-2(2)	2(2)
C(8)	40(3)	40(4)	40(3)	-15(3)	-1(3)	3(3)
C(10)	43(4)	68(5)	79(5)	-45(4)	-6(4)	-11(4)

Table 5. Hydrogen coordinates (x 10^4) and isotropic displacement parameters ($Å^2$x 10^3)
for sh2793.

	x	y	z	U(eq)
H(4A)	9876	1414	5656	31
H(4B)	8036	2306	5072	31
H(6A)	12277	15	2415	37
H(6B)	10699	437	3157	37
H(2)	4739	401	5655	45
H(4)	7161	-919	2396	56
H(8A)	5510	9106	-87	59
H(8B)	7081	8084	393	59
H(8C)	7473	9042	716	59
H(10A)	1387	7700	1698	87
H(10B)	3250	7089	1205	87
H(10C)	1838	8085	532	87

Er-Hg complex (3).

Table 1. Crystal data and structure refinement for **Er-Hg** complex .

Identification code	sh2472	
Empirical formula	C32 H66 Cl6 Er2 Hg I2 O9	
Formula weight	1596.46	
Temperature	170(2) K	
Wavelength	0.71073 Å	
Crystal system	Triclinic	
Space group	$P\bar{1}$	
Unit cell dimensions	a = 9.1770(3) Å	α= 87.913(2)°.
	b = 15.7741(5) Å	β= 75.2440(10)°.
	c = 17.9528(8) Å	γ = 87.7110(10)°.
Volume	2510.19(16) $Å^3$	
Z	2	
Density (calculated)	2.112 Mg/m^3	
Absorption coefficient	7.954 mm^{-1}	

F(000)	1508
Crystal size	0.52 x 0.38 x 0.22 mm^3
Theta range for data collection	1.17 to 22.12°.
Index ranges	-9<=h<=9, -16<=k<=13, -18<=l<=18
Reflections collected	23683
Independent reflections	6137 [R(int) = 0.0339]
Completeness to theta = 22.12°	98.2 %
Absorption correction	Multiscan
Max. and min. transmission	0.2736 and 0.1040
Refinement method	Full-matrix least-squares on F^2
Data / restraints / parameters	6137 / 0 / 471
Goodness-of-fit on F^2	1.033
Final R indices [I>2sigma(I)]	R1 = 0.0314, wR2 = 0.0736
R indices (all data)	R1 = 0.0411, wR2 = 0.0782
Largest diff. peak and hole	0.695 and -1.852 e.$Å^{-3}$

Table 2. Atomic coordinates (x 10^4) and equivalent isotropic displacement parameters ($Å^2$x 10^3) for sh2472. U(eq) is defined as one third of the trace of the orthogonalized U^{ij} tensor.

	x	y	z	U(eq)
Er(1)	1347(1)	2608(1)	6604(1)	21(1)
Er(2)	8219(1)	2330(1)	2821(1)	26(1)
Hg	7292(1)	2656(1)	754(1)	41(1)
I(1)	9294(1)	3711(1)	-22(1)	62(1)
I(2)	4955(1)	1821(1)	642(1)	71(1)
Cl(1)	3294(2)	1395(1)	6153(1)	30(1)
Cl(2)	-680(3)	3794(1)	6972(1)	36(1)
Cl(3)	7418(3)	3189(1)	4047(1)	36(1)
Cl(4)	6357(3)	3295(1)	2216(1)	34(1)
Cl(5)	8839(3)	1520(1)	1502(1)	35(1)
Cl(6)	10059(3)	1342(2)	3316(1)	39(1)
O(1)	-284(6)	1884(3)	6022(3)	23(1)
O(2)	3346(6)	3572(3)	6360(3)	25(1)
O(3)	-129(6)	1673(4)	7550(3)	30(1)
O(4)	6230(6)	1437(4)	3251(3)	31(2)
O(5)	1724(6)	3146(4)	5312(3)	29(1)
O(6)	10104(7)	3232(4)	2273(4)	37(2)

O(8)	2065(7)	2708(4)	7728(4)	39(2)
O(9)	3848(8)	3761(4)	8189(4)	51(2)
O(10)	2038(10)	1430(5)	8732(4)	71(2)
C(3)	-1242(9)	842(5)	5388(5)	30(2)
C(4)	5884(10)	979(6)	3996(5)	32(2)
C(5)	5160(11)	1228(6)	2826(5)	36(2)
C(6)	161(9)	1303(6)	5386(5)	29(2)
C(7)	4941(9)	3339(6)	6256(6)	35(2)
C(8)	-2468(10)	1533(6)	5661(6)	33(2)
C(9)	9981(11)	4155(6)	2200(6)	43(3)
C(10)	598(11)	3590(7)	4982(6)	46(3)
C(11)	2695(12)	3185(7)	3962(5)	44(3)
C(12)	11632(11)	2954(7)	1842(7)	53(3)
C(14)	11453(15)	4436(7)	1743(8)	83(5)
C(13)	12436(14)	3751(9)	1637(10)	95(5)
C(15)	4342(10)	629(6)	4088(5)	34(2)
C(16)	4323(10)	477(6)	3258(5)	36(2)
C(18)	-110(11)	743(6)	7495(5)	38(2)
C(17)	-1923(9)	1956(6)	6267(6)	34(2)
C(21)	-1227(11)	1922(6)	8250(5)	41(3)
C(19)	-1309(14)	445(7)	8170(7)	65(4)
C(20)	-1955(19)	1150(9)	8583(9)	124(8)
C(22)	3122(10)	3090(6)	4708(5)	40(3)
C(23)	1404(12)	3849(7)	4175(6)	55(3)
C(24)	3185(11)	4486(6)	6329(6)	42(3)
C(26)	5759(11)	4164(6)	6084(8)	59(3)
C(25)	4659(13)	4817(7)	6295(9)	77(4)
C(29)	3265(13)	4454(7)	8670(7)	59(3)
C(31)	1652(16)	1382(11)	9557(7)	92(5)
C(28)	5310(20)	3873(11)	9057(10)	104(6)
C(30)	3189(16)	815(10)	8456(9)	95(5)
C(27)	5081(15)	3378(10)	8436(9)	91(5)
C(32)	2320(20)	554(11)	9749(10)	112(7)
C(33)	3690(20)	499(11)	9075(12)	122(7)
C(34)	4170(20)	4493(14)	9208(11)	149(9)

Table 3. Bond lengths [Å] and angles [°] for sh2472.

Er(1)-O(8)	2.289(6)
Er(1)-O(2)	2.373(5)
Er(1)-O(1)	2.379(5)
Er(1)-O(5)	2.385(5)
Er(1)-O(3)	2.388(5)
Er(1)-Cl(2)	2.565(2)
Er(1)-Cl(1)	2.572(2)
Er(2)-O(6)	2.283(6)
Er(2)-O(4)	2.307(6)
Er(2)-Cl(6)	2.554(2)
Er(2)-Cl(3)	2.556(2)
Er(2)-Cl(5)	2.652(2)
Er(2)-Cl(4)	2.653(2)
Hg-I(2)	2.615(9)
Hg-I(1)	2.620(8)
Hg-Cl(4)	2.760(2)
Hg-Cl(5)	2.761(2)
O(1)-C(6)	1.456(1)
O(1)-C(17)	1.456(1)
O(2)-C(24)	1.444(1)
O(2)-C(7)	1.461(1)
O(3)-C(21)	1.452(1)
O(3)-C(18)	1.473(1)
O(4)-C(5)	1.443(1)
O(4)-C(4)	1.464(1)
O(5)-C(22)	1.456(1)
O(5)-C(10)	1.460(1)
O(6)-C(9)	1.460(1)
O(6)-C(12)	1.476(1)
O(9)-C(29)	1.419(1)
O(9)-C(27)	1.423(1)
O(10)-C(30)	1.410(2)
O(10)-C(31)	1.432(1)
C(3)-C(6)	1.503(1)
C(3)-C(8)	1.534(1)
C(4)-C(15)	1.507(1)
C(5)-C(16)	1.514(1)

C(7)-C(26)	1.511(1)
C(8)-C(17)	1.496(1)
C(9)-C(14)	1.467(1)
C(10)-C(23)	1.499(1)
C(11)-C(22)	1.490(1)
C(11)-C(23)	1.531(2)
C(12)-C(13)	1.470(2)
C(14)-C(13)	1.367(2)
C(15)-C(16)	1.523(1)
C(18)-C(19)	1.490(1)
C(21)-C(20)	1.449(2)
C(19)-C(20)	1.385(2)
C(24)-C(25)	1.455(1)
C(26)-C(25)	1.405(2)
C(29)-C(34)	1.432(2)
C(31)-C(32)	1.49(2)
C(28)-C(34)	1.38(2)
C(28)-C(27)	1.446(2)
C(30)-C(33)	1.38(2)
C(32)-C(33)	1.51(2)

O(8)-Er(1)-O(2)	72.9(2)
O(8)-Er(1)-O(1)	143.0(2)
O(2)-Er(1)-O(1)	143.90(2)
O(8)-Er(1)-O(5)	144.8(2)
O(2)-Er(1)-O(5)	71.93(2)
O(1)-Er(1)-O(5)	72.27(2)
O(8)-Er(1)-O(3)	71.4(2)
O(2)-Er(1)-O(3)	144.26(2)
O(1)-Er(1)-O(3)	71.65(2)
O(5)-Er(1)-O(3)	143.81(2)
O(8)-Er(1)-Cl(2)	92.59(2)
O(2)-Er(1)-Cl(2)	92.95(1)
O(1)-Er(1)-Cl(2)	89.26(1)
O(5)-Er(1)-Cl(2)	86.32(2)
O(3)-Er(1)-Cl(2)	90.55(2)
O(8)-Er(1)-Cl(1)	91.55(2)
O(2)-Er(1)-Cl(1)	89.08(1)
O(1)-Er(1)-Cl(1)	86.92(1)

O(5)-Er(1)-Cl(1)	90.78(2)
O(3)-Er(1)-Cl(1)	89.97(1)
Cl(2)-Er(1)-Cl(1)	175.77(7)
O(6)-Er(2)-O(4)	173.7(2)
O(6)-Er(2)-Cl(6)	91.12(2)
O(4)-Er(2)-Cl(6)	93.43(2)
O(6)-Er(2)-Cl(3)	92.32(2)
O(4)-Er(2)-Cl(3)	91.61(2)
Cl(6)-Er(2)-Cl(3)	94.94(8)
O(6)-Er(2)-Cl(5)	88.33(2)
O(4)-Er(2)-Cl(5)	87.28(2)
Cl(6)-Er(2)-Cl(5)	90.61(7)
Cl(3)-Er(2)-Cl(5)	174.40(7)
O(6)-Er(2)-Cl(4)	88.81(2)
O(4)-Er(2)-Cl(4)	86.35(2)
Cl(6)-Er(2)-Cl(4)	175.97(7)
Cl(3)-Er(2)-Cl(4)	89.09(7)
Cl(5)-Er(2)-Cl(4)	85.36(7)
I(2)-Hg-I(1)	141.62(3)
I(2)-Hg-Cl(4)	102.64(5)
I(1)-Hg-Cl(4)	105.23(5)
I(2)-Hg-Cl(5)	103.91(5)
I(1)-Hg-Cl(5)	105.93(5)
Cl(4)-Hg-Cl(5)	81.31(7)
Er(2)-Cl(4)-Hg	96.02(7)
Er(2)-Cl(5)-Hg	96.02(7)
C(6)-O(1)-C(17)	109.3(6)
C(6)-O(1)-Er(1)	126.8(4)
C(17)-O(1)-Er(1)	124.0(5)
C(24)-O(2)-C(7)	108.6(6)
C(24)-O(2)-Er(1)	125.8(5)
C(7)-O(2)-Er(1)	125.5(5)
C(21)-O(3)-C(18)	109.0(6)
C(21)-O(3)-Er(1)	126.1(5)
C(18)-O(3)-Er(1)	124.8(5)
C(5)-O(4)-C(4)	109.5(6)
C(5)-O(4)-Er(2)	125.6(5)
C(4)-O(4)-Er(2)	124.8(5)
C(22)-O(5)-C(10)	107.5(7)

C(22)-O(5)-Er(1)	126.1(5)
C(10)-O(5)-Er(1)	126.4(5)
C(9)-O(6)-C(12)	108.2(7)
C(9)-O(6)-Er(2)	127.2(5)
C(12)-O(6)-Er(2)	124.2(5)
C(29)-O(9)-C(27)	108.2(8)
C(30)-O(10)-C(31)	108.2(1)
C(6)-C(3)-C(8)	101.5(7)
O(4)-C(4)-C(15)	105.5(7)
O(4)-C(5)-C(16)	105.6(7)
O(1)-C(6)-C(3)	105.3(7)
O(2)-C(7)-C(26)	105.5(7)
C(17)-C(8)-C(3)	102.5(7)
O(6)-C(9)-C(14)	106.6(8)
O(5)-C(10)-C(23)	106.1(8)
C(22)-C(11)-C(23)	100.2(8)
C(13)-C(12)-O(6)	103.9(9)
C(13)-C(14)-C(9)	108.2(1)
C(14)-C(13)-C(12)	111.1(1)
C(4)-C(15)-C(16)	102.3(7)
C(5)-C(16)-C(15)	102.7(7)
O(3)-C(18)-C(19)	105.5(7)
O(1)-C(17)-C(8)	105.5(7)
C(20)-C(21)-O(3)	105.7(8)
C(20)-C(19)-C(18)	107.9(9)
C(19)-C(20)-C(21)	111.7(1)
O(5)-C(22)-C(11)	106.4(8)
C(10)-C(23)-C(11)	103.4(8)
O(2)-C(24)-C(25)	106.8(8)
C(25)-C(26)-C(7)	106.5(8)
C(26)-C(25)-C(24)	109.0(9)
O(9)-C(29)-C(34)	106.7(1)
O(10)-C(31)-C(32)	104.6(1)
C(34)-C(28)-C(27)	107.1(1)
C(33)-C(30)-O(10)	107.7(1)
O(9)-C(27)-C(28)	107.7(1)
C(31)-C(32)-C(33)	99.7(1)
C(30)-C(33)-C(32)	104.4(1)
C(28)-C(34)-C(29)	110.1(1)

Table 4. Anisotropic displacement parameters ($Å^2 x\ 10^3$) for sh2472. The anisotropic displacement factor exponent takes the form: $-2\pi^2[\ h^2\ a^{*2}U^{11} + ... + 2\ h\ k\ a^*\ b^*\ U^{12}\ ]$

	U^{11}	U^{22}	U^{33}	U^{23}	U^{13}	U^{12}
Er(1)	19(1)	18(1)	25(1)	-2(1)	-5(1)	0(1)
Er(2)	26(1)	23(1)	27(1)	3(1)	-4(1)	-3(1)
Hg	48(1)	42(1)	35(1)	1(1)	-12(1)	-1(1)
I(1)	80(1)	59(1)	45(1)	14(1)	-11(1)	-19(1)
I(2)	64(1)	83(1)	70(1)	-18(1)	-23(1)	2(1)
Cl(1)	23(1)	22(1)	44(1)	-3(1)	-8(1)	4(1)
Cl(2)	32(1)	25(1)	50(2)	-12(1)	-8(1)	7(1)
Cl(3)	40(1)	34(1)	32(1)	-5(1)	-7(1)	3(1)
Cl(4)	39(1)	32(1)	30(1)	-1(1)	-8(1)	6(1)
Cl(5)	40(1)	31(1)	32(1)	-3(1)	-8(1)	8(1)
Cl(6)	40(1)	34(1)	44(1)	3(1)	-15(1)	6(1)
O(1)	18(3)	22(3)	28(3)	-4(3)	-3(3)	-4(3)
O(2)	21(3)	16(3)	40(4)	-4(3)	-10(3)	0(3)
O(3)	35(4)	28(4)	23(3)	0(3)	0(3)	-2(3)
O(4)	35(4)	30(4)	32(4)	9(3)	-13(3)	-9(3)
O(5)	26(3)	31(4)	31(3)	7(3)	-10(3)	-6(3)
O(6)	32(4)	23(4)	46(4)	5(3)	6(3)	-4(3)
O(8)	46(4)	42(4)	32(4)	-1(3)	-16(3)	-13(3)
O(9)	53(5)	46(5)	63(5)	-20(4)	-32(4)	4(4)
O(10)	92(6)	66(6)	42(5)	10(4)	-2(4)	29(5)
C(3)	23(5)	29(5)	37(5)	-3(4)	-8(4)	-5(4)
C(4)	38(6)	27(5)	32(5)	5(4)	-11(4)	-4(4)
C(5)	38(6)	42(6)	32(5)	2(5)	-14(5)	-6(5)
C(6)	24(5)	30(5)	33(5)	-14(4)	-5(4)	0(4)
C(7)	16(5)	34(6)	54(6)	-7(5)	-10(4)	10(4)
C(8)	23(5)	27(5)	54(6)	3(5)	-17(5)	-6(4)
C(9)	44(6)	27(6)	55(7)	-1(5)	-6(5)	3(5)
C(10)	42(6)	56(7)	43(6)	16(5)	-16(5)	2(5)
C(11)	57(7)	49(7)	30(6)	6(5)	-15(5)	-14(6)
C(12)	29(6)	41(7)	76(8)	-4(6)	7(6)	2(5)
C(14)	83(10)	32(7)	96(10)	-5(7)	47(8)	-15(7)

C(13)	43(8)	71(10)	149(14)	42(10)	10(8)	-19(8)
C(15)	36(6)	31(5)	33(5)	0(4)	-7(4)	-7(4)
C(16)	28(5)	41(6)	41(6)	-5(5)	-9(5)	-2(5)
C(18)	38(6)	29(6)	40(6)	4(5)	3(5)	-5(5)
C(17)	21(5)	31(5)	50(6)	-4(5)	-9(5)	-2(4)
C(21)	41(6)	38(6)	35(6)	-4(5)	6(5)	7(5)
C(19)	73(9)	30(6)	73(8)	10(6)	13(7)	-6(6)
C(20)	136(14)	74(10)	100(12)	-26(9)	93(11)	-45(10)
C(22)	34(6)	35(6)	43(6)	8(5)	5(5)	-8(5)
C(23)	54(7)	69(8)	50(7)	30(6)	-28(6)	-21(6)
C(24)	31(6)	28(6)	66(7)	-2(5)	-9(5)	-3(5)
C(26)	28(6)	31(6)	119(11)	-4(6)	-18(6)	-7(5)
C(25)	48(8)	33(7)	147(13)	9(7)	-18(8)	-12(6)
C(29)	65(8)	49(7)	68(8)	-4(6)	-29(7)	4(6)
C(31)	80(10)	140(14)	47(8)	-3(8)	-8(7)	37(10)
C(28)	119(14)	112(13)	116(13)	10(11)	-94(12)	-21(11)
C(30)	70(10)	105(13)	95(12)	-6(10)	-2(9)	33(9)
C(27)	70(10)	114(12)	108(12)	-28(10)	-58(9)	33(9)
C(32)	113(14)	130(15)	99(13)	89(12)	-43(11)	-48(12)
C(33)	156(19)	72(11)	162(19)	-18(12)	-89(17)	37(12)
C(34)	163(19)	200(20)	124(16)	-101(15)	-104(15)	71(17)

Table 5. Hydrogen coordinates (x 10^4) and isotropic displacement parameters ($Å^2$x 10^3) for sh2472.

	x	y	z	U(eq)
H(8A)	2859	3067	7749	80(40)
H(8B)	1568	2390	8173	160(70)
H(3A)	-1377	346	5750	35
H(3B)	-1229	654	4866	35
H(4A)	5880	1367	4417	38
H(4B)	6638	513	4001	38
H(5A)	5686	1076	2292	43
H(5B)	4453	1714	2807	43
H(6A)	966	899	5465	35
H(6B)	533	1619	4892	35
H(7A)	5291	2948	5823	41

H(7B)	5115	3059	6730	41
H(8A)	-2538	1936	5235	40
H(8B)	-3465	1283	5879	40
H(9A)	9728	4410	2714	52
H(9B)	9184	4325	1938	52
H(10A)	174	4095	5285	56
H(10B)	-235	3211	4979	56
H(11A)	2348	2646	3811	53
H(11B)	3537	3396	3542	53
H(12A)	12121	2578	2167	63
H(12B)	11597	2650	1374	63
H(14A)	11364	4676	1238	99
H(14B)	11825	4882	2016	99
H(13A)	13155	3802	1959	113
H(13B)	13019	3741	1091	113
H(15A)	3538	1044	4331	40
H(15B)	4221	94	4400	40
H(16A)	4849	-66	3076	44
H(16B)	3278	474	3200	44
H(18A)	886	493	7516	46
H(18B)	-327	582	7007	46
H(17A)	-2268	2559	6305	40
H(17B)	-2303	1669	6776	40
H(21A)	-723	2177	8610	49
H(21B)	-1973	2342	8131	49
H(19A)	-2082	145	7994	78
H(19B)	-868	48	8499	78
H(20A)	-1877	1075	9121	149
H(20B)	-3038	1198	8591	149
H(22A)	3646	2535	4743	48
H(22B)	3800	3546	4757	48
H(23A)	1795	4427	4156	66
H(23B)	730	3832	3825	66
H(24A)	2434	4690	6792	50
H(24B)	2846	4676	5867	50
H(26A)	6523	4189	6385	71
H(26B)	6274	4216	5529	71
H(25A)	4873	5292	5912	93
H(25B)	4674	5032	6804	93

H(29A)	2199	4366	8944	70
H(29B)	3321	4989	8359	70
H(31A)	544	1399	9767	110
H(31B)	2082	1857	9767	110
H(28A)	5265	3506	9522	125
H(28B)	6308	4136	8905	125
H(30A)	2793	352	8213	113
H(30B)	4028	1075	8067	113
H(27A)	6001	3371	8005	109
H(27B)	4856	2786	8618	109
H(32A)	1638	81	9762	134
H(32B)	2603	566	10245	134
H(33A)	4510	844	9158	146
H(33B)	4066	-96	8993	146
H(34A)	4620	5059	9169	178
H(34B)	3537	4410	9739	178

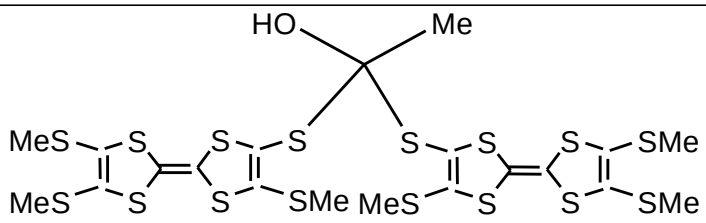

$(Me_3TTF)_2C(OH)Me$

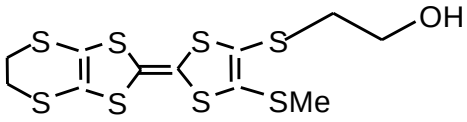

HETMT-EDTTTF

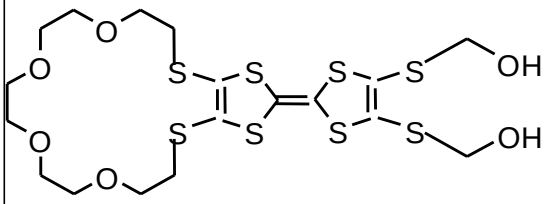

$((\text{-}O(CH_2)_2\text{-})_4\text{-}TTF(CH_2OH)_2$

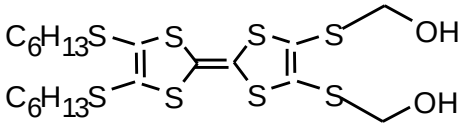

DHMT-DHTTTF

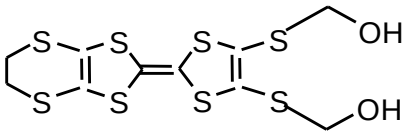

DHMT-EDTTTF

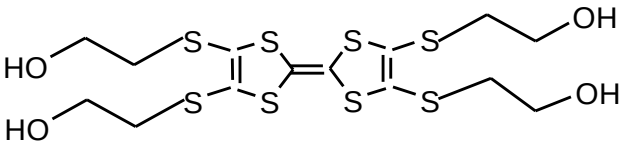

THET-TTF

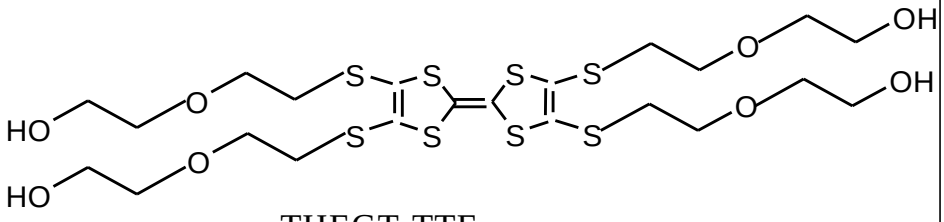

THEGT-TTF

Scheme H-1: Representation of the molecules discussed in the Chapter B (see Table B-4)